A Data-Driven Frequency-Domain Approach for Robust Controller Design via Convex Optimization

THIS IS A TEMPORARY TITLE PAGE
It will be replaced for the final print by a version
provided by the service academique.

Thèse n. 8305
présenté le 4 Decembre 2017
à la Faculté des Sciences et Techniques de L'ingénieur
laboratoire d'automatique
programme doctoral en Génie Electrique
École Polytechnique Fédérale de Lausanne

pour l'obtention du grade de Docteur ès Sciences
par

Achille Nicoletti

acceptée sur proposition du jury:

Prof. Colin Jones, président du jury
Dr. Alireza Karimi, directeur de thèse
Dr. Michele Martino, co-directeur de thèse
Prof. Drazen Dujic, rapporteur
Prof. Simone Formentin, rapporteur
Prof. Marcel Heertjes, rapporteur

Lausanne, EPFL, 2017

CERN-THESIS-2017-322
04/12/2017

It is the perfection of God's works that they are all done with the greatest simplicity.
— Isaac Newton

You must be ready to give up even the most attractive ideas when experiment shows them to be wrong.
— Alessandro Volta

To my parents...

Acknowledgements

The writing and completion of this dissertation would not have been possible without the assistance, support, and guidance of the many special people in my life. Firstly, I would like to thank God for giving me the capability to contribute to the engineering world and hopefully assist the future civilizations in creating technologies for the good of mankind. I hope that ethical values will be exercised and that the technologies arising from the new frontiers of science are used in conscientious manners.

Secondly, I would like to thank my EPFL advisor, Dr. Alireza Karimi. I have learned many things from him since starting my Ph.D, and I thank him for accepting me into his program. His contributions and patience were key factors in the successful completion of this dissertation. I would also like to thank my CERN supervisor, Dr. Michele Martino. He has been very helpful during my Ph.D studies, and I have enjoyed the numerous technical discussions I had with him; I always learned something new from each discussion, and am very appreciative for that. Among my other CERN colleagues, I would like to also thank Miguel Cerqueira Bastos, Quentin King, Olivier Michele, Davide Aguglia, Todor Todorvic, Ivan Jovetic, Olivier Founier, and Louis De Mallac. The knowledge that I have acquired from Michele and my numerous colleagues will be something that I will foster and cherish for the rest of my life. Among other EPFL personnel and members of other universities that I have collaborated with, I would like to thank Prof. Colin Jones (president of my jury committee), Prof. Dan Simon, Prof. Dominique Bonvin, Prof. Kiril Streletzky, Prof. Marcel Heertjes, and Prof. Simone Formentin.

In addition to my work colleagues, I would also like to thank Zlatko Emedji and Jose Manuel De Paco Soto for being good friends and providing the emotional support I needed. Also a thank you to Predrag Milosavljevic and Christoph Kammer for being good competitors at Foosball during my time at EPFL. Additionally, I would like to thank Michael Davis, Hugo Lebreton, Miguel Hermo Serans, Mahdieh Sadat Sad Abadi, Ioannis Lymperopoulos, Timm Faulwasser, Philippe Muellhaupt, and all other CERN and EPFL colleagues for our random technical and non-technical discussions. A special thank you to Ruth Benassi for her continued support for all administrative work and Christophe Salzmann for his support on technical related issues in the laboratories.

Finally, I would like to thank my family for their support during this endeavour. To my wife Iuliia for her continued support and love, I thank you for everything you have done and being born into this world. I am utterly grateful to be with you and could not wish for anything else. My sisters Carmen, Marie, and Elizabeth have been great inspirations to me; they shaped me into the person I am today and can honestly say that without them, I may not have been so

successful. To my mother, I thank you for everything you have done for me during my 34 years on this planet. I appreciate all of the hard work that you have done to support the family, and I will always carry your love in my heart. And finally, to my father, I wish you could have still been with us to witness this moment in my life. I know that you would have been proud of me, and am very grateful for all of the sacrifices you made for the family.

Geneva, 15 December 2017 Achille Nicoletti

Abstract

The objective of this dissertation is to develop data-driven frequency-domain methods for designing robust controllers through the use of convex optimization algorithms. Many of today's industrial processes are becoming more complex, and modeling accurate physical models for these plants using first principles may be impossible. Albeit a model may be available; however, such a model may be too complex to consider for an appropriate controller design. With the increased developments in the computing world, large amounts of measured data can be easily collected and stored for processing purposes. Data can also be collected and used in an on-line fashion. Thus it would be very sensible to make full use of this data for controller design, performance evaluation, and stability analysis. The design methods imposed in this work ensure that the dynamics of a system are captured in an experiment and avoids the problem of unmodeled dynamics associated with parametric models. The devised methods consider robust designs for both linear-time-invariant (LTI) single-input-single-output (SISO) systems and certain classes of nonlinear systems.

In this dissertation, a data-driven approach using the frequency response function of a system is proposed for designing robust controllers with $\mathscr{H}_\infty$ performance. Necessary and sufficient conditions are derived for obtaining $\mathscr{H}_\infty$ performance while guaranteeing the closed-loop stability of a system. A convex optimization algorithm is formulated to obtain the controller parameters which ensure system robustness; the controller is robust with respect to the frequency-dependent uncertainties of the frequency response function. For a certain class of nonlinearities, the proposed method can be used to obtain a best-linear-approximation with an associated frequency-dependent uncertainty to guarantee the stability and performance for the underlying linear system that is subject to nonlinear distortions.

The controller for this design scheme is presented as a ratio of two linearly-parameterized transfer functions; in this manner, the numerator and denominator of a controller are simultaneously optimized. With this construction, it can be shown that as the controller order increases, the solution to the convex problem converges to the global optimal solution of the $\mathscr{H}_\infty$ problem. This method is then extended to the 2-degree-of-freedom discrete-time controller where the necessary and sufficient conditions are imposed for multiple weighted sensitivity functions.

The concepts behind these design methods are then used to devise necessary and sufficient conditions for ensuring the closed-loop stability of systems with sector-bounded nonlinearities. The conditions are simple convex feasibility constraints which can be used to stabilize systems with multi-model uncertainty. Additionally, a method is proposed for obtaining $\mathscr{H}_\infty$

performance for systems with uncertain gains within these sectors.
By convexifying the $\mathscr{H}_\infty$ problem, the global optimal solution to an approximate problem is obtained. For low-order controllers, the solution to this approximate problem may lead to solutions far from the optimal solution of the true $\mathscr{H}_\infty$ problem. Thus two methods are proposed to address this issue for low-order controllers. In one method, a non-convex problem is formulated which optimizes the basis function parameters of a controller while guaranteeing the stability of the closed-loop systems. In another method, a set of convex problems are solved in an iterative fashion to obtain the desired performance (which also guarantees the closed-loop stability of the system). With both methods, the local solution to the $\mathscr{H}_\infty$ problem for fixed-structure controllers is obtained. However, the convex problem is computationally tractable and can also consider $\mathscr{H}_2$ performance.
The effectiveness of the proposed method(s) is illustrated by considering several case studies that require robust controllers for achieving the desired performance. The main applicative work in this dissertation is with respect to a power converter control system at the European Organization for Nuclear Research (CERN) (which is used to control the current in a magnet to produce the desired field in controlling particle trajectories in particle accelerators). The proposed design methods are implemented in order to satisfy the challenging performance specifications set by the application while guaranteeing the system stability and robustness using data-driven design strategies.

Key words: Convex optimization, data-driven control, fixed-structure control, $\mathscr{H}_\infty$ control, $\mathscr{H}_2$ control, nonlinear control, power converter control, robust control, sector nonlinearity.

Résumé

L'objectif de cette thèse est de développer des méthodes de domaine fréquentiel pilotées par les données pour la conception de contrôleurs robustes grâce à l'utilisation d'algorithmes d'optimisation convexe. De nombreux procédés industriels actuels deviennent de plus en plus complexes et il peut être impossible de modéliser des modèles physiques précis pour ces plantes en utilisant les principes premiers. Bien qu'un modèle puisse être disponible ; cependant, un tel modèle peut être trop complexe à considérer pour une conception de contrôleur appropriée. Avec les développements accrus dans le monde informatique, de grandes quantités de données mesurées peuvent être facilement collectées et enregistrées à des fins de traitement. Les données peuvent également être collectées et utilisées en ligne. Il serait donc judicieux de tirer pleinement parti de ces données pour la conception du contrôleur, l'évaluation des performances et l'analyse de la stabilité. Les méthodes de conception imposées dans ce travail garantissent que la dynamique d'un système est capturée dans une expérience et évite le problème de la dynamique non modélisée associée aux modèles paramétriques. Les méthodes développées prennent en compte des conceptions robustes pour les systèmes à entrée unique à sortie unique (SISO) linéaire invariant de temps (LTI) et pour certaines classes de systèmes non-linéaires.

Dans cette thèse, une approche basée sur les données utilisant la fonction de réponse en fréquence d'un système est proposée pour concevoir des contrôleurs robustes avec des performances $\mathscr{H}_\infty$. Les conditions nécessaires et suffisantes sont dérivées pour obtenir des performances $\mathscr{H}_\infty$ tout en garantissant la stabilité en boucle fermée d'un système. Un algorithme d'optimisation convexe est implémenté pour obtenir les paramètres du contrôleur qui assurent la robustesse du système ; le contrôleur est robuste par rapport aux incertitudes dépendantes de la fréquence de la fonction de réponse en fréquence. En effet, pour une certaine classe de non-linéarités, la méthode proposée peut être utilisée pour obtenir une meilleure approximation linéaire avec une incertitude dépendante de la fréquence associée pour garantir la stabilité et la performance du système linéaire sous-jacent aux distorsions non-linéaires.

Le contrôleur pour ce schéma de conception est présenté comme un ratio de deux fonctions de transfert paramétrées linéairement ; dans cette manière, le numérateur et le dénominateur d'un contrôleur sont simultanément optimisés. Avec cette construction, on peut montrer qu'à mesure que l'ordre du contrôleur augmente, la solution au problème convexe converge vers la solution optimale globale du problème $\mathscr{H}_\infty$. Cette méthode est ensuite étendue au contrôleur à temps discret à 2 degrés-de-liberté où les conditions nécessaires et suffisantes sont imposées

pour des fonctions de sensibilité pondérées multiples.
Les concepts qui sous-tendent ces méthodes de conception sont ensuite utilisés pour concevoir les conditions nécessaires et suffisantes pour assurer la stabilité en boucle fermée des systèmes avec des non-linéarités liées au secteur. Les conditions sont de simples contraintes de faisabilité convexes qui peuvent être utilisées pour stabiliser des systèmes avec une incertitude multimodèle. De plus, une méthode est proposée pour obtenir des performances $\mathscr{H}_\infty$ pour les systèmes dont les gains sont incertains dans ces secteurs.
En convexisant le problème $\mathscr{H}_\infty$, on obtient la solution optimale globale à un problème approximatif. Pour les contrôleurs de bas-ordre, la solution à ce problème approximatif peut conduire à des solutions loin de la solution optimale du vrai problème $\mathscr{H}_\infty$. Ainsi, deux méthodes sont proposées pour résoudre ce problème pour les contrôleurs de bas-ordre. Dans une méthode, un problème non convexe est formulé qui optimise les paramètres de fonction de base d'un contrôleur tout en garantissant la stabilité des systèmes en boucle fermée. Dans une autre méthode, un ensemble sur des problèmes convexes est résolu de manière itérative pour obtenir la performance désirée (ce qui garantit également la stabilité en boucle fermée du système). Avec les deux méthodes, la solution locale au problème $\mathscr{H}_\infty$ pour les contrôleurs de structure fixe est obtenue. Cependant, le problème convexe est informatiquement tractable et peut également considérer $\mathscr{H}_2$ performance.
L'efficacité de la méthode proposée est illustrée en considérant plusieurs exemples qui nécessitent des contrôleurs robustes pour atteindre la performance souhaitée. Le principal travail applicatif de cette thèse porte sur un système de contrôle de convertisseur de puissance au CERN (qui est utilisé pour contrôler le courant dans un aimant afin de produire le champ souhaité pour contrôler les trajectoires de particules dans les accélérateurs). Les méthodes de conception proposées sont mises en œuvre afin de satisfaire les spécifications de performance difficiles définies par l'application tout en garantissant la stabilité et la robustesse du système à l'aide de stratégies de conception pilotées par les données.

Mots clefs : Optimisation convexe, contrôle piloté par les données, contrôle à structure fixe, contrôle $\mathscr{H}_\infty$, contrôle $\mathscr{H}_2$, contrôle non-linéaire, contrôle du convertisseur de puissance, contrôle robuste, non-linéarité sectorielle.

Abbreviations

1DOF	1-Degree-Of-Freedom
2DOF	2-Degree-Of-Freedom
ARE	Algebraic Riccati Equations
BLA	Best Linear Approximation
BP	Bilinear Programming
CbT	Correlation-based Tuning
CERN	Conseil Européen pour la Recherche Nucléaire (European Organization for Nuclear Research)
CPU	Central Processing Unit
DF	Describing Function
FGC	Function Generator Controller
FRF	Frequency Response Function
HJI	Hamilton-Jacobi-Isaacs
ICbT	Iterative Correlation based Tuning
IFT	Iterative Feedback Tuning
KYP	Kalman-Yakubovich-Popov
LMI	Linear Matrix Inequality
LP	Linearly Parameterized
LPV	Linear Parameter-Varying
LQG	Linear-Quadratic-Gaussian
LTI	Linear Time-Invariant
MFAC	Model-Free Adaptive Control
MIMO	Multiple-Input-Multiple-Output
MPC	Model Predictive Control
MRAC	Model Reference Adaptive Control
MRC	Model Reference Control
PI	Proportional-Integral
PID	Proportional-Integral-Derivative
PRBS	Pseudorandom Binary Sequence
PSO	Particle Swarm Optimization
RL	Resistive(R)-Inductive(L)
SDP	Semi-Definite Programming
SDPT3	Semi-Definite Programming Toolbox

SDRE	State-Dependent Riccati Equation
SIP	Semi-Infinite Programming
SISO	Single-Input-Single-Output
SPR	Strictly Positive Real
UC	Unfalsified Control
VRFT	Virtual Reference Feedback Tuning

Nomenclature

List of Operators and Conventions

$\mathbf{RH}_\infty$	The set of all stable, proper, real-rational transfer functions with bounded infinity norms.
$\boldsymbol{\rho}^\top$	Transpose of the vector $\boldsymbol{\rho}$.
$\boldsymbol{H} \prec 0$	Strict matrix inequality of a symmetric matrix $\boldsymbol{H}$.
$\Im\{\cdot\}$	Imaginary part of a complex variable.
$\mathbb{C}$	The set of all complex numbers.
$\mathbb{R}$	The set of all real numbers.
$\mathbb{R}^n$	The set of all real vectors of dimension n.
$\mathbb{R}^{m\times n}$	The set of real $m \times n$ matrices.
$\mathbb{R}_+$	The set of all real numbers greater than zero.
$\mathbb{Z}$	The set of non-negative integers.
$\mathscr{F}\{\cdot\}$	Fourier transform of the argument.
$\Phi(u)$	Nonlinear function of an input signal u.
$\Re\{\cdot\}$	Real part of a complex variable.
$\sigma^2_{xy} = \frac{1}{Q-1}\sum_{q=1}^{Q}(x^{[q]}-x)(y^{[q]}-y)^*$	Sample covariance of Q realizations of x and y.
$\sigma^2_x = \frac{1}{Q-1}\sum_{q=1}^{Q}\lvert x^{[q]}-x\rvert^2$	Sample variance of Q realizations of x.
$A(j\omega)$	Frequency response function of $A(s)$.
$A(e^{j\omega})/A(e^{-j\omega})$	Frequency response function of $A(z)/A(z^{-1})$.
$A(s)$	Transfer function of continuous-time system.
$A(z)/A(z^{-1})$	Transfer function of discrete-time system.

A^*	Complex conjugate of the complex number A.
$C(\beta, r_d)$	Disk associated with Circle criterion (centered at β with radius r_d).
$f : A \rightarrow B$	f is a function on the set of the domain of $f \subseteq A$ into the set B.
$\|A\| = \sqrt{[\Re\{A\}]^2 + [\Im\{A\}]^2}$	The magnitude of a complex number A.
$\|\|A\|\|_\infty = \sup_\omega \|A(j\omega)\|$	Infinity norm of the complex function $A(j\omega)$ (the same operation applies for $A(e^{-j\omega})$) .
$\|\|A\|\|_p = \left[\frac{1}{2\pi}\int_{\Omega_c} \|A(j\omega)\|^p d\omega\right]^{p^{-1}}$	p-norm of $A(j\omega)$ for $p \in [1,2,\ldots,\infty[$.

List of Symbols

α	Uncertain gain within a sector-bounded nonlinearity.
α_p	The significance level of a χ^2 distribution.
β	Center of the disk $C(\beta, r_d)$.
β_1, β_2	Slopes of the lines which bound a sector nonlinearity.
$\boldsymbol{\phi}$	Vector of stable orthogonal basis functions.
$\boldsymbol{\rho}$	Vector of decision variables.
$\boldsymbol{\theta}_p$	Vector of parameteric uncertainties.
δ_m	Additive disk uncertainty parameter associated with the coprime M.
δ_n	Additive disk uncertainty parameter associated with the coprime N.
ℓ	Number of models of a multimodel process.
ι	Constriction coefficient of PSO algorithm.
$\mathscr{D}_i$	Frequency spectrum of a process input disturbance.
$\mathscr{D}_o$	Frequency spectrum of a process output disturbance.
$\mathscr{N}_d$	Describing function of a nonlinearity.

$\mathscr{N}_t$	The set of all sector-bounded time-varying nonlinearities.
$\mathscr{R}$	Frequency spectrum of the signal r.
$\mathscr{S}_q$	q^{th} sensitivity function of a closed-loop system.
$\mathscr{S}_q^d$	Desired q^{th} sensitivity function of a closed-loop system.
$\mathscr{S}_q^i$	q^{th} sensitivity function of a closed-loop system with respect to the i^{th} plant model.
$\mathscr{U}$	Frequency spectrum of the signal u.
$\mathscr{U}_n$	Frequency spectrum of u_n.
$\mathscr{V}$	A class of nonlinear systems (i.e., Wiener systems).
$\mathscr{X}$	Frequency spectrum of a signal for identifying the coprime factors of a linear system in a nonlinear closed-loop structure.
$\mathscr{Y}$	Frequency spectrum of the signal y.
$\mathscr{Y}_S$	Spectrum of error term which is used to describe a nonlinear system in $\mathscr{V}$.
Ω	The set of discrete-time frequencies.
ω	Frequency in $\text{rad}\,\text{s}^{-1}$.
Ω_c	The set of continuous-time frequencies.
σ_A^2	Variance associated with the measurements of system A.
$\theta_1, \theta_2, \theta_3$	Cognitive learning rate, social learning rate, and learning rate, respectively (used in the PSO algorithm).
$\tilde{M}$	Set of additive uncertainty associated with coprime M.
$\tilde{N}$	Set of additive uncertainty associated with coprime N.
ϑ	PSO penalty factor.
ξ	Laguerre parameter for continuous-time controller.
ξ_z	Laguerre parameter for discrete-time controller.

ζ_d	Desired damping factor associated with a second order transfer function.
ζ_i	Poles of a generalized orthonormal basis function.
f_d	Desired closed-loop bandwidth.
G	General representation of a linear plant model.
G_i	i^{th} model of a multimodel process.
$G_{\mathscr{V}}$	A plant model which belongs to the class of systems in $\mathscr{V}$.
K	Controller for 1-degree-of-freedom structure.
L	General representation of an open-loop system.
M	Coprime factor of a plant model G.
m_p	m_p sided polygon to approximate the ellipse from a model's parameteric uncertainty.
N	Coprime factor of a plant model G.
n_r, n_s, n_t	Order of the polynomials R, S, and T, respectively.
p_x	Number of particles in PSO algorithm.
R	Polynomial of discrete-time controller.
r	Reference input of a closed-loop system.
r_d	Radius of the disk $C(\beta, r_d)$.
S	Polynomial of discrete-time controller.
s	Laplace transform variable.
T	Polynomial of discrete-time 2DOF RST controller.
T_s	Sampling time of a discrete-time system.
u	Input signal of a plant/process.
u_n	Output signal of a sector-bounded nonlinearity.
W_q	Weighting filter associated with the q^{th} sensitivity function $\mathscr{S}_q$.
X	Coprime factor of controller K.

Y	Coprime factor of controller K.
y	Output signal of a plant/process.
z	Z-transform variable.

Contents

Acknowledgements **i**

Abstract (English/Français) **iii**

Abbreviations **vii**

Nomenclature **ix**

List of figures **xix**

List of tables **xxiii**

1 Introduction **1**
1.1 Motivation . . . 1
1.1.1 Brief History on Automatic Control . . . 1
1.1.2 The Data-Driven Paradigm . . . 2
1.2 State of the Art . . . 3
1.2.1 Data-driven Control . . . 3
1.2.2 Fixed-Structure Controller Design . . . 5
1.2.3 Nonlinear Control . . . 7
1.3 Research Objectives . . . 9
1.3.1 Global Solution of $\mathscr{H}_\infty$ problem . . . 9
1.3.2 Fixed-Structure Controller Design . . . 10
1.3.3 Contributions . . . 11
1.4 Dissertation Structure . . . 12

2 Preliminaries **15**
2.1 Class of models . . . 15
2.1.1 General Plant Representation . . . 15
2.1.2 Coprime Representation . . . 18
2.1.3 Nonlinear Models . . . 20
2.2 Class of controllers . . . 26
2.2.1 Polynomial 1DOF Controller . . . 26
2.2.2 *RST* 2DOF Controller . . . 27
2.2.3 Coprime 1DOF Controller . . . 27

2.3 Control Performance . . . 28
2.3.1 Sensitivity Functions for 1DOF Structure . . . 29
2.3.2 Sensitivity Functions for RST Structure . . . 29
2.4 Optimization Problems . . . 30
2.5 Conclusion . . . 32

3 Robust $\mathscr{H}_\infty$ Controller Design 33
3.1 Introduction . . . 33
3.2 Convex parameterization of robust controllers . . . 33
3.2.1 Controller objective . . . 33
3.2.2 Nominal and robust performance . . . 36
3.2.3 Multi-model and frequency-domain polytopic uncertainty . . . 38
3.3 Fixed-order controller design . . . 41
3.3.1 Controller parameterization . . . 41
3.3.2 Convergence to the optimal solution . . . 42
3.3.3 Finite number of constraints . . . 43
3.3.4 Solution by linear programming . . . 44
3.4 Case Studies . . . 44
3.4.1 Case 1: Multi-model uncertainty . . . 44
3.4.2 Case 2: Convergence to optimal performance . . . 46
3.4.3 Case 3: Flexible Transmission System . . . 47
3.5 Conclusion . . . 48

4 Robust RST Controller Design with Applications to Power Converters 51
4.1 Introduction . . . 51
4.2 $\mathscr{H}_\infty$ Performance via Convex Optimization . . . 52
4.2.1 General Design Specifications . . . 52
4.2.2 Robust Design . . . 56
4.2.3 Controller Stability . . . 57
4.2.4 Tracking Specifications . . . 58
4.2.5 Convex Optimization via Semi-Definite Programming . . . 59
4.3 Simulation Examples . . . 60
4.3.1 Case 1: Multi-model uncertainty . . . 60
4.3.2 Case 2: Nonlinear Distortions . . . 61
4.4 Case Study: Power Converter Control . . . 67
4.4.1 Power Converters for Particle Accelerators . . . 67
4.4.2 Experimental Test Setup . . . 68
4.4.3 Control Objective . . . 69
4.4.4 Weighting filter selection . . . 70
4.4.5 Synthesis and Experimental Results . . . 71
4.5 Case Study: Torsional Control . . . 73
4.5.1 Weighting filter selection . . . 75
4.5.2 Experimental results . . . 76

4.6 Conclusion . . . 77

5 Robust Control of Systems With Sector Nonlinearities 79
5.1 Introduction . . . 79
5.2 The Circle Criterion Revisited . . . 80
5.3 Stabilization via the Circle Criterion . . . 82
5.3.1 Case 1: $0 < \beta_1 < \beta_2$ . . . 82
5.3.2 Case 2: $\beta_1 < 0 < \beta_2$ . . . 85
5.3.3 Case 3: $0 = \beta_1 < \beta_2$ . . . 87
5.4 A Multi-Model Approach for Ensuring $\mathscr{H}_\infty$ Performance . . . 87
5.4.1 Convex Optimization via Semi-Definite Programming . . . 89
5.5 Case Study . . . 90
5.5.1 Stabilization via the Circle Criterion . . . 92
5.5.2 Stabilization with Performance . . . 93
5.6 Conclusion . . . 96

6 $\mathscr{H}_\infty$ Design for Low-Order Fixed-Structure Controllers 99
6.1 Introduction . . . 99
6.1.1 Robust Performance via Convex Optimization . . . 100
6.2 Optimization Problems For Fixed-Struture Design . . . 101
6.2.1 Bilinear Programming . . . 102
6.2.2 Particle Swarm Optimization . . . 103
6.3 Simulation Examples . . . 105
6.3.1 Case 1: Robust PID Design . . . 106
6.3.2 Case 2: Multi-model Uncertainty . . . 108
6.4 Conclusion . . . 112

7 Model-Reference Control for Particle Accelerator Power Converters 113
7.1 Introduction . . . 113
7.2 Control Performance . . . 114
7.2.1 Convex Approximation . . . 114
7.2.2 $\mathscr{H}_\infty$ Performance . . . 116
7.2.3 $\mathscr{H}_2$ Performance . . . 116
7.2.4 $\mathscr{H}_1$ Performance . . . 117
7.3 Stability Analysis . . . 119
7.3.1 Initial Stabilizing Controller . . . 121
7.4 Simulation Examples . . . 122
7.4.1 Case 1: Heat Conductor . . . 123
7.4.2 Case 2: Unstable robot prototype . . . 125
7.5 Case Study: Power Converter Control . . . 127
7.5.1 Controller Design . . . 127
7.6 Conclusion . . . 133

8 Conclusion and Future Outlook **135**
8.1 Conclusion 135
8.1.1 Future Outlook 137

A H_∞ Smith Predictor Design for Time-Delayed MIMO Systems via Convex Optimization **139**
A.1 Introduction 139
A.2 Problem Formulation 140
A.2.1 Class of models 140
A.2.2 Class of controllers 141
A.2.3 Design specifications 141
A.3 Proposed method 142
A.3.1 Primary controller design 144
A.4 Industrial Case Studies 145
A.4.1 Case 1 - SP with fixed time delays 145
A.4.2 Case 2 - SP with uncertain time delays 146
A.4.3 Case 3 - The Shell control problem 148
A.5 Conclusion 152

Bibliography **153**

Curriculum Vitae **165**

List of Figures

2.1 Nonlinear sector that is bounded by two lines with slopes β_1 and β_2. 21
2.2 Representation of a nonlinear system by a linear system for a certain class of inputs. 22
2.3 Procedure for measuring the BLA from the FRF of the nonlinear system. $G^{[q,p]}$ is the FRF estimate of the p^{th} period of the q^{th} experiment. 23
2.4 Structure to be used in obtaining the coprimes for an unstable process. 26
2.5 RST controller structure. 27

3.1 Graphical representation of the constraint in 3.1. 34
3.2 Illustration of the constraints for polytopic uncertainty with 3 vertices. 40
3.3 Step responses for the family of closed-loop systems. 46
3.4 $\gamma_n^\star$ versus the controller order with different Laguerre parameters. 47
3.5 Flexible transmission system 48
3.6 Experimental identification data. 49
3.7 Nyquist diagram of the spectral model together with uncertainty disks. 49
3.8 Magnitude of the FRF of sensitivity function $\mathscr{S}_s$. 50

4.1 The graphical interpretation of $\mathscr{H}_\infty$ constraints in the complex plane. 53
4.2 Optimal solution $\gamma^\star$ as a function of the controller order. Solutions obtained with the proposed method (dashed-blue line); solutions obtained with the method which requires the selection of a desired open-loop transfer function (dashed-red line). 62
4.3 Random phase multi-sine input $r(t)$ along with the plant input $u(t)$ and output $y(t)$. For presentation purposes, the signals are shown for 2 full periods. 63
4.4 N (dashed-blue line) with the associated uncertainties at each frequency (black circles). The FRF obtained between r to y for a given experiment with no uncertainties (dashed-red line). 64
4.5 M (dashed-blue line) with the associated uncertainties at each frequency (black circles). The FRF obtained between r to u for a given experiment with no uncertainties (dashed-red line). 64
4.6 Variances of coprimes caused by nonlinear distortions 65

4.7 Step response of the nonlinear system. The desired closed-loop response (black line); the response with the proposed method (including uncertainties in design) (blue line); the response with no uncertainties considered (red line). 66
4.8 Power converter control system. 67
4.9 Fractional dynamics of magnet caused by Eddy currents. 68
4.10 The CANCUN used for the control application. 69
4.11 The desired reference current profile. The blue-dashed line indicates the time when the error must remain within ±1000 parts-per-million (ppm); the red-dashed line indicates the time when the error must remain within ±100 ppm. . 70
4.12 PRBS signal used for the input voltage $v(t)$ of the open-loop system along with the resulting output current $i(t)$. 71
4.13 Comparison between the error resulting from the model-based design (solid-black line with red error-bars) and the error resulting with the proposed method (solid-black line with green error-bars). 72
4.14 Torsional apparatus (ECP model 205a) used for the experimental analysis. The three disks are comprised of block masses which can be added or removed to alter the inertia of each disk (and thus alter the dynamics of the system). Each disk is vertically suspended on a spring with a variable spring constant. The actuator is located on the bottom of the device. 73
4.15 Time-domain response of the closed-loop system with a PRBS excitation signal (shown only for the system configuration with two block masses on the top disk): the PRBS reference input $r(t)$ with a register length of 511 (solid-blue); control output $u(t)$ (solid-red); output response $y(t)$ (solid-black). 74
4.16 FRF's of the plant model obtained from the closed-loop time-domain response of each system configuration. The loads on the bottom and middle disk are fixed while the load on the top disk is varied: FRF with one block mass on the top disk (solid-blue); FRF with two block masses on the top disk (solid-green); FRF with four block masses on the top disk (solid-red). 75
4.17 Step response for each load configuration: response with one block mass on the top disk (solid-blue); response with two block masses on the top disk (solid-green); response with four block masses on the top disk (solid-red). 77
4.18 Closed-loop frequency response functions of all three system configurations: closed-loop FRF with one block mass on the top disk (solid-blue); closed-loop FRF with two block masses on the top disk (solid-green); closed-loop FRF with four block masses on the top disk (solid-red). 78

5.1 Discrete-time controller structure. 79
5.2 Equivalent block diagram in autonomous form. 80
5.3 Absolute stability condition for the sector nonlinearity in (2.14) when different conditions for β_1 and β_2 are considered. 81
5.4 A graphical interpretation of the constraint (5.5) in the complex plane. 83

5.5 Time-varying sector nonlinearity used for the case study. The nonlinearity switches at every positive integer multiple of T_n between the dashed-red line and the solid-red line. 91
5.6 Nyquist plot of $L_i(e^{-j\omega})$ for $i = 1,\ldots,4$ (solid-blue line); disk $C(-2.76, 2.26)$ (solid-red line). The Nyquist criterion for the sector-bounded nonlinearity is satisfied for all models. 93
5.7 The PRBS signal injected as the reference signal $r(t)$ with the measured responses for $u_n(t)$, $x(t)$ and $y(t)$. For illustrative purposes, the figure displays only a small portion of the total signal for the plant G_1. 94
5.8 Calculated FRFs for N_1 (solid-blue line), N_2 (solid-red line), N_3 (solid-orange line), N_4 (solid-purple line). 94
5.9 Calculated FRFs for M_1 (solid-blue line), M_2 (solid-red line), M_3 (solid-orange line), M_4 (solid-purple line). 95
5.10 Closed-loop step responses for all models G_i. The reference signal is shown with the dashed-black line. 96
5.11 Nyquist plot of L_1 with the stability constraint (blue-line) and without the stability constraint (red-line). 97

6.1 Optimal solution to the convex problem for varying ξ. 107
6.2 Optimal solution to (6.21) using the proposed bilinear and PSO algorithms. The optimal solution produced by `hinfstruct` (solid-red line). 108
6.3 Step response of $\mathscr{S}_s(s)$ for all seven models using the controller designed with `hinfstruct` (with 200 random initializations). 111
6.4 Step response of $\mathscr{S}_s(s)$ for all seven models using the proposed PSO algorithm. 111

7.1 Closed-loop FRFs for each G_i obtained by solving the $\mathscr{H}_2$ problem (dashed-blue) and solving the $\mathscr{H}_\infty$ problem (dashed-red). The desired closed-loop FRF is shown with the solid-black line. 124
7.2 Closed-loop step response for the nominal plant model with $\mathscr{H}_1$ performance (blue-line), $\mathscr{H}_2$ performance (green-line), and $\mathscr{H}_\infty$ performance (red-line). The dashed-black line is the desired response. 127
7.3 The desired reference current i_R. The error between the blue-dashed line and the red-dashed line must remain within ± 1000 ppm; the error after the red-dashed line must remain within ± 100 ppm. 128
7.4 PRBS signal used for the input voltage $v(t)$ of the open-loop system along with the resulting output current $i(t)$. 130
7.5 Errors obtained using the proposed designs (blue, green and orange lines); error obtained using the `SYSTUNE` controller (red line). 132
7.6 $|\mathscr{S}_2|$ for all of the design methods discussed in this work. 132
7.7 $G(e^{-j\omega})$ (dashed-blue line) with the frequency-dependent uncertainty disks (blue circles) and $G_m(e^{-j\omega})$ (solid-red line). 133

A.1 MIMO representation of the Smith Predictor 142

A.2 Closed loop comparison between time delayed MIMO system with unity feedback and time delayed MIMO SP: unit step reference signal (black, dash), response from system with no SP structure (red, solid), response with SP and with diag$(\mathbf{L}_D(s)) = \frac{1}{30s}$ (blue, solid), response with SP and with diag$(\mathbf{L}_D(s)) = \frac{1}{5s}$ (green, solid). 147
A.3 MIMO response to a unit step input: reference signal (black,dash), the remaining $\Omega = 16$ closed-loop responses are for all possible combinations of the time delay parameters in (A.22). 148
A.4 Gershgorin bands centered at L_{qq} with the largest time delay combination in (A.22): performance filter with $|W_{1_q}| = 0.5$ (green circle), Gershgorin bands corresponding to $q = 1$ (blue circles), Gershgorin bands corresponding to $q = 2$ (red circles). Note that $Z(j\omega)$ is simply the complex number representation of each circle in the plot. 149
A.5 MIMO SP closed-loop response to a unit step input with $\tau_{qp} = \zeta_{qp}\ \forall\ \{p,q\}$: reference signal (black,dash), output response with the proposed optimization method (blue, solid), output response with the “squared down" method. 151
A.6 MIMO SP closed-loop response to a unit step input with $\tau_{qp} = 1.2\zeta_{qp}\ \forall\ \{p,q\}$: reference signal (black,dash), output response with the proposed optimization method (blue, solid), output response with the “squared down" method. 151
A.7 MIMO SP controller output response to a unit step reference: Controller output response of proposed method with $\tau_{qp} = \zeta_{qp}$ (blue, solid), controller output response of “squared down" method with $\tau_{qp} = \zeta_{qp}$ (red, solid), controller output response of proposed method with $\tau_{qp} = 1.2\zeta_{qp}$ (blue, dash), controller output response of “squared down" method with $\tau_{qp} = 1.2\zeta_{qp}$ (red, dash) 152

List of Tables

3.1 Procedure for optimizing low-order controllers. 41

4.1 Procedure for computing an RST controller 60
4.2 Parameters resulting from the bisection algorithm. 66

5.1 Procedure for computing a controller with $\mathscr{H}_\infty$ performance (with respect to the fundamental frequency of a sector-bounded nonlinearity) 90

6.1 Procedure for executing the PSO algorithm 105
6.2 Comparison of optimal solutions from convex and non-convex problems (with optimization time) 108
6.3 Comparison between optimal solutions and optimization time for multi-model problem 110

7.1 Procedure for obtaining local optimal solution with convex formulation 118
7.2 Optimization results for $\mathscr{H}_2$ and $\mathscr{H}_\infty$ problems 124
7.3 Performance for different optimization criteria 126
7.4 Performance values for all methods 132

1 Introduction

1.1 Motivation

1.1.1 Brief History on Automatic Control

The initial use and implementation of feedback control is claimed to have originated from the Hellenic worlds; the earliest known construction of a feedback control mechanism was an ancient water clock invented by a Greek mechanician named Ktesibios in the third century B.C. [1]. The invention of devices for automatic control of temperature (i.e., the thermostat) and windmills were established in the 17^{th} and 18^{th} century. The flyball governor (initially conceptualized by James Watt in 1788) was a feedback system that implemented the principle of proportional control to regulate steam engines; an analysis of this type of system was performed by James Clerk Maxwell [2]. This system led to an uprising in the art of modern control theory which sprouted the industrial revolution. The increased use of engines in the modern era led to further investigation of feedback control by Bode [3] (who introduced the notions of gain and phase margins) and Nyquist [4] who published his celebrated frequency-domain encirclement criterion. Poincaré and Lyapunov also published important works in modern and state space approaches.

As time progressed, the emergence of other sophisticated control algorithms of feedback systems have been devised in response to the technological advances of industrial settings. The introduction of digital technologies in the late 1950s brought enormous changes to automatic control. Digital computers made it possible to implement more advanced control algorithms that were being developed in the 1970s [5]. Control methods such as adaptive control have a long history; however, it was the digital computer which offered the advantage of identifying the system parameters, making decisions about the required modifications to the control algorithm, and implementing the changes in a timely manner. Optimal and robust control techniques (such as model-predictive-control (MPC), linear-quadratic-Gaussian (LQG) and $\mathscr{H}_\infty$ approaches) could not be realized for practical applications without the help of digital computers [6]. However, at that time, computers were not sophisticated enough to solve such problems in a reasonable manner and solutions for these problems were attempted

to be derived analytically (which was a very difficult task). However, as time progressed, technological advances were made in the computing world which allowed computers to solve these problems very efficiently. As our increasingly advanced technologies enable us to build larger, more capable, more complex systems, the role of design becomes ever more important. Due to the complexity of many of today's industrial processes (transportation systems, aerospace systems, communication systems, etc.,), the modeling of these systems by using first principles may be impossible. Even though a physical model is available, these models tend to be too complex for analysis and controller implementation. Data-driven control schemes seek to alleviate this problem by synthesizing controllers without the need of a physical model.

1.1.2 The Data-Driven Paradigm

In industrial schemes, the dynamics of plants are typically approximated by low-order models, since the controller synthesis is easier to implement for lower order processes. However, this approximation can impede the performance of a controller, since low-order models are subject to model uncertainty. In a data-driven design setting, a controller is designed by directly using online or offline input/output data (instead of designing a controller based on first modeling of a given plant). Data-driven methods aim to design controllers through direct usage of the process data while eliminating the challenging and tedious issues associated with the modeling process. In this manner, stability and performance can still be guaranteed under certain reasonable assumptions. A survey on the differences associated with model-based control and data-driven control has been addressed in [7] and [8]; the authors assert that model-based control methods are inherently less robust due to the unmodeled dynamics of a process, and that these controllers may possibly be unsafe for practical applications. With the data-driven control scheme, the parametric uncertainties and the unmodeled dynamics (for linear time-invariant systems) are irrelevant and the only source of uncertainty comes from the measurement process.

Given the available resources of a digital computer, access to huge amounts of measured process data can easily be collected due to the well-developed information technology (i.e., collected information from stored historical data or online data in real-time during process runs). The information can be collected and interpreted in the time-domain or frequency-domain. The frequency-domain approach offers many advantages compared to time-domain methods:

- Without knowledge of the transfer function, the dynamics of a system can be captured experimentally through the frequency response.
- Relative and absolute stability of a closed-loop system can be determined with the knowledge of the open-loop frequency response.
- Noise disturbance generated in the system can be easily determined using frequency

analysis.

- Frequency-domain analysis can also be carried out for nonlinear systems (including systems with strong nonlinearities such as chaos and bifurcation [9]).

In addition to avoiding the problem of unmodeled dynamics, the use of controllers with pre-defined structures is also important. In the classical robust control design method, the order of the resulting full-order controllers can be quite large; in fact, the order can be as large as the order of the augmented plant [10]. This can be problematic since it is known that computers possess cost-limited hardware and are limited in computing resources. However, the increased dependency on computers for control systems has fostered a need for control designs in a digital framework. Thus the notion of fixed-structure controller synthesis becomes an important subject in today's controller design scheme. In fact, the proportional-integral and proportional-integral-derivative (PI/PID) controllers are still the most widely used controller structures in today's industry due to their ease of implementation. It is known that more than 90% of all control loops are PID [11].

Fixed-structure robust controller design schemes for linear systems (in a data-driven setting) have been the focus of ongoing research. To a certain degree, the effects of nonlinearities could be ignored because they did not impair system performance. However, due to the increased performance demands on today's industrial systems, the effects of certain nonlinearities can impact the behavior of these systems. For many of today's systems, the effects of nonlinearities can no longer be neglected (see [12] and [13]). Due to the extensive use of frequency-domain techniques for linear systems within the control systems community, and given the need for analyzing the effects of nonlinear systems, it is thus natural to extend the frequency-domain analysis and control schemes for linear systems where nonlinear distortions can occur. A comparative study of frequency-domain methods for nonlinear systems has recently been addressed in [14].

1.2 State of the Art

In this section, a review of the current literature on data-driven control schemes that include fixed-structure $\mathscr{H}_2$ and $\mathscr{H}_\infty$ design methods for linear systems is presented, as this is one of the major research topics covered in this dissertation. Additionally, a review of nonlinear controller design methods (using frequency-domain data) is also presented.

1.2.1 Data-driven Control

Data-driven controller design is a very attractive research field within the control community (see [8, 7, 15]). In this method, a controller is designed by using either the time-domain or frequency-domain data of a system rather than using a parametric model of the plant (where the intermediate identification procedure or first principle modeling is not required).

A comparative analysis shows that although model-based approaches are statistically more efficient in terms of the variance of the controller parameters, a data-driven approach can outperform the model-based approach in terms of the final control cost [16]. Data-driven controllers can be synthesized either on-line or off-line.

On-line Methods

On-line methods refer to design schemes where the parameters of a controller are adjusted in real-time while the system is running in closed-loop operation. The classical model-reference adaptive control (MRAC) [17] may be considered as the first data-driven attempt to solve the model-reference problem in an on-line manner. This method attempts to minimize the tracking error and adjust the controller parameters from an on-line identification of the process model.

Model-free adaptive control (MFAC) [18] is a more recent data-driven approach that implements a dynamic linearization of the process whose controller design and stability analysis merely depend on the measured input and output data of the controlled plants. This method can be used to design discrete-time controllers for nonlinear systems and multiple-input-multiple-output (MIMO) processes [19, 20]. More recent extensions and applications which implement this method can be found in [21, 22, 23, 24].

Unfalsified control (UC) [25] is yet another on-line control strategy which uses a fictitious reference signal to control a closed-loop system. The unfalsified control theory views the control problem as an identification problem where a control law is identified based on control performance goals, problem constraints, and evolving observational data. With this method, a controller is discarded when the fictitious signals do not satisfy the desired specifications. A non-iterative approach for controller design using unfalsified control is presented in [26]; however, this method is limited to stable systems. [27] extends on the concepts of unfalsified control by using Riccati-based parameterization of $\mathscr{H}_\infty$ controllers. Note that an off-line non-iterative method for UC has recently been proposed in [28].

Off-line Methods

Off-line design schemes can synthesize controllers before they are applied to a system. Thus when there is no need for adaptation (and the process is time-invariant), these methods are favorable due to their ease of implementation. However, these methods rely on finite amount of data that is generated from a given identification experiment. The widely used PID controller is usually tuned based on a set of time-domain or frequency-domain data. The first examples of automated tuning using PID controllers were based on empirical methods proposed by Ziegler and Nichols [29].

Iterative feedback tuning (IFT) [30, 31] is an offline control methodology that uses an iterative technique to solve a non-convex problem to obtain the controller parameters; this method can

consider fixed-structure controllers. The main goal is to obtain unbiased gradient estimates and optimize for time-domain performance. The gradient of a criterion (with respect to the controller parameters) is computed such that a desired specification is satisfied (which is usually accomplished by minimizing a desired performance criterion). A typical performance criterion is to minimize the error between the reference signal and the actual output. The controller parameters are updated based on data obtained from multiple experiments. However, stability is not guaranteed with this method. Some works which devised robust stability conditions for the IFT method are asserted in [32, 33], and recent applications of robust IFT controller design methods have been addressed in [34, 35].

The virtual reference feedback tuning (VRFT) [36] is an offline one-shot method which minimizes the (filtered) $\mathscr{H}_2$ norm of the difference between a desired reference model and the achieved closed-loop system. In this method, a controller is computed based on the measured plant input when fed by a "virtual" error. This signal is computed assuming that the experiment was "virtually" performed in closed-loop with the controller achieving the desired specifications based on a given reference model. This idea was first proposed in [37], where it was denoted as Virtual Reference Direct Design. The authors in [38] give an overview of data-driven methods for the general $\mathscr{H}_2$ control problem. Recent developments and extensions using the VRFT technique for SISO systems ([39],[40]) and MIMO systems ([41],[42],[43]) have also been studied.

Iterative Correlation based Tuning (ICbT) [44] is another off-line approach where the objective is to adjust and fine tune the controller parameters by decorrelating the closed-loop output error and the reference signal. It implements the concepts of system identification where the predictor of the plant output is adjusted to make the prediction error uncorrelated with the plant input. An extension of this method to MIMO systems has been presented in [45]. However, in [46], a correlation-based tuning (CbT) approach is presented (which is a non-iterative version of ICbT) where the stability issue and the influence of measurement noise in the model-reference problem are studied.

A comparative study of different data-driven model-reference methods for non-minimum phase plants has been recently given in [47]. Note that VRFT, IFT, CbT, and the unfalsified control strategies are model-reference based schemes; these types of problems require special care since minimization of a desired reference model can lead to poor stability and robustness margins.

1.2.2 Fixed-Structure Controller Design

Controller synthesis methods belonging to the $\mathscr{H}_\infty$ control framework minimizes the $\mathscr{H}_\infty$ norm of a weighted closed-loop sensitivity function. In the general $\mathscr{H}_\infty$ synthesis problems, controllers are computed using semidefinite programing (SDP) algorithms [48] or algebraic Riccati equations [49]. The solutions of these $\mathscr{H}_\infty$ control problems refer to the full-order case (which are convex). The controllers that result from these algorithms, however, are

typically of very high order, which complicates implementation. As discussed above, due to the ease of implementation of low-order controllers (such as the PID) and the limited computational resources of today's embedded systems, the control engineer is confined to design fixed-structure controllers. It is well known that fixed-structure controller design in the model-based setting is a non-convex optimization problem. In fact, some of the problems in [49] for fixed-structure controllers are regarded as NP-hard [50], which makes the $\mathscr{H}_\infty$ problem (with fixed-structure controllers) an inherently difficult problem to solve. Non-smooth optimization methods for fixed-structure controllers are used in [51], [52] and [53]; these methods are implemented in the `MATLAB` Robust Control Toolbox (which is called with the `hinfstruct` command). In parallel, a code package for fixed-order optimization called `HIFOO` was being developed that considered the same non-smooth problem formulation as [51], but can consider $\mathscr{H}_2$ synthesis as well. However, these non-smooth techniques cannot synthesize controllers based on the frequency response of the system (they need a parametric model), and are limited to certain system dynamics (i.e., a pure delay must be approximated by a Padé function).

Design Using Frequency-Domain Data

Frequency-domain based controller synthesis methods are design schemes that continue to spark the interest of many researchers. Controller design methods which synthesize controllers by only using the frequency-domain data of a process can be categorized as a data-driven control scheme (since no parametric model is used for the actual synthesis). Therefore, given the fact that the modeling process for today's systems is inherently problematic, it is natural to implement and develop a data-driven design methodology to design robust controllers.

A robust frequency-domain controller design method has been established in [54]. In this method, upper and lower bounds are set on the desired closed-loop specifications where rational controllers are computed; however, this method requires a solution to a nonlinear optimization problem. Additionally, closed-loop stability is not guaranteed *a-priori*. Another frequency-domain loop-shaping approach to design fixed-structure controllers is presented in [55]. In this method, a convex optimization problem can be formulated if a linearly parameterized (LP) controller is considered; however, as in [54], the closed-loop stability is not guaranteed and should be verified *a-posteriori*. A more recent loop-shaping method has been proposed in [56] where the authors address the $\mathscr{H}_\infty$ problem for stable SISO and MIMO systems. The authors impose multiple line constraints in the Nyquist diagram to achieve both the closed-loop stability and performance. Feasibility constraints are proposed which are multilinear when LP controllers are used; for special controller cases, the feasibility constraints become convex.

In [57], a frequency-domain approach is realized where a convex optimization algorithm is formulated by considering a convex approximation of the $\mathscr{H}_\infty$ criterion. The constraints are convexified around a desired open-loop transfer function where a non-iterative algorithm is proposed to optimize a set of LP controllers that guarantee the closed-loop stability. This

method is extended to data-driven gain-scheduled controller design in [58] and multivariable decoupling controller design in [59]. A toolbox that implements the methods used in these works has been devised in [60].

In [61, 62], a frequency-response method is proposed based on the Q-parametrization to guarantee the $\mathscr{H}_\infty$ performance for fixed-structure controllers. This method linearizes the non-convex $\mathscr{H}_\infty$ constraint using a first-order Taylor expansion around an operating point; in this manner, the local solution to the fixed-structure $\mathscr{H}_\infty$ problem is obtained. An initial stabilizing controller is needed in order to guarantee the closed-loop stability. Another frequency-domain approach for computing LP controllers is presented in [63] where the $\mathscr{H}_\infty$ constraints are convexified around an initial stabilizing controller; an iterative algorithm is used that converges to a local optimal solution of the non-convex problem. In [64], the authors also linearize a non-convex constraint around an initial stabilizing controller and implement an iterative method for obtaining a local solution; however, in this work, the objective was to minimize the integrated error under $\mathscr{H}_\infty$ robustness constraints. The convex-concave approximation of the $\mathscr{H}_\infty$ constraint in [64] leads to the same constraint as in [57] for PID controllers. The extension of this method to design multivariable PID controllers for stable systems is presented in [65] (where the linearization is performed with respect to a quadratic matrix inequality). More recent works that implement an iterative method that ensures $\mathscr{H}_\infty$ performance have been devised in [66]. The non-convex $\mathscr{H}_\infty$ constraints here are also linearized around an initial stabilizing controller, but the method is not limited to LP controllers and stable systems and can consider $\mathscr{H}_2$ performance as well.

1.2.3 Nonlinear Control

In principle, all real-world systems are nonlinear and it would seem appropriate to consider nonlinear control theory for real applications. In general, it is very difficult to generalize a controller design method to apply to all nonlinear systems; thus various theories have been developed by considering specific classes of nonlinear systems. The limit cycle theory, Poincaré maps, Lyapunov stability theory, and describing functions are some methods that are used for stabilizing and controlling systems that include specific classes of nonlinearities. The theory of nonlinear control is very broad; in this dissertation, the focus is placed on nonlinear control using the $\mathscr{H}_\infty$ criterion and in a data-driven setting (as this is the framework of this dissertation).

$\mathscr{H}_\infty$ Control of Nonlinear Systems

There are many works that have addressed the $\mathscr{H}_\infty$ problem in the linear framework; however, only several works have been established for $\mathscr{H}_\infty$ control of nonlinear systems. In [67], a solution of the problem of disturbance attenuation with internal stability via measurement feedback is presented. The authors in [68] derived the necessary conditions for the existence of an output feedback controller such that the Hamilton-Jacobi-Isaacs (HJI) equations related

to the closed-loop system have a positive smooth solution; they confirmed the separation principle for the nonlinear $\mathscr{H}_\infty$ control problem (although stability was not guaranteed). The HJI equations are a set of nonlinear partial differential equations which in general cannot be solved analytically [69]. The solution to these equations give necessary and sufficient optimal control conditions for systems modeled by nonlinear dynamics. When the system is LTI, the HJI equations reduce to the familiar algebraic Riccati equations (AREs). The work in [70] implements a Galerkin approximation to obtain the solution of the HJI equations for $\mathscr{H}_\infty$ control. In [71], state-dependent Riccati equation (SDRE) techniques are used in an iterative fashion (i.e., by solving a set of convex optimization problems) to approximate the solution of the HJI equations and obtain $\mathscr{H}_2$ or $\mathscr{H}_\infty$ performance. SDREs, however, are computationally expensive where convergence to a solution may take significant time. The recent work in [72], however, proposed an update algorithm *in a data-driven setting* to learn the solution of HJI equations iteratively and provide a convergence proof.

Data-Driven Control of Nonlinear Systems

Data-driven methods for controlling systems with nonlinearities is a field which continues to grow and evolve. The describing function (DF) method was first conceptualized by the authors in [73] and is one of the few widely applicable methods for analyzing a certain class of nonlinear systems. This method uses the frequency response method for analyzing linear systems that are subject to time-invariant odd nonlinearities. DFs approximate the dynamics of a nonlinearity by only considering the fundamental component of the nonlinear response; the justification for considering only the fundamental component is made by the fact that for real physical systems, the linear subsystem of the overall nonlinear system is a low-pass filter which attenuates the higher frequency components of the nonlinearity. In this manner, an approximate model can be formed for the nonlinearity. Some recent works and applications using the DFs are proposed in [74, 75, 76]. The DF method, however, can fail badly for systems which emphasize higher harmonics of the nonlinearity. Some examples of this have been presented in [77] for bang-bang systems.

More recent data-driven methodologies for controlling nonlinear systems have also been studied in the literature. The authors in [19] present a model-free approach to design controllers that guarantee stability for a class of nonlinear discrete-time systems; in [20], this method is extended to the MIMO nonlinear system. A VRFT method is proposed in [78] to design controllers for nonlinear plant models using a direct “one-shot" method. The authors in [79] build on the iterative learning control data-driven algorithm to design controllers for a class of nonlinear autoregressive exogenous models. A method for designing controllers in a data-driven setting for constrained linear systems is presented in [80]. A specific 2-degree-of-freedom (2DOF) controller structure is used in [81, 82] where a nonlinear controller is used in parallel with a linear controller to control nonlinear systems by using the VRFT design approach. The work in [83] extends on the concept of the VRFT method and implements a data-driven scheme to design linear parameter-varying (LPV) model-reference controllers.

Frequency-domain methods for stabilizing systems with nonlinearities has also been investigated in literature. One of the most remarkable theories in systems and control theory is the Kalman – Yakubovich – Popov (KYP) lemma [84, 85], which established the equivalence between frequency-domain conditions (e.g., Circle and Popov criteria) and time-domain conditions for absolute stability of Lur'e systems. The Circle and Popov criterion have proposed frequency-domain methods that stabilize systems with sector-bounded nonlinearities. There are many variations of these theories that have been recently proposed in literature to control nonlinear systems [86, 87, 88, 89, 90, 91, 92].

1.3 Research Objectives

1.3.1 Global Solution of $\mathscr{H}_\infty$ problem

The first objective of this dissertation is to implement a data-driven method (using frequency-domain data) and develop a convex optimization problem such that the global optimal solution to the $\mathscr{H}_\infty$ problem is obtained. Formulating convex problems are desired since (1) they are computationally tractable, and (2), a convex objective function ensures that all local optima are global optima [93]. Many works have been published for optimizing LP controllers using frequency domain-data and convex optimization algorithms. In these works, LP controllers were specifically chosen since this convexifies the $\mathscr{H}_\infty$ problem.

In this dissertation, it is desired to develop a necessary and sufficient (convex) condition for attaining $\mathscr{H}_\infty$ performance while guaranteeing the closed-loop stability of a system (using controllers that are not LP where a controller's numerator and denominator are simultaneously optimized). By convexifying the $\mathscr{H}_\infty$ problem, the global solution to an approximate problem is obtained; given the necessity and sufficiency of the convex problem, the solution to the convex problem will converge to the global optimal solution of the true $\mathscr{H}_\infty$ problem as the controller order is increased.

The outcome of the objective asserted in the previous paragraph is based on systems with 1-degree-of-freedom controller structures in a continuous-time framework. Since the proposed method in this dissertation implements a data-driven frequency-domain approach for controller synthesis, it is natural to extend the above controller design methodology for

- systems using a 2-degree-of-freedom controller in a discrete-time framework
- systems which are corrupted by nonlinear distortions
- systems which require constraints on multiple sensitivity functions

It will be desired to implement the proposed data-driven methodology to a particle accelerator power converter control system at CERN. In this system, the controller structure is fixed with a 2-degree-of-freedom discrete-time RST controller; this type of controller is implemented

due to the fact that these systems require both very precise tracking capabilities and sufficient robustness margins.

The next objective is to further extend the proposed design methodology to nonlinear systems with sector-bounded nonlinearities. The Circle criterion provides a necessary and sufficient condition for stabilizing this class of nonlinear systems; thus the data-driven scheme can be combined with the ideas presented by the Circle criterion to achieve closed-loop stability. The main objective, however, is to formulate necessary and sufficient (convex) feasibility conditions for achieving the desired stability requirements.

1.3.2 Fixed-Structure Controller Design

With the objectives asserted in the previous subsection, it is evident that although convergence to the global optimal solution of the $\mathscr{H}_\infty$ problem is obtained with increasing controller order, the solution may be far from optimal for low-order controllers (since the global solution to an *approximate* problem is obtained). Thus the next research objective is to optimize the controller performance for low-order controllers using frequency-domain data (while guaranteeing the closed-loop stability of the system); this can be accomplished by finding a local solution to the $\mathscr{H}_\infty$ problem using fixed-structure low-order controllers. Two methods are proposed for achieving this specification:

- Solve a non-convex problem (in a data-driven setting) to obtain a local solution to the fixed-structure $\mathscr{H}_\infty$ problem.
- Solve a set of convex problems in an iterative fashion (in a data-driven setting) to obtain a local solution to the fixed-structure $\mathscr{H}_\infty$ problem

Note that the objective here is to optimize non-LP fixed-structure controllers. In the previous subsection, the objective was to formulate a convex problem using non-LP controllers; the solution to this convex problem, however, does not guarantee that the local solution to the $\mathscr{H}_\infty$ problem (for fixed-structure low-order controllers) is obtained. *Thus the main difference between the objective here and the objective discussed in the previous subsection is that convergence to a local solution for a given controller order is desired.*

The non-convex $\mathscr{H}_\infty$ constraints do not guarantee the closed-loop stability of a given system; thus it is desired to formulate a non-convex problem which optimizes all of the fixed-structure controller parameters while guaranteeing the closed-loop stability. It is known that non-convex problems are difficult to solve since the quality of solutions depend heavily on the initial conditions. Thus a particle swarm optimization (PSO) algorithm is presented to solve this problem; PSO is a powerful optimization method that can solve both linear and nonlinear problems and can be used to solve problems without specifying initial conditions. However, when the problem is of large dimension, the quality of the solution or the optimization time can be inadmissible. Thus it is desired to compare the local solutions obtained from the non-

convex $\mathscr{H}_\infty$ problem and the convex $\mathscr{H}_\infty$ problem (for fixed-structure non-LP controllers, linearized around a stabilizing operating point) to determine the validity and practicability of both methods.

The fixed-structure design is implemented on the same CERN converter that was discussed in the previous subsection, but with a different load and a different reference signal to track. The local solution to the fixed-structure problem is obtained using the convex formulation since (1), this method can consider other performance criterion (i.e., $\mathscr{H}_1$ and $\mathscr{H}_2$ performance), and (2), the method is more efficient in a computational sense.

1.3.3 Contributions

The following main contributions of this dissertation are highlighted as follows:

- It derives the necessary and sufficient conditions for achieving robust stability and robust performance *in a data-driven setting* by minimizing the infinity norm of a weighted sensitivity function. The designed controller is robust with respect to the uncertainties captured in an identification experiment (which can be modeled as additive uncertainties).
- It derives the necessary and sufficient conditions for a certain class of models with frequency-domain polytopic uncertainties that are caused by measurement noise or multi-model incertitude.
- It shows that the solution to a convex problem converges monotonically to the global solution of the true $\mathscr{H}_\infty$ problem as the controller order increases (while guaranteeing the closed-loop stability).
- It proposes a method to design controllers for linear systems that are subjected to nonlinear distortions.
- It derives necessary and sufficient conditions for stabilizing systems with sector-bounded nonlinearities. It also derives a sufficient condition for guaranteeing the closed-loop performance for all uncertain gains within the sector nonlinearity.
- It presents a method for obtaining the local optimal solution of the $\mathscr{H}_\infty$ problem for fixed-structure controllers. This method uses a PSO algorithm for achieving the solution in a data-driven setting.
- It proposes a convex model-reference problem for fixed-structure non-LP controllers where local optimal solutions to the $\mathscr{H}_2$ or $\mathscr{H}_\infty$ problems are obtained. Closed-loop stability of the system is guaranteed with a given initial stabilizing controller. It also proposes a method for obtaining $\mathscr{H}_1$ performance.
- It implements the design methods for a power converter control system at CERN.

1.4 Dissertation Structure

The structure and general layout of this dissertation is now provided. Since the class of models and controllers vary from chapter to chapter, a dedicated chapter has been inserted in order to clarify all of the class of models and controllers that are presented in this work.

Chapter 2: Preliminaries

This chapter is dedicated to defining all of the class of models, uncertainties, and controllers that are used throughout the paper.

Chapter 3: Robust $\mathscr{H}_\infty$ Controller Design

This chapter deals with the problem of robust stability and robust performance for LTI-SISO systems. Necessary and sufficient conditions are derived for guaranteeing the stability of the closed-loop system and $\mathscr{H}_\infty$ performance. A convex optimization problem is formulated in which a controller is parameterized as a ratio of two LP transfer functions; in this manner, the controllers numerator and denominator are optimized. It is shown that as the controller order increases, the global optimal solution to the $\mathscr{H}_\infty$ problem is obtained. The robustness of the closed-loop system is established by considering an additive uncertainty of coprime factors (which can be easily obtained by spectral analysis of measured data). With this method, conditions for ensuring the performance and stability for systems with frequency-domain polytopic uncertainties are also derived. The simulation and experimental results at the end of the chapter show the effectiveness of the proposed method.

Chapter 4: RST Controller Design for Particle Accelerator Power Converters

In this chapter, the necessary and sufficient conditions for obtaining $\mathscr{H}_\infty$ performance that were developed in Chapter 3 are extended to multiple weighted sensitivity functions where the controller structure used is a 2-degree-of-freedom RST controller. Additionally, a method for obtaining $\mathscr{H}_\infty$ performance for linear systems which are subjected to nonlinear distortions is presented. The main idea of this approach is to model a nonlinear system as a linear system with an added noise source. The methods presented in this chapter are applied in simulation and for a power converter control system at CERN where the objective is to control the current in a magnet given a desired reference signal.

Chapter 5: Robust Control of Systems With Sector Nonlinearities

This chapter uses the celebrated Circle criterion to develop necessary and sufficient (convex) feasibility conditions for stabilizing systems with sector-bounded nonlinearities (in a data-driven setting). The conditions are developed for several different cases in which the lines that bound the nonlinearity can vary (i.e., lines with positive and negative slopes). Additionally, a sufficient condition is presented for obtaining $\mathscr{H}_\infty$ performance for systems with uncertain gains that lie within the sector nonlinearity. A case study is presented which considers multi-model uncertainty for a class of switched time-varying nonlinear systems.

Chapter 6: $\mathscr{H}_\infty$ Design for Low-Order Fixed-Structure Controllers

In this chapter, the necessary and sufficient conditions presented in Chapter 3 are used to design low-order fixed-structure controllers. This problem, however, is non-convex; thus a sufficient condition is presented which ensures that the local solution of the $\mathscr{H}_\infty$ problem is obtained for fixed-structure controllers. The proposed optimization problem can be expressed in a bilinear form if the controllers are LP. However, in the case when the controllers are not LP, a PSO algorithm is proposed to obtain the local solution of the problem.

Chapter 7: Model-Reference Control for Particle Accelerator Power Converters

In this chapter, a sufficient condition is developed for obtaining the local solution to the $\mathscr{H}_2$ and $\mathscr{H}_\infty$ problems through the usage of linear matrix inequalities (LMIs). Non-convex constraints are linearized around an operating point such that the closed-loop stability is guaranteed if the initializing controllers of the algorithm are stabilizing. This method optimizes fixed-structure controllers for the model-reference problem; however, the methods described in this chapter can also be applied to minimize a desired weighted sensitivity function. Additionally, a 2-step method is proposed for obtaining $\mathscr{H}_1$ performance (which is a desired criterion for many applications). The methods in this chapter are applied to several problems including the power converter control system that was studied in Chapter 4 (with a different load and a different reference signal to track).

Chapter 8: Conclusion

This chapter states the concluding remarks and discusses the possible future outlook of the research presented in this dissertation.

Appendix

The appendix contains the work related to frequency-domain approaches for controlling MIMO time-delayed processes using the Smith predictor structure [94]. However, the control methodology here differs from the methods discussed in the main chapters of this dissertation.

2 Preliminaries

This chapter is devoted to classifying the class of models and controllers that are used throughout this work. Each chapter of this dissertation implements a particular process and controller structure, and it is convenient to first define them here. The process models will be represented in both polynomial form and coprime form; the set of uncertainties for these processes are also defined. This dissertation also presents methods for controlling certain classes of nonlinear systems; these classes are also defined in this chapter. The controllers considered in this work will be 1-degree-of-freedom (1DOF) (continuous-time and discrete-time controllers) and 2DOF discrete-time RST controllers.

2.1 Class of models

The class of models considered in this dissertation are defined in this section.

2.1.1 General Plant Representation

Given a process input signal $u(t)$ and output signal $y(t)$ of a continuous-time LTI-SISO plant model $G(s)$ (with $\mathscr{U}(j\omega)$ and $\mathscr{Y}(j\omega)$ defined as the frequency spectrums of $u(t)$ and $y(t)$, respectively), then the frequency response function (FRF) of the plant model is represented as $G(j\omega)$, where the following relation holds:

$$\mathscr{Y}(j\omega) = G(j\omega)\mathscr{U}(j\omega), \quad \forall \omega \in \Omega_c,$$

where $\Omega_c := \mathbb{R} \cup \{\infty\}$.

A similar representation can be made for discrete-time systems. Given a process input signal $u[k]$ and output signal $y[k]$ of a discrete-time LTI-SISO plant model $G(z^{-1})$ (with $\mathscr{U}(e^{-j\omega})$ and $\mathscr{Y}(e^{-j\omega})$ defined as the frequency spectrums of $u[k]$ and $y[k]$, respectively), then the FRF of

the plant model is represented as $G(e^{-j\omega})$, where the following relation holds:

$$\mathscr{Y}(e^{-j\omega}) = G(e^{-j\omega})\mathscr{U}(e^{-j\omega}), \quad \forall \omega \in [-\pi/T_s, \pi/T_s],$$

where T_s [s] is defined as the sampling period of the discrete-time system, and k is a discrete-time instant. Note that due to the symmetry of the spectrums, it is sufficient to consider $\omega \in \Omega := [0, \pi/T_s]$ for practical applications.

Remark. *When the Shannon-Nyquist sampling theorem is met for discrete-time systems, the FRFs for continuous-time and discrete-time processes are nearly identical (i.e., $G(j\omega) \approx G(e^{-j\omega})$). For the remaining portions of this chapter, when the dependency in ω is neglected, it signifies that the definition/equation applies to both continuous-time and discrete-time systems.*

Class of Uncertainties

Multimodel Uncertainty:

In general, a set $\mathscr{G}$ can be formulated to represent a plant model containing ℓ FRF models:

$$\mathscr{G} = \{G_i(e^{-j\omega}); \quad i = 1, \ldots, \ell; \quad \forall \omega \in \Omega\}$$

for discrete-time systems and

$$\mathscr{G}_c = \{G_i(j\omega); \quad i = 1, \ldots, \ell; \quad \forall \omega \in \Omega_c\}$$

for continuous-time systems. These sets define a system which is subject to multi-model uncertainty.

Multiplicative Uncertainty:

The set of all LTI-SISO strictly proper frequency response models belonging to the family of perturbed plants with multi-model and multiplicative uncertainty can be defined as

$$\mathscr{G}_m = \{G_i[1 + \Delta W_{2_i}]; \quad i = 1, \ldots, \ell\}, \tag{2.1}$$

where G_i is the nominal FRF of the process, W_{2_i} is an uncertainty weight with bounded infinity norm, and Δ is an unknown stable transfer function satisfying $\|\Delta\|_\infty < 1$.

Parametric uncertainty:

The approach proposed in this dissertation requires only the frequency response of a model to design a robust controller. However, if a parametric model is available, the approach can still be used by computing the frequency response of the model. It is well known that the interval deterministic parametric uncertainty cannot be converted to the ellipsoid uncertainty in the frequency-domain. In a data-driven framework, for an identified parametric model using noisy data, the parametric uncertainties have stochastic bounds and can be transferred to the

frequency-domain in a stochastic sense.

In a data-driven approach, a parametric model of the plant is identified together with its parametric uncertainty using the classical prediction error methods (see [95]). The parametric uncertainty is characterized by an ellipsoid in the parameter space and can be computed using the asymptotic covariance matrix of the parameters for a given probability level. Thanks to the invariance property of the Maximum Likelihood Estimators, any function of the estimated parameters will converge to a normal distribution with a covariance matrix that can be computed based on the derivative of the function with respect to the parameters and its covariance matrix. In the complex plane, this parametric uncertainty is represented by an ellipse at each frequency that is well approximated with an m_p-sided polygon ($m_p > 2$) of minimum area that circumscribes each ellipse. In this manner, the parametric uncertainty can be taken into account using the frequency-domain polytopic uncertainty with almost no conservatism.

Suppose that a stable parametric model $\hat{G}(\boldsymbol{\theta}_p)$ is identified from a set of noisy data and the covariance matrix of the parameters, $\text{cov}(\boldsymbol{\theta}_p)$, is computed (where $\boldsymbol{\theta}_p \in \mathbb{R}^n$ is a vector of parametric uncertainties). Then, the frequency response of the identified model can be computed with its real and imaginary parts put in vector form as

$$\hat{G}_v(\omega, \boldsymbol{\theta}_p) = \begin{bmatrix} \Re\{\hat{G}(\boldsymbol{\theta}_p)\} & \Im\{\hat{G}(\boldsymbol{\theta}_p)\} \end{bmatrix}^\top. \tag{2.2}$$

This vector has a joint normal distribution with the covariance $C_G(\omega, \boldsymbol{\theta}_p)$ that can be estimated from $\text{cov}(\boldsymbol{\theta}_p)$ using a linear approximation as follows:

$$C_G(\omega) = \left(\frac{\partial \hat{G}_v(\omega, \boldsymbol{\theta}_p)}{\partial \boldsymbol{\theta}_p} \right) \text{cov}(\boldsymbol{\theta}_p) \left(\frac{\partial \hat{G}_v(\omega, \boldsymbol{\theta}_p)}{\partial \boldsymbol{\theta}_p} \right)^\top. \tag{2.3}$$

Note that $\text{cov}(\boldsymbol{\theta}_p) \in \mathbb{R}^{n \times n}$ and $C_G(\omega, \boldsymbol{\theta}_p) \in \mathbb{R}^{2 \times 2}$. Then, the true frequency response will belong to the following ellipse in the complex plane with a probability of $1 - \alpha_p$:

$$\begin{bmatrix} \bar{x} - \Re\{\hat{G}(\boldsymbol{\theta}_p)\} \\ \bar{y} - \Im\{\hat{G}(\boldsymbol{\theta}_p)\} \end{bmatrix}^\top C_G^{-1}(\omega, \boldsymbol{\theta}_p) \begin{bmatrix} \bar{x} - \Re\{\hat{G}(\boldsymbol{\theta}_p)\} \\ \bar{y} - \Im\{\hat{G}(\boldsymbol{\theta}_p)\} \end{bmatrix} \leq \chi_2^2(\alpha_p), \tag{2.4}$$

where χ_2^2 is the chi-square distribution with two degrees of freedom. For a confidence interval of 0.95 ($\alpha_p = 0.05$), we have $\chi_2^2(0.05) = 5.99$. Since the uncertainty set is an ellipse, an m_p-sided polygon with minimum area that circumscribes it can be used to represent the uncertainty, and is approximated by frequency-domain polytopic uncertainty as

$$G(\lambda, \boldsymbol{\theta}_p) = \sum_{k=1}^{m_p} \lambda_i \hat{G}_k(\boldsymbol{\theta}_p), \tag{2.5}$$

where

$$\hat{G}_k(\boldsymbol{\theta}_p) = \hat{G}(\boldsymbol{\theta}_p) + [1 \quad j]\sqrt{5.99C_G(\omega,\boldsymbol{\theta}_p)}\begin{bmatrix}\frac{\cos(2\pi k/m_p)}{\cos(\pi/m_p)}\\ \frac{\sin(2\pi k/m_p)}{\cos(\pi/m_p)}\end{bmatrix}. \tag{2.6}$$

The last vector in (2.6) represents the k-th coordinate of a vertex of a polygon circumscribing the unit circle while the matrix $\sqrt{5.99C_G(\omega,\boldsymbol{\theta}_p)}$ designates the size and direction of the uncertainty (for 0.95 probability).

Acquisition of FRFs

Suppose that $u[k]$ and $y[k]$ are measurable and that these signals are noise-free and have zero initial and final conditions (i.e., $u[k] = y[k] = 0$ for $k \leq 0$ and $k > K_s$). Then, the FRF of the system is obtained as $G(e^{-j\omega}) = \mathscr{Y}(e^{-j\omega})\mathscr{U}^{-1}(e^{-j\omega})$, where

$$\mathscr{U}(e^{-j\omega}) = \sum_{k=0}^{K_s} u[k]e^{-j\omega T_s k} \tag{2.7}$$

$$\mathscr{Y}(e^{-j\omega}) = \sum_{k=0}^{K_s} y[k]e^{-j\omega T_s k} \tag{2.8}$$

are the frequency spectrums of the input and output signals. Under these assumptions, it is evident that from a set of sampled time-domain data, one is able to obtain a continuous FRF. If the data is noisy, then $G(e^{-j\omega})$ is characterized as the Empirical Transfer Function Estimate (ETFE) and is asymptotically unbiased [95]. For such systems, an additive uncertainty model can be considered to ensure robustness in the presence of noise perturbations.

The FRF of the process can be determined by considering the frequency response of a parametric model or from a set of input/output data. For example, a Pseudorandom binary sequence (PRBS) signal can be used as an excitation signal to identify the dynamics of a plant, since this type of signal has properties similar to white noise and excites all frequencies. Sine-sweep methods can also be used for this identification.

2.1.2 Coprime Representation

Suppose that a SISO unity feedback control system structure is used, where the plant is represented as $G(s) = N(s)M^{-1}(s)$ such that $\{N(s), M(s)\} \in \mathbf{RH}_\infty$. As asserted in [10] and [96], if $N(s)$ and $M(s)$ are coprime, then $G(s) = N(s)M^{-1}(s)$ is called a *coprime factorization* of $G(s)$ over $\mathbf{RH}_\infty$.

The frequency response of such a factorized SISO system is given by:

$$G(j\omega) = N(j\omega)M^{-1}(j\omega), \quad \omega \in \Omega_c, \tag{2.9}$$

where $N(j\omega), M(j\omega)$ are the FRFs of bounded analytic functions in the right half plane. It is also assumed that $G(j\infty) = 0$, which implies that $N(j\infty) = 0$ and $M(j\infty) \neq 0$. This representation includes time-delayed systems as well as unstable plants with unbounded infinity norms.

A similar coprime factorization can be considered for discrete-time systems. In this case, the plant is represented as $G(z^{-1}) = N(z^{-1})M^{-1}(z^{-1})$ such that $\{N(z^{-1}), M(z^{-1})\} \in \mathbf{RH}_\infty$ (where $N(z^{-1})$ and $M(z^{-1})$ are coprime factorizations over $\mathbf{RH}_\infty$). Let the FRF of the plant be defined as $G(e^{-j\omega}) = N(e^{-j\omega})M^{-1}(e^{-j\omega})$ for all $\omega \in \Omega$. $N(e^{-j\omega})$ and $M(e^{-j\omega})$ must be FRFs of bounded analytic functions outside the unit circle.

Class of Uncertainties

Additive coprime uncertainty:

Suppose that the frequency response of the coprimes are represented with additive uncertainty, given as

$$\begin{aligned} \tilde{N} &= N + |W_n|\delta_n e^{j\theta_n} \\ \tilde{M} &= M + |W_m|\delta_m e^{j\theta_m}, \end{aligned} \tag{2.10}$$

where $|\delta_n| \leq 1$, $|\delta_m| \leq 1$; $\theta_n, \theta_m \in [0\,, 2\pi]$; W_n and W_m are computed from the covariance of the estimates for a given confidence interval. These types of models can be easily obtained by spectral analysis of measured data. Suppose that N is obtained from the Fourier transform of the input signal u and output signal y such that $\mathscr{Y} = N\mathscr{U}$. The estimates of $\Re\{N\}$ and $\Im\{N\}$ are asymptotically uncorrelated and normally distributed (thanks to the central limit theorem) with a variance of $\Theta_v(\omega)/2|\mathscr{U}|^2$, where $\Theta_v(\omega)$ is the spectrum of the disturbance v at the output of the plant [95]. As a result, the model uncertainty in the complex plane will be a disk centered at N and its radius $|W_n|$ will follow the Rayleigh distribution and can be computed for any probability level. For example, the true frequency response at each frequency belongs to a disk of radius $|W_n|$ with a probability of 0.95, where

$$|W_n| = \sqrt{\frac{5.99\Theta_v(\omega)}{2|\mathscr{U}|^2}}. \tag{2.11}$$

The spectrum of disturbance can be estimated from the data by [95]:

$$\Theta_v(\omega) = \Theta_y(\omega) - \frac{|\Theta_{uy}(\omega)|}{\Theta_u(\omega)}, \tag{2.12}$$

where $\Theta_u(\omega)$ is the input spectrum, $\Theta_y(\omega)$ is the output spectrum and $\Theta_{uy}(\omega)$ is the cross-spectral density of input and output signals.

Frequency-domain polytopic uncertainty:

Let the frequency-domain polytopic uncertainty be defined as

$$G(\lambda, j\omega) = N(\lambda, j\omega)M^{-1}(\lambda, j\omega), \tag{2.13}$$

where

$$N(\lambda, j\omega) = \sum_{i=1}^{\ell} \lambda_i N_i(j\omega) \qquad ; \qquad M(\lambda, j\omega) = \sum_{i=1}^{\ell} \lambda_i M_i(j\omega)$$

and $\lambda_i \geq 0$, $\sum_{i=1}^{w} \lambda_i = 1$. Note that $\boldsymbol{\lambda}$ is a w-dimensional vector that belongs to the convex hull of λ_i's. This uncertainty should not be confused with the parametric polytopic uncertainty, which is defined in the parameter space in model-based robust control approaches.

Acquisition of FRFs

Finding the coprime factors of a given linear plant is a standard problem in control when the model of the plant is available [97]. Although, the coprime factors are not unique for a given system, their choice has only an effect for low-order controller design and this effect will be reduced by increasing the controller order (as will be shown in the next chapter). In a data-driven setting, for stable systems, a trivial choice is $N = G$ and $M = 1$.

For unstable systems, a stabilizing controller is needed in order to properly formulate N and M. In this case, N is the FRF between the reference signal and the measured output, while M is the FRF between the reference signal and the plant input. Given these formulations, it is evident that NM^{-1} represents the FRF of the plant model.

2.1.3 Nonlinear Models

There are two classes of nonlinear systems that will be considered in this work: nonlinear systems that can be represented by a linear system with additive stochastic distortions and linear systems which are in cascade with sector-bounded nonlinearities.

Nonlinear Wiener Systems

The class of nonlinearities for these types of systems are now addressed with the following definition:

Definition 2.1. ***Class $\mathcal{V}$ of nonlinear systems.*** *$\mathcal{V}$ is the set of nonlinear systems for which the following properties hold:*

- *The influence of the initial conditions vanishes asymptotically.*
- *The steady state response to a periodic input is a periodic signal with the same period as the input. Phenomena such as bifurcation, chaos, and sub-harmonics are excluded; however, strong nonlinearities such as saturation and discontinuities are permitted.*

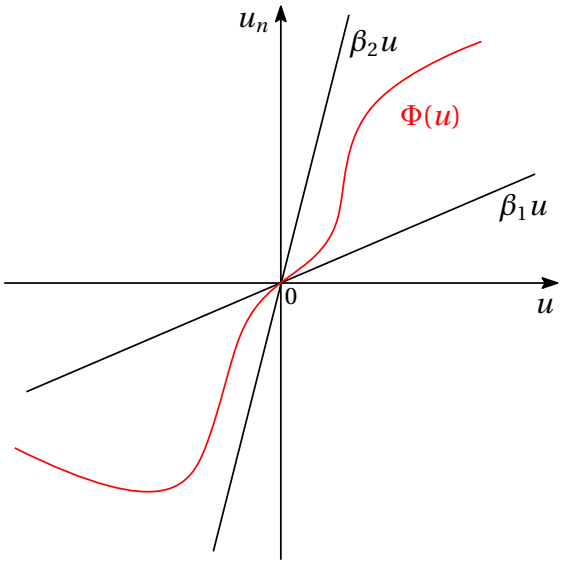

Figure 2.1 – Nonlinear sector that is bounded by two lines with slopes β_1 and β_2.

- *Only a point wise approximation of the output is obtained.*

A common type of nonlinearity in $\mathcal{V}$ is the sector-bounded time-invariant (memoryless) nonlinearity in which the input u_n to a linear plant model is a nonlinear function of the process input u (i.e., $u_n = \Phi(u)$). However, the nonlinear systems described by $\mathcal{V}$ include a wider class of nonlinearities (i.e., the so called Wiener systems [98]). A nonlinear system which abides by the above definition will be denoted as $G_{\mathcal{V}}(\cdot)$ (i.e., $G_{\mathcal{V}}(\cdot) \in \mathcal{V}$).

Sector-Bounded Time-Varying Nonlinearities

The second class of nonlinearities that will be addressed in this work is of the sector type (which will be denoted as $\Phi(\cdot)$) and is defined as

$$\mathcal{N}_t = \{\Phi(t,u) : \beta_1 u < \Phi(t,u) < \beta_2 u, \forall\, t \geq 0, \forall\, u \in [a,b]\}, \tag{2.14}$$

where u is the input signal of the nonlinearity, $\{\beta_1, \beta_2\} \in \mathbb{R}$ and $\{(a,b) \in \mathbb{R} : a < 0 < b\}$. This condition can be interpreted as a nonlinearity which is bounded by two straight lines with slopes β_1 and β_2 that pass through the origin. Let u_n represent the output signal of the nonlinear function $\Phi(\cdot)$; Fig. 2.1 depicts this sector nonlinearity when $\mathcal{N}_t$ in (2.14) holds globally (i.e., when the nonlinearity remains bounded for all values of u).

Acquisition of FRFs

Nonlinear Wiener Systems:

Suppose that the signals $u[k]$ and $y[k]$ are measurable; according to [99], for a certain class

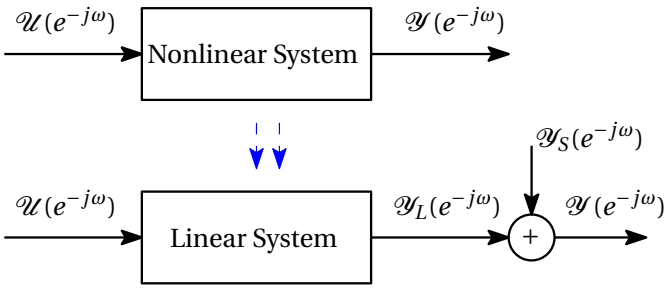

Figure 2.2 – Representation of a nonlinear system by a linear system for a certain class of inputs.

of reference signals and nonlinear systems, the FRF obtained during an experiment with a nonlinear plant can be described by a linear system plus an error term $\mathcal{Y}_S(e^{-j\omega})$ (see Fig. 2.2). The class of nonlinear systems that can be considered with this approach are those in $\mathcal{V}$.

The idea asserted in [99] is to perform multiple experiments with full or random phase multi-sines as the reference input. Averaging of the FRFs over the consecutive periods quantifies the noise level. Averaging of these mean FRFs over multiple experiments quantifies the level of the stochastic nonlinear distortions (with the sum of the remaining noise level). A best-linear-approximation (BLA) of the nonlinear system can then be obtained with an associated variance (which fully characterizes the underlying linear system).

Definition 2.2. ***Random Phase Multi-sine****: $u(t)$ is a random phase multi-sine if*

$$u(t) = \sum_{k=-K_s/2+1}^{K_s/2-1} \mathcal{U}_k e^{j2\pi f_s k t/K_s}, \tag{2.15}$$

where $\mathcal{U}_k = \mathcal{U}_{-k}^* = |\mathcal{U}_k| e^{j\varphi_k}$, $(\cdot)^*$ denotes the complex conjugate of the argument, f_s is the clock frequency of the waveform generator, K_s is the number of samples in the signal period, and the phases φ_k are a realization of an independent distributed random process in $[0, 2\pi)$, where the expected value of $e^{j\varphi_k}$ is equal to zero.

Stable Plant:

Let us first consider the case when the plant model is stable; for a given known input signal, an open-loop experiment can be performed to obtain the FRF BLA and the variance. Let us define $G^{[q,p]}(e^{-j\omega})$ as the FRF estimate of $G_{\mathcal{V}}(\cdot)$ for the p-th period of a q-th experiment (with P denoting the total number of periods in each experiment and Q being the total number of experiments):

$$\begin{aligned} G^{[q,p]}(e^{-j\omega}) &= \frac{\mathcal{Y}^{[q,p]}(e^{-j\omega})}{\mathcal{U}^{[q]}(e^{-j\omega})} \\ &= G(e^{-j\omega}) + G_S^{[q]}(e^{-j\omega}) + E_G^{[q,p]}(e^{-j\omega}), \end{aligned} \tag{2.16}$$

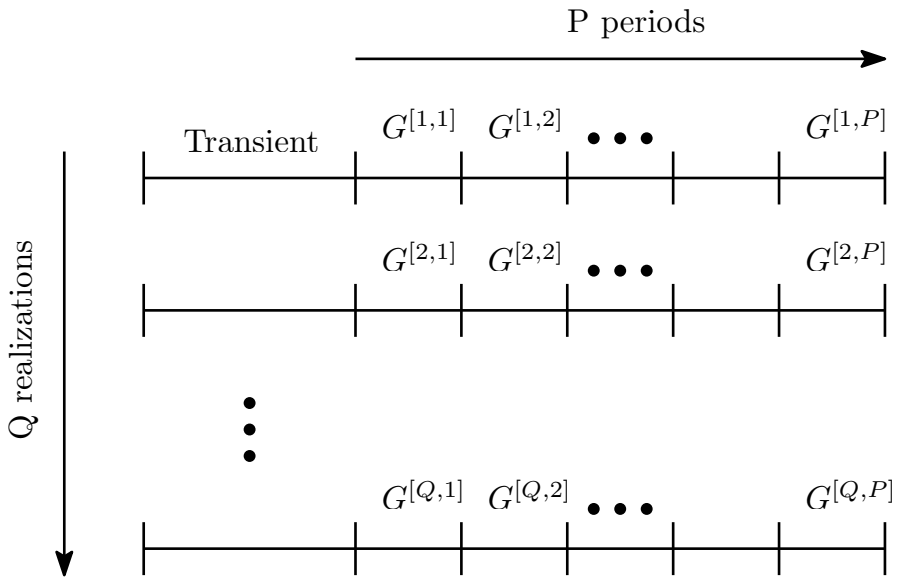

Figure 2.3 – Procedure for measuring the BLA from the FRF of the nonlinear system. $G^{[q,p]}$ is the FRF estimate of the p^{th} period of the q^{th} experiment.

where G is the FRF BLA, $G_S^{[q]} = \mathscr{Y}_S^{[q]}/\mathscr{U}^{[q]}$ (i.e., the stochastic nonlinear contributions) and $E_G^{[q,p]}$ are the errors due to the output noise; Fig. 2.3 shows the measurement process of this estimate. The sample mean and the sample variance of the FRF estimates over P periods are determined as follows:

$$\begin{aligned} G^{[q]}(e^{-j\omega_k}) &= \frac{1}{P}\sum_{p=1}^{P} G^{[q,p]}(e^{-j\omega_k}) \\ \sigma_n^{2[q]}(k) &= \frac{1}{P(P-1)}\sum_{p=1}^{P}\left|G^{[q,p]}(e^{-j\omega_k}) - G^{[q]}(e^{-j\omega_k})\right|^2, \end{aligned} \tag{2.17}$$

where $\sigma_n^{2[q]}$ is the sample noise variance of the sample mean $G^{[q]}$. The BLA of the plant G with the associated sample total variance σ_G^2 can then be determined with the following relations [99]:

$$\begin{aligned} G(e^{-j\omega_k}) &= \frac{1}{Q}\sum_{q=1}^{Q} G^{[q]}(e^{-j\omega_k}) \\ \sigma_G^2(k) &= \frac{1}{Q(Q-1)}\sum_{q=1}^{Q}\left|G^{[q]}(e^{-j\omega_k}) - G(e^{-j\omega_k})\right|^2. \end{aligned} \tag{2.18}$$

Unstable Plant:

Let us now consider the case when the plant model is unstable; in this case, an open-loop experiment cannot be performed to obtain the FRFs. A stabilizing controller would first need to be implemented in order to stabilize the closed-loop system. Now, suppose that the signal

r is measurable, where the spectrum of r is denoted as $\mathscr{R}(e^{-j\omega})$. Additionally, let us define $N(e^{-j\omega})$ as the FRF BLA between the signals r to y and $M(e^{-j\omega})$ as the FRF BLA between the signals r to u. Since the nonlinear system is described by a linear system plus an error term $\mathscr{Y}_S(e^{-j\omega})$, then it is evident that the FRF BLA of the plant model $G(e^{-j\omega}) = N(e^{-j\omega})M^{-1}(e^{-j\omega})$. This is known as a *coprime factorization* of the FRF G, where N and M are coprime functions which are analytic outside the unit circle [10].

According to [99], the sample means and total (co)variances can be determined as follows:

$$\begin{aligned}
\mathscr{Y}(e^{-j\omega_k}) &= \frac{1}{Q}\sum_{q=1}^{Q}\mathscr{Y}^{[q]}(e^{-j\omega_k}) \\
\sigma^2_{\mathscr{Y}}(k) &= \frac{1}{Q(Q-1)}\sum_{q=1}^{Q}|\mathscr{Y}^{[q]}(e^{-j\omega_k}) - \mathscr{Y}(e^{-j\omega_k})|^2 \\
\sigma^2_{\mathscr{Y}\mathscr{R}}(k) &= \frac{1}{Q(Q-1)}\sum_{q=1}^{Q}\left[\mathscr{Y}^{[q]}(e^{-j\omega_k}) - \mathscr{Y}(e^{-j\omega_k})\right]\left[\mathscr{R}^{[q]}(e^{-j\omega_k}) - \mathscr{R}(e^{-j\omega_k})\right]^* \\
\sigma^2_{\mathscr{U}\mathscr{R}}(k) &= \frac{1}{Q(Q-1)}\sum_{q=1}^{Q}\left[\mathscr{U}^{[q]}(e^{-j\omega_k}) - \mathscr{U}(e^{-j\omega_k})\right]\left[\mathscr{R}^{[q]}(e^{-j\omega_k}) - \mathscr{R}(e^{-j\omega_k})\right]^*,
\end{aligned} \tag{2.19}$$

where the spectrums and variances for the signals u (i.e., $\mathscr{U}(e^{-j\omega_k})$ and $\sigma^2_{\mathscr{U}}(k)$) and r (i.e., $\mathscr{R}(e^{-j\omega_k})$ and $\sigma^2_{\mathscr{R}}(k)$) are computed in the same manner as $\mathscr{Y}(e^{-j\omega_k})$ and $\sigma^2_{\mathscr{Y}}(k)$, respectively. Finally, the FRF of the BLA for each coprime can then be obtained as

$$N(e^{-j\omega_k}) = \mathscr{Y}(e^{-j\omega_k})\mathscr{R}^{-1}(e^{-j\omega_k}), \quad M(e^{-j\omega_k}) = \mathscr{U}(e^{-j\omega_k})\mathscr{R}^{-1}(e^{-j\omega_k}), \tag{2.20}$$

where the associated total variance for each coprime is calculated as follows:

$$\begin{aligned}
\sigma^2_N(k) &= \left|N(e^{-j\omega_k})\right|^2\left(\frac{\sigma^2_{\mathscr{Y}}(k)}{|\mathscr{Y}(e^{-j\omega_k})|^2} + \frac{\sigma^2_{\mathscr{R}}(k)}{|\mathscr{R}(e^{-j\omega_k})|^2} - 2\Re\left\{\frac{\sigma^2_{\mathscr{Y}\mathscr{R}}(k)}{\mathscr{Y}(e^{-j\omega_k})\mathscr{R}^*(e^{-j\omega_k})}\right\}\right) \\
\sigma^2_M(k) &= \left|M(e^{-j\omega_k})\right|^2\left(\frac{\sigma^2_{\mathscr{U}}(k)}{|\mathscr{U}(e^{-j\omega_k})|^2} + \frac{\sigma^2_{\mathscr{R}}(k)}{|\mathscr{R}(e^{-j\omega_k})|^2} - 2\Re\left\{\frac{\sigma^2_{\mathscr{U}\mathscr{R}}(k)}{\mathscr{U}(e^{-j\omega_k})\mathscr{R}^*(e^{-j\omega_k})}\right\}\right).
\end{aligned} \tag{2.21}$$

Remark. *Note that in [99], the FRF estimate of $G(e^{-j\omega})$ (and the associated uncertainty) can be obtained from the signals u and y directly. However, the coprime formulation was needed in this chapter in order to apply the proposed controller design schemes (which are asserted in subsequent chapters).*

Given the BLA of the nonlinear system and total variance of each coprime, the additive uncertainty relations in (2.10) can be used to ensure that the dynamics of the underlying linear system are captured in the frequency response measurements. For example, if it is desired to construct an uncertainty disk such that the true frequency response lies within the disk with a

probability level of 0.95, then the radius of this disk(s) associated with the set in (2.10) will be

$$\begin{aligned} |W_n(e^{-j\omega_k})| &= \sqrt{5.99\sigma_N^2(k)} \\ |W_m(e^{-j\omega_k})| &= \sqrt{5.99\sigma_M^2(k)}. \end{aligned} \tag{2.22}$$

Remark. *Note that for stable systems, $N(e^{-j\omega}) = G(e^{-j\omega})$ and $M(e^{-j\omega}) = 1$ can be selected for the coprimes. In this case,*

$$\hat{N}(e^{-j\omega}) = G(e^{-j\omega}) + |W_g(e^{-j\omega})|\delta_g e^{j\theta_g},$$

where $|\delta_g| \leq 1; \theta_g \in [0, 2\pi]; |W_g(e^{-j\omega})| = \sqrt{5.99\sigma_G^2}$.

Sector-Bounded Time-Varying Nonlinearities:

The method to obtain the coprimes for the linear system with the sector-bounded nonlinearity will now be formulated (i.e., with $\Phi(\cdot) \in \mathcal{N}_t$). To keep the context of the work presented in this section in a data-driven framework, the following assumption is asserted:

Assumption 1. *The signal u_n is assumed to be measurable, which allows the dynamics of the linear system to be captured in an identification experiment.*

- *Stable Process*: If the plant is stable, then a simple choice for the coprimes is $N(e^{-j\omega}) = G(e^{-j\omega})$ and $M(e^{-j\omega}) = 1$. In a data-driven setting, $G(e^{-j\omega})$ can be obtained by simply performing an open-loop experiment and applying an excitation signal (such as a PRBS or sine-sweep signal) at the input of the process. The FRF is then obtained as $G(e^{-j\omega}) = \mathscr{Y}(e^{-j\omega})/\mathscr{U}_n(e^{-j\omega})$ (where $\mathscr{U}_n(e^{-j\omega})$ is the frequency spectrum of the signal $u_n[k]$).
- *Unstable Process*: If the plant is unstable, we assume that a stabilizing controller $K(z^{-1})$ exists that can be used for data acquisition. In this case, the closed-loop system is excited with an excitation signal and $u_n[k]$ and $y[k]$ are recorded. Then, in an offline manner, the signal $x[k]$ will be generated using the structure shown in Fig. 2.4 (where the frequency spectrum of $x[k]$ can be obtained, which is denoted as $\mathscr{X}(e^{-j\omega})$). The fixed gain β_l should be selected inside the sector nonlinearity such that if we replaced the sector nonlinearity with the fixed gain β_l, the resulting linear closed-loop system would be stable (i.e., the roots of $1 + \beta_l G(k^{-1})K(z^{-1})$ are inside the unit circle). With the structure shown in Fig. 2.4, it is easy to see that the transfer function between x and u_n (that can be called $M(z^{-1})$) is

  $$M(z^{-1}) = \left[1 + \beta_l G(z^{-1})K(z^{-1})\right]^{-1},$$

  which is stable. Furthermore, the transfer function between x and y (that can be called $N(z^{-1})$) is

  $$N(z^{-1}) = G(z^{-1})\left[1 + \beta_l G(z^{-1})K(z^{-1})\right]^{-1},$$

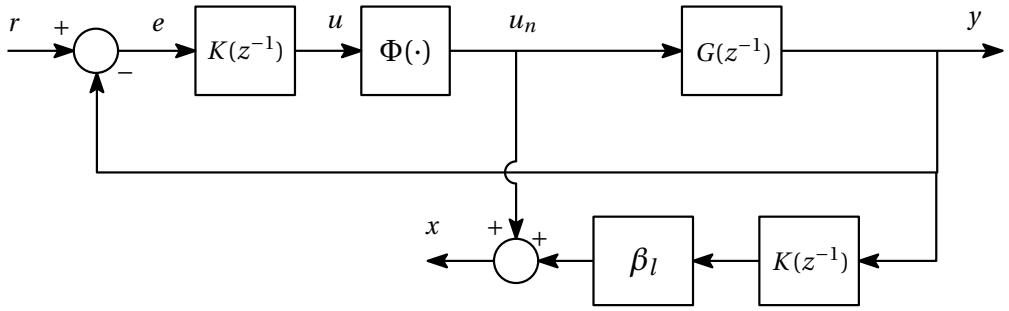

Figure 2.4 – Structure to be used in obtaining the coprimes for an unstable process.

which is also stable. Therefore, with a closed-loop experiment where the identifying signal is injected into the reference input, the coprimes can be obtained as

$$N(e^{-j\omega}) = \frac{\mathscr{Y}(e^{-j\omega})}{\mathscr{X}(e^{-j\omega})}, \quad M(e^{-j\omega}) = \frac{\mathscr{U}_n(e^{-j\omega})}{\mathscr{X}(e^{-j\omega})}, \tag{2.23}$$

where it is evident that $G(e^{-j\omega}) = N(e^{-j\omega})M^{-1}(e^{-j\omega})$.

2.2 Class of controllers

This dissertation considers various types of controller structures. Thus it is appropriate to define all of the class of controllers considered in this work.

2.2.1 Polynomial 1DOF Controller

The structure of this controller is represented as a ratio of two polynomial functions $K(z^{-1}) = R(z^{-1},\boldsymbol{\rho})S^{-1}(z^{-1},\boldsymbol{\rho})$. The functions $R(z^{-1},\boldsymbol{\rho})$ and $S(z^{-1},\boldsymbol{\rho})$ each represent polynomials in z^{-1}, i.e.,

$$R(z^{-1},\boldsymbol{\rho}) = r_0 + r_1 z^{-1} + \cdots + r_{n_r} z^{-n_r} \tag{2.24}$$

$$S(z^{-1},\boldsymbol{\rho}) = 1 + s_1 z^{-1} + \cdots + s_{n_s} z^{-n_s}, \tag{2.25}$$

where r_i and s_i are the controller parameters and $\{n_r, n_s\}$ are the orders of the polynomials R and S, respectively. The vector of controller parameters $\boldsymbol{\rho}$ is defined as

$$\boldsymbol{\rho}^\top = [r_0, r_1, \ldots, r_{n_r}, s_1, s_2, \ldots, s_{n_s}], \tag{2.26}$$

where $\boldsymbol{\rho} \in \mathbb{R}^{n_{rs}}$ with $n_{rs} = n_r + n_s + 1$.

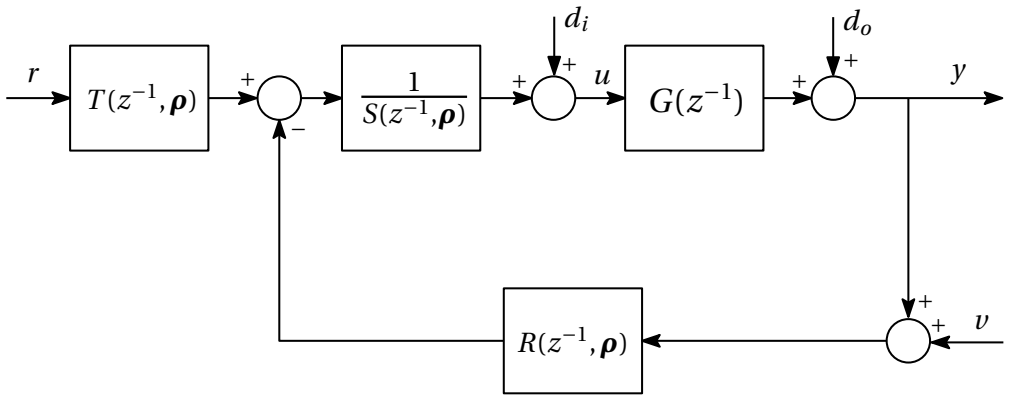

Figure 2.5 – RST controller structure.

2.2.2 RST 2DOF Controller

The RST controller is a 2DOF controller which can be used to synthesize the tracking and regulation requirements independently from each other [100]. The general structure of this controller is shown in Fig. 2.5. Each controller is realized as a polynomial function as follows:

$$R(z^{-1},\boldsymbol{\rho}) = r_0 + r_1 z^{-1} + \cdots + r_{n_r} z^{-n_r} \tag{2.27}$$

$$S(z^{-1},\boldsymbol{\rho}) = 1 + s_1 z^{-1} + \cdots + s_{n_s} z^{-n_s} \tag{2.28}$$

$$T(z^{-1},\boldsymbol{\rho}) = t_0 + t_1 z^{-1} + \cdots + t_{n_t} z^{-n_t}, \tag{2.29}$$

where $\{n_r, n_s, n_t\}$ are the orders of the polynomials R, S and T, respectively. The controller parameter vector $\boldsymbol{\rho} \in \mathbb{R}^{n_{rst}}$ (vector of decision variables) is defined as

$$\boldsymbol{\rho}^\top = [r_0, r_1, \ldots, r_{n_r}, s_1, s_2, \ldots, s_{n_s}, t_0, t_1, \ldots, t_{n_t}],$$

where $n_{rst} = n_r + n_s + n_t + 2$.

2.2.3 Coprime 1DOF Controller

Consider the controller structure, $K(s) = X(s)Y^{-1}(s)$, where $X(s)$ and $Y(s)$ are stable transfer functions with bounded infinity norm ($X(s), Y(s) \in \mathbf{RH}_\infty$). These transfer functions may be discrete- or continuous-time[1].

The functions X and Y are linearly parameterized as $X(\boldsymbol{\rho}) = \boldsymbol{\rho}_x^\top \boldsymbol{\phi}$ and $Y(\boldsymbol{\rho}) = \boldsymbol{\rho}_y^\top \boldsymbol{\phi}$, where $\boldsymbol{\rho}_x^\top = [\rho_{x_0}, \ldots, \rho_{x_n}]$ and $\boldsymbol{\rho}_y^\top = [1, \rho_{y_1}, \ldots, \rho_{y_n}]$ are the vectors of the controller parameters (where $\boldsymbol{\rho}_x \in \mathbb{R}^{n+1}$ and $\boldsymbol{\rho}_y \in \mathbb{R}^{n+1}$) and $\boldsymbol{\phi}^\top = [1, \phi_1 \cdots, \phi_n]$ is a vector of stable orthogonal basis functions. A

[1] Note that the term "coprime controller" is used in this dissertation to remain in the same convention as that of the coprime plant model. However, the functions X and Y are not actually coprime factorizations of K (i.e., they do not necessarily have to satisfy the Bezout identity $NX + MY = 1$). The are simply transfer functions that belong in $\mathbf{RH}_\infty$.

simple choice is the Laguerre basis functions given by [101]:

$$\phi_i(s) = \frac{\sqrt{2\xi}(s-\xi)^{i-1}}{(s+\xi)^i} \tag{2.30}$$

with $\xi > 0$ and $i = 1, \cdots, n$ for continuous-time systems and

$$\phi_i(z) = \frac{\sqrt{1-\xi_z^2}}{z-\xi_z}\left(\frac{1-\xi_z z}{z-\xi_z}\right)^{i-1} \tag{2.31}$$

with $-1 < \xi_z < 1$ for discrete-time systems.

A PID controller can also be represented in this form. Suppose that the desired controller structure is given as

$$K(s,\boldsymbol{\rho}) = k_p + k_i\frac{1}{s} + k_d\frac{s}{T_f s+1}, \tag{2.32}$$

where $T_f \in \mathbb{R}_+$. Then the controller can be expressed as $K(\boldsymbol{\rho}) = X(\boldsymbol{\rho})Y^{-1}(\boldsymbol{\rho})$ with

$$\begin{aligned} \boldsymbol{\rho}_x^\top &= [\rho_1 \;\; \rho_2 \;\; \rho_3] \\ \boldsymbol{\rho}_y^\top &= [T_f \;\; 1 \;\; 0] \\ \boldsymbol{\phi}(s,\xi) &= [s^2 \;\; s \;\; 1]^\top (s+\xi)^{-2}, \end{aligned} \tag{2.33}$$

where the parameters of $\boldsymbol{\rho}_x$ are $\rho_1 = k_p T_f + k_d$, $\rho_2 = k_p + k_i T_f$, $\rho_3 = k_i$.

2.3 Control Performance

Throughout this dissertation, the objective will be to design a controller that meets some constraints on the infinity norm of the weighted sensitivity functions. Thus it is convenient to now define the various sensitivity functions for the different structures considered in this work. Before defining these quantities, it is appropriate to first define the notion of Hurwitz and Schur systems.

Definition 2.3. *(Hurwitz system) A continuous-time transfer function $A(s)$ is called Hurwitz if the poles of $A(s)$ are located in the open left half-plane of the complex plane, that is, the real part of every pole is negative.*

Definition 2.4. *(Schur system) A discrete-time transfer function $A_d(z)$ is called Schur if the poles of $A_d(z)$ lie in the open unit disk of the complex plane, that is, the magnitude of each pole is less than one.*

Note that both Hurwitz and Schur systems relate the notion of stability for both continuous-time and discrete-time processes. Therefore, the terms “stable” and “Hurwitz” (or “stable” and “Schur”) are used interchangeably throughout this dissertation.

2.3.1 Sensitivity Functions for 1DOF Structure

The sensitivity functions associated with the unity feedback control system structure (using a 1DOF coprime controller and a coprime representation for the plant model) are given by:

$$\mathscr{S}_s(\boldsymbol{\rho}) = \frac{\mathscr{E}}{\mathscr{R}} = \frac{1}{1+GK(\boldsymbol{\rho})} = \frac{MY(\boldsymbol{\rho})}{NX(\boldsymbol{\rho})+MY(\boldsymbol{\rho})} \tag{2.34}$$

$$\mathscr{S}_t(\boldsymbol{\rho}) = \frac{\mathscr{Y}}{\mathscr{R}} = \frac{GK(\boldsymbol{\rho})}{1+GK(\boldsymbol{\rho})} = \frac{NX(\boldsymbol{\rho})}{NX(\boldsymbol{\rho})+MY(\boldsymbol{\rho})} \tag{2.35}$$

$$\mathscr{S}_u(\boldsymbol{\rho}) = \frac{\mathscr{U}}{\mathscr{R}} = \frac{K(\boldsymbol{\rho})}{1+GK(\boldsymbol{\rho})} = \frac{MX(\boldsymbol{\rho})}{NX(\boldsymbol{\rho})+MY(\boldsymbol{\rho})} \tag{2.36}$$

$$\mathscr{S}_v(\boldsymbol{\rho}) = \frac{\mathscr{Y}}{\mathscr{D}_i} = \frac{G}{1+GK(\boldsymbol{\rho})} = \frac{NY(\boldsymbol{\rho})}{NX(\boldsymbol{\rho})+MY(\boldsymbol{\rho})}, \tag{2.37}$$

where $\mathscr{E} = \mathscr{R} - \mathscr{Y}$ and $\mathscr{D}_i$ is the frequency spectrum of the plant input disturbance. For the 1DOF controllers that are represented in polynomial form, a similar representation of the above sensitivity functions can be made with $X(\boldsymbol{\rho}) = R(\boldsymbol{\rho})$ and $Y(\boldsymbol{\rho}) = S(\boldsymbol{\rho})$.

2.3.2 Sensitivity Functions for RST Structure

It is appropriate to consider the various sensitivity functions associated with the RST controller structure (since the definitions differ from the 1DOF case). Some sensitivity functions for this process (using a coprime representation for the plant) can be asserted as follows:

$$\mathscr{S}_1(\boldsymbol{\rho}) = \frac{\mathscr{Y}}{\mathscr{D}_o} = \frac{MS(\boldsymbol{\rho})}{NR(\boldsymbol{\rho})+MS(\boldsymbol{\rho})} = \frac{MS(\boldsymbol{\rho})}{\psi(\boldsymbol{\rho})} \tag{2.38}$$

$$\mathscr{S}_2(\boldsymbol{\rho}) = \frac{\mathscr{Y}}{\mathscr{R}} = \frac{NT(\boldsymbol{\rho})}{NR(\boldsymbol{\rho})+MS(\boldsymbol{\rho})} = \frac{NT(\boldsymbol{\rho})}{\psi(\boldsymbol{\rho})} \tag{2.39}$$

$$\mathscr{S}_3(\boldsymbol{\rho}) = \frac{\mathscr{E}}{\mathscr{R}} = \frac{NR(\boldsymbol{\rho})+MS(\boldsymbol{\rho})-NT(\boldsymbol{\rho})}{NR(\boldsymbol{\rho})+MS(\boldsymbol{\rho})} = \frac{\psi(\boldsymbol{\rho})-NT(\boldsymbol{\rho})}{\psi(\boldsymbol{\rho})} \tag{2.40}$$

$$\mathscr{S}_4(\boldsymbol{\rho}) = \frac{\mathscr{U}}{\mathscr{R}} = \frac{MT(\boldsymbol{\rho})}{NR(\boldsymbol{\rho})+MS(\boldsymbol{\rho})} = \frac{MT(\boldsymbol{\rho})}{\psi(\boldsymbol{\rho})}, \tag{2.41}$$

where $\psi(\boldsymbol{\rho}) = NR(\boldsymbol{\rho}) + MS(\boldsymbol{\rho})$ and $\mathscr{D}_o$ is the frequency spectrum of the output disturbance. Note that all of the sensitivity functions are Schur if the zeros of $\psi(\boldsymbol{\rho})$ lie within the unit circle. The sensitivity functions defined above (and all other sensitivity functions of interest) all contain the same transfer function $\psi(\boldsymbol{\rho})$. Therefore, a general construction of the sensitivity function can be expressed as $\mathscr{S}_q(\boldsymbol{\rho}) = \Delta_q(\boldsymbol{\rho})/\psi(\boldsymbol{\rho})$, where $\Delta_q(\boldsymbol{\rho})$ is a linear function of $R(\boldsymbol{\rho})$, $S(\boldsymbol{\rho})$ and/or $T(\boldsymbol{\rho})$. The subscript $q \in \{1,2,\ldots,c\}$ denotes the q-th sensitivity of interest and c is the total number of sensitivity functions.

Remark. *The proposed data-driven methods in this work do not consider parametric models in the synthesis problems; for this reason, both continuous-time and discrete-time models can be considered in the framework of this dissertation. Thus discrete-time controllers can be synthesized for continuous-time models, and vice versa. This is a typical scenario in real*

applications since continuous-time systems are usually controlled with discrete-time controllers (which is the case with the CERN power converter control system).

2.4 Optimization Problems

Throughout this dissertation, convex and quasi-convex optimization problems will be formulated for optimizing controllers based on a given criterion. Thus it is convenient to define what convex functions are along with some properties associated with convex problems.

Definition 2.5. *(Convex set) A set C is convex if the line segment between any two points in C lies in C. In other words, if for any $x_1, x_2 \in C$ and any λ with $0 \leq \lambda \leq 1$, we have*

$$\lambda x_1 + (1-\lambda) x_2 \in C.$$

Definition 2.6. *(Convex function) A function $f : \mathbb{R}^n \to \mathbb{R}$ is convex if the domain of f is a convex set and if for all x_1, x_2 in this domain, and λ with $0 \leq \lambda \leq 1$, we have*

$$f(\lambda x_1 + (1-\lambda) x_2) \leq \lambda f(x_1) + (1-\lambda) f(x_2).$$

Definition 2.7. *(Quasi-convex function) A function $f : \mathbb{R}^n \to \mathbb{R}$ is called quasi-convex if its domain and all its sublevel sets*

$$S_\alpha = \{x | f(x) \leq \alpha_q\},$$

for $\alpha_q \in \mathbb{R}$, are convex.

Based on the decision variables defined for the controllers in Section 2.2, the following notation is used to describe the problem of finding a $\boldsymbol{\rho}$ that minimizes $f_0(\boldsymbol{\rho})$ among all $\boldsymbol{\rho}$ that satisfy the conditions $f_i(\boldsymbol{\rho}) \leq 0, i = 1, ..., m_f$, and $h_i(\boldsymbol{\rho}) = 0, i = 1, ..., m_h$:

$$\begin{aligned} \underset{\boldsymbol{\rho}}{\text{minimize}} \quad & f_0(\boldsymbol{\rho}) \\ \text{subject to:} \quad & f_i(\boldsymbol{\rho}) \leq 0, \quad i = 1, ..., m_f, \\ & h_i(\boldsymbol{\rho}) = 0, \quad i = 1, ..., m_h. \end{aligned} \tag{2.42}$$

The decision vector $\boldsymbol{\rho}$ is the optimization variable (whose dimension varies based on the controller structure used), while $f_0(\boldsymbol{\rho})$ is the objective function to be minimized. A point $\boldsymbol{\rho}_o^\star$ is a global optimum if it is feasible and if $f_0(\boldsymbol{\rho}_o^\star) \leq f_0(\boldsymbol{\rho})$ for all feasible $\boldsymbol{\rho}$. If the objective function or any of the constraints are non-convex functions of $\boldsymbol{\rho}$, then, in general, one can only guarantee a local optimal solution to the problem.

Definition 2.8. *(Local optimum) A feasible point $\boldsymbol{\rho}^+$ is a local optimum of (2.42) if it is an optimum on some ball centered at $\boldsymbol{\rho}^+$, i.e., there exists a $B > 0$ such that*

$$f_0(\boldsymbol{\rho}^+) = \inf\left\{f_0(\boldsymbol{\rho}) : f_i(\boldsymbol{\rho}) \leq 0,\ i = 1, ..., m_f,\ h_i(\boldsymbol{\rho}) = 0,\ i = 1, ..., m_h,\ \|\boldsymbol{\rho} - \boldsymbol{\rho}^+\|_2 \leq B\right\}$$

The most important property of convex optimization problems is that any locally optimal point is also globally optimal. For the optimization problem in (2.42) to be convex (quasi-convex), $f_0(\boldsymbol{\rho})$ must be a convex (quasi-convex) function of $\boldsymbol{\rho}$ and $f_i(\boldsymbol{\rho})\ \forall i$ must be convex functions of $\boldsymbol{\rho}$ while $h_i(\boldsymbol{\rho})\ \forall i$ must be affine functions of $\boldsymbol{\rho}$. The problems formulated in this dissertation will be presented in epigraph form, i.e.,

$$\begin{aligned} \underset{\gamma,\boldsymbol{\rho}}{\text{minimize}} \quad & \gamma \\ \text{subject to:} \quad & f_0(\boldsymbol{\rho}) - \gamma \leq 0 \\ & f_i(\boldsymbol{\rho}) \leq 0, \quad i = 1,...,m_f, \\ & h_i(\boldsymbol{\rho}) = 0, \quad i = 1,...,m_h, \end{aligned} \tag{2.43}$$

where $\gamma \in \mathbb{R}$. This problem is equivalent to the problem in (2.42). The epigraph formulation is particularly useful for solving quasi-convex optimization problems. In this dissertation, many of the objective functions will posses the following form:

$$f_0(\boldsymbol{\rho}) = f_c(\boldsymbol{\rho}) f_l^{-1}(\boldsymbol{\rho}),$$

where $f_c(\boldsymbol{\rho})$ is a convex function of $\boldsymbol{\rho}$ such that $f_c(\boldsymbol{\rho}) \geq 0$, and $f_l(\boldsymbol{\rho})$ is a linear function of $\boldsymbol{\rho}$ such that $f_l(\boldsymbol{\rho}) > 0$ (with $\gamma \in \mathbb{R}_+$). With this formulation, it can be shown that the function $f_0(\boldsymbol{\rho})$ is indeed quasi-convex [93]. Given this construction for the objective function, note that

$$f_0(\boldsymbol{\rho}) \leq \gamma \iff f_c(\boldsymbol{\rho}) - \gamma f_l(\boldsymbol{\rho}) \leq 0,$$

where $f_c(\boldsymbol{\rho}) - \gamma f_l(\boldsymbol{\rho})$ is convex for a fixed γ. The usual manner in solving (2.43) with this formulation is by specifying upper and lower bounds on γ and implementing a *bisection* algorithm in order to obtain the global solution to the optimization problem (within a given tolerance).

Remark. *In the bisection method, an initial value is assigned for γ such that $\gamma_0 = 0.5(\gamma_{min} + \gamma_{max})$ to solve the optimization problem, where γ_{min} and γ_{max} are the minimum and maximum bounds set for γ. In an iterative algorithm, if the problem is feasible for γ_i, then $\gamma_{i+1} = 0.5(\gamma_{min} + \gamma_i)$, and the solution to the optimization problem in (2.43) is recalculated with γ_{i+1}. If the problem is infeasible for γ_i, then $\gamma_{i+1} = 0.5(\gamma_{max} + \gamma_i)$. This process is repeated until a solution is obtained within a given tolerance γ_{tol}.*

The following notation is used to characterize the type of solution obtained from a given optimization problem:

- For a given *convex* (or *quasi-convex*) optimization problem, the *global* optimal solutions are denoted as $\gamma^\star$ and $\boldsymbol{\rho}^\star$.
- For a given *non-convex* optimization problem, the *local* optimal solutions are denoted as γ^+ and $\boldsymbol{\rho}^+$.

2.5 Conclusion

This chapter has asserted all of the necessary class of models and controllers for the work presented in this dissertation. The models considered in this work consist of both linear and nonlinear systems. The linear plant model can be represented in a coprime form; the same principle can be applied to a controller. This representation is needed in order to develop some important theoretical results (which will be seen in subsequent chapters). Additionally, 1DOF and 2DOF controllers are considered for various types of applications that will be analyzed in this dissertation. In the beginning of each remaining chapter, the class of models and controllers will be referenced appropriately to the sections of this chapter.

3 Robust $\mathscr{H}_\infty$ Controller Design

3.1 Introduction

In this chapter, the necessary and sufficient conditions for the existence of robust controllers that guarantee bounded infinity norm on the sensitivity functions are developed. It is shown that these conditions depend only on the frequency response of the plant model and can be represented by convex constraints with respect to the controller parameters. By using fixed-order rational controllers, a convex optimization problem is formulated which produces a solution that ensures $\mathscr{H}_\infty$ performance. The results are extended to systems with frequency-domain polytopic uncertainties that are caused by measurement noise or multi-model incertitude. The developed conditions are necessary and sufficient for Hurwitz systems and only sufficient for unstable systems with polytopic uncertainties.

In this chapter, a continuous-time representation of coprime processes (see Section 2.1.2) with 1DOF coprime controllers (see Section 2.2.3) are considered. Thus the sensitivity functions with a 1DOF structure are considered.

3.2 Convex parameterization of robust controllers

3.2.1 Controller objective

An upper bound on the infinity-norm of $H(j\omega,\boldsymbol{\rho}) = W_1(j\omega)\mathscr{S}_s(j\omega,\boldsymbol{\rho})$ will be considered, where $W_1 : \mathbb{R}\cup\{\infty\} \to \mathbb{C}$ is the frequency function of a Hurwitz system with bounded infinity norm and $\mathscr{S}_s : \mathbb{R}^{2n+1} \times (\mathbb{R}\cup\{\infty\}) \to \mathbb{C}$ is the FRF of the sensitivity function in (2.34) (with n denoting the controller order). Therefore, the control objective is to find a stabilizing controller $K(\boldsymbol{\rho})$ such that

$$\sup_{\omega\in\Omega_c} |H(j\omega,\boldsymbol{\rho})| < \gamma, \tag{3.1}$$

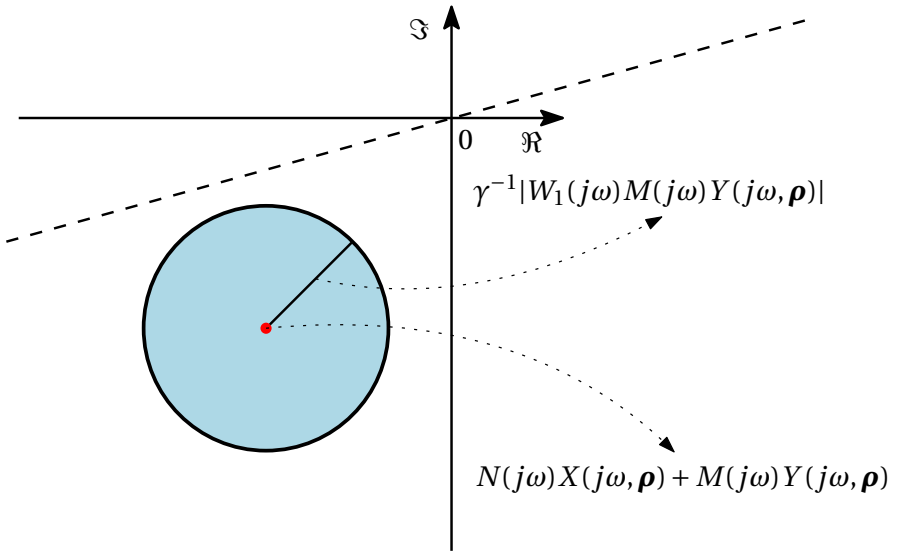

Figure 3.1 – Graphical representation of the constraint in 3.1.

where $\gamma \in \mathbb{R}_+$. This condition can easily be extended to the other weighted sensitivity functions asserted in equations (2.35-2.37). There are two problems associated with the condition in (3.1); the constraint is not convex and a controller which satisfies this condition does not necessarily guarantee the closed-loop stability of a system.

The main objective is to find a set of convex constraints (with respect to X and Y) to satisfy the constraint in (3.1). Note that this constraint can be expressed as

$$\gamma^{-1}\left|W_1(j\omega)M(j\omega)Y(j\omega,\boldsymbol{\rho})\right| < |N(j\omega)X(j\omega,\boldsymbol{\rho})+M(j\omega)Y(j\omega,\boldsymbol{\rho})|, \quad \forall\omega\in\Omega_c. \tag{3.2}$$

For any given frequency $\omega \in \Omega_c$, this condition is equivalent to a disk in the complex plane that is centered at

$$N(j\omega)X(j\omega,\boldsymbol{\rho})+M(j\omega)Y(j\omega,\boldsymbol{\rho})$$

and has a radius of $\gamma^{-1}\left|W_1(j\omega)M(j\omega)Y(j\omega,\boldsymbol{\rho})\right|$; this circle does not intersect with or include the origin. Fig. 3.1 displays a graphical interpretation of this condition. The following results are recalled before preceding with the theoretical contributions of this chapter.

Definition 3.1. *(Strictly Positive Real (SPR) System [102]) A transfer function $A(s)$ is strictly positive real if*

$$\Re\{A(s)\} > 0, \quad \forall \Re\{s\} > 0.$$

Lemma 3.1. *(Conditions of SPR Systems [102]) A transfer function $A(s)$ is strictly positive real if and only if*

- *$A(s)$ is Hurwitz*
- *$\Re\{A(j\omega)\} > 0$ for all $\omega \in \Omega_c$*

- *The poles of $A(s)$ on the $j\omega$ axis are simple (i.e., distinct) and the associated residues are real and non-negative*

The geometrical construction in Fig. 3.1 will now be used to prove the following lemma:

Lemma 3.2. *Suppose that*

$$H(j\omega,\boldsymbol{\rho}) = W_1(j\omega)M(j\omega)Y(j\omega,\boldsymbol{\rho})\left[N(j\omega)X(j\omega,\boldsymbol{\rho}) + M(j\omega)Y(j\omega,\boldsymbol{\rho})\right]^{-1}$$

is the frequency response of a bounded analytic function in the right half plane. Then, (3.1) is met if and only if there exists a stable proper rational transfer function $F(s)$ that satisfies

$$\Re\left\{\left[N(j\omega)X(j\omega,\boldsymbol{\rho}) + M(j\omega)Y(j\omega,\boldsymbol{\rho})\right]F(j\omega)\right\} > \gamma^{-1}\left|W_1(j\omega)M(j\omega)Y(j\omega,\boldsymbol{\rho})F(j\omega)\right|, \quad \forall\omega\in\Omega_c.$$

Proof: The basic idea is similar to that of the proof of Theorem 1 in [103]. It is clear that (3.1) is satisfied if and only if the disk of radius $\gamma^{-1}|W_1(j\omega)M(j\omega)Y(j\omega,\boldsymbol{\rho})|$ centered at $N(j\omega)X(j\omega,\boldsymbol{\rho})+M(j\omega)Y(j\omega,\boldsymbol{\rho})$ does not include the origin for all $\omega\in\Omega_c$, i.e.,

$$|N(j\omega)X(j\omega,\boldsymbol{\rho}) + M(j\omega)Y(j\omega,\boldsymbol{\rho})| > \gamma^{-1}|W_1(j\omega)M(j\omega)Y(j\omega,\boldsymbol{\rho})|.$$

This is equivalent to the existence of a line passing through the origin that does not intersect the disk. Therefore, at every given frequency, ω, there exists a complex number $f(j\omega)$ that can rotate the disk such that it lays inside the right hand side of the imaginary axis. Hence, we have

$$\Re\left\{\left[N(j\omega)X(j\omega,\boldsymbol{\rho}) + M(j\omega)Y(j\omega,\boldsymbol{\rho}) - \gamma^{-1}|W_1(j\omega)M(j\omega)Y(j\omega,\boldsymbol{\rho})|e^{j\theta}\right]f(j\omega)\right\} > 0 \qquad \forall\omega\in\Omega_c, \forall\theta\in[0\,,\,2\pi[. \tag{3.3}$$

Since $f(j\omega) = |f(j\omega)|e^{j\theta_f}$, then the above condition can be expressed as

$$\Re\left\{\left[N(j\omega)X(j\omega,\boldsymbol{\rho}) + M(j\omega)Y(j\omega,\boldsymbol{\rho})\right]f(j\omega)\right\} > \gamma^{-1}|W_1(j\omega)M(j\omega)Y(j\omega,\boldsymbol{\rho})f(j\omega)|\cos(\theta+\theta_f) \qquad \forall\omega\in\Omega_c, \forall\theta\in[0\,,\,2\pi[. \tag{3.4}$$

However, (3.4) is satisfied if and only if:

$$\Re\left\{\left[N(j\omega)X(j\omega,\boldsymbol{\rho}) + M(j\omega)Y(j\omega,\boldsymbol{\rho})\right]f(j\omega)\right\} > \gamma^{-1}|W_1(j\omega)M(j\omega)Y(j\omega,\boldsymbol{\rho})f(j\omega)|, \quad \forall\omega\in\Omega_c. \tag{3.5}$$

In [103], it is shown that $f(j\omega)$ can be approximated arbitrarily well by the frequency response of a stable transfer function $F(s)$ if and only if

$$Z = \left(N(j\omega)X(j\omega,\boldsymbol{\rho}) + M(j\omega)Y(j\omega,\boldsymbol{\rho}) - \gamma^{-1}|W_1(j\omega)M(j\omega)Y(j\omega,\boldsymbol{\rho})|e^{j\theta}\right)^{-1} \tag{3.6}$$

is analytic in the right half plane for all $\gamma_0 > \gamma$ and all $\theta \in [0, 2\pi[$. However, $[N(j\omega)X(j\omega,\boldsymbol{\rho}) + M(j\omega)Y(j\omega,\boldsymbol{\rho})]^{-1}$ is stable because of the stability of $H(j\omega,\boldsymbol{\rho})$. On the other hand, by decreasing γ_0 from infinity to γ, the poles of Z move continuously with γ_0. Therefore, Z is not analytic in the right half plane if and only if $Z^{-1}(j\omega) = 0$ for a given frequency, which is not the case because the origin is not in the interior of the circle $\gamma_0^{-1}|W_1(j\omega)M(j\omega)Y(j\omega,\boldsymbol{\rho})|e^{j\theta}$ for all $\omega \in \Omega_c$. ■

For notation purposes, and for the remaining sections of this chapter, the dependency in $j\omega$ will be omitted and reiterated when deemed necessary. However, the dependency in $\boldsymbol{\rho}$ will continue to be highlighted.

3.2.2 Nominal and robust performance

The set of all controllers that meet the nominal performance condition defined by the weighted norm of sensitivity functions is asserted in the following theorem.

Theorem 3.1. *Given the frequency response model G in (2.9) and the frequency response of a bounded weighting filter W_1, the following statements are equivalent:*
(a) *There exists a controller $K(\boldsymbol{\rho})$ that stabilizes G and*

$$\sup_{\omega\in\Omega_c} \left| W_1 \left[1 + GK(\boldsymbol{\rho})\right]^{-1} \right| < \gamma. \tag{3.7}$$

(b) *There exist $X(\boldsymbol{\rho}), Y(\boldsymbol{\rho}) \in \mathbf{RH}_\infty$ with $K(\boldsymbol{\rho}) = X(\boldsymbol{\rho})Y^{-1}(\boldsymbol{\rho})$, such that*

$$\gamma^{-1} \left| W_1 MY(\boldsymbol{\rho}) \right| < \Re\left\{ NX(\boldsymbol{\rho}) + MY(\boldsymbol{\rho}) \right\}, \quad \forall \omega \in \Omega_c. \tag{3.8}$$

Proof: (**b** ⇒ **a**)
$NX(\boldsymbol{\rho}) + MY(\boldsymbol{\rho})$ is analytic in the right half plane and its real part is positive for all $\omega \in \Omega_c$. However, it is evident that

$$\Re\left\{ NX(\boldsymbol{\rho}) + MY(\boldsymbol{\rho}) \right\} > 0 \iff \Re\left\{ [NX(\boldsymbol{\rho}) + MY(\boldsymbol{\rho})]^{-1} \right\} > 0, \quad \forall \omega \in \Omega_c.$$

Thus by the SPR condition in Lemma 3.1, $[NX(\boldsymbol{\rho}) + MY(\boldsymbol{\rho})]^{-1}$ is Hurwitz and therefore $K(\boldsymbol{\rho})$ stabilizes G. On the other hand, we have

$$\left| NX(\boldsymbol{\rho}) + MY(\boldsymbol{\rho}) \right| \geq \Re\left\{ NX(\boldsymbol{\rho}) + MY(\boldsymbol{\rho}) \right\}, \quad \forall \omega \in \Omega_c,$$

which leads to

$$\left| W_1 MY(\boldsymbol{\rho}) \right| < \gamma \left| NX(\boldsymbol{\rho}) + MY(\boldsymbol{\rho}) \right|, \quad \forall \omega \in \Omega_c$$

and consequently to (3.7) in Statement (**a**).

(**a** ⇒ **b**)
Assume that $K(\boldsymbol{\rho}') = X(\boldsymbol{\rho}')Y^{-1}(\boldsymbol{\rho}')$ satisfies Statement (**a**) but not Statement (**b**). Then, ac-

cording to Lemma 3.2, there exists a stable proper rational transfer function $F(s)$ such that

$$\Re\{[NX(\boldsymbol{\rho}')+MY(\boldsymbol{\rho}')]F\} > \gamma^{-1}\left|W_1MY(\boldsymbol{\rho}')F\right|, \quad \forall\omega\in\Omega_c.$$

Therefore, there exist $X(\boldsymbol{\rho})=X(\boldsymbol{\rho}')F$ and $Y(\boldsymbol{\rho})=Y(\boldsymbol{\rho}')F$ with $K(\boldsymbol{\rho})=X(\boldsymbol{\rho})Y^{-1}(\boldsymbol{\rho})=X(\boldsymbol{\rho}')Y^{-1}(\boldsymbol{\rho}')$, such that Statement (**b**) holds. ■

Robust stability:

The necessary and sufficient conditions for robust stability of closed-loop systems with disk-type frequency-domain uncertainty can be developed in a similar manner. The robust stability condition for the coprime factor uncertainty is given by [96, 104]

$$\left\|\left|W_m\mathscr{S}_s(\boldsymbol{\rho})M^{-1}\right|+\left|W_n\mathscr{S}_t(\boldsymbol{\rho})N^{-1}\right|\right\|_\infty < 1. \tag{3.9}$$

This condition can be written in the frequency domain as

$$\left|W_mY(\boldsymbol{\rho})\right|+\left|W_nX(\boldsymbol{\rho})\right| < \left|NX(\boldsymbol{\rho})+MY(\boldsymbol{\rho})\right|, \qquad \forall\omega\in\Omega_c. \tag{3.10}$$

Therefore, by the necessary and sufficient conditions in Theorem 3.1, the following convex constraint ensures robust stability:

$$\left|W_mY(\boldsymbol{\rho})\right|+\left|W_nX(\boldsymbol{\rho})\right| < \Re\left\{NX(\boldsymbol{\rho})+MY(\boldsymbol{\rho})\right\}, \qquad \forall\omega\in\Omega_c. \tag{3.11}$$

Robust performance:

On the other hand, if we consider the nominal performance as $\|W_1\mathscr{S}_s(\boldsymbol{\rho})\|_\infty<\gamma$, the performance will be satisfied for all models in the uncertainty set in (2.10) if $\|W_1\tilde{\mathscr{S}}_s(\boldsymbol{\rho})\|_\infty<\gamma$, or:

$$\left|W_1\tilde{M}Y(\boldsymbol{\rho})\right| < \gamma\left|\tilde{M}Y(\boldsymbol{\rho})+\tilde{N}X(\boldsymbol{\rho})\right|, \quad \forall\omega\in\Omega_c. \tag{3.12}$$

By substituting the relations from (2.10) into the above condition, we obtain the following constraint:

$$\begin{aligned}\left|W_1MY(\boldsymbol{\rho})+W_1|W_m|\delta_m e^{j\theta_m}Y(\boldsymbol{\rho})\right| < \gamma\Big|&MY(\boldsymbol{\rho})+NX(\boldsymbol{\rho})\\ &+|W_m|\delta_m e^{j\theta_m}Y(\boldsymbol{\rho})+|W_n|\delta_n e^{j\theta_n}X(\boldsymbol{\rho})\Big|\\ &\forall\omega\in\Omega_c,\forall\theta_m\in[0\,,2\pi],\forall\theta_n\in[0\,,2\pi].\end{aligned} \tag{3.13}$$

As a worst case consideration, $\delta_n=\delta_m=1$ can be considered (which represents the outermost disk of the uncertain set in (2.10)). A sufficient condition for the above constraint is:

$$\sup_{\omega\in\Omega_c} \frac{\left|W_1 MY(\boldsymbol{\rho})\right| + \left|W_1 W_m Y(\boldsymbol{\rho})\right|}{\left|NX(\boldsymbol{\rho}) + MY(\boldsymbol{\rho})\right| - \left|W_n X(\boldsymbol{\rho})\right| - \left|W_m Y(\boldsymbol{\rho})\right|} < \gamma. \tag{3.14}$$

Equivalently, for any $\omega \in \Omega_c$, a disk of radius

$$r_\mu(\boldsymbol{\rho}) = \gamma^{-1}|W_1 MY(\boldsymbol{\rho})| + \gamma^{-1}|W_1 W_m Y(\boldsymbol{\rho})| + |W_n X(\boldsymbol{\rho})| + |W_m Y(\boldsymbol{\rho})| \tag{3.15}$$

centered at $NX(\boldsymbol{\rho}) + MY(\boldsymbol{\rho})$ should not include the origin. This can be presented as a set of convex constraints with respect to $X(\boldsymbol{\rho})$ and $Y(\boldsymbol{\rho})$ as

$$r_\mu(\boldsymbol{\rho}) < \Re\left\{NX(\boldsymbol{\rho}) + MY(\boldsymbol{\rho})\right\}, \quad \forall\omega \in \Omega_c. \tag{3.16}$$

Note that the above constraint ensures also the robust stability constraint in (3.11).

Remark. *The conservatism of the constraint in (3.14) can be reduced by choosing:*

$$r_\mu(\boldsymbol{\rho},\theta_m) < \Re\left\{NX(\boldsymbol{\rho}) + MY(\boldsymbol{\rho}) + |W_m| e^{j\theta_m} Y(\boldsymbol{\rho})\right\}, \qquad \forall\omega \in \Omega_c, \forall\theta_m \in [0\,, 2\pi], \tag{3.17}$$

where

$$r_\mu(\boldsymbol{\rho},\theta_m) = \gamma^{-1}\left|W_1 MY(\boldsymbol{\rho}) + W_1|W_m| e^{j\theta_m} Y(\boldsymbol{\rho})\right| + \left|W_n X(\boldsymbol{\rho})\right|. \tag{3.18}$$

The implementation of this constraint requires gridding in ω and θ_m, which leads to a significant increase in the number of constraints and computational burden. However, for Hurwitz systems, since $M = 1$ and there is no disk uncertainty associated to M, the term $W_1|W_m|e^{j\theta_m} Y$ will be removed from the above equation.

3.2.3 Multi-model and frequency-domain polytopic uncertainty

It is clear that the following constraints

$$\gamma^{-1}\left|W_1 M_i Y(\boldsymbol{\rho})\right| < \Re\left\{N_i X(\boldsymbol{\rho}) + M_i Y(\boldsymbol{\rho})\right\}, \quad \forall\omega \in \Omega_c \quad , \quad \text{for } i = 1,\ldots,\ell \tag{3.19}$$

are necessary and sufficient conditions for robust performance of the closed-loop system with multi-model uncertainty. However, it can be shown that there are only sufficient conditions for frequency-domain polytopic uncertainty. It suffices to compute the convex combination of the constraints in (3.19) as

$$\gamma^{-1}\sum_{i=1}^{\ell}\lambda_i\left|W_1 M_i Y(\boldsymbol{\rho})\right| < \Re\left\{\sum_{i=1}^{\ell}\lambda_i\left[N_i X(\boldsymbol{\rho}) + M_i Y(\boldsymbol{\rho})\right]\right\}, \quad \forall\omega \in \Omega_c.$$

Noting that:

$$\left|\sum_{i=1}^{\ell}\lambda_i W_1 M_i Y(\boldsymbol{\rho})\right| \leq \sum_{i=1}^{\ell}\lambda_i |W_1 M_i Y(\boldsymbol{\rho})|, \tag{3.20}$$

we obtain:

$$\gamma^{-1}\left|W_1 M(\lambda) Y(\boldsymbol{\rho})\right| < \Re\left\{N(\lambda)X(\boldsymbol{\rho}) + M(\lambda)Y(\boldsymbol{\rho})\right\}, \quad \forall \omega \in \Omega_c.$$

Then, according to Theorem 3.1, the upper bound for the weighted sensitivity function is satisfied for all λ.

Although the constraints for polytopic uncertainty are only sufficient, necessary and sufficient conditions can be developed for some class of models and some sensitivity functions. The following theorem represents the results for systems that have frequency-domain polytopic uncertainty only in N.

Theorem 3.2. *Consider the model given in (2.13) with* $N(\lambda, j\omega) = \sum_{i=1}^{\ell}\lambda_i N_i(j\omega)$ *and* $M(\lambda, j\omega) = M(j\omega)$. *Then, the following statements are equivalent:*
(a) *Controller* $K(\boldsymbol{\rho})$ *stabilizes* $G(\lambda) = N(\lambda)M^{-1}$ *and*

$$\sup_{\omega\in\Omega_c}\left|W_1\left[1 + G(\lambda)K(\boldsymbol{\rho})\right]^{-1}\right| < \gamma.$$

(b) *There exist* $X(\boldsymbol{\rho}), Y(\boldsymbol{\rho}) \in \mathbf{RH}_\infty$ *such that* $K(\boldsymbol{\rho}) = X(\boldsymbol{\rho})Y^{-1}(\boldsymbol{\rho})$, *and*

$$\gamma^{-1}\left|W_1 M Y(\boldsymbol{\rho})\right| < \Re\left\{N_i X(\boldsymbol{\rho}) + M Y(\boldsymbol{\rho})\right\}, \quad \forall \omega \in \Omega_c, \quad \textit{for} \quad i = 1, \ldots, \ell. \tag{3.21}$$

Proof : (**b** $\Rightarrow$ **a**)
The convex combination of the constraints in (3.21) leads to

$$\gamma^{-1}\left|W_1 M Y(\boldsymbol{\rho})\right| < \Re\left\{N(\lambda)X(\boldsymbol{\rho}) + M Y(\boldsymbol{\rho})\right\} \tag{3.22}$$

for all $\omega \in \Omega_c$ and for all λ. So Statement (**a**) can be concluded using the result of Theorem 3.1.

(**a** $\Rightarrow$ **b**)
Suppose that (**a**) is satisfied with the controller $K(\boldsymbol{\rho}') = X(\boldsymbol{\rho}')Y^{-1}(\boldsymbol{\rho}')$. Therefore, all disks of the same radius, $\gamma^{-1}|W_1 M Y(\boldsymbol{\rho}')|$, centered inside a polygon with ℓ vertices, $N_i X(\boldsymbol{\rho}') + M Y(\boldsymbol{\rho}')$, do not include the origin. This represents a convex set, which is the convex hull of the ℓ disks. Therefore, there exists a line that passes through the origin and does not intersect this convex set. As a result, similar to the proof of Lemma 3.2, there exists a stable transfer function $F(s)$ such that:

$$\Re\left\{\left[N_i X(\boldsymbol{\rho}') + M Y(\boldsymbol{\rho}') - \gamma^{-1}|W_1 M Y(\boldsymbol{\rho}')|\right]F(j\omega)\right\} > 0, \quad \forall \omega \in \Omega_c, \quad \text{for} \quad i = 1, \ldots, \ell.$$

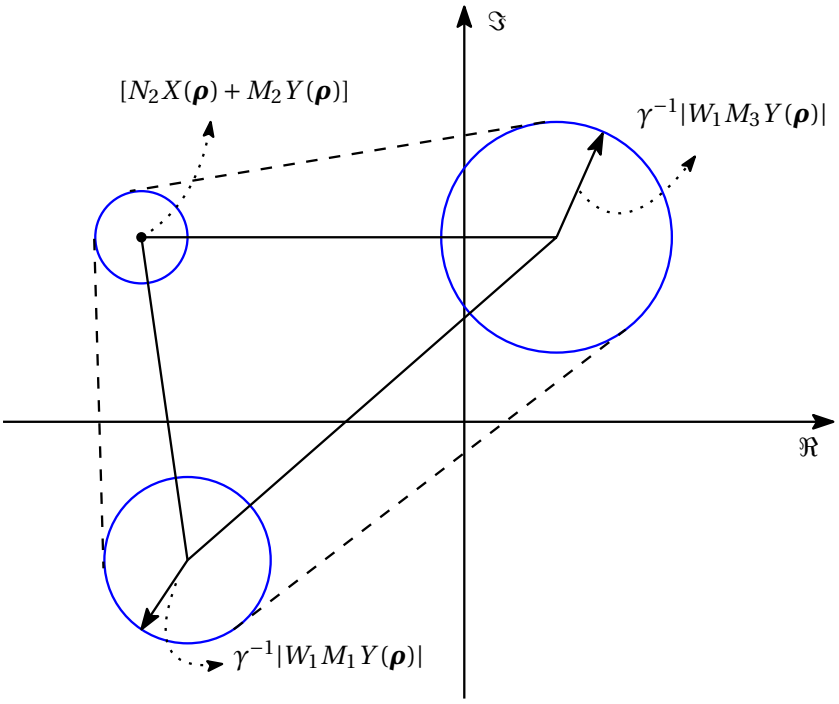

Figure 3.2 – Illustration of the constraints for polytopic uncertainty with 3 vertices.

Hence $X = X(\boldsymbol{\rho}')F$ and $Y = Y(\boldsymbol{\rho}')F$ satisfies the inequalities in Statement (**b**). ■

Theorem 3.2 considers only the plant model with polytopic uncertainty in N. This represents the class of Hurwitz systems that may have some fixed poles on the imaginary axis. The theorem also holds for unstable systems with no uncertainty in M. A polytopic uncertainty in M will change the radius of the disks centered at $N_iX(\boldsymbol{\rho}) + M_iY(\boldsymbol{\rho})$, such that the whole set of the disks will not be necessarily convex. Figure 3.2 shows a case in which the set of the disks is not convex but is inside the convex hull of the disks. This is always true because of the constraint in (3.20). In the special case shown in Fig. 3.2, we observe that the set of disks does not include the origin but the convex hull does. Similarly, Statement (**b**) in Theorem 3.2 is a sufficient condition for satisfying an upper bound on the weighted sensitivity functions $\mathscr{S}_t(\boldsymbol{\rho})$ or $\mathscr{S}_v(\boldsymbol{\rho})$, since the radius of the disks, at each frequency, will not be constant for the whole polygon. However, it will be necessary and sufficient for an upper bound on the weighted sensitivity function $\mathscr{S}_u(\boldsymbol{\rho})$ in (2.36).

Table 3.1 – Procedure for optimizing low-order controllers.

Algorithm: Convex optimization for low-order controller design

1. Choose a large arbitrary value for ζ and a very large controller order n. Then, compute X_n and Y_n by solving the optimization problem in (3.23).

2. Find $n^\circ \ll n$ dominant poles $[\zeta_1, \ldots, \zeta_{n^\circ}]$ of X_n and Y_n by frequency analysis or model reduction methods.

3. Consider a generalized orthonormal basis function [105] using the estimated dominant poles as

$$\phi_i(s) = \frac{\sqrt{\Re\{\zeta_{i-1}\}}}{s+\zeta_{i-1}} \prod_{k=1}^{i-2} \left(\frac{s-\zeta_k^*}{s+\zeta_k} \right), \qquad i = 2, \ldots, n^\circ + 1, \tag{3.24}$$

where ζ_k^* is the complex conjugate of ζ_k. Then, compute X_{n° and Y_{n° using the optimization problem in (3.23).

3.3 Fixed-order controller design

The minimization of $\|W_1 \mathscr{S}_s(\boldsymbol{\rho})\|_\infty$ becomes an optimization problem that can be solved as follows:

$$\begin{aligned} \underset{\gamma,\boldsymbol{\rho}}{\text{minimize}} \quad & \gamma \\ \text{subject to:} \quad & \left| W_1 M Y(\boldsymbol{\rho}) \right| < \gamma \Re\left\{ N X(\boldsymbol{\rho}) + M Y(\boldsymbol{\rho}) \right\} \\ & \forall \omega \in \Omega_c. \end{aligned} \tag{3.23}$$

In general, this optimization problem is not convex. However, by linearly parameterizing the coprime factors of the controller $X(\boldsymbol{\rho})$ and $Y(\boldsymbol{\rho})$, it becomes a quasi-convex optimization problem and can be solved by using a bisection algorithm to obtain the optimal solution for γ. Within a given tolerance, the bisection algorithm ensures the convergence to the global optimum solution. There are several practical and implementation issues in this optimization problem that will be addressed in this section.

3.3.1 Controller parameterization

The basis functions defined in (2.30) have only one parameter to be selected (ξ). It will be shown that for high-order controllers, the choice of the basis function is not important. However, for low-order controllers, this choice has a significant effect on the performance. Although a rigorous method for the optimal choice of the basis functions is an open problem, a three-step practical procedure (for continuous-time systems) is described in Table 3.1.

3.3.2 Convergence to the optimal solution

In this sub-section, we will show that the optimal solution ($\gamma_n^\star$) to the optimization problem in (3.23) (for a linear parameterization of $X(\boldsymbol{\rho})$ and $Y(\boldsymbol{\rho})$ by the orthogonal basis functions of order n) will converge to the least upper bound of the infinity norm of the weighted sensitivity function when n goes to infinity. The following Lemma is required to prove this convergence:

Lemma 3.3. *Let $X_n^\dagger(s)$ be the projection of $X_o(s) \in \mathbf{RH}_\infty$ into the subspace spanned by the orthogonal basis functions $\phi(s)$ in (2.30). Then [106] :*

$$\lim_{n\to\infty} \left\| X_o - X_n^\dagger \right\|_\infty = 0.$$

Theorem 3.3. *Suppose that the controller $K_o(s)$ achieves the optimal $\mathscr{H}_\infty$ performance for the plant model $G = NM^{-1}$ such that*

$$\gamma_o^\star = \inf_K \sup_\omega \left| W_1(1+GK)^{-1} \right| = \sup_\omega \left| W_1(1+GK_o)^{-1} \right|.$$

Suppose also that $\gamma_n^\star$ is the optimal solution of the convex optimization problem in (3.23) when X and Y are parameterized by an n dimensional orthogonal basis function. Then $\gamma_n^\star$ converges monotonically from above to $\gamma_o^\star$ when $n \to \infty$.

Proof : According to Theorem 3.1, there exist $X_o(s), Y_o(s) \in \mathbf{RH}_\infty$ such that $K_o(s) = X_o(s)Y_o^{-1}(s)$ and

$$\gamma_o^\star = \sup_{\omega\in\Omega_c} \left| \frac{W_1 M Y_o}{\Re\{NX_o + MY_o\}} \right|. \tag{3.25}$$

Take $X_n^\dagger$ and $Y_n^\dagger$ as the projections of X_o and Y_o into the subspace spanned by n-dimensional orthogonal basis functions and define

$$\gamma_n^\dagger = \sup_{\omega\in\Omega_c} \left| \frac{W_1 M Y_n^\dagger}{\Re\{NX_n^\dagger + MY_n^\dagger\}} \right|. \tag{3.26}$$

We assume that $\gamma_n^\dagger$ is bounded, i.e., $\Re\{NX_n^\dagger + MY_n^\dagger\} \neq 0$ for all $\omega \in \Omega_c$. This can be proved if n is large enough using contradiction and based on the fact that $\Re\{NX_o + MY_o\} > \epsilon > 0$. Assume that $j\omega^\dagger$ is a zero of $\Re\{NX_n^\dagger + MY_n^\dagger\}$. Therefore, at $\omega = \omega^\dagger$, one has

$$\Re\{NX_o + MY_o\} = \Re\{N(X_o - X_n^\dagger) + M(Y_o - Y_n^\dagger)\} > \epsilon. \tag{3.27}$$

However, $\Re\{N(X_o - X_n^\dagger) + M(Y_o - Y_n^\dagger)\}$ can be made arbitrarily small by increasing n, which shows that for large but finite n, $\Re\{NX_n^\dagger + MY_n^\dagger\} \neq 0$.

Now, let us compute $|\gamma_o^\star - \gamma_n^\dagger|$ using (3.25) and (3.26):

$$\left|\gamma_o^\star - \gamma_n^\dagger\right| \leq \sup_{\omega\in\Omega_c} \left| \frac{|W_1 M Y_o|}{\Re\{NX_o + MY_o\}} - \frac{|W_1 M Y_n^\dagger|}{\Re\{NX_n^\dagger + MY_n^\dagger\}} \right|. \tag{3.28}$$

On the other hand, according to Lemma 3.3 we have

$$\lim_{n\to\infty} \left\| X_o - X_n^\dagger \right\|_\infty = 0, \quad \lim_{n\to\infty} \left\| Y_o - Y_n^\dagger \right\|_\infty = 0.$$

Therefore, $\lim_{n\to\infty} |Y_n^\dagger| \to |Y_o|, \lim_{n\to\infty} \Re\{X_n^\dagger\} \to \Re\{X_o\}$ and $\lim_{n\to\infty} \Re\{Y_n^\dagger\} \to \Re\{Y_o\}$ for all $\omega \in \Omega_c$. As a result, we obtain

$$\lim_{n\to\infty} \left|\gamma_o^\star - \gamma_n^\dagger\right| = 0. \tag{3.29}$$

On the other hand, $\gamma_n^\star$, the solution of the optimization problem in (3.23), is always less than or equal to $\gamma_n^\dagger$ and greater than the optimal solution $\gamma_o^\star$. Thus $\gamma_n^\star$ converges from above to $\gamma_o^\star$ and this convergence is monotonic because the basis functions of order n are a subset of those of order $n+1$, which ensures that $\gamma_{n+1}^\star \leq \gamma_n^\star$. ■

This result shows that there is a trade-off between the controller complexity and the achieved performance. Increasing the controller order leads to a more complex optimization problem and possible numerical implementation problems associated with high-order controllers.

3.3.3 Finite number of constraints

The constraints in (3.23) should be satisfied for all $\omega \in \Omega_c$, which is an infinite set. This problem is known as a semi-infinite programming (SIP) problem and there exist different methods to solve it. A very simple and practical solution to this problem is to choose a finite set of frequencies $\Omega_\eta = \{\omega_1, \omega_2, \cdots, \omega_\eta\}$ and satisfy the constraints for this set. In this manner, the optimization problem is converted to a SDP problem which can be solved efficiently with solvers that are readily available.

The frequency points may be equally spaced, logarithmically spaced or chosen based on some information about the frequency response of the plant model and the desired bandwidth (more frequency points around the resonance frequencies and closed-loop bandwidth). The optimal choice of the frequency points is an open problem. However, the complexity of the optimization algorithm grows linearly with the number of frequency points (since the problem is quasi-convex) and so it can be chosen large enough.

An alternative is to use a randomized approach where the constraints are satisfied for a finite set of randomly chosen frequencies. In this approach, a bound on the violation probability of the constraints can be derived and approaches zero when the number of samples goes to infinity (see [107] and [108]). It should be mentioned that in a data-driven framework, the frequency domain uncertainties are given by some stochastic bounds. Therefore, even if the

constraints are met for all ω, the stability, robustness and performance are guaranteed within a probability level. As a result, the use of randomized methods to solve the robust optimization problem in (3.23) is fully compatible with the uncertainty description of the frequency-domain model of the proposed approach.

3.3.4 Solution by linear programming

The convex constraints in (3.23) are equivalent to the following linear constraints:

$$\Re\left\{NX(\boldsymbol{\rho})+MY(\boldsymbol{\rho})-\gamma^{-1}e^{j\theta}W_1MY(\boldsymbol{\rho})\right\}>0,\quad \forall\omega\in\Omega_c \tag{3.30}$$

and $\forall\theta\in[0,2\pi[$. In fact, $\gamma^{-1}e^{j\theta}W_1MY(\boldsymbol{\rho})$ represents the circle in Fig. 3.1. Note that $e^{j\theta}$ can be very well approximated by a polygon of $p_c>2$ vertices with least area that circumscribes it. By gridding ω and bounding the circle $e^{j\theta}$, a finite set of linear constraints can be obtained as

$$\Re\left\{N(j\omega_i)X(j\omega_i,\boldsymbol{\rho})+M(j\omega_i)Y(j\omega_i,\boldsymbol{\rho})-\gamma^{-1}\frac{e^{j2\pi k/p_c}}{\cos(\pi/p_c)}W_1(j\omega_i)M(j\omega_i)Y(j\omega_i,\boldsymbol{\rho})\right\}>0 \tag{3.31}$$

for $i=1,\ldots,\eta$ and $k=1,\ldots,p_c$. Therefore, the convex constraints in (3.30) can be replaced by $\eta\times p_c$ linear constraints. and then γ can be minimized by an iterative bisection algorithm. At each iteration, a linear feasibility problem can be solved efficiently even if the number of constraints are large.

3.4 Case Studies

3.4.1 Case 1: Multi-model uncertainty

In this example, a simulation is carried out to compare the traditional μ-synthesis method and the proposed approach for a set of unstable models. The controlled plants are taken from an example in the robust control toolbox of `MATLAB`. The nominal plant model is a first-order unstable system $G_0(s)=2(s-2)^{-1}$, and the family of perturbed plants are variations of $G_0(s)$ as follows:

$$\begin{aligned}
G_1(s)&=G_0(s)\frac{1}{0.06s+1} & G_4(s)&=G_0(s)e^{-0.04s}\\
G_2(s)&=G_0(s)\frac{50^2}{s^2+10s+50^2} & G_5(s)&=\frac{2.4}{s-2.2}\\
G_3(s)&=G_0(s)\frac{70^2}{s^2+28s+70^2} & G_6(s)&=\frac{1.6}{s-1.8}
\end{aligned} \tag{3.32}$$

Compared with the nominal plant, G_1 has an extra lag, G_2 and G_3 have high frequency resonance modes, G_4 has an additional time delay, G_5 and G_6 have pole and gain migrations.

Remark. *It is imperative to note that these models are simply used to obtain the frequency response functions of the perturbed plants. The actual controller synthesis does not rely on these parametric models.*

The control task is to design a linear controller to simultaneously stabilize this family of unstable plants and minimize the infinity norm of the weighted sensitivity functions, i.e.:

$$\begin{aligned} \underset{\gamma,\boldsymbol{\rho}}{\text{minimize}} \quad & \gamma \\ \text{subject to:} \quad & \left\| W_1 \mathscr{S}_s^i(\boldsymbol{\rho}) \right\|_\infty < \gamma \\ & \left\| W_2 \mathscr{S}_t^i(\boldsymbol{\rho}) \right\|_\infty < \gamma \\ & \text{for } i = 0, \ldots, 6, \quad \forall \omega \in \Omega_c, \end{aligned}$$

where

$$W_1(s) = \frac{0.33s + 4.248}{s + 0.008496} \quad ; \quad W_2(s) = \frac{0.1975s^2 + 0.6284s + 1}{7.901 \cdot 10^{-5} s^2 + 0.2514s + 400}$$

and where $\mathscr{S}_s^i(\boldsymbol{\rho})$ and $\mathscr{S}_t^i(\boldsymbol{\rho})$ represent the sensitivity functions with respect to the i^{th} plant model in G_i. The μ-synthesis method from the `MATLAB` robust control toolbox is used to solve this problem. The multi-model uncertainty is approximated with a fourth-order uncertainty weighting filter and a 18th-order controller is designed that achieves a performance of $\gamma_\mu^\star = 1.0248$. Comparable performance is achieved after reducing the controller order to 6.

Continuous-time Laguerre basis functions of order 5 with $\xi = 20$ and an integrator are used for the controller parameterization. A high frequency pole at 100 is used for constructing N_i and M_i for the models. For example, for $G_6(s) = N_6(s)M_6^{-1}(s)$:

$$N_6(s) = \frac{1.6}{s + 100}, \qquad M_6(s) = \frac{s - 1.8}{s + 100}.$$

The frequency response of the model is computed at $\eta = 200$ logarithmically spaced frequency points between 10^{-3} and 10^4 rad s^{-1}. The linearized constraints in (3.31) are used with a polygon of $p_c = 25$ vertices for over bounding $e^{j\theta}$. Solving the optimization problem leads to the following controller:

$$K(s) = \frac{0.26773(s+1)(s+2348)(s^2+19.82s+131.3)(s^2+28.5s+3510)}{s(s+7.759)(s^2+27.77s+556.5)(s^2+94.5s+12440)}$$

which leads to the step disturbance response depicted in Fig. 3.3. The resulting performance obtained from the proposed optimization problem is $\gamma^\star = 0.8852$. This is much smaller than that of the μ-synthesis method; in the proposed approach, there is no conservatism in modeling the multi-model uncertainties. It should be mentioned that in the μ-synthesis approach, the time delay in $G_4(s)$ is approximated with a first-order Padé function; in the proposed approach, the time-delay is taken into account with no approximation.

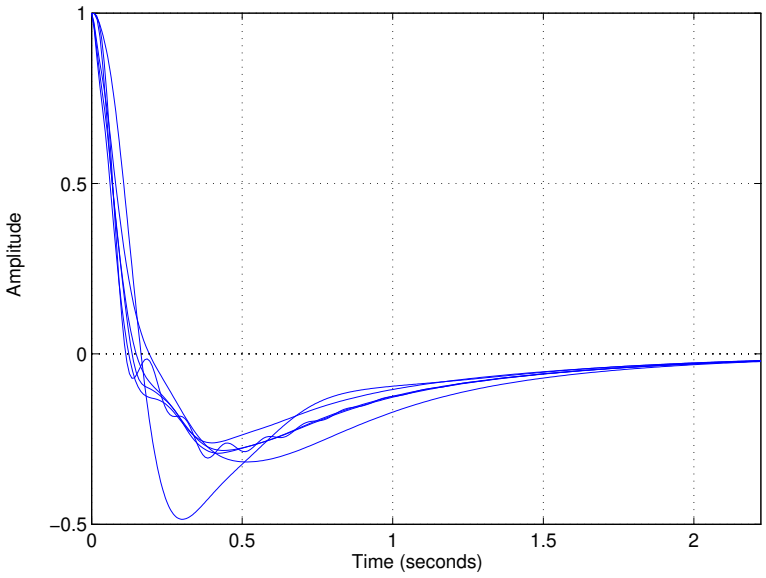

Figure 3.3 – Step responses for the family of closed-loop systems.

3.4.2 Case 2: Convergence to optimal performance

Consider a discrete-time SISO system given as

$$G(z) = \frac{z - 0.186}{z^3 - 1.116z^2 + 0.465z - 0.093}, \tag{3.33}$$

which uses a sampling time of $T_s = 1$ s. The goal is to design a controller with an integrator that minimizes $\left\| W_1 \mathscr{S}_s(\boldsymbol{\rho}) \right\|_\infty$, where

$$W_1(z) = \frac{0.4902(z^2 - 1.0431z + 0.3263)}{(z-1)(z-0.282)}. \tag{3.34}$$

For discrete-time controller synthesis, the controller is parameterized by discrete-time Laguerre basis functions as follows:

$$K(z) = X(z)Y^{-1}(z) \quad ; \quad X(z) = \boldsymbol{\rho}_x^T \phi(z)\,,\; Y(z) = \boldsymbol{\rho}_y^T \phi(z),$$

where $\boldsymbol{\phi}^T(z) = [1, \phi_1(z), \ldots, \phi_n(z)]$ and n is the controller order (with the Laguerre functions defined in (2.31)). It will be shown that by increasing the controller order, the side effect of the selection of the Laguerre parameter, ξ_z, is reduced.

In this example, $\eta = 50$ equally spaced frequency points between 0 and π are chosen. In order to have an integrator in the controller and to avoid unboundedness of W_1 at $\omega = 0$, the basis functions for $Y(z)$ are multiplied by $(z-1)/z$. Since the system is Schur, we choose

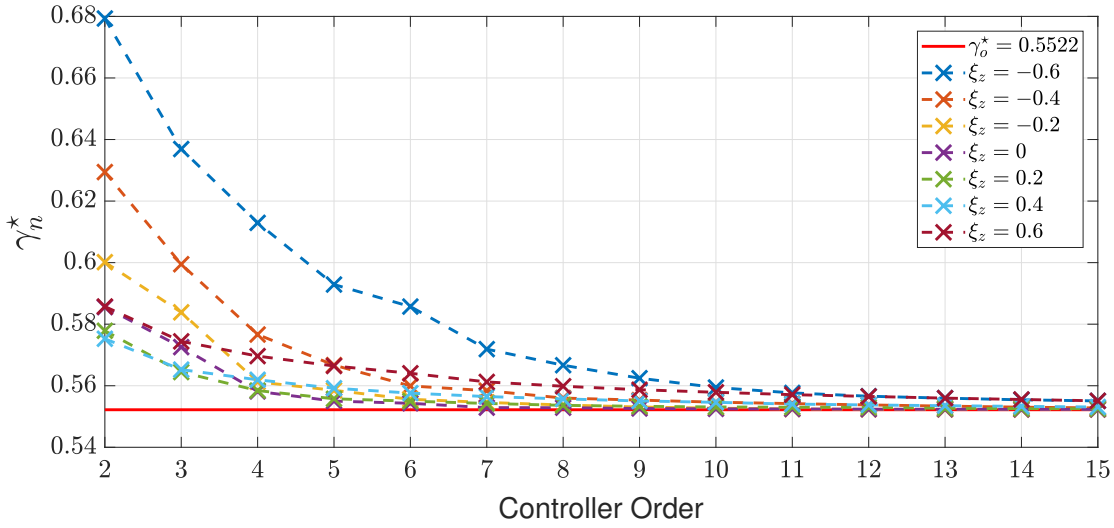

Figure 3.4 – $\gamma_n^\star$ versus the controller order with different Laguerre parameters.

$N(e^{j\omega}) = G(e^{j\omega})$ and $M(e^{j\omega}) = 1$. The convex constraints are linearized by approximating $e^{j\theta}$ with a polygon of $p_c = 50$ vertices.

The standard $\mathscr{H}_\infty$ control method in the Robust Control toolbox of MATLAB leads to the global optimal value of $\gamma_o^\star = 0.5522$ with a 6th order controller. Fig. 3.4 shows the optimal value, $\gamma_n^\star$, for different values of the parameter ξ_z in the Laguerre basis functions for varying controller orders n. It can be observed that the optimal solution converges monotonically and is independent of the value of ξ_z.

3.4.3 Case 3: Flexible Transmission System

In this example, experimental data is used to compute a robust controller which takes into consideration the frequency-domain uncertainty from the measurement process. An electro-mechanical flexible transmission system which consists of three disks connected by elastic belts was considered. The first disk was coupled to a servo motor which is derived by a current amplifier. The position of the third disk was measured with an incremental encoder and controlled by a proportional controller. The input of the system was the reference position for the third disk (see Fig. 3.5). This system was excited by a Pseudorandom binary sequence (PRBS) signal with a sampling period of $T_s = 40$ ms where data with length 765 was collected. Figure 3.6 shows the experimental data that was used to identify a frequency domain model using the spa command in the Identification toolbox of MATLAB. The Nyquist diagram of this spectral model together with the uncertainty disks of 0.95 probability are given in Fig. 3.7. The uncertainty disks were approximated by a polygon of $m = 20$ vertices and the goal was to

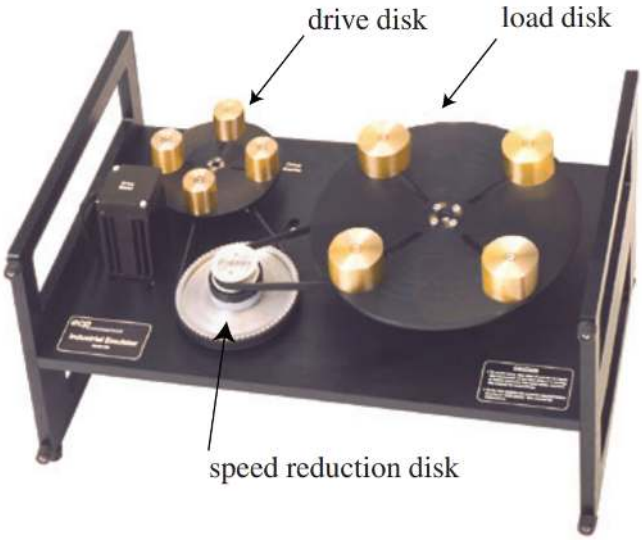

Figure 3.5 – Flexible transmission system

design a stabilizing controller that minimized γ, where $\left\| W_1 \mathscr{S}_s(\boldsymbol{\rho}) \right\|_\infty < \gamma$, with

$$W_1(z) = \frac{z - 0.96}{z - 1}.$$

In the proposed method, discrete-time Laguerre basis functions of order 4 with $\xi_z = 0$ (FIR filter) are considered for X and Y. The resulting controller is

$$K(z) = \frac{20.3(z^2 - 1.88z + 0.92)(z^2 - 1.278z + 0.6057)}{(z + 0.72)(z - 1)(z^2 + 0.209z + 0.563)},$$

which achieves an optimal performance of $\gamma^\star = 2.12$. Figure 3.8 shows the magnitude of the Bode diagram of the sensitivity function for the nominal model. It can be observed that the sensitivity function is small at low frequencies and its maximum value is less than 5dB, which guarantees a good stability margin.

3.5 Conclusion

A robust controller design method for LTI-SISO systems based on frequency-domain data is proposed. The necessary and sufficient conditions for the existence of a robust controller are represented by an infinite set of convex constraints and approximated with a finite set of linear constraints. This method can be easily applied to both continuous-time systems and discrete-time systems with time delay and multi-model uncertainty. In comparison with the classical $\mathscr{H}_\infty$ controller design methods, the following features can be highlighted:

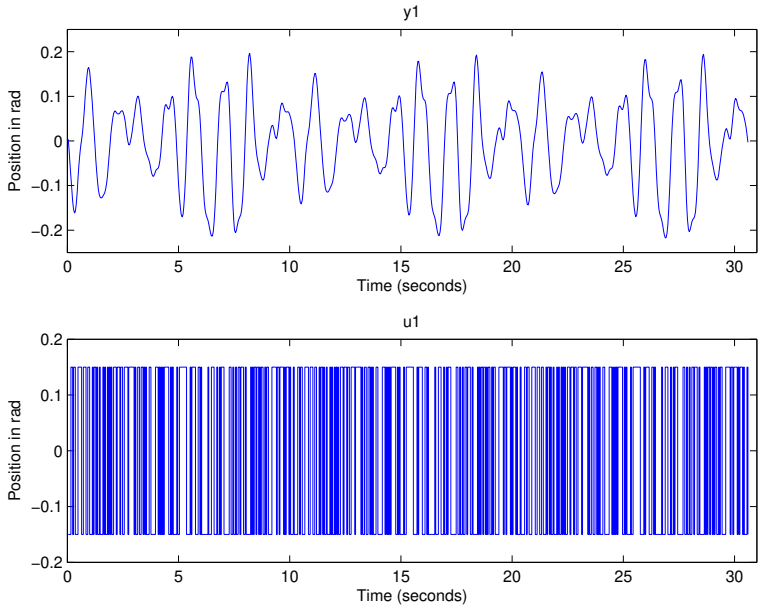

Figure 3.6 – Experimental identification data.

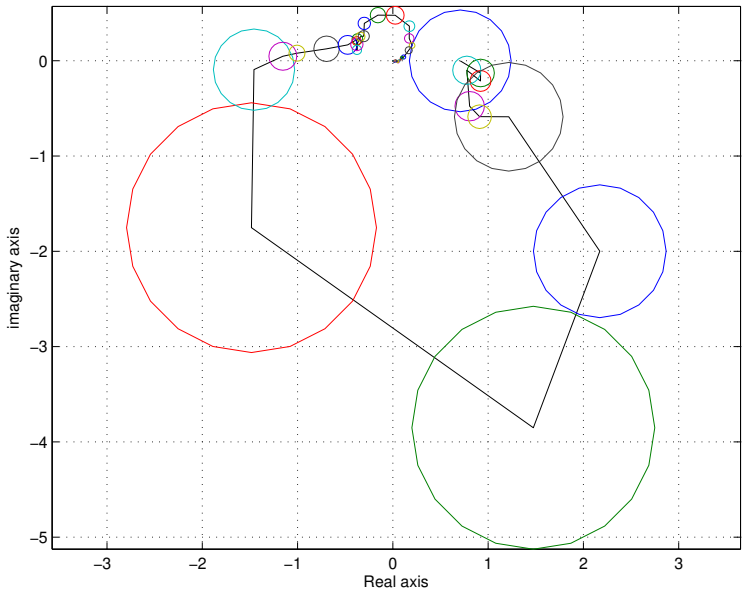

Figure 3.7 – Nyquist diagram of the spectral model together with uncertainty disks.

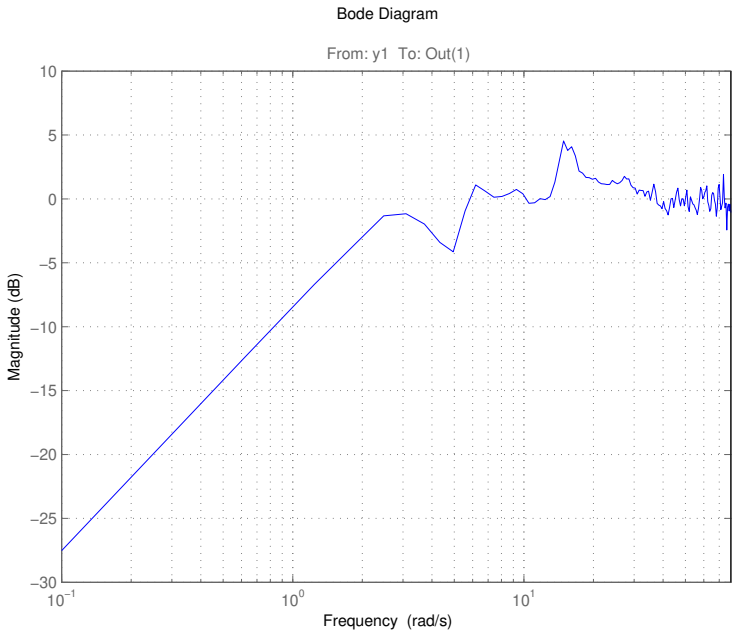

Figure 3.8 – Magnitude of the FRF of sensitivity function $\mathscr{S}_s$.

- The frequency response of the plant is the only requisite for controller synthesis where no parametric model is required
- Pure input/output time delay is considered with no approximation.
- Frequency-domain uncertainty is taken into account with reduced conservatism.
- Parametric uncertainty in identified models with noisy data can be considered in a stochastic sense with reduced conservatism.
- Fixed-order controllers can be designed in a convex optimization problem that considers a finite amount of constraints in the frequency domain.

It is shown that the choice of the basis functions affects the optimization results for low-order controllers. Chapters 6 and 7 will address this issue and consider designs for low-order controllers.

4 Robust RST Controller Design with Applications to Power Converters

4.1 Introduction

The method proposed in this chapter is an extension of the work in Chapter 3, where the necessary and sufficient conditions that ensures the $\mathscr{H}_\infty$ performance for multiple weighted sensitivity functions are presented using a discrete-time RST controller structure. The methods presented in Chapter 3 are combined with the ideas presented in [99] to develop a data-driven controller design methodology that guarantees $\mathscr{H}_\infty$ performance and closed-loop stability for linear systems that are subject to nonlinear distortions. With this method, a nonlinear system in $\mathscr{V}$ can be modeled as a BLA with an associated frequency-dependent uncertainty. By performing a set of identification experiments on the nonlinear system, the dynamics of the underlying linear system are guaranteed to lie in the set of these uncertainties. Additionally, since the parameters of the controller's denominator are the optimization variables, this method can lead to unstable controllers. Therefore, a sufficient condition is presented to ensure that the controller remains stable. Moreover, it is shown that as the controller order increases, the solution to the convex $\mathscr{H}_\infty$ problem converges to the global solution (for the RST controller structure that considers multiple weighted sensitivity functions). The proposed method is used to design robust controllers for four different case studies; two in simulation and two for real applications. For one of the industrial-based case studies, (which constitutes the main applicative focus of this chapter), a robust RST controller is designed for power converters in particle accelerators at CERN. The designed controller is implemented in the power converters to control their output current with extremely high precision, which represent its major challenge. The main advantage of the proposed data-driven method for this application is to simultaneously ensure the robustness margins, attain the required closed-loop bandwidth, guarantee the controller stability, and ensure a small tracking error while avoiding the long and tedious manual tuning process intrinsically involved in the classical pole-placement model-based approach.

In this chapter, a discrete-time representation of coprime processes (see Section 2.1.2) with RST controllers (see Section 2.2.2) are considered. Thus the sensitivity functions with the

RST structure in Section 2.3.2 are considered.

4.2 $\mathscr{H}_\infty$ Performance via Convex Optimization

4.2.1 General Design Specifications

As discussed in the previous chapter, the objective of the general $\mathscr{H}_\infty$ control problem is to find the controller parameter vector $\boldsymbol{\rho}$ such that

$$\sup_{\omega\in\Omega}\left|H_q(e^{-j\omega},\boldsymbol{\rho})\right|<\gamma, \tag{4.1}$$

where $\gamma\in\mathbb{R}_+$, $H_q(e^{-j\omega},\boldsymbol{\rho})=W_q(e^{-j\omega})\mathscr{S}_q(e^{-j\omega},\boldsymbol{\rho})$ and $W_q:\mathbb{R}\to\mathbb{C}$ is the FRF of a Schur weighting filter such that $H_q(e^{-j\omega},\boldsymbol{\rho})$ has a bounded infinity norm. For notation purposes, the dependency in $e^{-j\omega}$ will be omitted, and will only be reiterated when deemed necessary. The condition in (4.1) can also be expressed as follows:

$$\gamma^{-1}\left|W_q\Delta_q(\boldsymbol{\rho})\right|<\left|\psi(\boldsymbol{\rho})\right|,\quad\forall\omega\in\Omega. \tag{4.2}$$

It is desired to minimize the upper bound γ such that the $\mathscr{H}_\infty$ performance condition is satisfied. Therefore, the following optimization problem can be considered:

$$\begin{aligned}&\underset{\gamma,\boldsymbol{\rho}}{\text{minimize}}\quad\gamma\\&\text{subject to:}\quad\gamma^{-1}\left|W_q\Delta_q(\boldsymbol{\rho})\right|<\left|\psi(\boldsymbol{\rho})\right|\\&\qquad\qquad\forall\omega\in\Omega\quad;\quad q\in\mathscr{Q}\subset\{1,2,\ldots,c\}.\end{aligned} \tag{4.3}$$

Notice that (4.3) is a non-convex optimization problem.

Consider a circle in the complex plane at a specific frequency in Ω which is centered at $\psi(\boldsymbol{\rho})$ and has radius $\gamma^{-1}|W_q\Delta_q(\boldsymbol{\rho})|$. As described in Chapter 3 (in the case with a 1DOF controller), the constraint in (4.2) ensures that for any frequency point in Ω, the circle associated with this frequency point will not encircle the origin. Fig. 4.1 displays the graphical interpretation of this condition. The following results are recalled (for discrete-time systems) before preceding with the theoretical contributions of this chapter.

Lemma 4.1. *(Conditions of SPRness for discrete-time systems [109]) A transfer function $A_d(z^{-1})$ is strictly positive real if and only if*

- *$A_d(z^{-1})$ is Schur.*
- *$\Re\left\{A_d(e^{-j\omega})\right\}>0,\ \forall\omega\in\Omega$.*
- *The poles of $A_d(z^{-1})$ on the unit circle are simple and distinct and the associated residues are real and non-negative.*

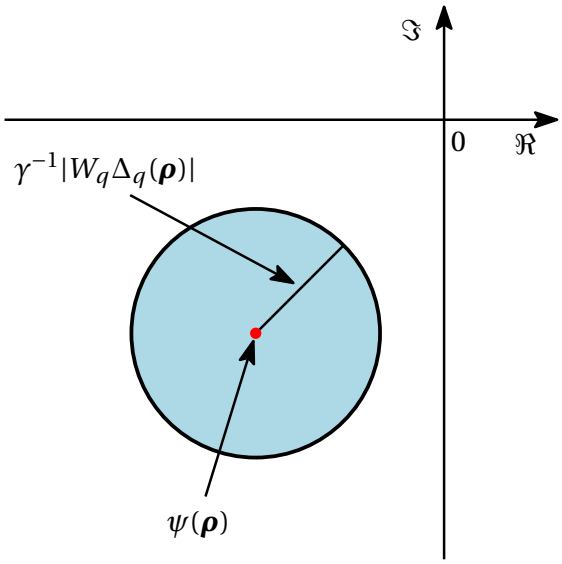

Figure 4.1 – The graphical interpretation of $\mathscr{H}_\infty$ constraints in the complex plane.

The geometrical construction in Fig. 4.1 will now be used to prove the following Lemma:

Lemma 4.2. *Suppose that*

$$H_q(e^{-j\omega},\boldsymbol{\rho}) = W_q(e^{-j\omega})\Delta_q(e^{-j\omega},\boldsymbol{\rho})\psi^{-1}(e^{-j\omega},\boldsymbol{\rho})$$

is the frequency response of a bounded analytic function outside the unit circle. Then, the following constraint is met

$$\sup_{\omega\in\Omega}\left|H_q(e^{-j\omega},\boldsymbol{\rho})\right| < \gamma \tag{4.4}$$

if and only if there exists a stable function $F(z^{-1})$ that satisfies

$$\Re\left\{\psi(\boldsymbol{\rho})F(e^{-j\omega})\right\} > \gamma^{-1}\left|W_q\Delta_q(\boldsymbol{\rho})F(e^{-j\omega})\right|, \qquad \forall\omega\in\Omega$$

Proof : The basic idea is similar to that of the proof of Lemma 3.2. It is clear that (4.4) is satisfied if and only if the disk of radius $\gamma^{-1}|W_q\Delta_q(\boldsymbol{\rho})|$ centered at $\psi(\boldsymbol{\rho})$ does not include the origin for all $\omega\in\Omega$, i.e. $|\psi(\boldsymbol{\rho})| > \gamma^{-1}|W_q\Delta_q(\boldsymbol{\rho})|$. This is equivalent to the existence of a line passing through the origin that does not intersect the disk. Therefore, at every given frequency ω, there exists a complex number $f(e^{-j\omega})$ that can rotate the disk such that it lays inside the right hand side of the imaginary axis. Hence, we have

$$\Re\left\{\left[\psi(\boldsymbol{\rho}) - \gamma^{-1}|W_q\Delta_q(\boldsymbol{\rho})|e^{j\theta}\right]f(e^{-j\omega})\right\} > 0, \quad \forall\omega\in\Omega, \forall\theta\in[0\,,\,2\pi[. \tag{4.5}$$

Since $f(e^{-j\omega}) = |f(e^{-j\omega})|e^{j\theta_f}$, then (4.5) can be expressed as

$$\Re\left\{\psi(\boldsymbol{\rho})f(e^{-j\omega})\right\} > \gamma^{-1}\left|W_q\Delta_q(\boldsymbol{\rho})f(e^{-j\omega})\right|\cos(\theta+\theta_f), \quad \forall\omega\in\Omega, \forall\theta\in[0\,,2\pi[. \tag{4.6}$$

However, (4.6) is satisfied if and only if:

$$\Re\left\{\psi(\boldsymbol{\rho})f(e^{-j\omega})\right\} > \gamma^{-1}\left|W_q\Delta_q(\boldsymbol{\rho})f(e^{-j\omega})\right|, \quad \forall\omega\in\Omega. \tag{4.7}$$

In [103], it is shown that, $f(e^{-j\omega})$ can be approximated arbitrarily well by the frequency response of a stable transfer function or FIR function $F(z^{-1})$ if and only if

$$Z = \left(\psi(\boldsymbol{\rho}) - \gamma_0^{-1}|W_q\Delta_q(\boldsymbol{\rho})|e^{j\theta}\right)^{-1} \tag{4.8}$$

is analytic outside the unit circle for all $\gamma_0 > \gamma$ and all $\theta\in[0\,,2\pi[$. However, $\psi^{-1}(\boldsymbol{\rho})$ is stable because of the stability of $H_q(\boldsymbol{\rho})$. On the other hand, by decreasing γ_0 from infinity to γ, the poles of Z move continuously with γ_0. Therefore, Z is not analytic outside the unit circle (i.e., Z has poles outside the unit circle) if and only if $Z^{-1}(e^{-j\omega}) = 0$ for a given frequency, which is not the case because the origin is not in the interior of the circle $\gamma_0^{-1}|W_q\Delta_q(\boldsymbol{\rho})|e^{j\theta}$. ■

The set of all controllers that meet the performance condition defined by the weighted norm of sensitivity functions is asserted in the following theorem.

Theorem 4.1. *Given the frequency response function $G(e^{-j\omega}) = N(e^{-j\omega})M^{-1}(e^{-j\omega})$ and the frequency response of a weighting filter $W_q(e^{-j\omega})$, then the following statements are equivalent for a given $q\in\mathcal{Q}$:*

(a) *There exists an RST controller that stabilizes G and*

$$\sup_{\omega\in\Omega}\left|W_q\mathcal{S}_q(\boldsymbol{\rho})\right| < \gamma. \tag{4.9}$$

(b) *There exists an RST controller such that*

$$\Re\left\{\psi(\boldsymbol{\rho})\right\} > \gamma^{-1}\left|W_q\Delta_q(\boldsymbol{\rho})\right|, \quad \forall\omega\in\Omega. \tag{4.10}$$

Proof: (**b** ⇒ **a**)
$\psi(\boldsymbol{\rho})$ is analytic outside the unit circle and its real part is positive for all $\omega\in\Omega$. Additionally, note that

$$\Re\left\{\psi(\boldsymbol{\rho})\right\} > 0 \iff \Re\left\{\psi^{-1}(\boldsymbol{\rho})\right\} > 0.$$

Therefore, by the conditions in Lemma 4.1, $\psi^{-1}(\boldsymbol{\rho})$ is Schur. This implies that $R(\boldsymbol{\rho})$ and $S(\boldsymbol{\rho})$ stabilizes G. On the other hand, we have

$$\left|\psi(\boldsymbol{\rho})\right| \geq \Re\left\{\psi(\boldsymbol{\rho})\right\}, \quad \forall\omega\in\Omega$$

which leads to $|W_q\Delta_q(\boldsymbol{\rho})| < \gamma|\psi(\boldsymbol{\rho})|$ for all $\omega \in \Omega$ and to (4.9) in Statement (**a**).

(**a** $\Rightarrow$ **b**)
Assume that $R(\boldsymbol{\rho}')$, $S(\boldsymbol{\rho}')$, and/or $T(\boldsymbol{\rho}')$ satisfies Statement (**a**) but not Statement (**b**). Then, according to Lemma 4.2, there exists a FIR function $F(z^{-1})$ such that

$$\Re\left\{\psi(\boldsymbol{\rho}')F(e^{-j\omega})\right\} > \gamma^{-1}\left|W_q\Delta_q(\boldsymbol{\rho}')F(e^{-j\omega})\right| \tag{4.11}$$

for all $\omega \in \Omega$. Therefore, there exists a higher order RST controller with $R = R(\boldsymbol{\rho}')F$, $S = S(\boldsymbol{\rho}')F$, and/or $T = T(\boldsymbol{\rho}')F$ such that Statement (**b**) holds. ■

The above theorem gives a necessary and sufficient condition for satisfying the $\mathscr{H}_\infty$ criterion for *one* sensitivity function. However, in typical control system applications, it is desired to shape several sensitivity functions simultaneously and impose multiple constraints on the weighted sensitivity functions. The following theorem ensures necessity and sufficiency of the $\mathscr{H}_\infty$ criterion when multiple sensitivity functions are considered:

Theorem 4.2. *Given the frequency response function $G(e^{-j\omega}) = N(e^{-j\omega})M^{-1}(e^{-j\omega})$ and the frequency response of weighting filters $W_q(e^{-j\omega})$ for $\forall\, q \in \mathscr{Q}$, then the following statements are equivalent:*

(a) *There exists an RST controller that stabilizes G and*

$$\sup_{\omega\in\Omega}\left|W_q\mathscr{S}_q(\boldsymbol{\rho})\right| < \gamma, \quad \forall\, q \in \mathscr{Q}. \tag{4.12}$$

(b) *There exists an RST controller such that*

$$\Re\left\{\psi(\boldsymbol{\rho})\right\} > \gamma^{-1}\left|W_q\Delta_q(\boldsymbol{\rho})\right|, \quad \forall\omega \in \Omega, \forall\, q \in \mathscr{Q}. \tag{4.13}$$

Proof: (**b** $\Rightarrow$ **a**)
The proof for this condition is similar to the proof presented in Theorem 4.1. By satisfying the constraint in (4.13) for all $q \in \mathscr{Q}$, the condition in (4.12) for each corresponding q is obtained.

(**a** $\Rightarrow$ **b**)
Assume that $R(\boldsymbol{\rho}')$, $S(\boldsymbol{\rho}')$, and/or $T(\boldsymbol{\rho}')$ satisfies Statement (**a**) but not Statement (**b**). Then, according to Lemma 4.2, there exist FIR transfer functions $F_q(z^{-1})$ such that

$$\Re\left\{F_q\psi(\boldsymbol{\rho}') - \gamma^{-1}\left|F_qW_q\Delta_q(\boldsymbol{\rho}')\right|\right\} > 0 \tag{4.14}$$

for all $\omega \in \Omega$ and for all $q \in \mathscr{Q}$. For Statement (**b**) to hold, there must exist a common F for all $q \in \mathscr{Q}$ such that $R = R(\boldsymbol{\rho}')F$, $S = S(\boldsymbol{\rho}')F$, and/or $T = T(\boldsymbol{\rho}')F$.

For a given frequency, the constraints in (4.12) will represent disks in the complex-plane that

are centered exactly at $\psi(\boldsymbol{\rho}')$ with varying radii (where the radii depend on each q). Let us define the following quantities at every $\omega \in \Omega$:

$$\begin{aligned}\Psi(e^{-j\omega},\boldsymbol{\rho}') &= \left\{\left|W_1\Delta_1(e^{-j\omega},\boldsymbol{\rho}')\right|,\ldots,\left|W_c\Delta_c(e^{-j\omega},\boldsymbol{\rho}')\right|\right\}\\ r_\Psi(e^{-j\omega},\boldsymbol{\rho}') &= \gamma^{-1}\max_{q\in\mathcal{Q}}\Psi(e^{-j\omega},\boldsymbol{\rho}').\end{aligned} \tag{4.15}$$

For any ω, the disk with radius $r_\Psi(\boldsymbol{\rho}')$ does not include the origin, and all of the other disks with smaller radii are enclosed in the disk with radius $r_\Psi(\boldsymbol{\rho}')$, i.e. :

$$\gamma^{-1}\left|W_q\Delta_q(e^{-j\omega},\boldsymbol{\rho}')\right| \le r_\Psi(e^{-j\omega},\boldsymbol{\rho}').$$

Therefore, for a given frequency, the complex number f_q which is used to rotate the disk associated with radius $r_\Psi(e^{-j\omega},\boldsymbol{\rho}')$ ensures that all of the disks with $\gamma^{-1}|W_q\Delta_q(e^{-j\omega},\boldsymbol{\rho}')| \le r_\Psi(e^{-j\omega},\boldsymbol{\rho}')$ are also rotated such that they all lie in the right-hand side of the imaginary axis. Therefore, there will always exist a common F that interpolates all f_q (different q in different frequencies) such that the conditions in (4.14) hold true for all $q \in \mathcal{Q}$. ■

4.2.2 Robust Design

With the proposed method, it is possible to design a fixed-structure controller which accounts for the uncertainties of a given FRF. Given the additive uncertainty in (2.10), a desired performance condition $\|W_q\mathcal{S}_q(\boldsymbol{\rho})\|_\infty < \gamma$ will be satisfied for all models in the uncertain set (2.10) if $\|W_q\tilde{\mathcal{S}}_q(\boldsymbol{\rho})\|_\infty < \gamma$, where $\tilde{\mathcal{S}}_q(\boldsymbol{\rho}) = \tilde{\Delta}_q/\tilde{\psi}(\boldsymbol{\rho})$ and $\tilde{\psi}(\boldsymbol{\rho}) = \tilde{N}R(\boldsymbol{\rho}) + \tilde{M}S(\boldsymbol{\rho})$. For example, consider the nominal performance condition $\|W_3\tilde{\mathcal{S}}_3(\boldsymbol{\rho})\|_\infty < \gamma$, where $W_3 : \mathbb{R} \to \mathbb{C}$ and $\tilde{\mathcal{S}}_3 : \mathbb{R}^{n_{rst}} \times \mathbb{R} \to \mathbb{C}$ with

$$\tilde{\Delta}_3(\boldsymbol{\rho}) = \tilde{M}S(\boldsymbol{\rho}) + \tilde{N}[R(\boldsymbol{\rho}) - T(\boldsymbol{\rho})].$$

As a worst case consideration, δ_m and δ_n can be selected to be equal to one in (2.10) (which ensures that the uncertainty in the entire disk is taken into account). By substituting the expressions in (2.10) into this condition, the following constraint can be devised:

$$\begin{aligned}&\left|W_3\left[\psi(\boldsymbol{\rho}) - NT(\boldsymbol{\rho}) + S(\boldsymbol{\rho})|W_m|e^{j\theta_m} + C(\boldsymbol{\rho})|W_n|e^{j\theta_n}\right]\right|\\ &\qquad < \gamma\left|\psi(\boldsymbol{\rho}) + R(\boldsymbol{\rho})|W_n|e^{j\theta_n} + S(\boldsymbol{\rho})|W_m|e^{j\theta_m}\right|\end{aligned} \tag{4.16}$$

$\forall\omega \in \Omega, \forall\{\theta_n,\theta_m\} \in [0,2\pi[$, where $C(\boldsymbol{\rho}) = R(\boldsymbol{\rho}) - T(\boldsymbol{\rho})$. For notation purposes, let $\psi'(\boldsymbol{\rho},\theta_n) := \psi(\boldsymbol{\rho}) + R(\boldsymbol{\rho})|W_n|e^{j\theta_n}$ be defined. Then for a given $\{\omega,\theta_n,\theta_m\}$, (4.16) represents a circle centered at $\psi'(\boldsymbol{\rho},\theta_n) + S(\boldsymbol{\rho})|W_m|e^{j\theta_m}$ with a radius of

$$x_p(\boldsymbol{\rho},\theta_m,\theta_n) = \gamma^{-1}|W_3|\left|\psi'(\boldsymbol{\rho},\theta_n) + S(\boldsymbol{\rho})|W_m|e^{j\theta_m} - T(\boldsymbol{\rho})[N + |W_n|e^{j\theta_n}]\right|. \tag{4.17}$$

According to Theorem 4.1, a necessary and sufficient condition for (4.16) can be constructed as follows:

$$x_p(\boldsymbol{\rho},\theta_m,\theta_n) < \Re\left\{\psi'(\boldsymbol{\rho},\theta_n) + S(\boldsymbol{\rho})|W_m|e^{j\theta_m}\right\}, \quad \forall\omega\in\Omega, \forall\{\theta_m,\theta_n\}\in[0,2\pi[. \tag{4.18}$$

By gridding in ω, θ_m and θ_n, then (4.18) becomes a convex constraint (with respect to $\boldsymbol{\rho}$); however, gridding in all of these variables can be computationally expensive. Therefore, a sufficient condition for (4.16) can be devised as follows:

$$\sup_{\omega\in\Omega}\frac{|W_3|\left[|\psi(\boldsymbol{\rho})-NT(\boldsymbol{\rho})|+|C(\boldsymbol{\rho})W_n|+|S(\boldsymbol{\rho})W_m|\right]}{|\psi(\boldsymbol{\rho})|-|R(\boldsymbol{\rho})W_n|-|S(\boldsymbol{\rho})W_m|} < \gamma. \tag{4.19}$$

With this condition, the dependency in θ_m and θ_n has been removed, and gridding in only one variable (i.e., ω) is required.

The condition in (4.19) can be represented as a disk in the complex plane which is centered at $\psi(\boldsymbol{\rho})$ and has radius

$$x_r(\boldsymbol{\rho}) = \gamma^{-1}|W_3|\left[|\psi(\boldsymbol{\rho})-NT(\boldsymbol{\rho})|+|C(\boldsymbol{\rho})W_n|+|S(\boldsymbol{\rho})W_m|\right]+|R(\boldsymbol{\rho})W_n|+|S(\boldsymbol{\rho})W_m|. \tag{4.20}$$

Therefore, a set of convex constraints is devised with $x_r(\boldsymbol{\rho}) < \Re\{\psi(\boldsymbol{\rho})\}$ for all $\omega\in\Omega$. This constraint has the same structure as that of the sensitivity functions and so can readily be included in the optimization problem. Note that (4.19) introduces some conservatism; however, this conservatism can always be reduced by imposing (4.18) (at the cost of a larger computation time).

Remark. *For stable plants, $M = 1$ may be selected. Therefore, the disk uncertainty associated with M is $|W_m| = 0$. From (4.17) and (4.18), it can be observed that with $|W_m| = 0$, the dependency on θ_m is removed, and no gridding in θ_m is required. The necessary and sufficient condition then becomes*

$$x_p(\boldsymbol{\rho},\theta_n) < \Re\left\{\psi'(\boldsymbol{\rho},\theta_n)\right\}, \quad \forall\omega\in\Omega, \forall\theta_n\in[0,2\pi[, \tag{4.21}$$

where $x_p(\boldsymbol{\rho},\theta_n) = \gamma^{-1}|W_3||\psi'(\boldsymbol{\rho},\theta_n) - T(\boldsymbol{\rho})[N+|W_n|e^{j\theta_n}]|$.

4.2.3 Controller Stability

For a stable plant, computation of an unstable controller should generally be avoided [100]. For the RST structure, it is evident that if the polynomial $S(z^{-1},\boldsymbol{\rho})$ possesses zeros outside the unit circle, then the open-loop system will become unstable. In order to avoid this impairment, it is required to impose a constraint such that the polynomial $S(z^{-1},\boldsymbol{\rho})$ possesses zeros inside the unit circle. This rationalization leads to the following lemma:

Lemma 4.3. *Suppose that $S(z^{-1},\boldsymbol{\rho})$ is parameterized as in (2.28). Then a sufficient (convex)*

condition to ensure that the zeros of $S(z^{-1},\boldsymbol{\rho})$ *remain inside the unit circle is*

$$\Re\{S(\boldsymbol{\rho})\} > 0, \quad \forall \omega \in \Omega. \tag{4.22}$$

Proof : $\Re\{S(\boldsymbol{\rho})\} > 0$ implies that $\Re\{S^{-1}(\boldsymbol{\rho})\} > 0$; from Lemma (4.1), this further implies that $S^{-1}(\boldsymbol{\rho})$ is Schur. ■

4.2.4 Tracking Specifications

In certain design strategies, it may sometimes be desired to track different reference signals with no steady-state error, such as a step or a ramp input. For the systems addressed in this thesis, it will be desired to track a step input. Minimization of the error sensitivity function is a soft constraint, and may not lead to the ideal tracking performance. Therefore it is advantageous to consider conditions that ensure proper tracking of a step input by imposing hard convex constraints. Note that in an *RST* structure, the existence of an integrator in the open-loop transfer function does not guarantee a zero steady-state error for tracking a step input. The necessary and sufficient condition for a zero steady-state error is recalled in the following lemma.

Lemma 4.4. *Suppose that the reference signal is a step function given as* $r(z^{-1}) = A(1-z^{-1})^{-1}$, *where A is the amplitude of the step function. Additionally, suppose that the controller* $S(z^{-1},\boldsymbol{\rho})$ *possesses an integrator (i.e.,* $S(z^{-1},\boldsymbol{\rho}) = (1-z^{-1})S'(z^{-1},\boldsymbol{\rho})$, *where* $S'(z^{-1},\boldsymbol{\rho})$ *is linearly parameterized). A necessary and sufficient condition to obtain a zero steady-state error for a step input is*

$$R(1,\boldsymbol{\rho}) = T(1,\boldsymbol{\rho}) \neq 0. \tag{4.23}$$

Proof. The proof for this condition can be established by using the final value theorem. For perfect tracking of an arbitrary reference signal $r[k]$, it is required that $\lim_{k\to\infty}(r[k]-y[k]) = 0$, or

$$\lim_{z\to 1}(1-z^{-1})r(z^{-1})[1-\mathscr{S}_2(z^{-1},\boldsymbol{\rho})] = 0. \tag{4.24}$$

For a step input, the condition for achieving a zero steady-state error can be expressed as

$$\lim_{z\to 1}[1-\mathscr{S}_2(z^{-1},\boldsymbol{\rho})] = 0. \tag{4.25}$$

By substituting (2.39) into (4.25) (and noting that $S(z^{-1},\boldsymbol{\rho}) = (1-z^{-1})S'(z^{-1},\boldsymbol{\rho})$), one can arrive to the following condition:

$$\lim_{z\to 1}\frac{N(z^{-1})[R(z^{-1},\boldsymbol{\rho})-T(z^{-1},\boldsymbol{\rho})]}{M(z^{-1})S(z^{-1},\boldsymbol{\rho})+N(z^{-1})R(z^{-1},\boldsymbol{\rho})} = \frac{R(1,\boldsymbol{\rho})-T(1,\boldsymbol{\rho})}{R(1,\boldsymbol{\rho})} = 0 \tag{4.26}$$

which evidently leads to the condition asserted in (4.23). ■

4.2.5 Convex Optimization via Semi-Definite Programming

Suppose that it is desired to obtain $\mathscr{H}_\infty$ performance for a sensitivity function (i.e., minimize γ in $\|W_q\mathscr{S}_q(\boldsymbol{\rho})\|_\infty < \gamma$). Then according to the results in Theorem 4.2, one can formalize an optimization problem to obtain the admissible $R(\boldsymbol{\rho})$, $S(\boldsymbol{\rho})$, and/or $T(\boldsymbol{\rho})$ controllers as follows:

$$\begin{aligned} \underset{\gamma,\boldsymbol{\rho}}{\text{minimize}} \quad & \gamma \\ \text{subject to:} \quad & \gamma^{-1}\left|W_q\Delta_q(\boldsymbol{\rho})\right| < \Re\left\{\psi(\boldsymbol{\rho})\right\} \\ & \forall\omega\in\Omega \quad ; \quad q\in\mathscr{Q}. \end{aligned} \tag{4.27}$$

For LP controllers, the optimization problem in (4.27) is quasi-convex. The classical solution to this problem is to implement a bisection algorithm in order to obtain the global solution.

As in the problems considered in Chapter 3, the problem in (4.27) is a SIP problem since there are a finite number of optimization variables and an infinite number of constraints. To solve this problem, the optimization algorithm can be converted to a SDP problem. A predefined frequency grid can be implemented in order to solve a finite number of constraints.

It can be shown that by increasing the controller order, the optimal solution to (4.27) converges to the global optimal solution of the $\mathscr{H}_\infty$ problem.

Lemma 4.5. *Suppose that the RST controller achieves the optimal $\mathscr{H}_\infty$ performance for the plant model $G = NM^{-1}$ such that*

$$\gamma_o^\star = \sup_\omega \left|W_q\Delta_q(\boldsymbol{\rho})\psi^{-1}(\boldsymbol{\rho})\right|, \quad \forall\, q\in\mathscr{Q}.$$

Additionally, suppose that $\gamma_n^\star$ is the optimal solution of the convex optimization in (4.27) when $R(\boldsymbol{\rho})$, $S(\boldsymbol{\rho})$ and/or $T(\boldsymbol{\rho})$ are parameterized by an n-th order FIR filter. Then $\gamma_n^\star$ converges monotonically from above to $\gamma_o^\star$ when $n\to\infty$.

Proof: The proof of a similar condition has been established in Theorem 3.3 (for one sensitivity function and for a 1DOF controller), and has been omitted to conserve space. However, the necessary and sufficient condition from Theorem 4.2 can be combined with the ideas presented in Theorem 3.3 to ensure that the solution to (4.27) converges to the global optimal solution of the $\mathscr{H}_\infty$ problem as n increases ($\forall\, q\in\mathscr{Q}$). ■

Table. 4.1 displays a general method for designing a controller using the proposed approach.

Table 4.1 – Procedure for computing an RST controller

Algorithm: Convex optimization for optimal performance

1. Excite the system with a multi-sinus or PRBS signal and identify the FRF of the system. If the process is stable, select $N = G$ and $M = 1$. If the process is unstable, see Section 2.1.2 for obtaining the coprime factors.

2. Compute the uncertainty for W_n and W_m using the covariance of the estimates [95] and define the performance filters in $\|W_q \mathcal{S}_q(\boldsymbol{\rho})\|_\infty$.

3. Formulate the control problem as minimizing the infinity norm of multiple weighted sensitivity functions.

4. Start with a first-order RST controller (with $n = n_r = n_s = n_t$) and solve the optimization problem in (4.27) by using a frequency grid to obtain γ_n. The constraint should be modified based on which sensitivity function is considered.

5. If the desired performance is met, stop. Otherwise, increase the order by one (i.e., $n = n + 1$).

6. Solve the problem in (4.27) to obtain the new γ_n and go to Step 5.

4.3 Simulation Examples

4.3.1 Case 1: Multi-model uncertainty

Consider the following unstable system reported in [110] which describes the dynamics of a magnetic levitation system linearized around an operating point (airgap of 17 mm):

$$G(s) = \frac{a_1}{(s+131.3)(s-a_2)(s+a_2)}, \tag{4.28}$$

where $a_1 = 163863.6$ and $a_2 = 29.85$. The input u is proportional to the inductor current and the output y is proportional the measured airgap. To demonstrate the effectiveness of the proposed method, it is supposed that there exists some uncertainty with the mass of the steel ball where the gain and poles of the system belong in the sets $\tilde{a}_1 \in \{0.9a_1, a_1, 1.1a_1\}$ and $\tilde{a}_2 \in \{0.7a_2, a_2, 1.3a_2\}$. With the proposed approach, a multi-model design can be implemented where stability and performance is guaranteed for all of the uncertainties associated with the system. The plant can be expressed as $G_i(s)$ for $i = 1, \ldots, 9$ (which represents the plant model with respect to the i^{th} unique combination of the uncertain parameters).

Remark. *Note that these models are simply used to obtain the FRFs of the plants and the controller synthesis does not rely on these parametric models. As a result, both continuous- and discrete-time plant models can be considered for the synthesis.*

Performance Specifications

For this particular case study, it was desired to obtain the best performance for disturbance rejection (i.e., by minimizing $\|W_1\mathscr{S}_1^i(\boldsymbol{\rho})\|_\infty \; \forall i$, where $\mathscr{S}_1^i(\boldsymbol{\rho})$ denotes the sensitivity function with respect to the i^{th} plant model from the set G_i). Note that this is a regulation problem, and the polynomial $T(\boldsymbol{\rho})$ is not included in the design process. Additionally, in order to have a zero steady-state error, the controller should include an integrator (i.e., $S(\boldsymbol{\rho}) = (1-z^{-1})S'(\boldsymbol{\rho})$). The weighting filter was selected as $W_1(s) = (s+\omega_d)s^{-1}$, which was designed in accordance with the methods described in [10]. The rejection bandwidth ω_d [rad s^{-1}] was selected as $\omega_d = 100\pi$. Note that $W_1(j\omega)$ is unbounded at $\omega = 0$; however, due to the fixed integrator in the controller, $\|W_1\mathscr{S}_1^i(\boldsymbol{\rho})\|_\infty$ remains bounded $\forall i$ and $\forall\omega$.

Controller Synthesis

Since each model is unstable, then each coprime factor must be selected such that $\{N_i(s), M_i(s)\} \in \mathbf{RH}_\infty$ for all i. A simple choice is to divide both the numerator and denominator of each model by a factor $(s+10)^3$.

Remark. *If a parametric model is not available for acquiring the FRFs of these coprimes, then a closed-loop identification experiment can be performed to obtain them (see Section 2.1.2).*

The problem in (4.27) was solved for $q = 1$ by considering all models in the set G_i and a linearly-spaced grid of 300 points from 0 to π/T_s rad s^{-1} (where a working sampling time of $T_s = 0.002$ s was selected, as asserted in [110]). The optimal solution $\gamma^\star$ for various controller orders have been computed and compared with the solutions obtained with the frequency-domain method in [111] (which requires the selection of a desired open-loop transfer function). Fig. 4.2 depicts the optimal solution as a function of the controller order; it can be observed that as the controller order increases, the solution obtained with the proposed method achieves better performance (i.e., converges monotonically to the global optimal solution of the $\mathscr{H}_\infty$ problem). For comparative purposes, the optimization times with both the proposed method and the method in [111] for a 5^{th} order controller (with $\gamma_{max} = 5$, $\gamma_{min} = 10^{-3}$, and a tolerance of 10^{-5} set for the bisection algorithm) are 111.5 s and 9.8 s, respectively. The difference in optimization times stems from the fact that the method in [111] fixes the polynomial $S(\boldsymbol{\rho})$ *a-priori* such that $R(\boldsymbol{\rho})$ is the only polynomial to be optimized; with the proposed method, the parameters in both $R(\boldsymbol{\rho})$ and $S(\boldsymbol{\rho})$ are optimized. The optimization times were calculated based on a computer having the following hardware specifications: Intel-Core i7, 3.4 GHz CPU, 8 GB RAM. The optimization algorithm was run using `MATLAB` version (R2015b) on a Windows 7 platform (64-bit).

4.3.2 Case 2: Nonlinear Distortions

In this case study, a 1DOF controller (i.e., with $R(\boldsymbol{\rho}) = T(\boldsymbol{\rho})$ in the RST structure) for a DC motor with a typical nonlinearity encountered in practice is considered. The model of the

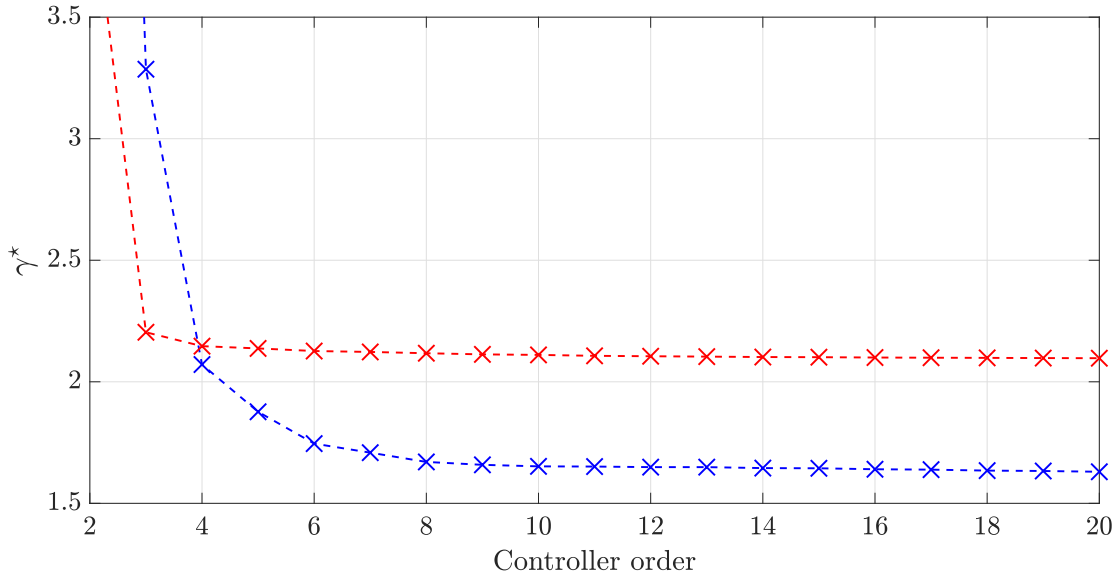

Figure 4.2 – Optimal solution $\gamma^\star$ as a function of the controller order. Solutions obtained with the proposed method (dashed-blue line); solutions obtained with the method which requires the selection of a desired open-loop transfer function (dashed-red line).

brushless DC motor is taken from [112]:

$$G(z) = \frac{0.0143z + 0.0142}{(z-1)(z-0.9725)}, \tag{4.29}$$

where the sampling time of the process is given as $T_s = 2.048$ ms. A typical nonlinearity that is encountered with motor applications is the dead-zone nonlinearity (see [113, 114]). This nonlinearity would occur at the input of the plant, and can be expressed as follows:

$$u_n = \begin{cases} 0, & \text{for } -d \leq u \leq d \\ m_n(u-d), & \text{for } u > d \\ m_n(u+d), & \text{for } u < -d \end{cases} \tag{4.30}$$

where u_n is the output to the nonlinearity, m_n is the slope of the line, and $d \in]0, \infty[$ is the value of u at which the discontinuity occurs. Note that this type of nonlinear system belongs to the class of systems in $\mathcal{V}$.

The objective of this case study will be to demonstrate the effectiveness of the proposed robust design method by applying a random-phase multi-sine signal that excites the dead-zone nonlinearity; the FRF obtained from this identification will then be used to model a BLA with an associated uncertainty (as discussed in Section 2.1.3) and design a robust controller that minimizes $\|W_3 \tilde{\mathscr{S}}_3(\boldsymbol{\rho})\|_\infty$. For simplicity, the values of the nonlinearity are selected as $m_n = 1$ and $d = 0.1$ for this case study. It will also be desired to investigate the response of a controller when the uncertainties in the design are neglected and the FRF of the coprimes are obtained

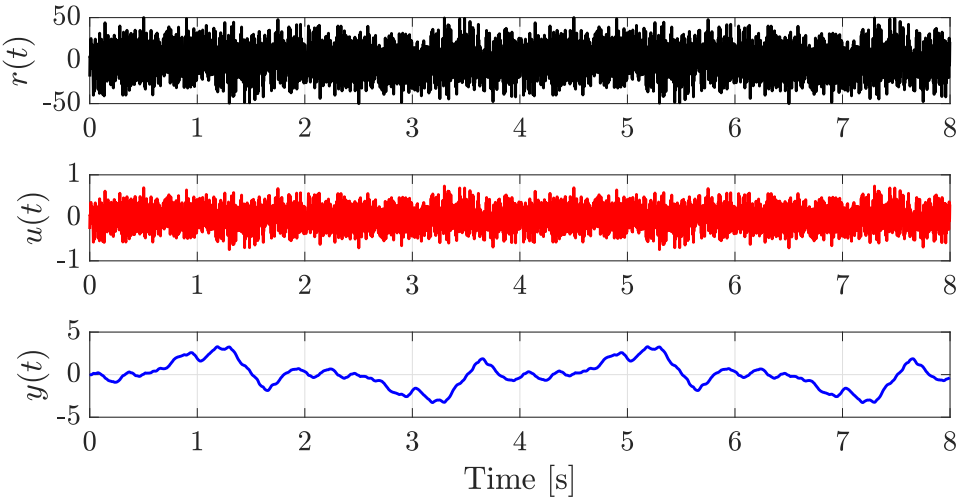

Figure 4.3 – Random phase multi-sine input $r(t)$ along with the plant input $u(t)$ and output $y(t)$. For presentation purposes, the signals are shown for 2 full periods.

from a given time-domain experiment.

Note that $G(z)$ possesses an integrator; therefore, the closed-loop method will be used where the BLAs for the coprimes N and M are formulated. To accomplish this task, the closed-loop system must first be stabilized. For this case study, the closed-loop system is stabilized when a proportional controller is implemented with a unity-feedback structure (with the value of the controller equal to 0.15). The closed-loop system was excited with a periodic random phase multi-sine (with an amplitude range of ± 50); 10 experiments were performed where the system was excited with 15 periods of this signal where the period length was 2000 samples and each period contains 500 sinusoids with random phases. The input and output time-domain signals are shown in Fig. 4.3.

For comparative purposes, it was desired to compare the design scheme when the uncertainties of the proposed method were neglected and the nominal FRF was obtained directly from the data in Fig. 4.3. The FRF BLAs with the associated uncertainties for $\tilde{N}$ and $\tilde{M}$ are shown in Fig. 4.4 and Fig. 4.5, respectively. The radii of the uncertainty circles for each coprime were computed using (2.22). It can be observed that at some frequencies, the FRF of the coprimes for a given experiment are not included in the uncertainty disks. The BLA variances for each coprime are shown in Fig. 4.6.

Controller Synthesis

With the BLA and the uncertainty for the coprimes, a controller was computed in order to obtain $\mathscr{H}_\infty$ performance for the underlying linear system. A SDP problem can be formulated to design robust controllers (which takes into account the uncertainties from the nonlinear

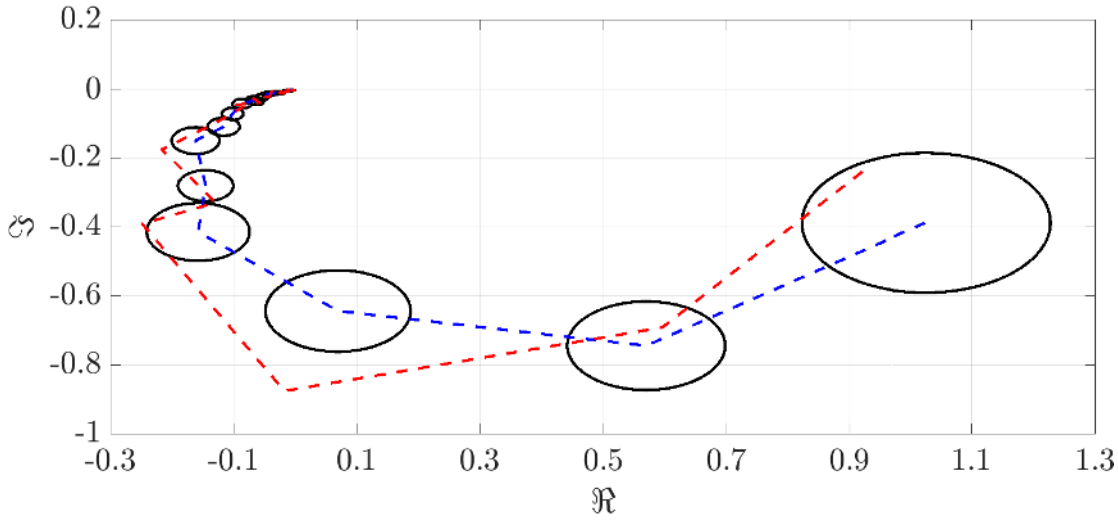

Figure 4.4 – N (dashed-blue line) with the associated uncertainties at each frequency (black circles). The FRF obtained between r to y for a given experiment with no uncertainties (dashed-red line).

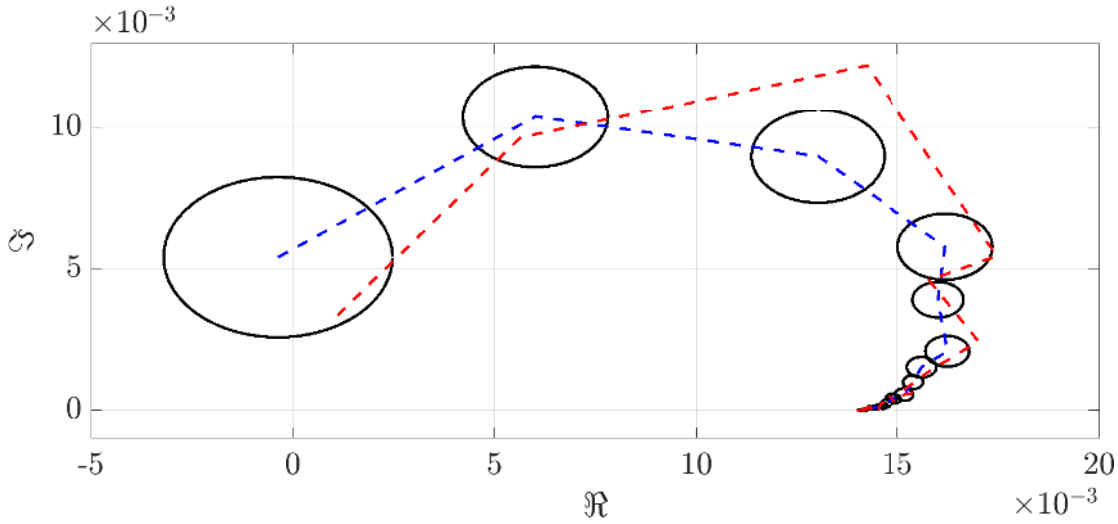

Figure 4.5 – M (dashed-blue line) with the associated uncertainties at each frequency (black circles). The FRF obtained between r to u for a given experiment with no uncertainties (dashed-red line).

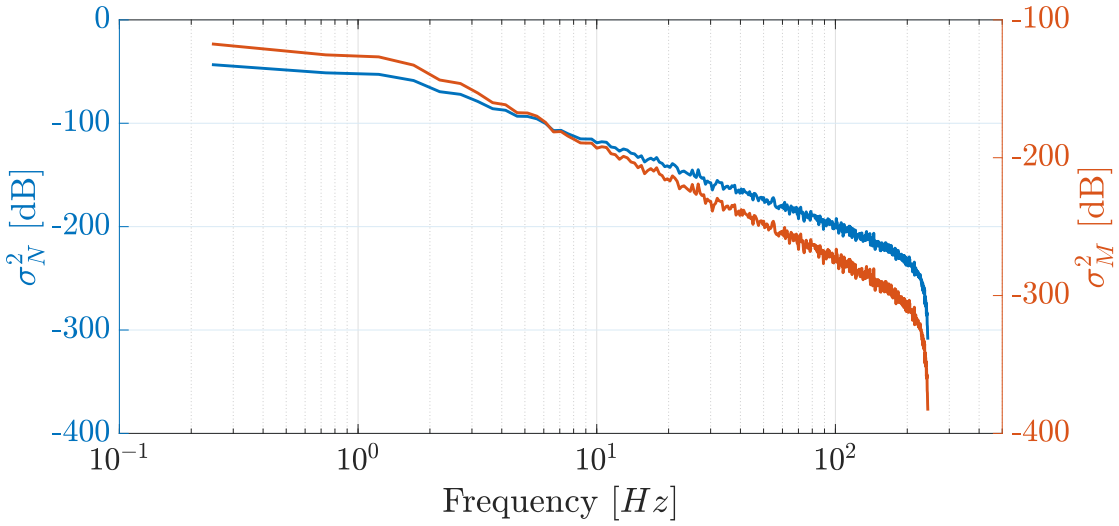

Figure 4.6 – Variances of coprimes caused by nonlinear distortions

distortions) as follows:

$$\begin{aligned} \underset{\boldsymbol{\rho},\gamma}{\text{minimize}} \quad & \gamma \\ \text{subject to:} \quad & \Re\left\{\psi(e^{-j\omega_k},\boldsymbol{\rho})\right\} > x_r(e^{-j\omega_k},\boldsymbol{\rho}) \\ & \text{for } k = 1,\ldots,\eta, \end{aligned} \tag{4.31}$$

where $\eta = 500$ and $x_r(e^{-j\omega_k},\boldsymbol{\rho})$ is defined as in (4.20). To invoke integral action, the controller will be prefixed with an integrator.

Weighting filter selection

The weighting filters W_n and W_m for the uncertainties in $\tilde{N}$ and $\tilde{M}$ were calculated using (2.22). The weighting filter W_3 was selected based on a desired closed-loop reference model. For the underlying *linear system*, it is known that $\mathscr{S}_2 + \mathscr{S}_3 = 1$. A simple first-order closed-loop reference model was selected as the desired complementary function $\mathscr{S}_2^d(z) = (1-c_d)(z-c_d)^{-1}$, where $c_d = e^{-\omega_d T_s}$ and ω_d [rad s^{-1}] is the desired bandwidth. For this case study, the desired bandwidth was selected as $\omega_d = 100\pi$. Thus W_3 was formulated as $[1-\mathscr{S}_2^d(z)]^{-1}$. Note that the controller was prefixed with an integrator, and $\|W_3\tilde{\mathscr{S}}_3(\boldsymbol{\rho})\|_\infty$ remains bounded $\forall\omega$.

Simulation Results

The problem in (4.31) was solved with a 5$^{\text{th}}$ order controller. Two design schemes were considered:

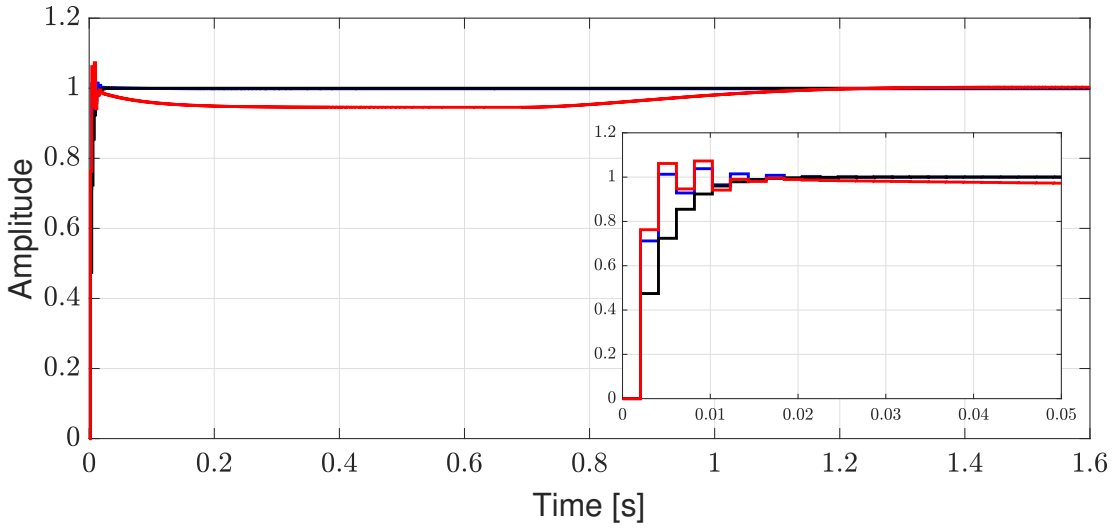

Figure 4.7 – Step response of the nonlinear system. The desired closed-loop response (black line); the response with the proposed method (including uncertainties in design) (blue line); the response with no uncertainties considered (red line).

Table 4.2 – Parameters resulting from the bisection algorithm.

Parameter	***Value***	***Unit***
$\gamma_{\max}$	5	-
$\gamma_{\min}$	0	-
γ_{tol}	10^{-3}	-
$\gamma^{\star}$	1.252	-
Optimization time	108.2	*s*
Number of constraints	500	-

- A design in which the FRF BLA with the associated frequency dependent uncertainties were considered.

- A design where no uncertainties are considered (i.e., $|W_n| = |W_m| = 0$) and the FRF of the coprimes is obtained from a given experiment.

The closed-loop step response of the nonlinear system is shown in Fig. 4.7; it can be observed that when the frequency-dependent uncertainties are considered in the design, good performance and stability is achieved. When the uncertainties are neglected in the design, the settling time is significantly larger. This is caused by the modeling error from the closed-loop experiment (which can be seen in figures 4.4 and 4.5 where the FRF lies outside the uncertainty disks at various frequency points). Thus with the proposed method, the performance and stability of the underlying linear system can be guaranteed by considering the frequency dependent uncertainties obtained from the random-phase multi-sine identification experiments performed on a nonlinear system.

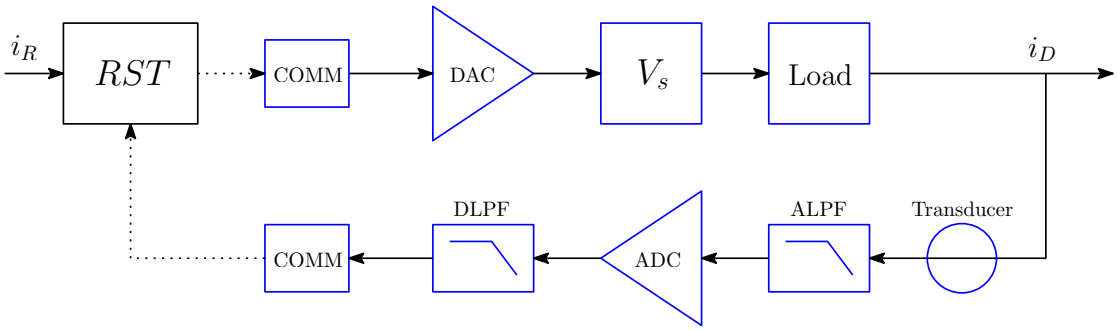

Figure 4.8 – Power converter control system.

4.4 Case Study: Power Converter Control

4.4.1 Power Converters for Particle Accelerators

The framework of the system discussed in this case study is part of the CERN Large Hadron Collider (LHC) Injector Upgrade Project [115], which was implemented to mitigate space-charge effects and to increase the beam brightness in order to fulfill the needs of the High Luminosity LHC [116]. The Q-STRIP magnet (i.e., the load, which is constituted of two chains of quadrupole magnets) is used in this framework to control the particle trajectories via the power converter control system.

Power converters can be seen as systems comprised of three main subsystems: (*i*) a power source (usually a voltage source) (*ii*) a measuring system and (*iii*) a controller unit. The current is usually measured with a particularly accurate current transducer called a direct current-current transformer (DCCT) [117]. The current measurement signal is fed back to a digital controller unit which usually includes a high precision analog-to-digital converter that implements the digital control algorithm([118], [119]).

The general configuration of the CERN power converter control system is depicted in Fig.4.8. The control loop consists of a magnet (i.e., the load), a voltage source V_s, low-pass anti-aliasing analog and digital filters (ALPF, DLPF), a digital-to-analog converter (DAC), and an analog-to-digital converter (ADC). The DAC (optional) and ADCs are integrated in the control unit labeled as the function generator controller (FGC, [120]) whose main function is to execute the control algorithm; it also implements all the diagnostics and communication functions with higher layers of the control architecture up to the accelerators control rooms. The DLPF may also include a decimator to reduce the sampling rate of the signal. The COMM block represents the delay associated with the communications link. The RST block represents the discrete-time controller that is used to control the magnet current i_D given a reference current i_R.

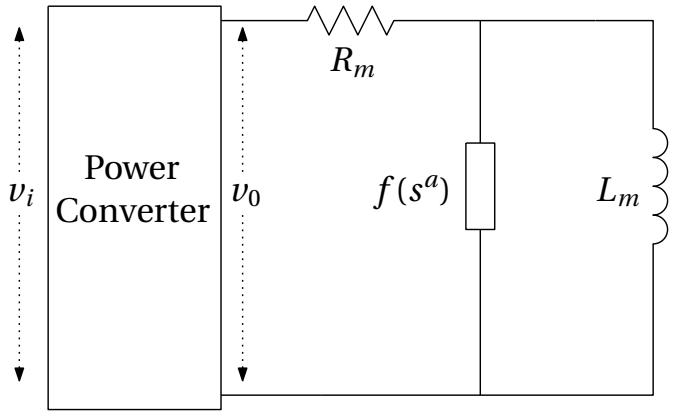

Figure 4.9 – Fractional dynamics of magnet caused by Eddy currents.

Magnet Dynamics

The magnet bearings of this system are subject to Eddy currents. In solid core structures, Faraday's law shows that Eddy currents are induced when the magnetic field changes in conductors [121]. These Eddy currents alter the dynamics of the magnet where simple integer-based transfer functions are incapable of modeling such systems with high precision.

Fig. 4.9 shows a basic schematic of the load dynamics with the effect of Eddy currents (where $f(s^a)$ is an impedance as a function of the fractional order Laplace variable with $0 < a < 1$). This impedance represents a fractional order system; in fact, it has been shown in [122, 123, 124] that fractional order systems correctly represent the dynamics of systems subject to Eddy currents. Therefore, the data-driven controller scheme using frequency-domain data is an appropriate technique for controlling such systems since all of the synthesis and stability criteria are addressed in the frequency-domain (where the performance and stability criteria in the frequency-domain is equivalent for fractional and non-fractional systems [125]).

4.4.2 Experimental Test Setup

The experimental test setup consists of a CERN AC-DC Narrow Converter (CANCUN), a dummy load and a proprietary software diagnostics tool:

- The CANCUN is based on a full bridge phase shifted topology followed by a 4 quadrant switching stage to allow 4 quadrant operation. Fig. 4.10 shows a CANCUN that incorporates three main parts: i) Two high precision current sensors (DCCTs) which are able to measure DC or pulsed current at the required precision; ii) A voltage (or power) module; iii) A digital controller (FGC3) which implements the digital control loop together with CERN designed control and diagnostics electronics. The ratings of the CANCUN for the Q-STRIP application is $\pm 100\,\mathrm{A}$ and $\pm 30\,\mathrm{V}$.
- The dummy load is (ideally) an RL-series load whose characteristics match those of the

Figure 4.10 – The CANCUN used for the control application.

Q-STRIP magnets.

- The software diagnostics tool interfaces with the main digital controller module, the FGC3 [120], and is able to acquire the relevant signals at a sampling rate of 10K samples per second. The acquired signals are the reference current and voltage, the measured current and voltage, and the current error.

4.4.3 Control Objective

The main objective is to design an RST controller such that the error obtained from a specific desired current profile, shown in Fig. 4.11, meets the desired specifications.

The magnet is represented as an RL circuit, and the dynamics of this circuit are dominant over the other components of the system. Thus a first order model with delay (i.e., $G_m(s) = e^{-sT_d}(L_m s + R_m)^{-1}$, where R_m is the circuit resistance, L_m is the circuit inductance, and T_d is the time delay) is appropriate to approximate the dynamics of the plant. For this case study, the model parameters are identified as: $R_m = 164.3\,\text{m}\Omega$, $L_m = 736.4\,\mu\text{H}$ and $T_d = 275.4\,\mu\text{s}$.

At CERN, the above model is discretized using the zero-order-hold method and used to design an RST controller based on the model-reference control (MRC) strategy [100]. The main difficulty is that the choice of the observer poles that lead to a good robustness margin is not trivial; the design of a working controller is a time consuming iterative process.

A PRBS signal was used as the input voltage reference of the open-loop system in order to capture the dynamics of the process. A total of 5 experiments were performed with the PRBS

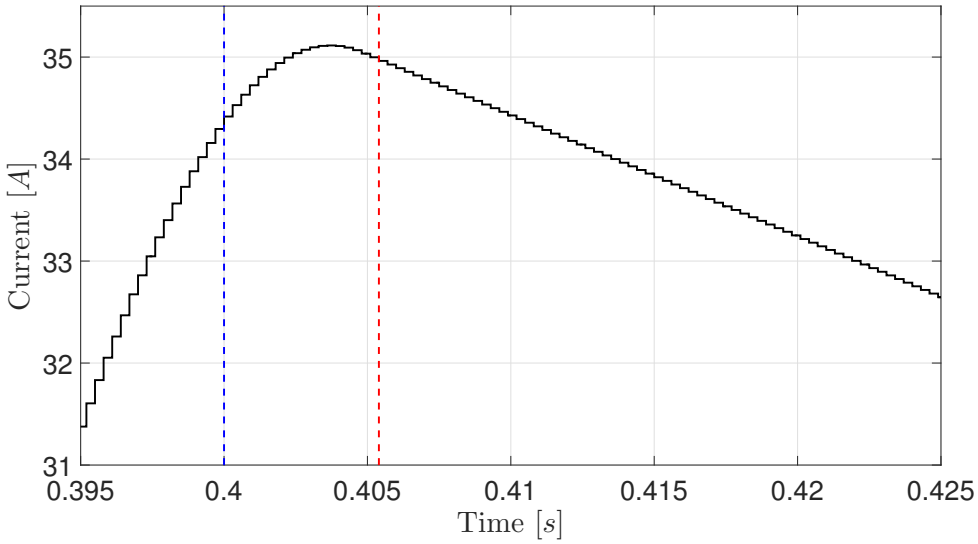

Figure 4.11 – The desired reference current profile. The blue-dashed line indicates the time when the error must remain within ±1000 parts-per-million (ppm); the red-dashed line indicates the time when the error must remain within ±100 ppm.

clock period $T_{cl} = 100\,\mu s$; the acquired periods (with transients removed in post-processing) could then be merged together. A custom FGC signal is limited to 1023 samples; therefore, a 9-bit PRBS signal was used for identification purposes. For a signal of length 511, the frequency resolution is limited to 255 points. The uncertainty was obtained from the covariance of the estimates with a 95% confidence interval. Fig. 4.12 shows the input and output signals acquired from the identification experiment.

4.4.4 Weighting filter selection

For this particular case study, it was desired to obtain the best tracking performance (i.e., by minimizing $\|W_3\mathcal{S}_3(\boldsymbol{\rho})\|_\infty$) while ensuring reasonable stability margins. It is evident that $\mathcal{S}_2^d + \mathcal{S}_3^d = 1$, where $\mathcal{S}_2^d$ and $\mathcal{S}_3^d$ are the desired complementary and error sensitivity functions, respectively. Based on this condition, the weighting filter W_3 was selected as $W_3 = [\mathcal{S}_3^d]^{-1}$. $\mathcal{S}_2^d$ was chosen as a standard second order model $\mathcal{S}_2^d(s) = \omega_d^2(s^2 + 2\zeta_d\omega_d s + \omega_d^2)^{-1}$, where ζ_d is the damping factor and

$$\omega_d = 2\pi f_d \left[1 - 2\zeta_d^2 + \sqrt{2 - 4\zeta_d^2 + 4\zeta_d^4}\right]^{-0.5}$$

and f_d [Hz] is the desired closed-loop bandwidth.

A simulation was performed to determine the required bandwidth to satisfy the desired error specifications. At CERN, the error is calculated with respect to a delayed reference input (i.e., $e(t) = r(t-\tau) - y(t)$); τ is determined by shifting the reference signal such that the

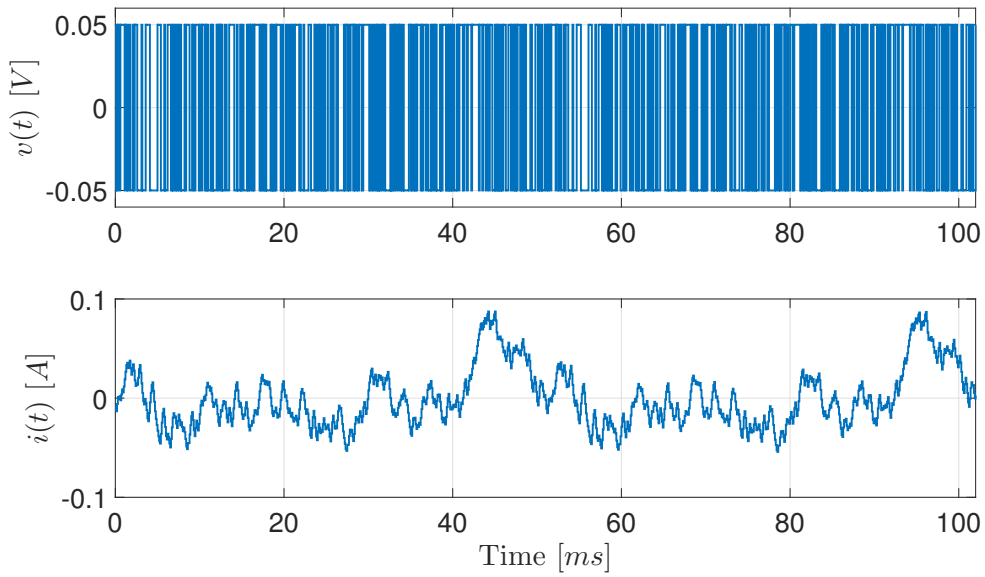

Figure 4.12 – PRBS signal used for the input voltage $v(t)$ of the open-loop system along with the resulting output current $i(t)$.

minimum peak error is achieved. By assuming that the closed-loop response behaves as $\mathscr{S}_2^d$, the bandwidth f_d can be selected such that the error between the delayed reference input and output remains within the requirements set by the application (which are shown in Fig. 4.11); the simulation results led to $f_d = 300\,\text{Hz}$ and $\zeta_d = 0.8$.

4.4.5 Synthesis and Experimental Results

The voltage applied to the magnet by the voltage source and the relative current are both sampled at 10 kHz while the control loop is run 3 times slower (i.e., $T_s = 300\,\mu\text{s}$). Since the plant is Schur, then a possible selection for the coprime factors is $N(e^{-j\omega}) = G(e^{-j\omega})$ and $M(e^{-j\omega}) = 1$. With a minimum value of $m_d = 0.5$ set for the modulus margin (i.e., the minimum distance between the critical point $(-1 + j0)$ and the Nyquist plot of the open-loop transfer function), the following optimization problem must be solved:

$$\begin{aligned} \underset{\gamma,\boldsymbol{\rho}}{\text{minimize}} \quad & \gamma \\ \text{subject to:} \quad & \Re\left\{\psi(e^{-j\omega_k},\boldsymbol{\rho})\right\} > x_r(e^{-j\omega_k},\boldsymbol{\rho}) \\ & \Re\left\{\psi(e^{-j\omega_k},\boldsymbol{\rho})\right\} > x_m(e^{-j\omega_k},\boldsymbol{\rho}) \\ & \Re\left\{S'(e^{-j\omega_k},\boldsymbol{\rho})\right\} > 0 \\ & R(1,\boldsymbol{\rho}) = T(1,\boldsymbol{\rho}) \neq 0 \end{aligned} \tag{4.32}$$

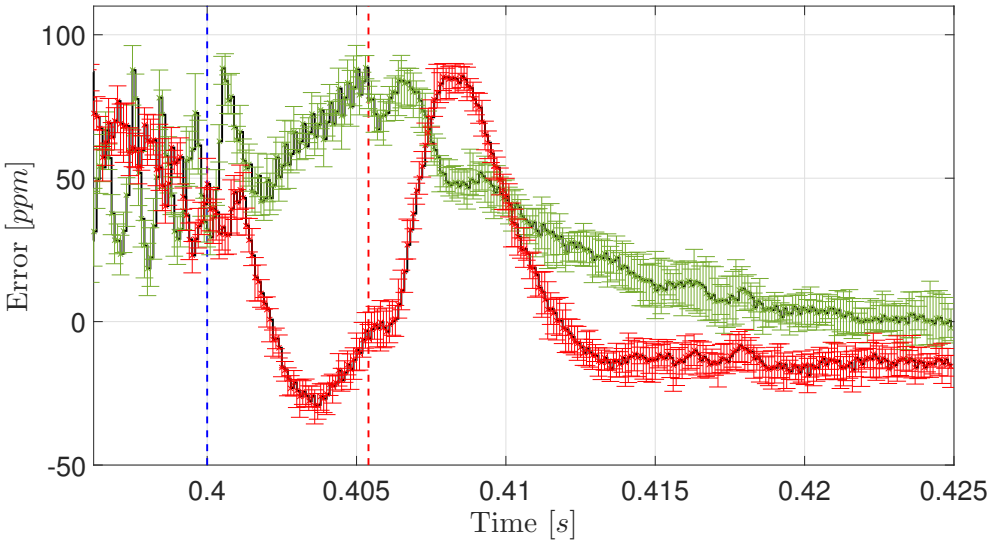

Figure 4.13 – Comparison between the error resulting from the model-based design (solid-black line with red error-bars) and the error resulting with the proposed method (solid-black line with green error-bars).

for $k = 1,\ldots,255$, where $S(z^{-1},\boldsymbol{\rho}) = (1-z^{-1})^2 S'(z^{-1},\boldsymbol{\rho})$, $x_r(e^{-j\omega_k},\boldsymbol{\rho})$ is defined as in (4.20), and $x_m(e^{-j\omega_k},\boldsymbol{\rho}) = |m_d S(e^{-j\omega_k},\boldsymbol{\rho})| + |R(e^{-j\omega_k},\boldsymbol{\rho})W_n(e^{-j\omega_k})|$. The first inequality in (4.32) ensures that $\mathscr{H}_\infty$ nominal performance is achieved for the RST structure whilst considering the frequency dependent uncertainties. The second inequality ensures that the modulus margin is at least 0.5 (a requirement for robust stability at CERN). The third inequality ensures that $S(\boldsymbol{\rho})$ has no unstable zeros (another requirement at CERN) while the fourth equality constraint ensures that the steady-state error is zero.

The semidefinite programming solver (SDPT3) was used in conjunction with `MATLAB` to perform the bisection algorithm [126]. A 9^{th} order controller was used to achieve the desired results (by following the steps outlined in Section 4.2.5). An optimal value of $\gamma^\star = 1.202$ was obtained after 61.3 s using the same computer as in the previous example.

A total of 10 experiments were performed; the error for both the model-based MRC method and data-driven based designs (with the associated error-bars showing the minimum and maximum errors at each sampling instant) are shown in Fig. 4.13. It can be observed that both designs are comfortably within the ±1000 ppm fast-transient requirement and within the ±100 ppm steady-state requirement. Indeed, both controllers achieve ±100 ppm even during the fast-transients. However, the proposed method ensures that all of the design requirements are met while eliminating the iterative process of attaining robust performance from the model-based methodology.

Figure 4.14 – Torsional apparatus (ECP model 205a) used for the experimental analysis. The three disks are comprised of block masses which can be added or removed to alter the inertia of each disk (and thus alter the dynamics of the system). Each disk is vertically suspended on a spring with a variable spring constant. The actuator is located on the bottom of the device.

4.5 Case Study: Torsional Control

An RST controller will now be designed for a multi-model torsional apparatus (ECP Model 205a), as shown in Fig.4.14. This system contains three disks with variable inertias suspended vertically on anti-friction ball bearings. The disks are connected through a non-rigid cable with an adjustable spring constant. The actuator (a high torque brushless motor with a 2 N m rating) is located at the bottom of the apparatus and is directly connected to the bottom disk via a rigid timing belt. The position of the disks are measured with a high resolution encoder (16,000 count/rev) and is used as feedback to control the closed-loop system. For this experiment, the dynamics of the apparatus will be altered by varying the inertias of the top disk.

An RST controller will be designed for various inertial configurations. Three different configurations will be considered for this design; the bottom disk and the middle disk will possess fixed inertias, while the inertia for the top disk will be varied. The inertia is varied by altering the number of block masses that are arranged on the disk.

The input to the system is the current of the actuator and the output is the position of the third disk. Therefore, the plant model has an integrator and is marginally stable; thus it is required to obtain the FRF's of the various configurations in a closed-loop structure. A stabilizing controller must be used to obtain $N(e^{-j\omega})$ and $M(e^{-j\omega})$. For this plant, a PID controller was designed to stabilize the closed-loop system. A reference input with a PRBS is implemented to

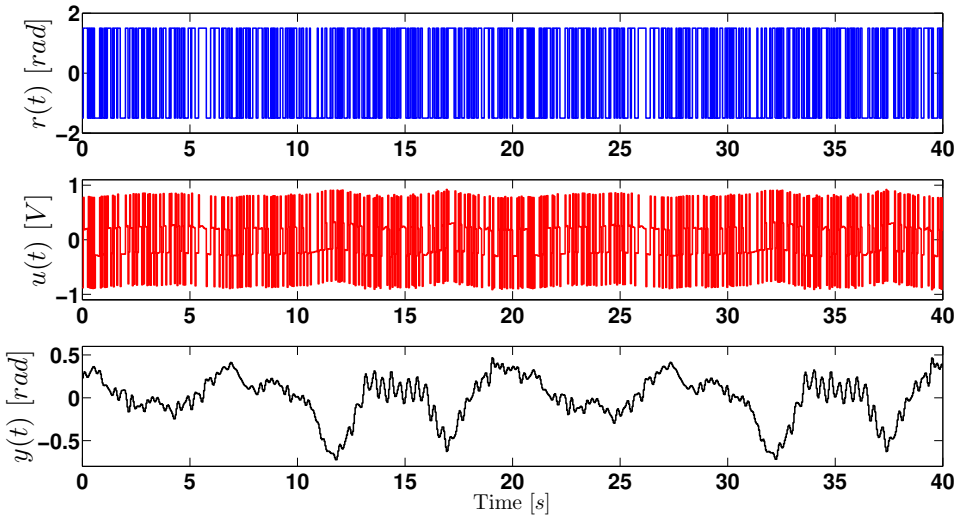

Figure 4.15 – Time-domain response of the closed-loop system with a PRBS excitation signal (shown only for the system configuration with two block masses on the top disk): the PRBS reference input $r(t)$ with a register length of 511 (solid-blue); control output $u(t)$ (solid-red); output response $y(t)$ (solid-black).

excite the closed-loop system with a sampling frequency of 25 Hz. The time-domain signals for the reference input $r(t)$, control output $u(t)$, and output $y(t)$ for this system are depicted in Fig.4.15 (for brevity, the figure shown is for one of the configurations). The FRF of $N(e^{-j\omega})$ is then obtained with the spectral analysis command in `MATLAB` (i.e., `spa(·)`) by using the time-domain data of $r(t)$ and $y(t)$. Similarly, the FRF of $M(e^{-j\omega})$ is obtained in a similar fashion by using the time-domain data of $r(t)$ and $u(t)$. The FRF of the plant model can then be described as $G(e^{-j\omega}) = N(e^{-j\omega})M^{-1}(e^{-j\omega})$. The FRFs for each of the three configurations are shown in Fig. 4.16.

It will be desired to minimize the tracking error and to reject a step disturbance at the output. In order to achieve these specifications, an integrator will be included in $S(z^{-1},\boldsymbol{\rho})$ (i.e., $S(z^{-1},\boldsymbol{\rho}) = (1-z^{-1})S'(z^{-1},\boldsymbol{\rho})$, where $S'(z^{-1},\boldsymbol{\rho})$ is linearly parameterized as in (2.28)). Additionally, a weight will be designated to limit the control effort. Therefore, the optimization problem formulated in (4.27) will be implemented for this design scheme with $q \in \{3,4\}$. Thus the following

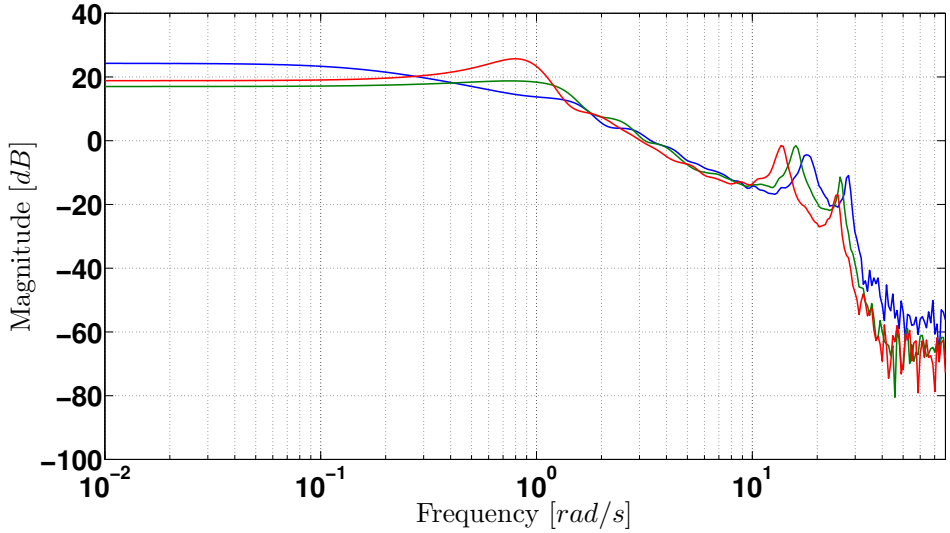

Figure 4.16 – FRF's of the plant model obtained from the closed-loop time-domain response of each system configuration. The loads on the bottom and middle disk are fixed while the load on the top disk is varied: FRF with one block mass on the top disk (solid-blue); FRF with two block masses on the top disk (solid-green); FRF with four block masses on the top disk (solid-red).

optimization problem will be considered:

$$
\begin{aligned}
\underset{\boldsymbol{\rho},\gamma}{\text{minimize}} \quad & \gamma \\
\text{subject to:} \quad & \gamma^{-1}\left|W_3(e^{-j\omega_k})[\psi_i(e^{-j\omega_k},\boldsymbol{\rho}) - N_i(e^{-j\omega_k})T(e^{-j\omega_k},\boldsymbol{\rho})]\right| - \Re\left\{\psi_i(e^{-j\omega_k},\boldsymbol{\rho})\right\} < 0 \\
& \gamma^{-1}\left|W_4(e^{-j\omega_k})M_i(e^{-j\omega_k})T(e^{-j\omega_k},\boldsymbol{\rho})\right| - \Re\left\{\psi_i(e^{-j\omega_k},\boldsymbol{\rho})\right\} < 0 \\
& R(1,\boldsymbol{\rho}) = T(1,\boldsymbol{\rho}) \neq 0 \\
& \text{for } i = 1,2,3 \text{ and } k = 1,\ldots,\eta,
\end{aligned}
\tag{4.33}
$$

where $\psi_i(e^{-j\omega_k},\boldsymbol{\rho}) = M_i(e^{-j\omega_k})S(e^{-j\omega_k},\boldsymbol{\rho}) + N_i(e^{-j\omega_k})R(e^{-j\omega_k},\boldsymbol{\rho})$.

4.5.1 Weighting filter selection

As in the previous case study, the weighting filter W_3 will be chosen based on the fact that $\mathscr{S}_2^d + \mathscr{S}_3^d = 1$. $\mathscr{S}_2^d$ is chosen as a first order transfer function such that the step response will have a time constant $\tau = 1\,\text{s}$ (which corresponds to a closed-loop bandwidth of $\omega_d = 1\,\text{rad}\,\text{s}^{-1}$). The transfer function which satisfies these requirements can be formulated as $\mathscr{S}_2^d(s) = (\tau s + 1)^{-1}$. Given this desired closed-loop model, an appropriate filter for the error

sensitivity function can be devised as $W_3(s) = (s+\omega_d)s^{-1}$. Note again that since the polynomial $S^{-1}(\boldsymbol{\rho})$ contains an integrator, $\|W_3\mathscr{S}_3(\boldsymbol{\rho})\|_\infty$ remains bounded for all ω.

It will also be desired to minimize the control effort at high frequencies; therefore, a viable choice for the control weighting function W_4 is

$$W_4(s) = \frac{s+\omega_u/M_u}{\omega_u}, \tag{4.34}$$

where M_u is the maximum controller gain, and ω_u is the controller bandwidth [10]. For the torsional system considered in this chapter, an appropriate choice for these parameters are $M_u = 10^3$ and $\omega_u = 3\,\mathrm{rad\,s^{-1}}$.

4.5.2 Experimental results

The optimization problem in (4.33) was solved by considering a logarithmically spaced frequency grid with $\eta = 400$ points. The SDPT3 software package was used in conjunction with `MATLAB` to solve the optimization problem. The algorithm in Table. 4.1 was used to design a 8^{th} order controller. The solution obtained from the bisection algorithm produces the following controllers:

$$R(z^{-1}) = 34.19 - 113.7z^{-1} + 160z^{-2} - 100.3z^{-3} - 10.66z^{-4} + 60.08z^{-5} \\ - 32.94z^{-6} - 2.093z^{-7} + 5.542z^{-8}$$

$$S(z^{-1}) = 1 + 0.3538z^{-1} + 0.2304z^{-2} - 0.07627z^{-3} - 0.2845z^{-4} - 0.2575z^{-5} - 0.08136z^{-6} \\ - 0.1705z^{-7} - 0.2921z^{-8} - 0.422z^{-9}$$

$$T(z^{-1}) = 0.00942 + 0.01295z^{-1} + 0.01548z^{-2} + 0.01646z^{-3} + 0.01116z^{-4} + 0.01683z^{-5} \\ + 0.01491z^{-6} + 0.01329z^{-7} + 0.01008z^{-8}$$

The optimal value of γ obtained from the optimization was $\gamma^\star = 2.228$. The step responses obtained for each of the inertial configurations are depicted in Fig. 4.17. From the multi-model step responses, it can be observed that the system is stable and robust to the dynamic variations of the torsional apparatus. Moreover, the load variations do not significantly impact the tracking performance (which is expected, since the same weighting filter was used in the multi-model optimization problem). The closed-loop FRF's of all three system configurations are shown in Fig. 4.18. It can be observed that the achieved closed-loop bandwidth for all three configurations is approximately $1\,\mathrm{rad\,s^{-1}}$, which was the bandwidth that was specified to form the weighting filter $W_3(s)$. This confirms the feasibility of the solution obtained from the

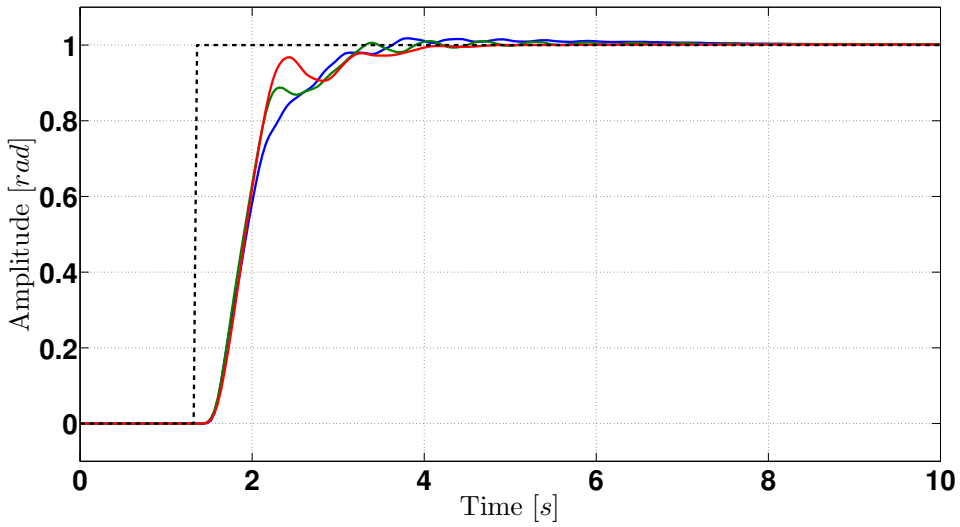

Figure 4.17 – Step response for each load configuration: response with one block mass on the top disk (solid-blue); response with two block masses on the top disk (solid-green); response with four block masses on the top disk (solid-red).

optimization problem in (4.33).

4.6 Conclusion

The necessary and sufficient conditions for the existence of RST controllers that achieve $\mathscr{H}_\infty$ performance for multiple weighted sensitivity functions have been established with a set of convex constraints. Additionally, a method has been devised to design controllers for linear systems that were subject to nonlinear distortions (where a nonlinear system was represented as a BLA with an associated uncertainty). Moreover, constraints have been devised in order to design a controller which considers the frequency dependent uncertainties and to assure the controller stability. The simulation and experimental results show that the proposed data-driven method offers an optimization-based systematic approach that leads to RST controllers meeting the challenging specifications required by each application.

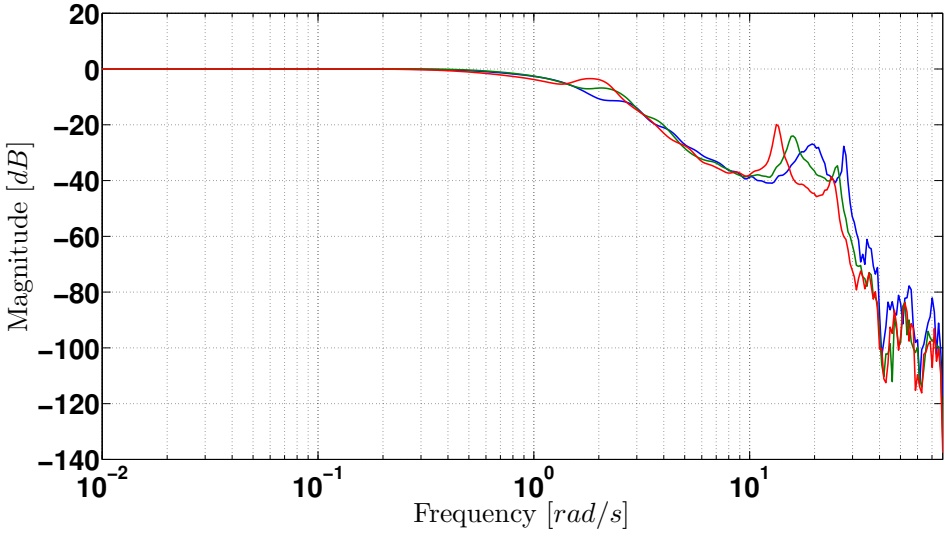

Figure 4.18 – Closed-loop frequency response functions of all three system configurations: closed-loop FRF with one block mass on the top disk (solid-blue); closed-loop FRF with two block masses on the top disk (solid-green); closed-loop FRF with four block masses on the top disk (solid-red).

5 Robust Control of Systems With Sector Nonlinearities

5.1 Introduction

In the previous chapters, robust controller design methods have been devised for *linear systems*. In Chapter 4, a method for designing controllers for linear systems subject to nonlinear distortions was considered; however, this method did not guarantee the stability or performance for the true nonlinear system. The objective of this chapter is to investigate systems with sector-bounded nonlinearities and use the Circle criterion to stabilize the closed-loop system in a data-driven setting. The necessary and sufficient conditions of stability using the Circle criterion are derived using only the FRF of a plant. The conditions are simple convex constraints that can be applied to systems with multi-model uncertainty as well. Moreover, a sufficient condition is presented to guarantee $\mathscr{H}_\infty$ performance and stability for systems with time-invariant sector-bounded nonlinearities represented by describing functions. The theory presented in this work extends on the concepts from chapters 3 and 4 to establish the stability and performance conditions for nonlinear systems.

In this chapter, a discrete-time representation of coprime processes (see Section 2.1.2) is used to represent the class of linear systems. The class of controllers used are the 1DOF polynomial structures asserted in Section 2.2.1. The class of nonlinear systems addressed in this chapter are the sector bounded nonlinearities asserted in Section 2.1.3. Fig. 5.1 shows the general structure of the overall closed-loop system.

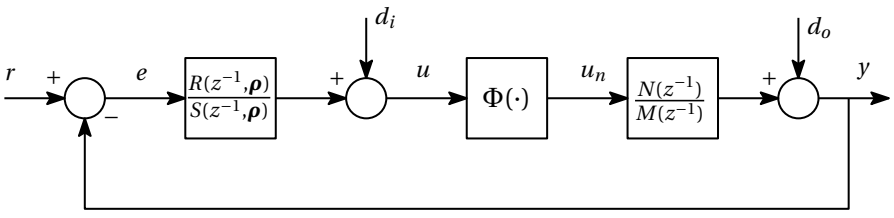

Figure 5.1 – Discrete-time controller structure.

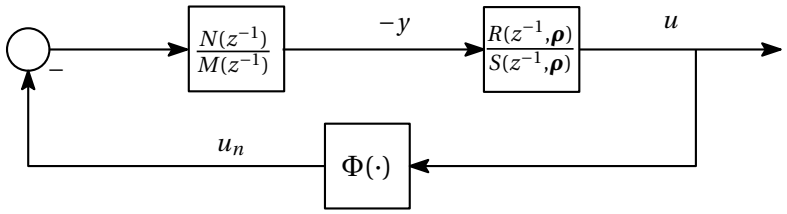

Figure 5.2 – Equivalent block diagram in autonomous form.

5.2 The Circle Criterion Revisited

The Circle criterion provides a necessary and sufficient condition for ensuring the closed-loop stability with a sector nonlinearity $\Phi(\cdot) \in \mathscr{N}_t$ [127]. In order to analyze the stability of the closed-loop system with the nonlinearity $\Phi(\cdot)$, let us consider the autonomous form of the block diagram in Fig. 5.1, which is shown in Fig. 5.2. The open-loop transfer function can be defined as

$$L(z^{-1},\boldsymbol{\rho}) = N(z^{-1})R(z^{-1},\boldsymbol{\rho})\left[M(z^{-1})S(z^{-1},\boldsymbol{\rho})\right]^{-1}.$$

One of the conditions for ensuring the closed-loop stability with $\Phi(\cdot) \in \mathscr{N}_t$ is as follows:

$$\Re\left\{\frac{1+\beta_2 L(e^{-j\omega},\boldsymbol{\rho})}{1+\beta_1 L(e^{-j\omega},\boldsymbol{\rho})}\right\} > 0, \quad \forall \omega \in \Omega, \tag{5.1}$$

where $L : \mathbb{R}^{n_{rs}} \times \mathbb{R} \to \mathbb{C}$. The condition in (5.1) can be interpreted as a disk $C(\beta, r_d)$ (with radius r_d centered at β) that does not intersect with $L(e^{-j\omega},\boldsymbol{\rho})$, where r_d and β are defined as follows:

$$\beta = -\frac{\beta_1+\beta_2}{2\beta_1\beta_2}, \quad r_d = \frac{1}{2}\left|\frac{\beta_2-\beta_1}{\beta_1\beta_2}\right|. \tag{5.2}$$

Depending on the signed values of β_1 and β_2, (5.1) can be interpreted in several different manners:

- If $0 < \beta_1 < \beta_2$, then (5.1) can be interpreted as a disk $C(\beta, r_d)$ in the complex plane such that the Nyquist plot of $L(e^{-j\omega},\boldsymbol{\rho})$ lies outside of the disk (without intersecting it).
- If $\beta_1 < 0 < \beta_2$, then (5.1) represents a disk $C(\beta, r_d)$ in the complex plane such that the Nyquist plot of $L(e^{-j\omega},\boldsymbol{\rho})$ lies completely in the interior of the disk (without intersecting it).
- If $0 = \beta_1 < \beta_2$, then (5.1) represents a vertical line in the complex plane that intersects the real axis at $-\beta_2^{-1}$, where the Nyquist plot of $L(e^{-j\omega},\boldsymbol{\rho})$ lies to the right of this line.

Fig. 5.3 displays the graphical representations for each case.

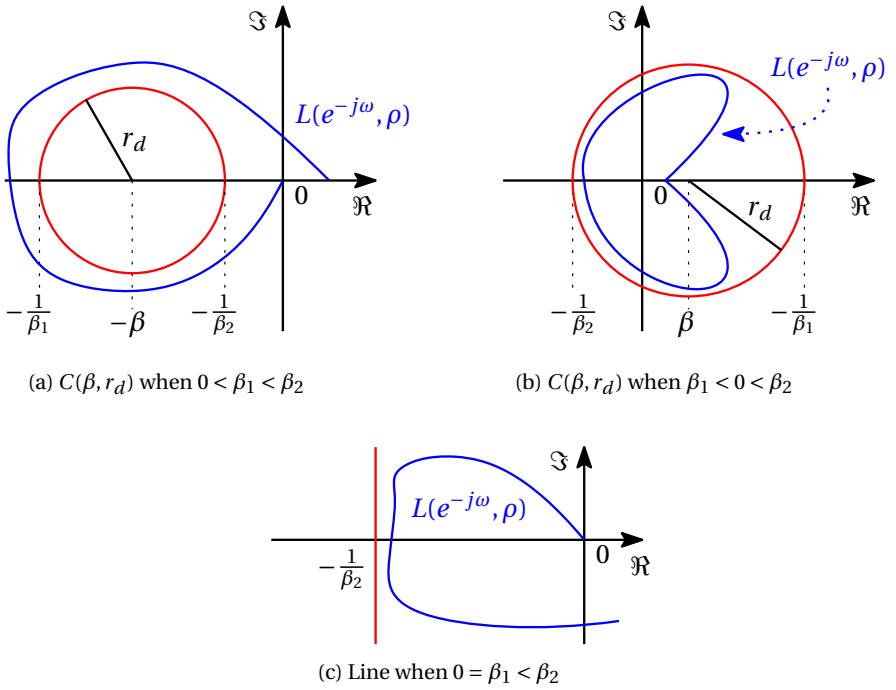

(a) $C(\beta, r_d)$ when $0 < \beta_1 < \beta_2$

(b) $C(\beta, r_d)$ when $\beta_1 < 0 < \beta_2$

(c) Line when $0 = \beta_1 < \beta_2$

Figure 5.3 – Absolute stability condition for the sector nonlinearity in (2.14) when different conditions for β_1 and β_2 are considered.

The Circle criterion states that given any sector nonlinearity in $\mathscr{N}_t$, the closed-loop system is globally asymptotically stable at the origin if and only if

$$L_T(e^{-j\omega}, \boldsymbol{\rho}) = L(e^{-j\omega}, \boldsymbol{\rho}) \left[\beta + L(e^{-j\omega}, \boldsymbol{\rho})\right]^{-1}$$

is Schur and the above disk conditions hold for the appropriate values of β_1 and β_2. By the Nyquist criterion, L_T is Schur if and only if the Nyquist plot of $L(e^{-j\omega}, \boldsymbol{\rho})$ does not intersect the point $(-\beta + j0)$ and encircles it exactly m times in the counterclockwise direction, where m is the number of poles of L with $|z| > 1$. The necessary and sufficient conditions of the Circle criterion for this class of nonlinearities is recalled from [127]:

Theorem 5.1. *Consider an open-loop transfer function $L(z^{-1})$ and $\{\beta_1, \beta_2\} \in \mathbb{R}$ with $\beta_1 < \beta_2$. Then the following two statements are equivalent:*

(a) *The negative feedback interconnection of $L(z^{-1})$ and any sector nonlinearity $\Phi(\cdot) \in \mathscr{N}_t$ is stable.*

(b) *The transfer function $L(z^{-1})$ satisfies one of the following conditions, as appropriate:*

- *Case 1:* $0 < \beta_1 < \beta_2$
  - *The Nyquist plot of $L(e^{-j\omega})$ does not intersect the interior of the disk $C(\beta, r_d)$ and encircles the interior of the disk $C(\beta, r_d)$ exactly m times in the counter-clockwise*

direction, where m is the number of poles of $L(z^{-1})$ *with* $|z| > 1$.

- *Case 2:* $\beta_1 < 0 < \beta_2$
  - $L(z^{-1})$ *is Schur and the Nyquist plot of* $L(e^{-j\omega})$ *lies in the interior of the disk* $C(\beta, r_d)$.
- *Case 3:* $\beta_1 = 0$
  - $L(z^{-1})$ *is Schur and*

$$\Re\left\{L(e^{-j\omega})\right\} > -\frac{1}{\beta_2}, \quad \forall \omega \in \Omega \tag{5.3}$$

Remark. *As discussed in [85] and [127], the Circle criterion provides only a sufficient condition for the stability of a closed-loop nonlinear system (with a sector-bounded nonlinearity) when the problem is concerned with a specific nonlinearity in a closed sector. However,* ***for any*** *nonlinearity in a closed-sector, the Circle criterion then becomes necessary and sufficient. The proof for the above Theorem can be found in [127].*

5.3 Stabilization via the Circle Criterion

This section is concerned with developing convex constraints for ensuring the closed-loop stability of the system in Fig. 5.1 given a nonlinearity in the set $\mathscr{N}_t$. The results of the Circle criterion asserted in the previous section will be used to formulate these conditions; the conditions for each case professed in Theorem 5.1 will be considered. For notation purposes, the dependency in $e^{-j\omega}$ will be omitted and will only be reiterated when deemed necessary. The dependency in $\boldsymbol{\rho}$ will continue to be highlighted.

5.3.1 Case 1: $0 < \beta_1 < \beta_2$

For this case, the condition from the Circle criterion can be expressed as follows:

$$\sup_{\omega\in\Omega}\left|\frac{r_d}{\beta + L(e^{-j\omega}, \boldsymbol{\rho})}\right| < 1. \tag{5.4}$$

This inequality will ensure that the Nyquist plot of $L(\boldsymbol{\rho})$ will remain outside the disk $C(\beta, r_d)$ and never intersect it. However, stability is not ensured with this condition since the inequality does not necessarily guarantee that the Nyquist criterion is met. Moreover, this constraint is not convex, which creates additional computation burdens. However, if $[\beta + L(\boldsymbol{\rho})]^{-1}$ is Schur, then by the Nyquist criterion, the Nyquist plot of $L(\boldsymbol{\rho})$ will not intersect the point $(-\beta + j0)$ and encircle it m times in the counterclockwise direction. Thus by Theorem 5.1, if $[\beta + L(\boldsymbol{\rho})]^{-1}$ is Schur and (5.4) is satisfied, then the closed-loop system with sector nonlinearity $\Phi(\cdot) \in \mathscr{N}_t$ is stable.

With the control structure used in this chapter, the condition in (5.4) can also be expressed as

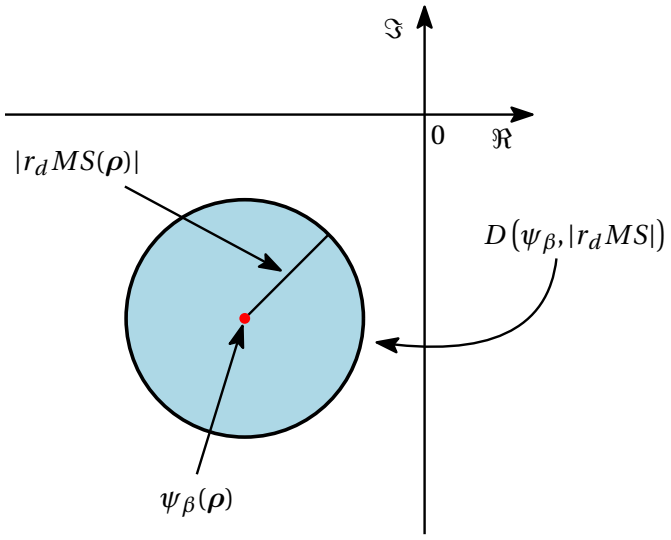

Figure 5.4 – A graphical interpretation of the constraint (5.5) in the complex plane.

follows:

$$\left|r_d MS(\boldsymbol{\rho})\right| < \left|\psi_\beta(\boldsymbol{\rho})\right|, \quad \forall \omega \in \Omega, \tag{5.5}$$

where $\psi_\beta(\boldsymbol{\rho}) = NR(\boldsymbol{\rho}) + \beta MS(\boldsymbol{\rho})$. Consider a disk in the complex plane $D(\psi_\beta, |r_d MS|)$ at a specific frequency in Ω which is centered at $\psi_\beta(\boldsymbol{\rho})$ and has radius $|r_d MS(\boldsymbol{\rho})|$. The constraint in (5.5) ensures that for any frequency point in Ω, the disk associated with this frequency point will not include the origin. Fig. 5.4 displays a graphical interpretation of this condition for a given ω. This geometrical construction will be used to prove the following Lemma:

Lemma 5.1. *The feedback interconnection of $L(z^{-1})$ and any sector nonlinearity $\Phi(\cdot) \in \mathscr{N}_t$ with $0 < \beta_1 < \beta_2$ is stable if and only if there exists a finite-impulse-response (FIR) function $F(z^{-1})$ that satisfies*

$$\Re\left\{\psi_\beta(\boldsymbol{\rho})F(e^{-j\omega})\right\} > \left|r_d MS(\boldsymbol{\rho})F(e^{-j\omega})\right|, \qquad \forall \omega \in \Omega. \tag{5.6}$$

Proof : From the necessary and sufficient condition in Theorem 5.1, stability of the closed-loop nonlinear system imposes the following condition:

$$\sup_{\omega\in\Omega}\left|\frac{r_d MS(\boldsymbol{\rho})}{\psi_\beta(\boldsymbol{\rho})}\right| < 1.$$

It is clear that the above condition is satisfied if and only if the disk $D(\psi_\beta, |r_d MS|)$ does not include the origin for all $\omega \in \Omega$, i.e. $|\psi_\beta(\boldsymbol{\rho})| > |r_d MS(\boldsymbol{\rho})|$. This is equivalent to the existence of a line passing through origin that does not intersect the disk. Therefore, at every given frequency, ω, there exists a complex number $f(e^{-j\omega})$ that can rotate the disk such that it lays

inside the right hand side of the imaginary axis. Hence, we have

$$\Re\left\{\left[\psi_\beta(\boldsymbol{\rho}) - |r_d MS(\boldsymbol{\rho})|e^{j\theta}\right] f(e^{-j\omega})\right\} > 0, \quad \forall\omega \in \Omega, \forall\theta \in [0\,, 2\pi[. \tag{5.7}$$

Since $f(e^{-j\omega}) = |f(e^{-j\omega})|e^{j\theta_f}$, then the above condition can be expressed as

$$\Re\left\{\psi_\beta(\boldsymbol{\rho}) f(e^{-j\omega})\right\} > \left|r_d MS(\boldsymbol{\rho}) f(e^{-j\omega})\right| \cos(\theta + \theta_f), \quad \forall\omega \in \Omega, \forall\theta \in [0\,, 2\pi[. \tag{5.8}$$

However, (5.8) is satisfied if and only if:

$$\Re\left\{\psi_\beta(\boldsymbol{\rho}) f(e^{-j\omega})\right\} > \left|r_d MS(\boldsymbol{\rho}) f(e^{-j\omega})\right|, \quad \forall\omega \in \Omega. \tag{5.9}$$

In [103], it is shown that, $f(e^{-j\omega})$ can be approximated arbitrarily well by the frequency response of a stable transfer function or FIR function $F(z^{-1})$ if and only if

$$Z = \left(\psi_\beta(\boldsymbol{\rho}) - \delta^{-1}|r_d MS(\boldsymbol{\rho})|e^{j\theta}\right)^{-1} \tag{5.10}$$

is analytic outside the unit circle for all $\theta \in [0\,, 2\pi[$ and for all $\delta > 1$. However, by the necessary and sufficient condition in Theorem 5.1, $\psi_\beta^{-1}(\boldsymbol{\rho})$ is Schur because the closed-loop nonlinear system is stable. Additionally, by decreasing δ from infinity to 1, the poles of Z move continuously with δ. Therefore, Z is not analytic outside the unit circle if and only if $Z^{-1}(e^{-j\omega}) = 0$ for a given frequency, which is not the case because the origin is not in the interior of the disk $D(\psi_\beta, |r_d MS|)$. ■

The set of all controllers that meet the stability condition given by the Circle criterion is asserted in the following theorem.

Theorem 5.2. *Given the frequency response function $G(e^{-j\omega}) = N(e^{-j\omega})M^{-1}(e^{-j\omega})$ and any sector nonlinearity $\Phi(\cdot) \in \mathscr{N}_t$ with $0 < \beta_1 < \beta_2$, then the following statements are equivalent:*

(a) *There exist polynomials R and S that stabilizes the nonlinear system.*

(b) *There exist polynomials R and S such that*

$$\Re\left\{\psi_\beta(\boldsymbol{\rho})\right\} > \left|r_d MS(\boldsymbol{\rho})\right|, \quad \forall\omega \in \Omega. \tag{5.11}$$

Proof: (**b** ⇒ **a**)
$\Re\{\psi_\beta(\boldsymbol{\rho})\} > 0$ signifies that the Nyquist plot of $\psi_\beta(\boldsymbol{\rho})$ will not encircle the origin $\forall\omega$. However, note that

$$\Re\left\{\psi_\beta(\boldsymbol{\rho})\right\} > 0 \iff \Re\left\{\frac{1}{\psi_\beta(\boldsymbol{\rho})}\right\} > 0.$$

By the SPR condition in Lemma (4.1), the positive real constraint implies that $\psi_\beta^{-1}(\boldsymbol{\rho}) = [MS(\boldsymbol{\rho})]^{-1}[\beta + L(\boldsymbol{\rho})]^{-1}$ is Schur. On the other hand, note that

$$\left|\psi_\beta(\boldsymbol{\rho})\right| \geq \Re\left\{\psi_\beta(\boldsymbol{\rho})\right\}, \quad \forall\omega \in \Omega. \tag{5.12}$$

From (5.11), this implies that

$$\left|r_d MS(\boldsymbol{\rho})\right| < \left|\psi_\beta(\boldsymbol{\rho})\right|, \quad \forall \omega \in \Omega \tag{5.13}$$

which leads to

$$\left|\frac{r_d}{\beta + L(\boldsymbol{\rho})}\right| < 1, \quad \forall \omega \in \Omega. \tag{5.14}$$

Therefore, the Nyquist plot of $L(\boldsymbol{\rho})$ does not intersect the disk $C(\beta, r_d)$ and consequently, according to Theorem 1, the closed-loop nonlinear system is stable.

(**a** $\Rightarrow$ **b**)
Assume that $R(\boldsymbol{\rho}')$, and $S(\boldsymbol{\rho}')$ satisfies Statement (**a**) but not Statement (**b**). Then, according to Lemma 5.1, there exists an FIR function $F(z^{-1})$ such that

$$\Re\left\{\psi_\beta(\boldsymbol{\rho}')F(e^{-j\omega})\right\} > \left|r_d MS(\boldsymbol{\rho}')F(e^{-j\omega})\right|, \quad \forall \omega \in \Omega. \tag{5.15}$$

Therefore, there exists a higher order controller with $R = R(\boldsymbol{\rho}')F$ and $S = S(\boldsymbol{\rho}')F$ such that Statement (**b**) holds. ■

5.3.2 Case 2: $\beta_1 < 0 < \beta_2$

For this case, the condition from the Circle criterion can be expressed as follows:

$$\sup_{\omega \in \Omega}\left|\frac{r_d}{\beta + L(\boldsymbol{\rho})}\right| > 1. \tag{5.16}$$

This inequality will ensure that the Nyquist plot of $L(\boldsymbol{\rho})$ will remain in the interior of the disk $C(\beta, r_d)$ and never intersect it. By Theorem 5.1, if $L(\boldsymbol{\rho})$ is Schur, then the above condition guarantees the stability of the closed-loop nonlinear system. With the control structure used in this chapter, the above condition can also be expressed as follows:

$$\left|\psi_\beta(\boldsymbol{\rho})\right| < \left|r_d MS(\boldsymbol{\rho})\right|, \quad \forall \omega \in \Omega. \tag{5.17}$$

Note that this condition is the same as that in (5.5) with the direction of the inequality sign changed. This condition represents a disk at a particular frequency in Ω in the complex plane which is centered at $r_d MS(\boldsymbol{\rho})$ and has radius $|\psi_\beta(\boldsymbol{\rho})|$. The constraint in (5.17) ensures that for any frequency point in Ω, the disk associated with this frequency point will not include the origin. Note that this geometrical construction is the same as (5.5), but with the radius and center interchanged (i.e., the disk is now represented as $D(r_d MS, |\psi_\beta|)$).

Lemma 5.2. *For a stable plant model, the feedback interconnection of $L(z^{-1})$ and any sector nonlinearity $\Phi(\cdot) \in \mathcal{N}_t$ with $\beta_1 < 0 < \beta_2$ is stable if and only if there exists a finite-impulse-*

response (FIR) function $F(z^{-1})$ *that satisfies*

$$\Re\left\{r_d MS(\boldsymbol{\rho})F(e^{-j\omega})\right\} > \left|\psi_\beta(\boldsymbol{\rho})F(e^{-j\omega})\right|, \quad \forall\omega\in\Omega. \tag{5.18}$$

Proof : The proof is very similar to the proof asserted in Lemma 5.1. By simply interchanging the radius and center from Lemma 5.1, the same steps can be carried out to prove the above statements. However, for this case, the open-loop system $L(\boldsymbol{\rho})$ must be Schur for ensuring the closed-loop stability of the nonlinear system.

Note that the constraint in (5.18) implies $\Re\{[r_d MS(\boldsymbol{\rho})F]^{-1}\} > 0$; from the SPR conditions in Lemma (4.1), $\Re\{[r_d MS(\boldsymbol{\rho})F]^{-1}\} > 0$ signifies that $[MS(\boldsymbol{\rho})F]^{-1}$ is Schur. Therefore, $S^{-1}(\boldsymbol{\rho})$ is stable (which ensures that $L(\boldsymbol{\rho})$ is Schur). ■

The set of all controllers that meet the stability condition given by the Circle criterion is asserted in the following theorem.

Theorem 5.3. *Given the frequency response function of a stable plant* $G(e^{-j\omega}) = N(e^{-j\omega})M^{-1}(e^{-j\omega})$ *and any sector nonlinearity* $\Phi(\cdot)\in\mathscr{N}_t$ *with* $\beta_1 < 0 < \beta_2$*, the following statements are equivalent:*

(a) *There exist polynomials R and S that stabilizes the nonlinear system.*

(b) *There exist polynomials R and S such that*

$$\Re\left\{r_d MS(\boldsymbol{\rho})\right\} > \left|\psi_\beta(\boldsymbol{\rho})\right|, \quad \forall\omega\in\Omega. \tag{5.19}$$

Proof : (**b** ⇒ **a**)
Since

$$\Re\left\{r_d MS(\boldsymbol{\rho})\right\} > 0 \Longleftrightarrow \Re\left\{\left[r_d MS(\boldsymbol{\rho})\right]^{-1}\right\} > 0,$$

then by the SPR condition in Lemma 4.1, $\Re\{r_d MS(\boldsymbol{\rho})\} > 0$ implies that $[r_d MS(\boldsymbol{\rho})]^{-1}$ is stable. This signifies that $S^{-1}(\boldsymbol{\rho})$ is stable (and thus $L(\boldsymbol{\rho})$ is Schur since G is stable). Furthermore, we have

$$\left|r_d MS(\boldsymbol{\rho})\right| \geq \Re\left\{r_d MS(\boldsymbol{\rho})\right\}, \quad \forall\omega\in\Omega \tag{5.20}$$

which leads to

$$\left|\psi_\beta(\boldsymbol{\rho})\right| < \left|r_d MS(\boldsymbol{\rho})\right|, \quad \forall\omega\in\Omega \tag{5.21}$$

and consequently to

$$\left|\frac{r_d}{\beta + L(\boldsymbol{\rho})}\right| > 1, \quad \forall\omega\in\Omega. \tag{5.22}$$

Therefore, the Nyquist plot of $L(\boldsymbol{\rho})$ remains inside the disk $C(\beta, r_d)$ and according to Theorem 1, the closed-loop nonlinear system is stable.

(**a** $\Rightarrow$ **b**)
The proof for this condition is very similar to the proof in Theorem 5.2 (by using the condition in Lemma 5.2 instead on Lemma 5.1). ■

5.3.3 Case 3: $0 = \beta_1 < \beta_2$

The necessary and sufficient condition for absolute stability in this case (as stated in Theorem 5.1) is that the Nyquist plot of $L(e^{-j\omega}, \boldsymbol{\rho})$ lies on the right-hand side of the vertical line intersecting the point $-\beta_2^{-1}$. A solution for realizing this case is to apply the necessary and sufficient convex constraints in Theorem 5.3 with $\beta_1 = -\epsilon$ (where $0 < \epsilon << 1$); this introduces some conservatism since we are restricting the Nyquist plot to be within the disk $C(\beta, r_d)$. However, this conservatism can be reduced by decreasing the value of ϵ (which expands the disk $C(\beta, r_d)$).

5.4 A Multi-Model Approach for Ensuring $\mathscr{H}_\infty$ Performance

In the previous section, necessary and sufficient conditions were developed for stabilizing systems with sector-bounded nonlinearities in $\mathscr{N}_t$. These conditions were established by using the properties of the Circle criterion. In this section, a method for ensuring $\mathscr{H}_\infty$ performance of the closed-loop system is developed. Since the $\mathscr{H}_\infty$ performance is well defined for linear systems, the performance is guaranteed for uncertain fixed gains inside the sector nonlinearity.

Consider replacing the nonlinearity $\Phi(u)$ in Fig. 5.1 with a simple gain α inside the sector; the entire control system then becomes linear. The output of this gain can then be expressed as $u_n = \alpha u$, which is a line in the $u - u_n$ plane with slope α in Fig. 2.1. This gain can be absorbed in the plant model as αNM^{-1}. In this linear framework, the sensitivity functions of the control system can be properly defined. As asserted in Chapter 2, a general construction of the sensitivity function can be expressed as $\mathscr{S}_q(\boldsymbol{\rho}) = \Delta_q(\boldsymbol{\rho})/\psi(\boldsymbol{\rho})$, where $\Delta_q(\boldsymbol{\rho})$ is a linear function of $R(\boldsymbol{\rho})$ or $S(\boldsymbol{\rho})$ and $\psi(\boldsymbol{\rho}) = \alpha NR(\boldsymbol{\rho}) + MS(\boldsymbol{\rho})$. The subscript $q \in \{s, t, u, v\}$ denotes the q-th sensitivity of interest. As an example, the sensitivity function $\mathscr{S}_s$ from r to $r - y$ is $\Delta_s(\boldsymbol{\rho})/\psi(\boldsymbol{\rho})$, where $\Delta_s(\boldsymbol{\rho}) = MS(\boldsymbol{\rho})$.

In the general $\mathscr{H}_\infty$ control problem for *linear systems*, the objective is to minimize an upper bound γ to find the controller parameter vector $\boldsymbol{\rho}$ such that

$$\sup_{\omega \in \Omega} \left| W_q(e^{-j\omega}) \mathscr{S}_q(e^{-j\omega}, \boldsymbol{\rho}) \right| < \gamma, \tag{5.23}$$

where $\mathscr{S}_q : \mathbb{R}^{n_{rs}} \times \mathbb{R} \to \mathbb{C}$, $\gamma \in \mathbb{R}_+$, and $W_q : \mathbb{R} \to \mathbb{C}$ is the FRF of a stable weighting filter such that $W_q \mathscr{S}_q(\boldsymbol{\rho})$ has a bounded infinity norm. The results from Theorem 4.1 are reiterated in this framework in order to establish the main results of this section.

Lemma 5.3. *Given the frequency response function $G(e^{-j\omega}) = \alpha N(e^{-j\omega}) M^{-1}(e^{-j\omega})$ and the frequency response of a weighting filter $W_q(e^{-j\omega})$, then the following statements are equivalent:*

(a) *There exist polynomials R and S that stabilize G and*

$$\sup_{\omega\in\Omega}\left|W_q\mathscr{S}_q(\boldsymbol{\rho})\right| < \gamma. \tag{5.24}$$

(b) *There exist polynomials R and S such that*

$$\Re\left\{\psi(\boldsymbol{\rho})\right\} > \gamma^{-1}\left|W_q\Delta_q(\boldsymbol{\rho})\right|, \quad \forall\omega\in\Omega. \tag{5.25}$$

Proof : The proof of a similar condition can be found in Theorem 4.1. ■

The above Lemma is only valid when the nonlinearity is replaced with a simple gain, and the overall system becomes linear. The following Theorem will now show how this result can be applied in order to guarantee $\mathscr{H}_\infty$ performance for all fixed gains in the sector.

Theorem 5.4. *Given the FRF of the modified plant model $G(e^{-j\omega}) = \alpha N(e^{-j\omega})M^{-1}(e^{-j\omega})$ and stable weighting filter $W_q(e^{-j\omega})$, the linearly parameterized functions $R(\boldsymbol{\rho})$ and $S(\boldsymbol{\rho})$ achieve $\mathscr{H}_\infty$ performance for all $\alpha\in[\beta_1,\beta_2]$ if*

$$\Re\left\{\psi(\boldsymbol{\rho})\right\} > \gamma^{-1}|W_q\Delta_q(\boldsymbol{\rho})|, \quad \alpha\in\{\beta_1,\beta_2\}, \forall\omega\in\Omega. \tag{5.26}$$

Proof : The inequality in (5.25) is linear with respect to α. Therefore, if the constraint (5.25) in Theorem 5.3 is satisfied for $\alpha=\beta_1$ *and* $\alpha=\beta_2$ (for the modified plant model $G=\alpha NM^{-1}$), then the constraint is satisfied for all $\alpha\in[\beta_1,\beta_2]$. ■

According to the results in Theorem 3.3, it can be shown that when γ is minimized, the optimal solution to the above problem converges to the global optimal solution of the true $\mathscr{H}_\infty$ problem as the controller order increases.

Let $\mathscr{N}_d(U)$ denote the describing function (DF) of $\Phi(u)$ when this nonlinearity is odd, time-invariant, and memoryless (where U is the amplitude of a sinusoidal signal injected at the input of $\Phi(u)$). Note that for this class of nonlinearities, $\mathscr{N}_d(U):\mathbb{R}\to\mathbb{R}$. Recall that the DF is obtained by applying a sinusoidal signal $U\sin(\omega t)$ at the input of the nonlinearity and calculating the ratio of the Fourier coefficient of the first harmonic at the output to U. Thus the expression for determining the DF is [85]:

$$\mathscr{N}_d(U) = \frac{2}{\pi U}\int_0^\pi \Phi(U\sin\theta)\sin\theta\; d\theta. \tag{5.27}$$

Note that the DF for a nonlinear element is *analogous* to the transfer function for a linear element, reducing identically to this transfer function in the purely linear case. For example, consider the sensitivity function $\mathscr{S}_s(\boldsymbol{\rho})$; if the nonlinearity is replaced with the DF, the

sensitivity function $\mathscr{S}_s(\boldsymbol{\rho})$ would then be expressed as

$$\mathscr{S}_s(\boldsymbol{\rho}) = \frac{MS(\boldsymbol{\rho})}{N\mathscr{N}_d(U)R(\boldsymbol{\rho}) + MS(\boldsymbol{\rho})}. \tag{5.28}$$

In [85], it was shown that when $\Phi(u)$ is sector-bounded by the lines with slopes β_1, β_2, then

$$\beta_1 \leq \mathscr{N}_d(U) \leq \beta_2, \quad \forall\, U \geq 0.$$

In other words, the describing function remains bounded by the slopes β_1, β_2 when the nonlinearity itself is bounded by the lines with slopes β_1, β_2. Therefore, by the results of Theorem 5.4, if the performance is guaranteed for all $\alpha \in [\beta_1, \beta_2]$, then the performance is also guaranteed for the system described by $\mathscr{N}_d(U)$. Thus stability and performance of a given (or multiple) sensitivity function(s) is guaranteed with respect to the fundamental frequency component of the nonlinearity.

5.4.1 Convex Optimization via Semi-Definite Programming

With the constraints developed in Theorem 5.4, an optimization problem can be formulated to guarantee $\mathscr{H}_\infty$ performance for the nonlinear system described by $\mathscr{N}_d(U)$ (i.e., the performance for the fundamental component of the nonlinearity) and for fixed uncertain gains in a sector. However, the closed-loop stability with the sector nonlinearity $\Phi(u) \in \mathscr{N}_t$ is guaranteed when the constraints in Theorem 5.2 and 5.3 (depending on the type of the sector) are added. Thus for $0 < \beta_1 < \beta_2$, the following optimization problem can be considered for the final design:

$$\begin{aligned} \underset{\gamma,\boldsymbol{\rho}}{\text{minimize}} \quad & \gamma \\ \text{subject to:} \quad & \Re\{\psi_i(\boldsymbol{\rho})\} > \gamma^{-1}\left|W_1 M_i S(\boldsymbol{\rho})\right| \\ & \Re\left\{\psi_{\beta,i}(\boldsymbol{\rho})\right\} > \left|r_d M_i S(\boldsymbol{\rho})\right| \\ & i = 1,\ldots,\ell;\ \alpha \in \{\beta_1,\beta_2\};\ \forall \omega \in \Omega, \end{aligned} \tag{5.29}$$

where $\psi_i(\boldsymbol{\rho}) = \alpha N_i R(\boldsymbol{\rho}) + M_i S(\boldsymbol{\rho})$ and $\psi_{\beta,i}(\boldsymbol{\rho}) = N_i R(\boldsymbol{\rho}) + \beta M_i S(\boldsymbol{\rho})$. The first constraint is related to the nominal performance, i.e., $\|W_1 \mathscr{S}_s^i\|_\infty < \gamma$ for all i, where $\mathscr{S}_s^i$ is the sensitivity function with respect to the i^{th} model in the set $\mathscr{G}$. The second inequality in the above problem can be altered for different sector cases. Therefore, closed-loop stability is guaranteed for $\Phi(\cdot) \in \mathscr{N}_t$ while the performance is guaranteed for the fundamental component of the (time-invariant) nonlinearity.

This optimization problem is quasi-convex. However, for a fixed γ, the problem becomes convex; therefore, to solve this problem, a bisection algorithm can be realized where an iterative approach is implemented in order to obtain an asymptotically convergent solution for γ. Additionally, as with the problems in chapters 3 and 4, the above optimization problem also possesses an infinite number of constraints; thus a SDP algorithm can be implemented

Table 5.1 – Procedure for computing a controller with $\mathscr{H}_\infty$ performance (with respect to the fundamental frequency of a sector-bounded nonlinearity)

Algorithm: Convex optimization for optimal performance

1. Excite the system with a multi-sinus or PRBS signal and identify $N(e^{-j\omega})$ and $M(e^{-j\omega})$ (as discussed in Section 2.1.3). The procedure can be repeated to find several models in different operating points.

2. Define the performance filters in $\|W_q \mathscr{S}_q^i(\boldsymbol{\rho})\|_\infty$ and formulate the control problem as minimizing the infinity norm of a multi-model process.

3. Start with a first-order controller (i.e., $n = n_r = n_s = 1$) and solve the optimization problem in (5.29) by using a frequency grid to obtain $\gamma_n^\star$. The constraint should be modified based on the sensitivity function to be minimized and the type of sector nonlinearity.

4. If the desired performance is met, stop. Otherwise, increase the order by one (i.e., $n = n + 1$).

5. Solve the problem in (5.29) to obtain the new $\gamma_n^\star$ and go to Step 4.

where a predefined frequency grid is used in order to solve a finite number of constraints.

Table. 5.1 displays a general method for designing a controller using the proposed approach.

5.5 Case Study

This section will now demonstrate the effectiveness of the proposed method(s) by investigating a case study that will implement the necessary and sufficient condition in Theorem 5.2 to design a stabilizing controller for a given time-varying sector-bounded nonlinearity. The condition in Theorem 5.4 is then used in conjunction with the condition in Theorem 5.2 to design controllers that provides stability for $\Phi(\cdot) \in \mathscr{N}_t$ and performance for the fundamental component of the nonlinearity.

The nonlinear system considered in this case study is of the switching type; a switched system is a family of dynamical systems endowed with a rule that determines, at every time, which dynamical system is responsible for the time evolution. Among the various problems in this field, much research has been devoted to the study of the stability of switched nonlinear systems [128, 129].

Two sector-bounded systems will be switched at every time instant $T_n\,[s]$. Let $\Phi_{t_d}(u)$ denote the nonlinearity that is switched on at time instant t_d. Then the time-varying nonlinear system for this case study can be characterized as follows:

$$\Phi_{2kT_n}(u) = \{u \in \mathbb{R} : u_n = u + \sin(u)\} \tag{5.30}$$

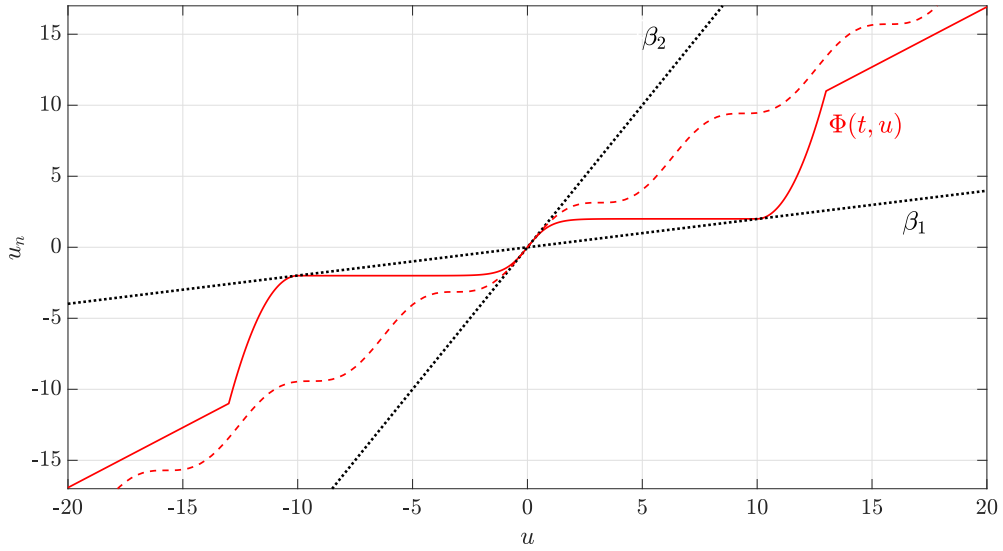

Figure 5.5 – Time-varying sector nonlinearity used for the case study. The nonlinearity switches at every positive integer multiple of T_n between the dashed-red line and the solid-red line.

while $\Phi_{(2k+1)T_n}(u)$ will possess the following characteristics:

$$u_n = \begin{cases} \kappa \tanh(u), & \text{for } |u| \leq a_1 \\ (u-a_1)^2 + \kappa, & \text{for } a_1 < u \leq a_2 \\ -(u+a_1)^2 - \kappa, & \text{for } -a_2 \leq u < -a_1 \\ \varsigma u, & \text{for } |u| > a_2 \end{cases} \tag{5.31}$$

for $k = 0, 1, \ldots, k_n$, where $a_1 = 10, a_2 = a_1 + 3, \kappa = 2$, and $\varsigma = a_2^{-1}[9 + \kappa]$. The bounding slopes can be analytically determined as follows:

$$\beta_1 = 2\left[\sqrt{a_1^2 + \kappa} - a_1\right], \ \beta_2 = \kappa. \tag{5.32}$$

Fig. 5.5 shows the time-varying sector nonlinearity for the conditions defined for $\Phi_d(u)$.

For this case study, the `MATLAB` software was used in conjunction with the `YALMIP` interface [130] to solve all of the problems in this work. A computer having the following hardware specifications was used: Intel-Core i7, 3.4 GHz CPU, 8GB RAM. The optimization algorithms were run using `MATLAB` version (R2017a) on a Windows 7 platform (64-bit).

5.5.1 Stabilization via the Circle Criterion

Consider the following family of unstable continuous-time systems:

$$\begin{aligned} G_1(s) &= \frac{10}{s^2-3s+1}, \quad G_2(s) = \frac{8}{2s^2-7s+3} \\ G_3(s) &= \frac{0.2s+5}{3s^2-5s+10}, \; G_4(s) = \frac{0.7s+10}{1.5s^2-4s+0.5}. \end{aligned} \tag{5.33}$$

This example will illustrate the effectiveness of the proposed method developed in Theorem 5.2 by designing one stabilizing $R(\boldsymbol{\rho})$ and $S(\boldsymbol{\rho})$ controller for all models $G_i(s)$ with the sector-bounded nonlinearity defined in (5.31). For the given values of this nonlinearity, the disk can be represented as $C(-2.76, 2.26)$; thus by the Circle criterion defined in Theorem 5.1, the open-loop FRF must encircle this disk $C(-2.76, 2.26)$ m times in the counter-clockwise direction.

The coprime factors $N_i(s)$ and $M_i(s)$ for each $G_i(s)$ must be selected such that $\{N_i(s), M_i(s)\} \in \mathbf{RH}_\infty$ for all i. A simple choice is to divide both the numerator and denominator of each coprime by $(s+1)^2$; for example, the coprimes for $G_1(s)$ can be selected as follows:

$$N_1(s) = \frac{10}{(s+1)^2}, \quad M_1(s) = \frac{s^2-3s+1}{(s+1)^2}, \tag{5.34}$$

where it is evident that $G_1(s) = N_1(s)M_1^{-1}(s)$. Note that selecting a different function in formulating the coprimes would not affect the stabilization of the closed-loop system.

The convex constraint in (5.11) is solved for all the models in (5.33) by implementing an SDP algorithm and considering a logarithmically spaced frequency grid of 500 points with $\omega \in [0.02\pi, \pi/T_s]$ (where $T_s = 2\,\text{ms}$ is the sampling time of the discrete-time controller). Note that (5.11) is a simple feasibility problem (i.e., the goal is to find a controller that satisfies the constraint with no objective function needed). A second-order polynomial was selected for both $R(\boldsymbol{\rho})$ and $S(\boldsymbol{\rho})$; the resulting controller is produced from the algorithm:

$$\begin{aligned} R(z^{-1}) &= 3.75 \cdot 10^4 (1-0.9978z^{-1})(1-0.2053z^{-1}) \\ S(z^{-1}) &= (1-0.2135z^{-1})(1+0.1891z^{-1}). \end{aligned} \tag{5.35}$$

Note that $S(z^{-1})$ has stable zeros; therefore, since $G_i(z^{-1})$ possesses 2 unstable poles for all i, the Nyquist plot of the open-loop FRF $L_i(e^{-j\omega})$ for each G_i must encircle the disk $C(-2.76, 2.26)$ 2 times in the counter-clockwise sense (without intersecting the disk). Fig. 5.6 shows the Nyquist plot of $L_i(e^{-j\omega})$ for all i along with the disk $C(-2.76, 2.26)$; it can be observed that the Nyquist plot for each plant model does indeed encircle the disk 2 times without intersecting it. Thus with a simple second-order controller, the closed-loop system is stable for the given family of unstable plants with a sector-bounded nonlinearity. The optimization time for obtaining this controller was calculated as 11.9 s.

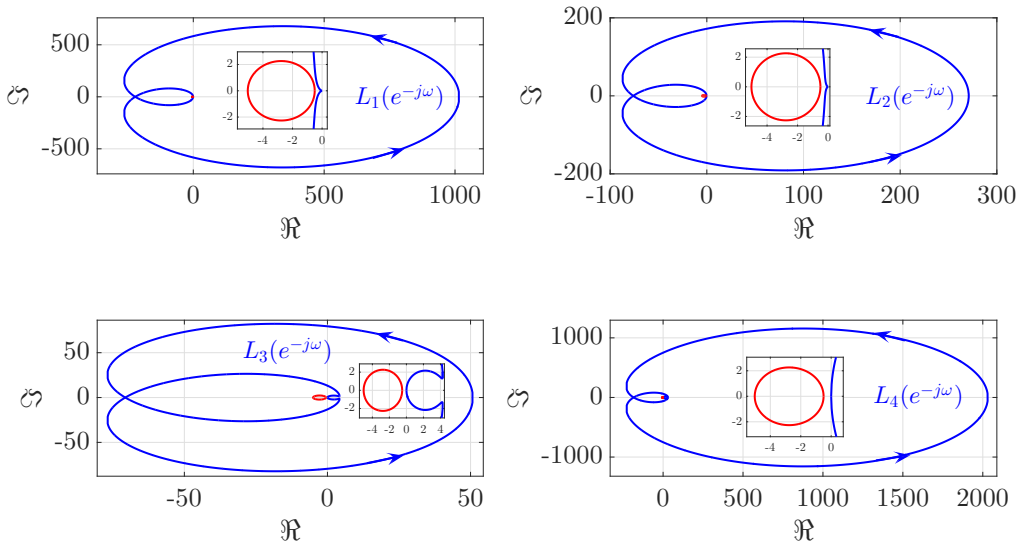

Figure 5.6 – Nyquist plot of $L_i(e^{-j\omega})$ for $i = 1,\ldots,4$ (solid-blue line); disk $C(-2.76, 2.26)$ (solid-red line). The Nyquist criterion for the sector-bounded nonlinearity is satisfied for all models.

5.5.2 Stabilization with Performance

The previous section illustrated how one can obtain stability of the closed-loop system with the sector-bounded nonlinearity; this section will now show how both stability for $\Phi \in \mathscr{N}_t$ and $\mathscr{H}_\infty$ performance can be obtained in the presence of this nonlinearity (when the nonlinearity is switched at a rate of $T_n = 0.02$ s). However, instead of simply defining the coprime factors parametrically (as in (5.34)), an identification experiment will be performed (in simulation) to obtain the FRFs of N_i and M_i.

Frequency Response Calculation: The case study considers a family of unstable systems. Therefore, the methods asserted in Section 2.1.3 can be used to obtain N_i and M_i. The controller in (5.35) was used to stabilize the closed-loop system. Since the bounds of the nonlinearity include $\Phi(\cdot) = 1$, then the gain β_l can be set to 1 in Fig. 2.4

There are many types of reference signals that can be used for identifying these coprimes. For this case study, a PRBS signal was used in order to capture the dynamics of the process. The PRBS is a deterministic signal which has characteristics similar to that of white noise and is usually used for system identification. In order to obtain good resolution at lower frequencies, a 15-period PRBS signal was injected as the reference input (where each period has a length of 32767 (15-bits))[1]. Fig. 5.7 displays a portion of the signals of interest (for the plant G_1) when the PRBS signal was injected. Note that the sampling time for this process is identical to that

[1]Note that the FRF is calculated based on one period of the PRBS (i.e., the final period, which is when the transients have disappeared.)

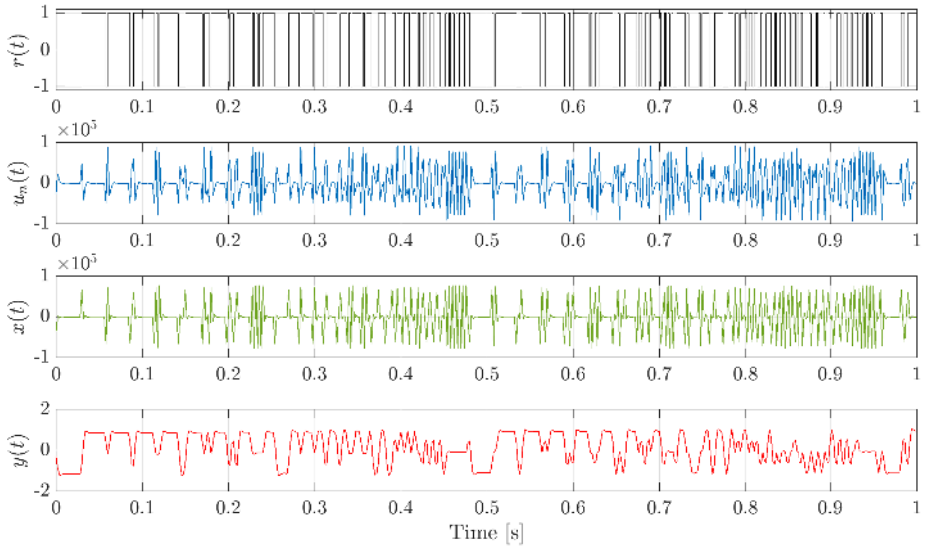

Figure 5.7 – The PRBS signal injected as the reference signal $r(t)$ with the measured responses for $u_n(t)$, $x(t)$ and $y(t)$. For illustrative purposes, the figure displays only a small portion of the total signal for the plant G_1.

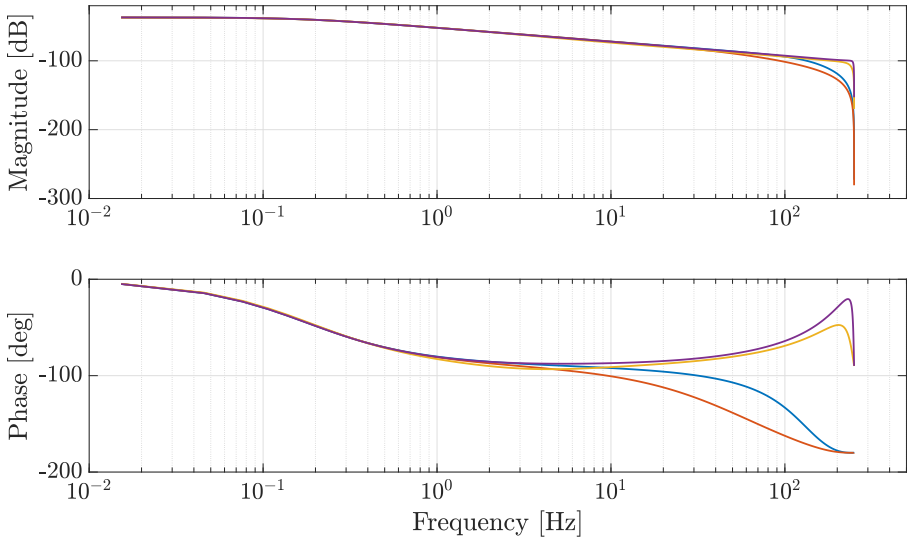

Figure 5.8 – Calculated FRFs for N_1 (solid-blue line), N_2 (solid-red line), N_3 (solid-orange line), N_4 (solid-purple line).

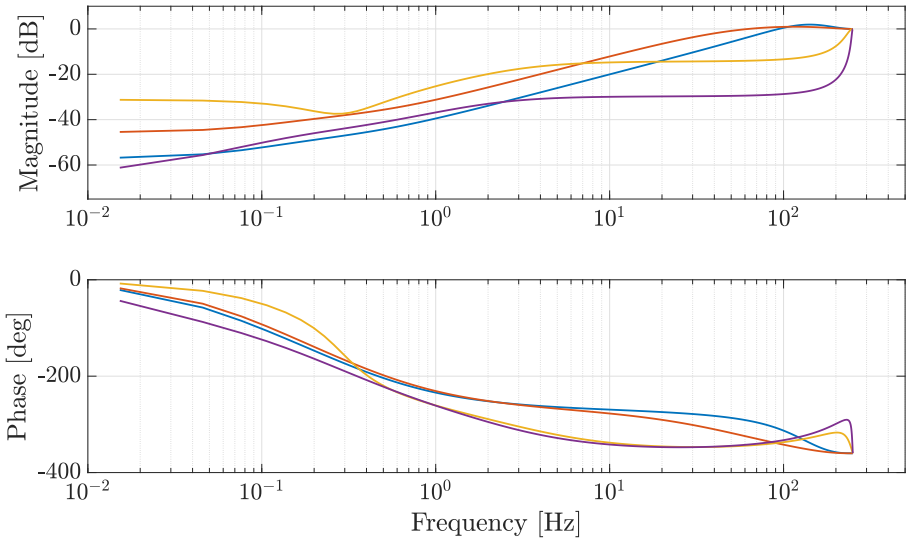

Figure 5.9 – Calculated FRFs for M_1 (solid-blue line), M_2 (solid-red line), M_3 (solid-orange line), M_4 (solid-purple line).

of the previous section (i.e., $T_s = 2$ ms). With these signals, the FRF of the coprimes were then calculated using the frequency spectrum of each time-domain signal (using the relations in (2.23)). Figures 5.8 and 5.9 show the resulting magnitude and phase for each coprime N_i and M_i, respectively.

Weighting filter selection: For nominal performance of the nonlinear system, the optimization problem in (5.29) can be used to synthesize a controller. The weighting filter W_1 was selected such that the closed-loop FRF is shaped based on the desired reference model given by $\mathscr{S}_t^d = (\tau s + 1)^{-1}$, where τ is the desired time constant. It is known that $\mathscr{S}_s + \mathscr{S}_t = 1$; thus it is also required that $\mathscr{S}_s^d + \mathscr{S}_t^d = 1$, where $\mathscr{S}_s^d$ is the desired FRF from r to $r - y$. Thus the weighting filter can be selected as $W_1(s) = [\mathscr{S}_s^d]^{-1} = s^{-1}(s + \tau^{-1})$. Note that the controller will be prefixed with an integrator (in order to have integral action); therefore, the weighted function $\|W_1 \mathscr{S}_s^i\|_\infty$ remains bounded $\forall\, i$ and for all ω.

Controller Synthesis and Results: A 5^{th}-order controller was designed such that it had integral action (by using the algorithm in Table 5.1). From the available frequency points obtained from the PRBS identification simulation (a total of 16384 linearly spaced points), 500 points were randomly selected from this grid using the methods described in [59] (with violation and confidence parameters set to 0.05). Thus by solving the problem in (5.29), a total of 6000 constraints must be satisfied (i.e., 1000 constrains for the performance criterion, 500 constraints for the stability requirement, satisfied for all 4 models). The desired closed-loop bandwidth was selected as 25 Hz, which corresponds to a time constant of $\tau = (50\pi)^{-1}$ s. The bisection algorithm was used to solve the problem in (5.29) with $\gamma_{max} = 2.5$, $\gamma_{min} = 0$, and $\gamma_{tol} = 10^{-4}$; with these parameters, the optimization time was calculated to be 291.1s and the

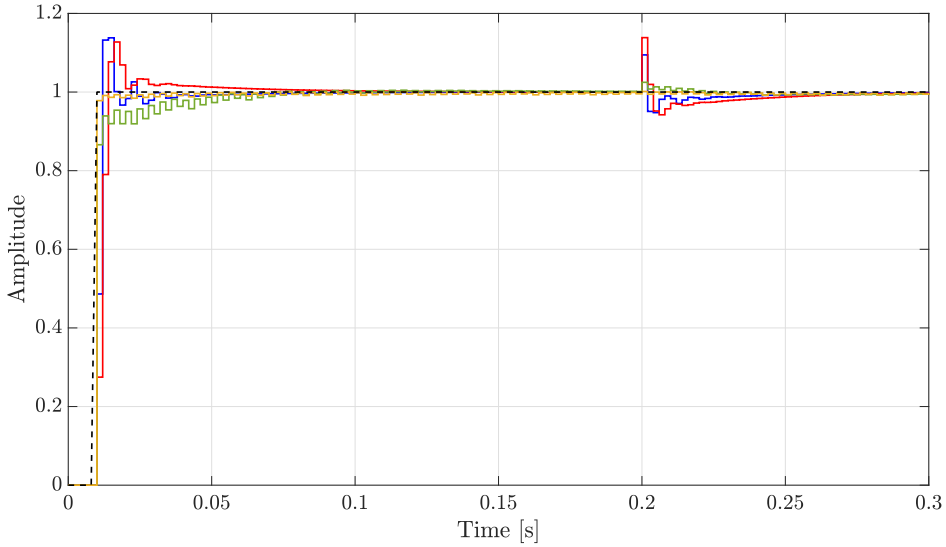

Figure 5.10 – Closed-loop step responses for all models G_i. The reference signal is shown with the dashed-black line.

optimal solution obtained was $\gamma^\star = 1.432$. The step response of the closed-loop nonlinear system for all 4 models is shown in Fig. 5.10. At $t = 0.2$ s, a step disturbance was injected at d_o with an amplitude of 0.2. It can be observed that the proposed approach ensures the closed-loop stability for the time-varying nonlinear system and good closed-loop performance is achieved.

Remark. *Fig. 5.11 shows the Nyquist plot of $L_1(e^{-j\omega})$ when (5.29) was solved with and without the time-varying stability constraint. It can be observed that without the time-varying stability constraint, the Nyquist plot of $L_1(e^{-j\omega})$ enters the disk $C(\beta, r_d)$; this is because the $\mathscr{H}_\infty$ performance criterion can only guarantee the stability and performance for the fundamental component of the nonlinearity and may violate the stability condition for the true nonlinear system. With the added stability constraint, it can be observed from Fig. 5.11 that the Nyquist plot of $L_1(e^{-j\omega})$ satisfies the Nyquist criterion for stabilizing the time-varying nonlinear system.*

5.6 Conclusion

In the previous chapter, a method for designing a controller for the underlying linear system of a nonlinear model was presented; however, stability or performance could not be guaranteed for the true nonlinear system. In this chapter, necessary and sufficient conditions have been formulated in order to design stabilizing controllers for systems with sector-bounded time-varying nonlinearities. This formulation used the results from the Circle criterion to derive conditions in a data-driven setting. All of the methods developed for stabilizing the true (time-varying) nonlinear system did not use any approximations or linearization techniques to achieve the desired results. Moreover, a sufficient condition was developed to achieve

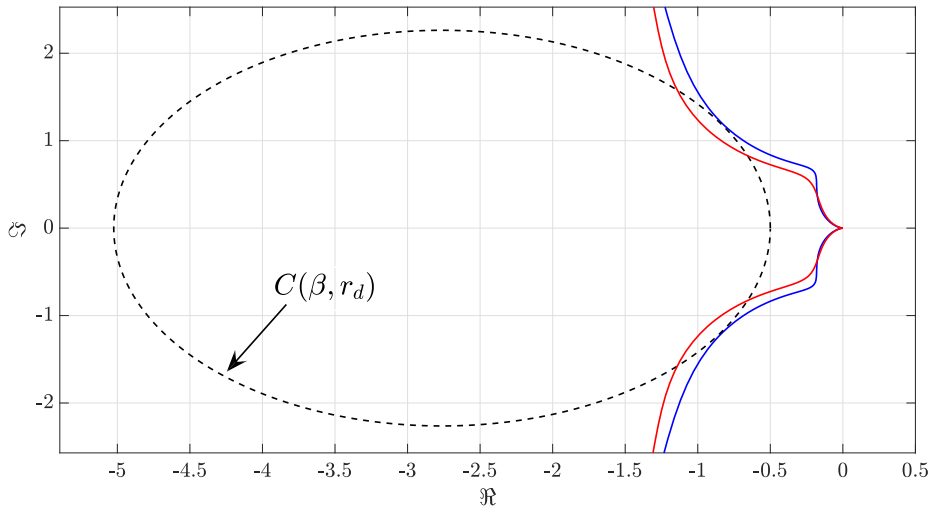

Figure 5.11 – Nyquist plot of L_1 with the stability constraint (blue-line) and without the stability constraint (red-line).

both stability and $\mathscr{H}_\infty$ performance for the nonlinear system represented by a describing function (i.e., the performance with respect to the fundamental frequency component of a sector-bounded (time-invariant) nonlinearity).

6 $\mathscr{H}_\infty$ Design for Low-Order Fixed-Structure Controllers

6.1 Introduction

In Chapter 3, a new data-driven method for $\mathscr{H}_\infty$ controller design by convex optimization was proposed; a controller was represented as a ratio of two transfer functions that were linearly parameterized using a vector of basis functions. It was shown that as the order of these transfer functions increased, the solution to the convex problem converged to the global optimal solution of the $\mathscr{H}_\infty$ problem (regardless of the basis function that was used). For a low-order controller, however, the results depend on the choice of the basis functions and is not necessarily optimal. By convexifying the $\mathscr{H}_\infty$ problem, the global optimal solution to an approximate problem is obtained; however, a question one may ask is why are convexification methods imposed to find a solution to the approximate $\mathscr{H}_\infty$ problem when one can simply use nonlinear solvers to find a local solution of the true $\mathscr{H}_\infty$ problem? This is the question that will be addressed in this chapter.

This chapter presents an extension of the work in Chapter 3, and its purpose is to devise a data-driven approach for improving the $\mathscr{H}_\infty$ performance for low-order fixed-structure controllers. Several non-convex optimization problems are proposed to optimize the basis function parameters for fixed-structure low-order controllers (while guaranteeing the closed-loop stability). In particular, a new PSO algorithm is formulated to optimize the controller parameters and guarantee the stability of the closed-loop system while ensuring robust performance (without any approximation). PSO is a very powerful population-based metaheuristic which uses an iterative method to improve a candidate solution and makes little to no assumptions about the problem being optimized. A major advantage of the PSO algorithm is that the cost function need not be differentiable; additionally, the algorithm can be applied to problems of large dimensions, and often produces quality solutions more rapidly than alternative methods. Recent works have utilized this method for solving the $\mathscr{H}_\infty$ problem [131, 132, 133]. As with all nonlinear solvers, there are trade-offs that exist between the optimization time and the quality of the optimal solution; these trade-offs will be investigated by comparing the optimal solutions from various methods.

In this chapter, a continuous-time representation of systems with multiplicative uncertainty are considered. The plant is represented in coprime form (see Section 2.1.2) and 1DOF coprime controllers (see Section 2.2.3) are considered. Thus the sensitivity functions with a 1DOF structure are considered.

6.1.1 Robust Performance via Convex Optimization

Consider a process from the multiplicative uncertainty set in (2.1). Given a performance weighting filter $W_1(j\omega)$ with bounded infinity norm, a necessary and sufficient condition for achieving robust performance is given by [96]:

$$\left\| |W_1 \mathscr{S}_s(\boldsymbol{\rho})| + |W_2 \mathscr{S}_t(\boldsymbol{\rho})| \right\|_\infty < \gamma, \tag{6.1}$$

where $\gamma = 1$. However, the problem of minimizing the upper bound γ will be considered in this chapter, where $\gamma \in \mathbb{R}_+$. The condition in (6.1) can also be expressed as

$$|W_1(j\omega)\mathscr{S}_s(j\omega,\boldsymbol{\rho})| + |W_2(j\omega)\mathscr{S}_t(j\omega,\boldsymbol{\rho})| < \gamma, \quad \forall \omega \in \Omega_c. \tag{6.2}$$

For notation purposes, the dependence in $j\omega$ will be omitted and will only be reiterated when deemed necessary. The dependence on $\boldsymbol{\rho}$ will continue to be highlighted. By substituting the frequency responses of (2.34) and (2.35) into (6.2), the condition for robust performance can be expressed as

$$\gamma^{-1}\left[|W_1 MY(\boldsymbol{\rho})| + |W_2 NX(\boldsymbol{\rho})|\right] < |\psi(\boldsymbol{\rho})|, \quad \forall \omega \in \Omega_c, \tag{6.3}$$

where $\psi(\boldsymbol{\rho}) = NX(\boldsymbol{\rho}) + MY(\boldsymbol{\rho})$. Consider a disk in the complex plane at a specific frequency in Ω_c which is centered at $\psi(\boldsymbol{\rho})$ and has radius

$$\gamma^{-1}\left[|W_1 MY(\boldsymbol{\rho})| + |W_2 NX(\boldsymbol{\rho})|\right].$$

As with the constraint presented in Chapter 3, the constraint in (6.3) ensures that for any frequency point in Ω_c, the disk associated with this frequency point will not encircle the origin. In Lemma 3.2, it was shown that there exists a function F that can rotate this disk such that it lies on the right-hand side of the $j\omega$ axis of the complex plane (i.e., all values on and within the disk have positive real parts). A necessary and sufficient condition for robust performance is considered with the following Lemma:

Lemma 6.1. *Suppose that*

$$H_1(\boldsymbol{\rho}) = W_1 MY(\boldsymbol{\rho})\psi^{-1}(\boldsymbol{\rho})$$
$$H_2(\boldsymbol{\rho}) = W_2 NX(\boldsymbol{\rho})\psi^{-1}(\boldsymbol{\rho})$$

are frequency responses of bounded analytic functions in the right-half plane. Then, the follow-

ing constraint is met

$$\sup_{\omega\in\Omega_c}\left(|H_1(\boldsymbol{\rho})|+|H_2(\boldsymbol{\rho})|\right)<\gamma \tag{6.4}$$

if and only if there exists a stable transfer function $F(s)$ that satisfies

$$\Re\left\{\psi(\boldsymbol{\rho})F\right\}>\gamma^{-1}\left[|W_1MY(\boldsymbol{\rho})F|+|W_2NX(\boldsymbol{\rho})F|\right]$$

for all $\omega\in\Omega_c$.

Proof: The proof has been omitted to conserve space. However, the proof of a similar condition can be found in Lemma 3.2. ■

With the above Lemma, a necessary and sufficient condition can be derived for attaining robust performance whilst ensuring the closed-loop stability. In Chapter 3, it was shown that if $X(\boldsymbol{\rho})$ and $Y(\boldsymbol{\rho})$ are linearly parameterized, then a quasi-convex optimization problem can be formulated as follows:

$$\begin{aligned}\underset{\gamma,\boldsymbol{\rho}}{\text{minimize}}\quad & \gamma\\ \text{subject to:}\quad & \gamma^{-1}\left[|W_1MY(\boldsymbol{\rho})|+|W_2NX(\boldsymbol{\rho})|\right]<\Re\{\psi(\boldsymbol{\rho})\}\\ & \forall\omega\in\Omega_c.\end{aligned} \tag{6.5}$$

This optimization problem is quasi-convex and can be solved by implementing a bisection algorithm. The problem is solved in a SDP form where a finite number of frequency points are defined *a-priori* (as discussed in Chapter 3).

6.2 Optimization Problems For Fixed-Struture Design

In order to preserve the convexity of the $\mathscr{H}_\infty$ problem in (6.5) (with fixed-structure controllers), it is necessary to invoke linearly parameterized transfer functions for $X(\boldsymbol{\rho})$ and $Y(\boldsymbol{\rho})$, where both transfer functions contain basis functions with fixed values. For example, if the Laguerre basis functions in (2.30) are used to formulate the controller, then the value of ξ (i.e., the Laguerre parameter) must be fixed *a priori*. In Chapter 3, it is shown that when the orders of $X(\boldsymbol{\rho})$ and $Y(\boldsymbol{\rho})$ increase, then γ from (6.5) converges monotonically to the global optimal solution of the $\mathscr{H}_\infty$ problem. However, it is impractical and sometimes impossible to implement the resulting high-order controllers to real systems. For low-order controllers, the optimal solution from the convex problem may be far from the global solution, and is very sensitive to the pre-set values of the basis function parameters. A solution to this problem is to simultaneously optimize the controller parameters $\boldsymbol{\rho}$ and the basis function parameter ξ by a nonlinear optimization algorithm.

An alternative is to formulate an optimization problem based on the results of Lemma 6.1 in order to improve the performance for low-order controllers.

Theorem 6.1. *The local optimal solution for obtaining $\mathscr{H}_\infty$ performance and closed-loop stability using the fixed-structure controllers $X(\boldsymbol{\rho})$ and $Y(\boldsymbol{\rho})$ is achieved if $F(\boldsymbol{\rho}_f)$ is parameterized with a set of stable orthogonal basis functions and the following optimization problem is realized:*

$$\begin{aligned} &\underset{\gamma,\boldsymbol{\rho},\boldsymbol{\rho}_f}{\textit{minimize}} && \gamma \\ &\textit{subject to:} && \gamma^{-1}|F(\boldsymbol{\rho}_f)|\big[|W_1MY(\boldsymbol{\rho})|+|W_2NX(\boldsymbol{\rho})|\big] < \Re\big\{F(\boldsymbol{\rho}_f)\psi(\boldsymbol{\rho})\big\} \\ &&& \forall \omega \in \Omega_c. \end{aligned} \tag{6.6}$$

Proof: According to Lemma 6.1, it is known that there exists a stable transfer function F such that the constraint to the $\mathscr{H}_\infty$ problem is satisfied. Therefore, $F = F(\boldsymbol{\rho}_f)$ can be chosen such that it incorporates stable basis functions (such as the Laguerre basis functions). Thus the local optimal solution to the $\mathscr{H}_\infty$ problem can be obtained by minimizing γ, fixing the orders of $X(\boldsymbol{\rho})$ and $Y(\boldsymbol{\rho})$, and implementing the optimization problem in (6.6).

The constraint in this problem implies that $\Re\{F(\boldsymbol{\rho}_f)\psi(\boldsymbol{\rho})\} > 0$, which further implies that $\Re\{[F(\boldsymbol{\rho}_f)\psi(\boldsymbol{\rho})]^{-1}\} > 0$ for all $\omega \in \Omega_c$. Therefore, by the SPR conditions professed in Lemma 3.1, $[F(\boldsymbol{\rho}_f)\psi(\boldsymbol{\rho})]^{-1}$ is Hurwitz and the closed-loop system is stable. ■

For continuous-time systems, the function $F(\boldsymbol{\rho}_f)$ can be selected as $F(\boldsymbol{\rho}_f) = \boldsymbol{\rho}_f^\top \boldsymbol{\phi}(\xi_f)$, where $\boldsymbol{\rho}_f^\top = [\rho_{f,0},\ldots,\rho_{f,n_f}]$ with $\boldsymbol{\rho}_f \in \mathbb{R}^{n_f+1}$ and $\boldsymbol{\phi}(\xi_f)$ is the vector of Laguerre basis functions asserted in (2.30) with the Laguerre parameter defined as $\xi_f \in \mathbb{R}_+$. It is imperative to note that $F(\boldsymbol{\rho}_f)$ is not part of the controller; it is a function which realizes the necessary and sufficient condition in Lemma 6.1. The type of optimization problem in (6.6) depends on the parameterization of $X(\boldsymbol{\rho})$, $Y(\boldsymbol{\rho})$, and $F(\boldsymbol{\rho}_f)$.

6.2.1 Bilinear Programming

If $X(\boldsymbol{\rho})$, $Y(\boldsymbol{\rho})$, and $F(\boldsymbol{\rho}_f)$ are linearly parameterized (where the Laguerre parameter ξ and ξ_f are fixed for each function), then the optimization problem in (6.6) becomes a bilinear problem (BP) when a bisection algorithm is used to compute the optimal γ. It is known that if (b_1^+, b_2^+) is a local solution to a BP given an objective function $f(b_1,b_2)$, then

$$\min_{b_1} f(b_1,b_2^+) = f(b_1^+,b_2^+) = \min_{b_2} f(b_1^+,b_2). \tag{6.7}$$

Given this property of BPs, the local solution to the BP can be obtained by solving a finite set of convex optimization problems until convergence is achieved. The advantage of this method is that the local solution is obtained without the need to explicitly solve a nonlinear problem where a SDP approach can be used. The basic idea for solving (6.6) in this manner is to first solve the problem with $X(\boldsymbol{\rho})$ and $Y(\boldsymbol{\rho})$ linearly parameterized while $F(\boldsymbol{\rho}_f) = 1$. The optimal solution to this convex problem will generate $X(\boldsymbol{\rho}^\star)$ and $Y(\boldsymbol{\rho}^\star)$. Now construct a 1^{st} order linearly parameterized function for $F(\boldsymbol{\rho}_f)$ and solve the following optimization problem

(using the bisection algorithm):

$$\begin{aligned} \underset{\gamma,\boldsymbol{\rho}_f}{\text{minimize}} \quad & \gamma \\ \text{subject to:} \quad & \gamma^{-1}|F(\boldsymbol{\rho}_f)|\big[|W_1MY(\boldsymbol{\rho}^\star)|+|W_2NX(\boldsymbol{\rho}^\star)|\big] < \Re\{F(\boldsymbol{\rho}_f)\psi(\boldsymbol{\rho}^\star)\} \\ & \forall \omega \in \Omega_c. \end{aligned} \tag{6.8}$$

The optimal solution to this convex problem will generate $F(\boldsymbol{\rho}_f^\star)$. Now repeat the process of linearly parameterizing $X(\boldsymbol{\rho})$ and $Y(\boldsymbol{\rho})$ and use $F(\boldsymbol{\rho}_f^\star)$ to solve the optimization problem. Once convergence is achieved, then the order of $F(\boldsymbol{\rho}_f)$ can be increased (while keeping the orders of $X(\boldsymbol{\rho})$ and $Y(\boldsymbol{\rho})$ fixed). This process is repeated for increasing n_f until the optimal solution $\gamma^\star$ converges to a constant value (i.e., converges to a local solution γ^+). This optimization technique is known as the “Mountain Climbing" method [134].

Remark. *Note that $\gamma^\star$ represents the global solution to the convex problem while γ^+ represents the local solution to the fixed-structure $\mathscr{H}_\infty$ problem.*

6.2.2 Particle Swarm Optimization

When the basis function parameters ξ and ξ_f in $X(\boldsymbol{\rho})$, $Y(\boldsymbol{\rho})$ and $F(\boldsymbol{\rho}_f)$ are decision variables, then the problem in (6.6) becomes nonlinear. One of the problems with solving this nonlinear problem is defining the initial values for the decision variables. Since there can be many variables involved in this optimization problem, defining the initial variables to achieve the global optimal solution to the $\mathscr{H}_\infty$ problem may not be trivial.

PSO is a powerful optimization method that can solve both linear and nonlinear problems and can be used to solve the problem in (6.6) without specifying initial conditions. It is based on the principle that groups of individuals work together to improve both their collective and individual performance [135]. Due to the constraints imposed in (6.6), an exterior method (i.e., Non-Death-Penalty approach) will be implemented in order to obtain the optimal solution to the problem. With this method, the constrained optimization problem can be transformed to the following unconstrained problem:

$$\underset{\boldsymbol{x}}{\text{minimize}} \;\; \Lambda(j\omega,\boldsymbol{x}), \tag{6.9}$$

where $\boldsymbol{x}^\top = [\boldsymbol{\rho}^\top, \boldsymbol{\rho}_f^\top, \boldsymbol{\xi}^\top, \gamma]$, $\boldsymbol{\xi} = [\xi, \xi_f]^\top$ is the vector of basis function parameters, and

$$\begin{aligned} \Lambda(j\omega,\boldsymbol{x}) &= \gamma + \frac{1}{\eta}\sum_{k=1}^{\eta} \vartheta_k Z_k(j\omega_k,\boldsymbol{x}) \\ Z_k(j\omega_k,\boldsymbol{x}) &= [\max(0, z_k(j\omega_k,\boldsymbol{x}))]^\wp \\ z_k(j\omega_k,\boldsymbol{x}) &= |W_1(j\omega_k)M(j\omega_k)Y(j\omega_k,\boldsymbol{x})F(j\omega_k,\boldsymbol{x})| \\ &\qquad + |W_2(j\omega_k)N(j\omega_k)X(j\omega_k,\boldsymbol{x})F(j\omega_k,\boldsymbol{x})| - \gamma\Re\left\{F(j\omega_k,\boldsymbol{x})\psi(j\omega_k,\boldsymbol{x})\right\}. \end{aligned} \tag{6.10}$$

The value of $\wp$ is usually taken to be 1 or 2 and $\vartheta_k \in \mathbb{R}_+$ is the penalty factor [135]. In this chapter, $\wp = 1$ will be considered. A very large penalty factor will ensure fast convergence to a local solution (even if it is far from the optimal), while a small penalty factor will cause the PSO algorithm to spend much time searching in infeasible regions and may converge to an infeasible solution [136]. For this particular problem, the value of ϑ_k will be a constant, since the weighting factor for each constraint should be the same ($\vartheta_k = \vartheta$). In other words, the constraint should not be weighted differently for varying frequencies.

The PSO algorithm seeks to find an optimal solution by implementing a swarm of p_x particles. Let $\boldsymbol{x}_i$ denote the position of the i^{th} particle; for the decision variables considered in (6.10), the i^{th} particle occupies the position

$$\boldsymbol{x}_i^\top := [\boldsymbol{\rho}_i^\top, \boldsymbol{\rho}_{f_i}^\top, \boldsymbol{\xi}_i^\top, \gamma_i]^\top, \tag{6.11}$$

where $i \in \{1, \ldots, p_x\}$. The velocity of the i^{th} particle (at which it moves though the search space) is denoted as $\boldsymbol{v}_i$. One approach in expressing the manner in which the position and velocity of the i^{th} particle is updated can be realized as

$$\begin{aligned} \boldsymbol{x}_i^{l+1} &= \boldsymbol{x}_i^l + \boldsymbol{v}_i^{l+1} \\ \boldsymbol{v}_i^{l+1} &= \iota\big[\boldsymbol{v}_i^l + \theta_1 r_{1,i}^l(\boldsymbol{b}_i^l - \boldsymbol{x}_i^l) + \theta_2 r_{2,i}^l(\boldsymbol{h}_i^l - \boldsymbol{x}_i^l) + \theta_3 r_{3,i}^l(\boldsymbol{g}^l - \boldsymbol{x}_i^l)\big], \end{aligned} \tag{6.12}$$

where $\iota \in \mathbb{R}_+$ is the constriction coefficient, and $\theta_c \in \mathbb{R}_+$ for $c \in \{1,2,3\}$ are the learning rates (θ_1 is the cognitive learning rate, θ_2 is the social learning rate, and θ_3 is the learning rate influencing the best individual found so far since the first generation). The random numbers $r_{c,i}^l$ are uniformly distributed in $[0,1]$ and represent the stochastic behavior associated with the algorithm. For a stable PSO algorithm, the constriction coefficient should be chosen as follows [135]:

$$\iota = \frac{2k_\vartheta}{\theta_T - 2}, \tag{6.13}$$

where $k_\vartheta \in (0,1)$ and $\theta_T = \theta_1 + \theta_2 + \theta_3$. The best-so-far position of the i^{th} particle is defined as

$$\boldsymbol{b}_i^l = \underset{\boldsymbol{x}_i^t}{\arg\min}\{\Lambda(\boldsymbol{x}_i^t), 0 \le t \le l\}. \tag{6.14}$$

For a given neighborhood size σ, the best-so-far position of σ close neighbors is determined as follows:

$$\boldsymbol{h}_i^l = \underset{\boldsymbol{x}_i^t}{\arg\min}\{\Lambda(\boldsymbol{x}_i^t), 0 \le t \le l \mid \boldsymbol{x}_i^t \in H_i^t\}, \tag{6.15}$$

where H_i^t are the σ nearest neighbors of $\boldsymbol{x}_i^t$. The best position of the entire swarm for the

Table 6.1 – Procedure for executing the PSO algorithm

Algorithm: PSO for optimal performance

1. Initialize a population of p_x particles with random positions $\boldsymbol{x}_i^0 \ \forall i$ and velocities $\boldsymbol{v}_i^0 = 0$. Set $l = 0$ and determine $\boldsymbol{b}_i^0$, $\boldsymbol{h}_i^0$, and $\boldsymbol{g}^0$.

2. Apply the update equations in (6.12) and evaluate the cost function with the new population.

3. If the termination criterion is satisfied, then the algorithm returns the optimal solution

$$\boldsymbol{x}^+ = \arg\min_{\boldsymbol{x}_i^k} \{\Lambda(\boldsymbol{x}_i^k), \forall i, k\}. \tag{6.17}$$

Otherwise, go to the next step.

4. Set $l = l + 1$ and determine $\boldsymbol{b}_i^l$, $\boldsymbol{h}_i^l$, and $\boldsymbol{g}^l$. Then return to Step 2.

current iteration l is defined as

$$\boldsymbol{g}^l = \arg\min_{\boldsymbol{x}_i^l} \{\Lambda(\boldsymbol{x}_i^l), \forall i\}. \tag{6.16}$$

The PSO algorithm can be implemented with the steps outlined in Table 6.1.

The optimal values of θ_c may vary depending on the problem that is being analyzed; in general, it is recommended that $\theta_c = 2.1 \ \forall c$ [135]. These will be the values used for the examples in the next section. A similar rationalization can be made with the selection of k_ϑ; a larger value of k_ϑ encourages exploration while a smaller value of k_ϑ bolsters exploitation.

6.3 Simulation Examples

Let us now consider two examples in order to determine the validity of the proposed method. The `YALMIP` library [130] in conjunction with `MATLAB` was used to solve the convex problem (i.e., the sequential set of convex problems to solve the BP).

For each example, the proposed method will be used where the non-convex problem is solved using three different approaches:

- **Method 1**: Linearly parameterizing $X(\boldsymbol{x})$, $Y(\boldsymbol{x})$, and $F(\boldsymbol{x})$ (where the basis function parameters in $\boldsymbol{\xi}$ are fixed *a-priori*) and use the BP algorithm to solve a sequential set of convex problems until convergence is achieved for increasing n_f.
- **Method 2**: Formulate non-LP functions for $X(\boldsymbol{x})$ and $Y(\boldsymbol{x})$ (with $F(\boldsymbol{x}) = 1$) and use the PSO algorithm to optimize $\boldsymbol{\rho}$ and ξ.

- **Method 3**: Formulate non-LP functions for $X(\boldsymbol{x})$, $Y(\boldsymbol{x})$ and $F(\boldsymbol{x})$ and use the PSO algorithm to optimize all parameters in $\boldsymbol{x}$.

It will be of interest to compare the solutions from each method with the associated optimization time. For comparative purposes, the solutions from all three methods will be compared to the solution obtained from the `hinfstruct` function in `MATLAB`. As a result, examples from the literature with parametric models are chosen.

Remark. *It is emphasized that a direct comparison with `hinfstruct` is not the objective of these examples, since the proposed method does not synthesize controllers based on parametric models (only the frequency data are used in the optimization problems).*

All optimization problems were solved using a computer with an Intel-i7 core (3.4 GHz) processor and with 8 GB of RAM running on a 64-bit Windows 7 platform. The `MATLAB` version (R2015b) was used for running all algorithms.

6.3.1 Case 1: Robust PID Design

Consider the unstable non-minimum phase system analyzed in [137] and [138] (which is subject to multiplicative uncertainty):

$$G(s) = \frac{s-1}{s^2+0.8s-0.2}. \tag{6.18}$$

The objective of this case study is to design a stabilizing PID controller such that the following performance condition is satisfied:

$$\|W_1\mathscr{S}_s(\boldsymbol{\rho})\|_\infty < \gamma \quad \text{and} \quad \|W_2\mathscr{S}_t(\boldsymbol{\rho})\|_\infty < \gamma. \tag{6.19}$$

The weighting filters for this design will be chosen as those defined in [137]: $W_1(s) = 10(100s+1)^{-1}$ and $W_2(s) = (s+0.1)(s+1)^{-1}$. Since $G(s)$ is unstable, the coprime functions can be selected as follows:

$$N(s) = \frac{s-1}{(s+1)^2}, \quad M(s) = \frac{(s^2+0.8s-0.2)}{(s+1)^2}, \tag{6.20}$$

where it is evident that $G(s) = N(s)M^{-1}(s)$. For a PID controller, the structure of the functions $X(\boldsymbol{x})$ and $Y(\boldsymbol{x})$ can be selected with the vectors defined in (2.33). Therefore, the following optimization problem is considered for satisfying (6.19):

$$\begin{aligned} \underset{\boldsymbol{x}}{\text{minimize}} \quad & \gamma \\ \text{subject to:} \quad & \gamma^{-1}|W_1MY(\boldsymbol{x})F(\boldsymbol{x})| < \Re\{\psi(\boldsymbol{x})F(\boldsymbol{x})\} \\ & \gamma^{-1}|W_2NX(\boldsymbol{x})F(\boldsymbol{x})| < \Re\{\psi(\boldsymbol{x})F(\boldsymbol{x})\} \\ & \omega \in \Omega_c. \end{aligned} \tag{6.21}$$

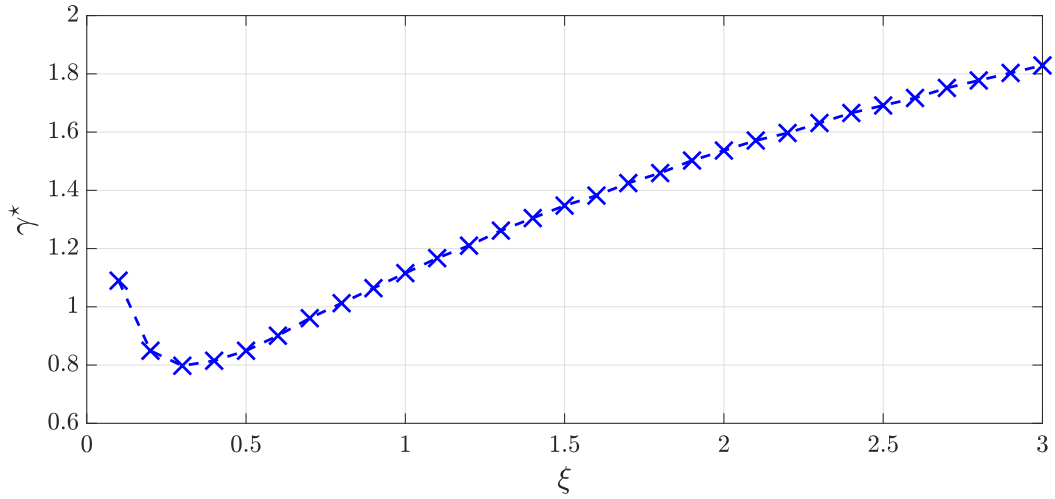

Figure 6.1 – Optimal solution to the convex problem for varying ξ.

Simulation Results

First, consider the optimal solution to the convex problem (i.e., $F(\boldsymbol{x}) = 1$ with $X(\boldsymbol{x})$ and $Y(\boldsymbol{x})$ linearly parameterized) as the basis function parameter ξ is varied. The problem is solved by converting it to an SDP problem and gridding the frequency from 10^{-2} to 10^{2} rad s^{-1} (using 200 logarithmically spaced points). Fig. 6.1 displays how the optimal solution γ varies with the basis function parameter ξ. It can be observed that the optimal solution to the convex problem is highly sensitive to the basis function parameter.

The problem in (6.21) is now solved using the proposed method with the same frequency grid. First, consider the case when the basis function parameters (i.e., ξ, ξ_f) are fixed and so $F(\boldsymbol{x})$ is linearly parameterized; this signifies that (6.21) becomes a BP and Method 1 must be considered. Let $\gamma^+_{n_f}$ denote the (local) optimal solution to the problem for a given order n_f of $F(\boldsymbol{x})$. The BP is solved with the iterative convex method (i.e., the Mountain Climbing method) for different basis function values (with $\xi = \xi_f$); Fig. 6.2 displays the optimal solution as a function of n_f. It can be observed that regardless of the basis function parameter, the solution converges to the same value (which in this case, is $\gamma^+ = 0.737$). The `hinfstruct` function from `MATLAB` produces the same value.

Now consider the parameterizations of Method 2 and Method 3; with Method 3, $F(\boldsymbol{x})$ was selected with $n_f = 2$. Since the PSO method implements a stochastic search algorithm, 5 iterations for each method were initiated where each iteration was terminated when convergence was achieved (within a tolerance of 10^{-5}). The minimum value of γ that achieves feasibility for all iterations was considered as the optimal. A swarm of $p_x = 50$ with a penalty factor $\vartheta = 10$ and $k_\vartheta = 0.95$ was used in the algorithm. Table. 6.2 compares the optimal solutions obtained with the optimization time for each method. The convex method refers to the algorithm in Chapter 3 with $\xi = 1$. Note that the optimization time of Method 1 varies based on which basis function parameter is used. The variation time shown in this table is based on the values used

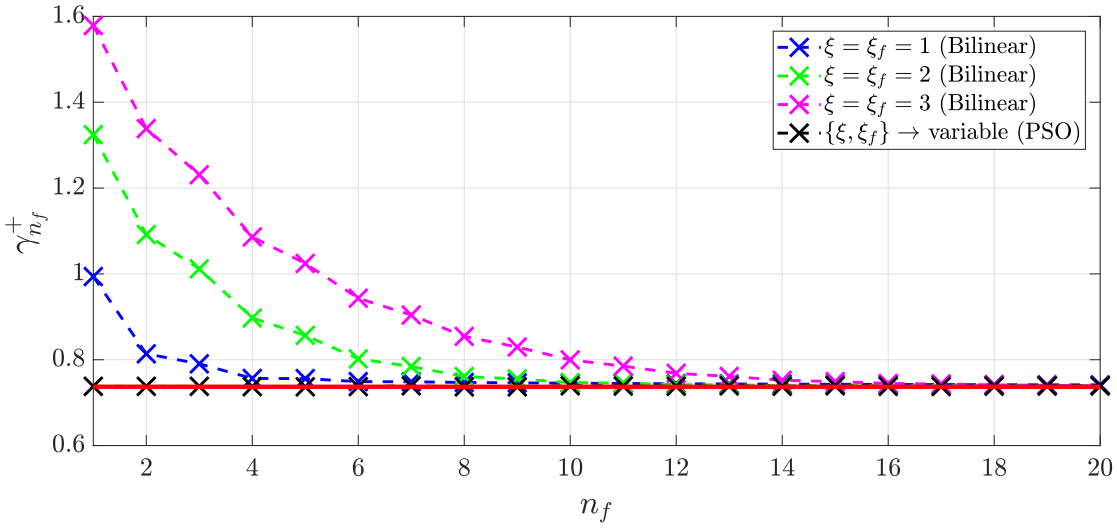

Figure 6.2 – Optimal solution to (6.21) using the proposed bilinear and PSO algorithms. The optimal solution produced by `hinfstruct` (solid-red line).

Table 6.2 – Comparison of optimal solutions from convex and non-convex problems (with optimization time)

	γ^+	Optimization Time [min]
Method 1	0.737	[4,21]
Method 2	0.799	0.48
Method 3	0.737	0.50
Convex Method	$\gamma^\star = 1.113$	0.84
`hinfstruct`	0.737	0.18

in Fig. 6.2. The advantage of Method 1 is that a sequence of convex problems are solved and no stochastic search algorithms are required (at the cost of a significantly larger optimization time). Method 3 achieves a low optimal value with little time; therefore, *in a data-driven sense*, optimizing $X(\boldsymbol{x})$, $Y(\boldsymbol{x})$ and $F(\boldsymbol{x})$ using the PSO algorithm proves to be the more efficient solution for this problem.

Fig. 6.2 also displays the solution for varying n_f using Method 3. It can be observed that when these basis function parameters are optimized, a 1$^{\text{st}}$ order function for $F(\boldsymbol{x})$ produces a solution approximately equal to the solution from `hinfstruct`. Thus optimizing the basis function parameters using the PSO algorithm proves to be more efficient, since convergence to a solution is obtained without implementing high orders of $F(\boldsymbol{x})$.

6.3.2 Case 2: Multi-model Uncertainty

For this example, a robust controller will be designed for a family of unstable systems. This example is taken from the Robust Control Toolbox of `MATLAB` (which is the same example

considered in Section 3.4.1). For this problem, the control objective is to minimize γ and satisfy the following criteria for all seven models:

$$\|W_1\mathscr{S}_s^i(\boldsymbol{\rho})\|_\infty < \gamma \quad \text{and} \quad \|W_2\mathscr{S}_t^i(\boldsymbol{\rho})\|_\infty < \gamma \tag{6.22}$$

for $i = 0,\ldots,6$. The weighting filters W_1 and W_2 are chosen to be equal to those in Section 3.4.1).

The `hinfstruct` function in `MATLAB`'s Robust Control Toolbox uses this criteria to design a controller, and achieves a local optimal solution of $\gamma^+ = 0.886$ (with 200 random initiations) when a 6^{th} order controller is used (with integral action).

The same problem is now solved using the proposed approach. First, the coprime factors $N_i(s)$ and $M_i(s)$ for $i = 0,\ldots,6$ must be established. Since each model is unstable, then each coprime factor must be selected such that $\{N_i(s), M_i(s)\} \in \mathbf{RH}_\infty$ for all i. A simple choice is to divide both the numerator and denominator of each model by a factor $(s+\upsilon)^{d_i}$, where $\upsilon \in \mathbb{R}_+$ and d_i is the largest degree of the denominator of the i-th respective plant model. For example, the coprime factors for the plant $G_2(s)$ can be formed as follows:

$$\begin{aligned} N_2(s) &= \frac{2\cdot 50^2}{(s+\upsilon)^3} \\ M_2(s) &= \frac{(s-2)(s^2+10s+50^2)}{(s+\upsilon)^3}. \end{aligned} \tag{6.23}$$

From these relations, it is evident that $G_2(s) = N_2(s)M_2^{-1}(s)$. To further simplify the design, the same $\upsilon = 100$ (as defined in the case study presented in Section 3.4.1) can be selected for each i-th coprime.

The optimization problem (with the proposed approach) for the mixed $\mathscr{H}_\infty$ criteria in (6.22) can be formulated as follows:

$$\begin{aligned} \underset{\boldsymbol{x}}{\text{minimize}} \quad & \gamma \\ \text{subject to:} \quad & \gamma^{-1}|W_1M_iY(\boldsymbol{x})F(\boldsymbol{x})| < \Re\{\psi_i(\boldsymbol{x})F(\boldsymbol{x})\} \\ & \gamma^{-1}|W_2N_iX(\boldsymbol{x})F(\boldsymbol{x})| < \Re\{\psi_i(\boldsymbol{x})F(\boldsymbol{x})\} \\ & \omega \in \Omega_c, i = 0,\ldots,6, \end{aligned} \tag{6.24}$$

where $\psi_i(\boldsymbol{x}) = N_iX(\boldsymbol{x}) + M_iY(\boldsymbol{x})$.

Simulation Results

The problem in (6.24) is solved by considering a logarithmically spaced frequency grid with 300 points from 10^{-1} to 10^4 rad s^{-1}. First, consider the parameterization process asserted in Method 1; a 6^{th} order controller is designed (5^{th} order controller with one integrator) using the Laguerre basis functions defined in (2.30) with $\xi = 20$ (as defined in Section 3.4.1) and with

Table 6.3 – Comparison between optimal solutions and optimization time for multi-model problem

	γ^+	Optimization Time [min]
Method 1	0.817	606
Method 2	0.880	207
Method 3	0.817	401
Convex Method	$\gamma^\star = 0.881$	15
`hinfstruct`	0.886	212

$\xi_f = 20$. The BP is then solved using the “Mountain Climbing" method until convergence is achieved (within 10^{-5}) for $n_f = 10$.

Now consider the parameterization method asserted in Method 2 and Method 3 (where Method 3 will use a function $F(\boldsymbol{x})$ with $n_f = 10$). Fifty iterations for each method were initiated where each iteration was terminated when convergence was achieved. The minimum value of γ that achieves feasibility for all iterations was considered as the optimal. For this problem, a swarm of $p_x = 150$ particles was used with a penalty factor $\vartheta = 2$ and $k_\vartheta = 0.95$. A comparison of the optimal solutions with the optimization time for each method satisfying the criteria in (6.22) are tabulated in Table.6.3 (where each method implements a 6^{th} order controller). From all of these algorithms, it can be observed that the proposed method using Method 1 and Method 3 yield the best solutions for this problem. Additionally, Method 2 achieves a better optimal solution than `hinfstruct` with a lower optimization time; however, it should be noted that selecting a lower number of random initializations (i.e., 10 initializations) with `hinfstruct` produces a solution very close to the solution with 200 initializations (with a difference of approximately 1%). In other words, there is no significant improvement in the optimal solution when the number of random initializations are increased.

In contrast with the solutions obtained in *Case 1*, the optimization time for the convex problem in the multi-model case is much lower than those using the other methods. Therefore, for larger order controllers with more problem constraints, there exists a trade-off between the optimization time and the quality of the optimal solution.

Figure. 6.3 shows the step response of $\mathscr{S}_s(s)$ (disturbance response) for all seven models using the solution obtained with the `hinfstruct` command, while Figure. 6.4 shows the step response of $\mathscr{S}_s(s)$ using the proposed PSO method (with function parameterization as asserted in Method 3). It can be observed that the proposed data-driven method produces shorter settling times and reduced overshoot (at the expense of a larger optimization time). However, all of the results are comparable.

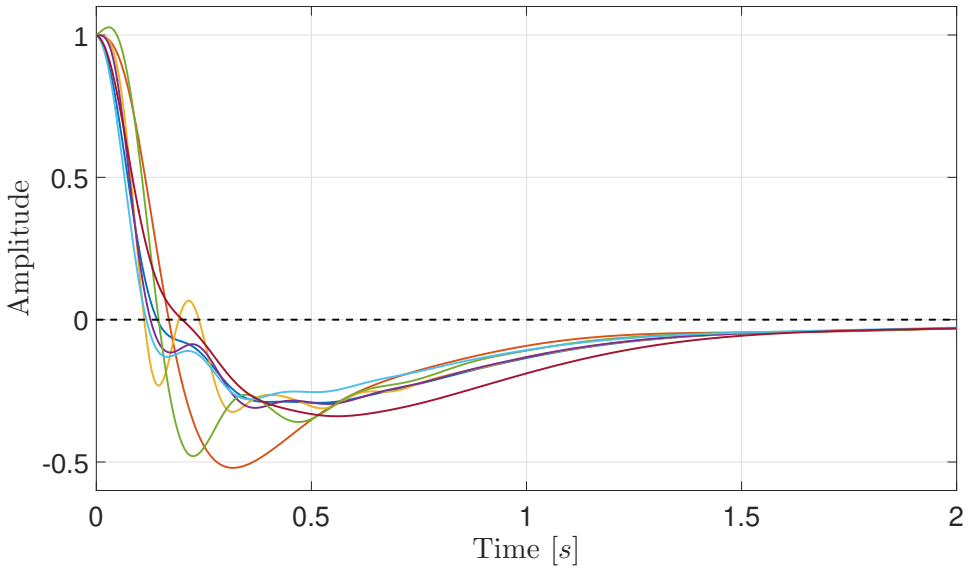

Figure 6.3 – Step response of $\mathscr{S}_s(s)$ for all seven models using the controller designed with `hinfstruct` (with 200 random initializations).

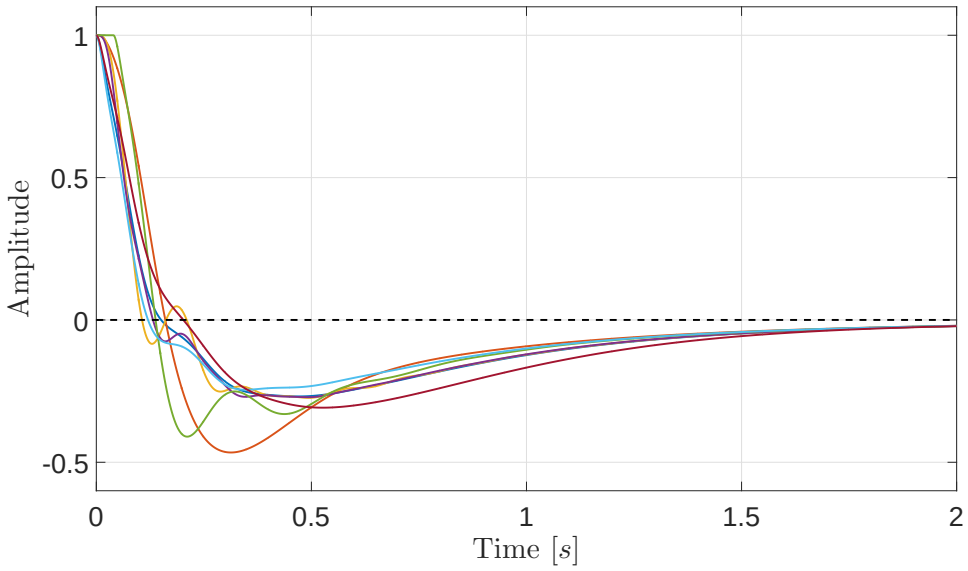

Figure 6.4 – Step response of $\mathscr{S}_s(s)$ for all seven models using the proposed PSO algorithm.

6.4 Conclusion

A data-driven approach has been implemented in order to design robust low-order controllers that achieve $\mathscr{H}_\infty$ performance. With the methods developed in chapters 3 and 4, the optimal solution obtained with low-order controllers may be far from the global solution of the $\mathscr{H}_\infty$ problem (since these methods solve an approximate (convex) problem). Therefore, in this chapter, an optimization problem was formulated to obtain a local solution to the $\mathscr{H}_\infty$ problem using fixed-structure low-order controllers (while guaranteeing the closed-loop stability). This optimization problem was non-convex; therefore, a PSO algorithm was formulated in a data-driven setting to solve this optimization problem and optimize all parameters of a fixed-structure controller. Thanks to the results obtained from Lemma 3.2, the local optimal solution to the true $\mathscr{H}_\infty$ problem (for fixed-structure controllers) was achieved. The simulation examples show that for very low-order controllers (such as the PID controller), the solutions to the non-convex optimization problems yield better results in a short amount of time. For higher order controllers, the convex method produces a reasonable value (with respect to the optimal values of the non-convex problems) in a relatively short time. For future work, it will be desired to compare the solutions and optimization times using other nonlinear solvers (such as genetic algorithms, evolutionary programming, and differential evolution).

7 Model-Reference Control for Particle Accelerator Power Converters

7.1 Introduction

The design methodology described in the previous chapter was based on computing fixed-structure controllers by finding the local solution to a non-convex problem. However, it was seen that for larger order controllers, the optimization time can be quite large; additionally, the selection of the free parameters of the nonlinear solver (i.e., the constriction coefficient, the learning rates, and the penalty factor) for larger order controllers can significantly alter the quality of the optimal solution. Therefore, since convex problems are computationally tractable, it is natural to extend on the methods in the previous chapter by finding the local solution to the $\mathscr{H}_\infty$ problem through a convex optimization algorithm. With the BP formulated in the previous chapter, a local solution was obtained by implementing the "Mountain Climbing" method (i.e., solving a set of convex problems); however, this method relied on an iterative scheme where multiple SDP problems were solved (using a bisection algorithm) until convergence was achieved, which was extremely time consuming for problems with many constraints.

The method proposed in this chapter is an extension of [66] and [139] to the model-reference control problem and invokes a data-driven control scheme to design fixed-structure controllers. In [139], a convex optimization problem was proposed in order to obtain the local solution to the $\mathscr{H}_\infty$ problem (for the model-reference objective); an LMI construction was realized where the local solution to the problem was obtained without the need to implement a bisection algorithm (which significantly reduces the computation time). In addition to obtaining $\mathscr{H}_\infty$ performance, this chapter presents a new approach for obtaining $\mathscr{H}_1$ and $\mathscr{H}_2$ performance using frequency-domain data. Two distinct methods are proposed to design a 2DOF controller by using convex optimization algorithms; however, the methods described in this chapter can also be applied to mixed $\mathscr{H}_2$ and $\mathscr{H}_\infty$ problems (i.e., minimizing the norm of weighted sensitivity functions). Additionally, with certain trivial initializations of the controller parameters, it is shown that the closed-loop stability is guaranteed. The methods presented in this chapter are implemented for a specific power converter application at CERN.

The class of models considered in this chapter will be LTI-SISO discrete-time systems where the FRF of the plant model is described as $G(e^{-j\omega})$. Unlike the system structure presented in previous chapters, the plant is not represented as a function of coprimes. It is assumed that $G(e^{-j\omega})$ is bounded in all frequencies except for a set B_g which includes a finite number of frequencies that correspond to the poles of G on the unit circle. Therefore, the set of frequencies defined for the FRF plant is

$$\omega \in \Omega_g := \left\{ \omega \,\middle|\, -\frac{\pi}{T_s} \leq \omega \leq \frac{\pi}{T_s} \right\} \setminus B_g.$$

In general, a set $\mathscr{G}_g$ can be formulated to represent a plant model containing ℓ FRF models:

$$\mathscr{G}_g = \{G_i(e^{-j\omega}); \quad i = 1, \ldots, \ell; \quad \forall \omega \in \Omega_g\}. \tag{7.1}$$

For simplicity, one model from the set $\mathscr{G}_g$ will be considered, and the subscript i will be omitted. However, in general, the design procedures outlined in this chapter can be applied to the multi-model case (as will be shown in the case studies).

The class of controllers will be the RST controller structure asserted in Section 2.2.2. Thus the sensitivity functions considered will be those in Section 2.3.2. Note that since the plant model is not represented in coprime form, then the sensitivity functions can be expressed with $N = G$ and $M = 1$. The set of frequencies of all roots of $S(z^{-1}, \boldsymbol{\rho})$ on the stability boundary (i.e., on the unit circle) is denoted by B_s. Note that $S(e^{-j\omega}, \boldsymbol{\rho})$ should be invertible for all $\omega \in \Omega := \Omega_g \setminus B_s$.

7.2 Control Performance

In this section, it will be demonstrated that the performance specification of the control problem will be achieved by formulating a convex optimization problem. The controllers will be synthesized by only considering the FRF of the system.

7.2.1 Convex Approximation

In subsequent sections, it will be shown that the type of optimization problem that will be considered will have the following form:

$$\begin{aligned} &\underset{\boldsymbol{\rho},\gamma}{\text{minimize}} && \gamma \\ &\text{subject to:} && g^*(\boldsymbol{\rho})\gamma^{-1}g(\boldsymbol{\rho}) - \psi^*(\boldsymbol{\rho})\psi(\boldsymbol{\rho}) < 0, \end{aligned} \tag{7.2}$$

where $\gamma \in \mathbb{R}_+$, $g : \mathbb{R}^{n_{rst}} \times \mathbb{R} \to \mathbb{C}$ and $\psi : \mathbb{R}^{n_{rs}} \times \mathbb{R} \to \mathbb{C}$ are linear functions of the decision vector $\boldsymbol{\rho}$ and $(\cdot)^*$ denotes the complex conjugate of the argument. This type of problem is convex-concave (due to the $-\psi^*(\boldsymbol{\rho})\psi(\boldsymbol{\rho})$ term). To convexify this constraint, the term $\psi^*(\boldsymbol{\rho})\psi(\boldsymbol{\rho})$ can be linearized around an initial operating point $\boldsymbol{\rho}_0$. It can be shown that $\psi^*(\boldsymbol{\rho})\psi(\boldsymbol{\rho})$ is always

greater than or equal to a linear function of $\boldsymbol{\rho}$ for any initial vector $\boldsymbol{\rho}_0$:

$$\psi^*(\boldsymbol{\rho})\psi(\boldsymbol{\rho}) \geq \psi^*(\boldsymbol{\rho})\psi_0 + \psi(\boldsymbol{\rho})\psi_0^* - \psi_0^*\psi_0, \tag{7.3}$$

where $\psi_0 = \psi(\boldsymbol{\rho}_0)$. The condition in (7.3) can easily be established by realizing the following inequality:

$$[\psi(\boldsymbol{\rho}) - \psi_0]^*[\psi(\boldsymbol{\rho}) - \psi_0] \geq 0. \tag{7.4}$$

With this linearization, a sufficient condition for the inequality in (7.2) can be developed as follows:

$$g^*(\boldsymbol{\rho})\gamma^{-1}g(\boldsymbol{\rho}) - \left[\psi^*(\boldsymbol{\rho})\psi_0 + \psi(\boldsymbol{\rho})\psi_0^* - \psi_0^*\psi_0\right] < 0. \tag{7.5}$$

By using the Shur Complement Lemma [140], the above condition can be expressed in terms of a LMI:

$$\begin{bmatrix} \psi^*(\boldsymbol{\rho})\psi_0 + \psi(\boldsymbol{\rho})\psi_0^* - \psi_0^*\psi_0 & g^*(\boldsymbol{\rho}) \\ g(\boldsymbol{\rho}) & \gamma \end{bmatrix} \succ 0. \tag{7.6}$$

This type of formulation will be used in the next section in order to construct a model-reference control objective.

For a Schur SISO system $X(z^{-1})$, the $\mathscr{H}_1$, $\mathscr{H}_2$ and $\mathscr{H}_\infty$ norms are defined as follows:

$$\|X\|_1 := \frac{T_s}{2\pi}\int_{-\pi/T_s}^{\pi/T_s} |X(e^{-j\omega})|\, d\omega$$
$$\|X\|_2 := \sqrt{\frac{T_s}{2\pi}\int_{-\pi/T_s}^{\pi/T_s} \left|X(e^{-j\omega})\right|^2 d\omega}$$
$$\|X\|_\infty := \sup_{\omega\in\Omega} |X(e^{-j\omega})|$$

It is imperative to note that the boundedness of spectral norm X does not guarantee the stability of X.

A model-reference criterion can be considered as a form of control performance. If $\mathscr{S}_2 : \mathbb{R}^{n_{rst}} \times \mathbb{R} \to \mathbb{C}$ is the closed-loop FRF and $\mathscr{S}_2^d : \mathbb{R} \to \mathbb{C}$ is the desired FRF, then one can consider minimizing $(\mathscr{S}_2(\boldsymbol{\rho}) - \mathscr{S}_2^d)$ in the $\mathscr{H}_p$ sense (for $p = \{1, 2, \infty\}$) in order to shape $\mathscr{S}_2$.

Remark. *Note that the theory developed in subsequent sections will discuss shaping the FRF of $\mathscr{S}_2$ (i.e., a model-reference control objective). However, one can consider shaping any sensitivity function of interest with the presented methods.*

7.2.2 $\mathscr{H}_\infty$ Performance

In this section, a method for optimizing the parameters of the RST polynomials in one optimization problem is presented (i.e., the RST polynomials are simultaneously optimized to obtain the desired $\mathscr{H}_2$ or $\mathscr{H}_\infty$ performance). The closed-loop FRF for the RST structure is $\mathscr{S}_2(\boldsymbol{\rho}) = \Delta_2(\boldsymbol{\rho})\psi^{-1}(\boldsymbol{\rho})$ (with $\Delta_2(\boldsymbol{\rho}) = GT(\boldsymbol{\rho})$, as given in (2.39) with $N = G$). In the $\mathscr{H}_\infty$ sense, the objective is to minimize $\|\mathscr{S}_2(\boldsymbol{\rho}) - \mathscr{S}_2^d\|_\infty$; an equivalent representation of this objective is to minimize γ such that $\|\mathscr{S}_2(\boldsymbol{\rho}) - \mathscr{S}_2^d\|_\infty^2 < \gamma$ (which is the epigraph form of the minimization criterion). This criterion is satisfied if the following optimization problem is considered:

$$\begin{aligned} &\underset{\boldsymbol{\rho},\gamma}{\text{minimize}} \quad \gamma \\ &\text{subject to:} \quad \left[\mathscr{S}_2(\boldsymbol{\rho}) - \mathscr{S}_2^d\right]^* \left[\mathscr{S}_2(\boldsymbol{\rho}) - \mathscr{S}_2^d\right] < \gamma \end{aligned} \tag{7.7}$$

for all $\omega \in \Omega$. It can be observed that the constraint in (7.7) is not convex. Given the definition of $\mathscr{S}_2(\boldsymbol{\rho})$, this constraint can be written as:

$$\left[\Delta_2(\boldsymbol{\rho}) - \psi(\boldsymbol{\rho})\mathscr{S}_2^d\right]^* \gamma^{-1} \left[\Delta_2(\boldsymbol{\rho}) - \psi(\boldsymbol{\rho})\mathscr{S}_2^d\right] - \psi^*(\boldsymbol{\rho})\psi(\boldsymbol{\rho}) < 0.$$

Note that this constraint has the exact form as the constraint in (7.2); therefore, the LMI formulation in (7.6) can be utilized to construct the model-reference optimization problem as follows:

$$\begin{aligned} &\underset{\boldsymbol{\rho},\gamma}{\text{minimize}} \quad \gamma \\ &\text{subject to:} \quad \begin{bmatrix} \psi^*(\boldsymbol{\rho})\psi_0 + \psi_0^*\psi(\boldsymbol{\rho}) - \psi_0^*\psi_0 & \left(\Delta_2(\boldsymbol{\rho}) - \psi(\boldsymbol{\rho})\mathscr{S}_2^d\right)^* \\ \Delta_2(\boldsymbol{\rho}) - \psi(\boldsymbol{\rho})\mathscr{S}_2^d & \gamma \end{bmatrix} \succ 0 \end{aligned} \tag{7.8}$$

for all $\omega \in \Omega$, where

$$\psi_0 = \psi(\boldsymbol{\rho}_0) = GR(\boldsymbol{\rho}_0) + S(\boldsymbol{\rho}_0)$$

and $\boldsymbol{\rho}_0$ is the vector of initializing parameters for R and S, i.e.,

$$\boldsymbol{\rho}_0 = [r_{0,0}, r_{1,0}, \ldots, r_{n_r,0}, s_{1,0}, s_{2,0}, \ldots, s_{n_s,0}].$$

7.2.3 $\mathscr{H}_2$ Performance

In a similar manner, an optimization problem can be formulated for minimizing the square of the $\mathscr{H}_2$ model-reference objective (i.e., minimizing $\|\mathscr{S}_2(\boldsymbol{\rho}) - \mathscr{S}_2^d\|_2^2$); the optimization problem

for this criteria can be expressed as follows:

$$\begin{aligned} \underset{\boldsymbol{\rho},\gamma,\Gamma}{\text{minimize}} \quad & \gamma = \int_{-\pi/T_s}^{\pi/T_s} \Gamma(\omega)\, d\omega \\ \text{subject to:} \quad & \left[\mathscr{S}_2(\boldsymbol{\rho}) - \mathscr{S}_2^d\right]^* \left[\mathscr{S}_2(\boldsymbol{\rho}) - \mathscr{S}_2^d\right] < \Gamma(\omega) \end{aligned} \tag{7.9}$$

for all $\omega \in \Omega$, where $\Gamma(\omega)$ is an unknown function of ω. Therefore, by using the results obtained in Section 7.2.1, the following convex optimization problem can be considered:

$$\begin{aligned} \underset{\boldsymbol{\rho},\gamma,\Gamma}{\text{minimize}} \quad & \gamma = \int_{-\pi/T_s}^{\pi/T_s} \Gamma(\omega)\, d\omega \\ \text{subject to:} \quad & \begin{bmatrix} \psi^*(\boldsymbol{\rho})\psi_0 + \psi_0^*\psi(\boldsymbol{\rho}) - \psi_0^*\psi_0 & \left(\Delta_2(\boldsymbol{\rho}) - \psi(\boldsymbol{\rho})\mathscr{S}_2^d\right)^* \\ \Delta_2(\boldsymbol{\rho}) - \psi(\boldsymbol{\rho})\mathscr{S}_2^d & \Gamma(\omega) \end{bmatrix} \succ 0 \end{aligned} \tag{7.10}$$

for all $\omega \in \Omega$. For this $\mathscr{H}_2$ problem, note that $\Gamma(\omega)$ can be selected as a simple linear polynomial function of finite order, i.e.,

$$\Gamma(\omega) = \sum_{i=0}^{h} \Gamma_i \omega^i, \tag{7.11}$$

where h is the order of the polynomial. In the case when the constraints are evaluated at a finite number of frequencies (i.e., $\omega \in \Omega_\eta = \{\omega_1, \ldots, \omega_\eta\}$), then $\Gamma(\omega)$ can be replaced by an optimization variable Γ_k at each frequency ω_k for $k = 1, \ldots, \eta$.

Remark. *Note that the choice of the initializing controllers in ψ_0 may affect the stability of the closed-loop system (for either the optimization problems concerning the $\mathscr{H}_\infty$ or $\mathscr{H}_2$ norms). Section 7.3 will discuss how to select these initializing controllers in order to ensure stability.*

To obtain the local optimal solution to the problem in (7.7) (respectively 7.9), the convex problem in (7.8) (respectively 7.10) must be solved in an iterative fashion. The basic procedure for implementing this iterative algorithm is summarized in Table 7.1 for the problem in (7.8) (which is similar to the procedure for the problem in (7.10)). By executing this algorithm, the solution to the convex problem converges to a local solution of the fixed-structure $\mathscr{H}_\infty$ (respectively $\mathscr{H}_2$) problem (i.e., $\lim_{l\to\infty} \gamma_l^\star \to \gamma^+$ and $\lim_{l\to\infty} \boldsymbol{\rho}_l^\star \to \boldsymbol{\rho}^+$).

7.2.4 $\mathscr{H}_1$ Performance

In the previous section, convex optimization problems were formulated in order to satisfy the model-reference problem; one convex optimization problem can be considered for this design approach to obtain all of the controller parameters and achieve either $\mathscr{H}_2$ or $\mathscr{H}_\infty$ performance (i.e., obtain the local solutions to the $\mathscr{H}_p$ problems for $p \in \{2, \infty\}$). However, in many applications (as in the power converter application considered in this work, which is discussed in Section 7.5), minimizing the $\mathscr{H}_1$ norm of the model-reference objective may be desired. It is known that minimizing different $\mathscr{H}_p$ norms in the frequency-domain will be

Table 7.1 – Procedure for obtaining local optimal solution with convex formulation

Algorithm: Convex optimization for optimal performance
1. Define a tolerance for γ (γ_{tol}) and set $l = 1$ (where l denotes the iteration number).
2. Solve the problem in (7.8) for a given controller order and a given ψ_0 and obtain the optimal solutions for $\gamma_l^\star$ and $\boldsymbol{\rho}_l^\star$. Formulate $\psi(\boldsymbol{\rho}_l^\star)$ and then let $l = l+1$.
3. Let $\psi_0 = \psi(\boldsymbol{\rho}_{l-1}^\star)$ and solve the problem in (7.8) to obtain $\gamma_l^\star$ and $\boldsymbol{\rho}_l^\star$.
4. If $\gamma_{l-1}^\star - \gamma_l^\star < \gamma_{tol}$, stop. Otherwise, let $l = l+1$ and return to step 3.

interpreted in different manners in the time-domain. For example, given a bounded discrete-time signal $x[k]$, the relationship between the frequency-domain and time-domain for the $\mathscr{H}_2$ norm is $\|X\|_2 = \|x\|_2$ according to the well-known Parseval theorem, where $X(e^{-j\omega})$ is the frequency spectrum of $x[k]$. The relationship between $\|X\|_1$ and $\|x\|_\infty$ is given as follows:

$$\begin{aligned}\|x\|_\infty &= \sup_k |x[k]| = \sup_k \left| \frac{T_s}{2\pi} \int_{-\pi/T_s}^{\pi/T_s} X(e^{-j\omega}) e^{jkT_s\omega} d\omega \right| \\ &\leq \sup_k \frac{T_s}{2\pi} \int_{-\pi/T_s}^{\pi/T_s} \left| X(e^{-j\omega}) e^{jkT_s\omega} \right| d\omega = \frac{T_s}{2\pi} \int_{-\pi/T_s}^{\pi/T_s} \left| X(e^{-j\omega}) \right| d\omega = \|X\|_1 .\end{aligned} \tag{7.12}$$

Similarly, it can be shown that $\|X\|_\infty \leq \|x\|_1$. Therefore, if one is interested in minimizing the peak error in the time-domain, then minimizing the $\mathscr{H}_1$ norm of the error in the frequency-domain can be considered.

The $\mathscr{H}_1$ model-reference problem can be formulated as follows:

$$\begin{aligned} \underset{\boldsymbol{\rho},\gamma,\Gamma}{\text{minimize}} \quad & \gamma = \int_{-\pi/T_s}^{\pi/T_s} \Gamma(\omega) d\omega \\ \text{subject to:} \quad & \left| \mathscr{S}_2(\boldsymbol{\rho}) - \mathscr{S}_2^d \right| < \Gamma(\omega) \end{aligned} \tag{7.13}$$

for all $\omega \in \Omega$. The convexification methods used to obtain $\mathscr{H}_2$ and $\mathscr{H}_\infty$ performance (as discussed in Sections 7.2.2 and 7.2.3) cannot be used in formulating the $\mathscr{H}_1$ problem since the constraint in this problem cannot be expressed as in (7.2). Linearization does not pose as a viable solution since $\Gamma(\omega)$ is a vector of decision variables and a straightforward bisection algorithm cannot be performed to obtain the local solution to the problem. Therefore, a different approach is taken to solve the $\mathscr{H}_1$ model-reference problem; a two-step design method is implemented where the $R(\boldsymbol{\rho})$ and $S(\boldsymbol{\rho})$ polynomials are optimized separately from the polynomial $T(\boldsymbol{\rho})$. For this reason, let us define the following vectors:

$$\boldsymbol{\rho}_1 = [r_0, r_1, \ldots, r_{n_r}, s_1, s_2, \ldots, s_{n_s}]; \quad \boldsymbol{\rho}_2 = [t_0, t_1, \ldots, t_{n_t}]. \tag{7.14}$$

A sequential set of convex problems are formulated as follows: in the first problem, the polynomials $R(\boldsymbol{\rho}_1)$ and $S(\boldsymbol{\rho}_1)$ are optimized for regulation. In this step, the appropriate stability and robustness margins can be attained for the closed-loop system. Once these polynomials are formulated, the sensitivity functions defined in Section 2.3.2 become linear functions of $\boldsymbol{\rho}_2$. A convex optimization problem for the $\mathscr{H}_1$ model-reference objective can then be easily implemented in order to obtain the final polynomial in the RST structure $T(\boldsymbol{\rho}_2)$.

Suppose that it is desired to obtain a minimum value for the modulus margin (which ensures both the closed-loop stability and sufficient robustness margins). The modulus margin is the minimum distance between the Nyquist plot of the open-loop FRF and the point $(-1+j0)$. Thus one must consider satisfying $\|m_d \mathscr{S}_1(\boldsymbol{\rho}_1)\|_\infty < 1$ for all $\omega \in \Omega$, where m_d is the desired minimum value of the modulus margin. By applying the methods described in Section 7.2.2, a convex constraint for satisfying the modulus margin criterion can be formulated as follows:

$$\begin{bmatrix} \psi^*(\boldsymbol{\rho}_1)\psi_0 + \psi_0^*\psi(\boldsymbol{\rho}_1) - \psi_0^*\psi_0 & \left(m_d S(\boldsymbol{\rho}_1)\right)^* \\ m_d S(\boldsymbol{\rho}_1) & 1 \end{bmatrix} \succ 0, \quad \forall \omega \in \Omega. \tag{7.15}$$

The above constraint ensures a sufficient robustness margin with the parameter m_d. With a feasible solution to the problem in (7.15), the admissible parameters for $R(\boldsymbol{\rho}_1^\star)$ and $S(\boldsymbol{\rho}_1^\star)$ are obtained (where $\boldsymbol{\rho}_1^\star$ is the feasible solution to the problem). The solution to (7.15) will guarantee the closed-loop stability and desired robustness margin if ψ_0 is chosen appropriately (which will be discussed in Section 7.3). Once the admissible parameters are obtained for $R(\boldsymbol{\rho}_1^\star)$ and $S(\boldsymbol{\rho}_1^\star)$, one then simply considers the following unconstrained model-reference optimization problem:

$$\underset{\boldsymbol{\rho}_2}{\text{minimize}} \quad \left\| \mathscr{S}_2(\boldsymbol{\rho}_1^\star, \boldsymbol{\rho}_2) - \mathscr{S}_2^d \right\|_1, \quad \forall \omega \in \Omega. \tag{7.16}$$

The feasible solution to this problem satisfies the $\mathscr{H}_1$ model-reference objective. Note that $\mathscr{S}_2(\boldsymbol{\rho}_1^\star, \boldsymbol{\rho}_2)$ is now linear with respect to the decision vector $\boldsymbol{\rho}_2$, and the objective function in (7.16) is convex.

7.3 Stability Analysis

The model-reference constraints developed in Sections 7.2.2 and 7.2.3 do not guarantee the stability of the closed-loop system. Setting a desired FRF to shape a closed-loop FRF is analogous to bounding the closed-loop FRF; it can be shown that unstable systems can still possess bounded FRFs.

The initializing controllers in ψ_0 play an important role in guaranteeing the stability of the closed-loop system. By using the Nyquist criterion, the stability of the closed-loop system can be ensured if certain conditions are met for these initializing controllers.

The following definition and properties will be needed in order to properly analyze the stability

conditions of the system:

Definition 7.1. *Let* wno$\{A(z)\}$ *refer to the winding number around the origin, in the counterclockwise sense, of the image of* $A(z)$ *when* z *traverses the Nyquist contour (with small detours around the poles of* $A(z)$ *on the unit circle). Then the following properties hold:*

$$\text{wno}\{A_1(z)A_2(z)\} = \text{wno}\{A_1(z)\} + \text{wno}\{A_2(z)\} \tag{7.17}$$

$$\text{wno}\{A(z)\} = -\text{wno}\{A^*(z)\} \tag{7.18}$$

$$\text{wno}\{A(z)\} = -\text{wno}\{A^{-1}(z)\} \tag{7.19}$$

The open-loop FRF of the RST structure is given as $L(\boldsymbol{\rho}) = GR(\boldsymbol{\rho})S^{-1}(\boldsymbol{\rho})$. By the Nyquist stability criterion, the closed-loop system is stable if and only if the Nyquist plot of

$$1 + L(\boldsymbol{\rho}) = 1 + GR(\boldsymbol{\rho})S^{-1}(\boldsymbol{\rho})$$

makes $n_G + n_K$ counterclockwise encirclements of the origin (where n_G and n_K are, respectively, the number of poles outside the unit circle of G and $R(\boldsymbol{\rho})S^{-1}(\boldsymbol{\rho})$). The Nyquist plot of $1 + L(\boldsymbol{\rho})$ must also not pass through the origin. Therefore, to ensure the closed-loop stability of the system, we must have $\text{wno}\{1 + L(\boldsymbol{\rho})\} = n_G + n_K$. Note that n_K is also equal to the number of zeros outside the unit circle of $S(\boldsymbol{\rho})$.

Theorem 7.1. *Suppose that* $R(\boldsymbol{\rho}_0)$ *and* $S(\boldsymbol{\rho}_0)$ *are stabilizing initial controllers and that* $R(\boldsymbol{\rho})$ *and* $S(\boldsymbol{\rho})$ *are feasible solutions to the following constraint:*

$$\psi^*(\boldsymbol{\rho})\psi_0 + \psi_0^*\psi(\boldsymbol{\rho}) > 0, \quad \forall \omega \in \Omega. \tag{7.20}$$

Then the closed-loop system is stable if $S(\boldsymbol{\rho})$ *and* $S(\boldsymbol{\rho}_0)$ *share the same zeros on the stability boundary (i.e., the zeros on the unit circle).*

Proof: The proof is based on the Nyquist stability criterion and the properties of the winding number. The winding number of $\psi^*(\boldsymbol{\rho})\psi_0$ is given as follows:

$$\begin{aligned}\text{wno}\{\psi^*(\boldsymbol{\rho})\psi_0\} &= \text{wno}\{\psi^*(\boldsymbol{\rho})\} + \text{wno}\{\psi_0\} \\ &= -\text{wno}\{GR(\boldsymbol{\rho}) + S(\boldsymbol{\rho})\} + \text{wno}\{GR(\boldsymbol{\rho}_0) + S(\boldsymbol{\rho}_0)\} \\ &= -\text{wno}\{S(\boldsymbol{\rho})\} - \text{wno}\{1 + L(\boldsymbol{\rho})\} + \text{wno}\{S(\boldsymbol{\rho}_0)\} + \text{wno}\{1 + L(\boldsymbol{\rho}_0)\}.\end{aligned} \tag{7.21}$$

Since $S(\boldsymbol{\rho})$ and $S(\boldsymbol{\rho}_0)$ share the same poles on the unit circle, the phase variation of $\psi^*(\boldsymbol{\rho})\psi_0$ for the small detours around the poles on the unit circle is zero and the winding number of $\psi^*(\boldsymbol{\rho})\psi_0$ can be evaluated over Ω instead of the Nyquist contour. Additionally, the constraint in (7.20) implies that $\Re\{\psi^*(\boldsymbol{\rho})\psi_0\} > 0$ since

$$\Re\{\psi^*(\boldsymbol{\rho})\psi_0\} = \frac{1}{2}\left[\psi^*(\boldsymbol{\rho})\psi_0 + \psi_0^*\psi(\boldsymbol{\rho})\right]$$

This signifies that the Nyquist plot of $\psi^*(\boldsymbol{\rho})\psi_0$ will not pass through or encircle the origin and

$\text{wno}\{\psi^*(\boldsymbol{\rho})\psi_0\} = 0$. Therefore, from (7.21), the following condition can then be realized:

$$\text{wno}\{1 + L(\boldsymbol{\rho})\} = \text{wno}\{S(\boldsymbol{\rho}_0)\} + \text{wno}\{1 + L(\boldsymbol{\rho}_0)\} - \text{wno}\{S(\boldsymbol{\rho})\}. \tag{7.22}$$

However, if the initializing controllers are stabilizing, then $\text{wno}\{1 + L(\boldsymbol{\rho}_0)\} = n_G + n_{K_0}$, where n_{K_0} is the number of poles outside the unit circle of $R(\boldsymbol{\rho}_0)S^{-1}(\boldsymbol{\rho}_0)$ (which is also equal to the number of zeros outside the unit circle of $S(\boldsymbol{\rho}_0)$). Note that the polynomial $S(\boldsymbol{\rho})$ in (2.28) is equivalent to

$$S(z, \boldsymbol{\rho}) = \frac{z^{n_s} + s_1 z^{n_s - 1} + \cdots + s_n}{z^{n_s}}. \tag{7.23}$$

Now, consider a contour that incorporates the unit circle; by the Cauchy principle of argument, it can be observed from (7.23) that

$$\text{wno}\{S(\boldsymbol{\rho})\} = n_s - n_K - n_s = -n_K.$$

By the same principle, it is evident that

$$\text{wno}\{S(\boldsymbol{\rho}_0)\} = n_{s_0} - n_{K_0} - n_{s_0} = -n_{K_0},$$

where n_{s_0} is the order of $S(\boldsymbol{\rho}_0)$. Therefore, from (7.22), we have the following condition:

$$\text{wno}\{1 + L(\boldsymbol{\rho})\} = -n_{K_0} + n_G + n_{K_0} + n_K = n_G + n_K \tag{7.24}$$

and the closed-loop system will be stable. ■

Remark. *According to the above Theorem, $S(\boldsymbol{\rho})$ and $S(\boldsymbol{\rho}_0)$ must share the same zeros on $|z| = 1$ to guarantee the closed-loop stability. Assume that the number of prefixed integrators in $S^{-1}(\boldsymbol{\rho})$ and $S^{-1}(\boldsymbol{\rho}_0)$ are identical. Therefore, to ensure that the criterion in the Theorem is met when the problems in Sections 7.2.2 or 7.2.3 are solved, the constraint $|S(\boldsymbol{\rho})| > 0 \; \forall \omega \in \Omega$ can be imposed (which ensures that $S(\boldsymbol{\rho})$ will not possess additional zeros on $|z| = 1$). However, $|S(\boldsymbol{\rho})| > 0$ is a concave function of $\boldsymbol{\rho}$; therefore, the linearization techniques implemented in Section 7.2.1 can be used to linearize this constraint as follows:*

$$S^*(\boldsymbol{\rho})S(\boldsymbol{\rho}_0) + S(\boldsymbol{\rho})S^*(\boldsymbol{\rho}_0) - S^*(\boldsymbol{\rho}_0)S(\boldsymbol{\rho}_0) > 0, \quad \forall \omega \in \Omega. \tag{7.25}$$

Thus imposing the above constraint to any of the optimization problems will ensure that the stability criterion in Theorem 7.1 is satisfied.

7.3.1 Initial Stabilizing Controller

In a data-driven setting, and for practical applications, a stabilizing controller is typically already available for unstable systems; these controllers can be used in ψ_0 to initialize the optimization algorithm. For stable systems a controller with small gain is always stabilizing,

however, one should take care of poles on the unit circle (such as pure integrators, as discussed in Theorem 7.1).

If a model has been given by an application, a feasibility problem can be formulated to design a stabilizing controller. The following Lemma can be used for this purpose:

Lemma 7.1. *Let the plant model be represented as*

$$G(e^{-j\omega}) = N(e^{-j\omega})M^{-1}(e^{-j\omega}),$$

where $N(e^{-j\omega})$ and $M(e^{-j\omega})$ are coprime factorizations of $G(e^{-j\omega})$ [96] and are both analytic outside the unit circle. Then the system with the RST structure is internally stable if a feasible solution is obtained in the following problem:

$$\begin{aligned} &\textit{find} && \boldsymbol{\rho}_0 \\ &\textit{subject to:} && \Re\left\{\psi(\boldsymbol{\rho}_0)\right\} > 0 \\ &&& \forall \omega \in \Omega, \end{aligned} \tag{7.26}$$

where $\psi(\boldsymbol{\rho}_0) = NR(\boldsymbol{\rho}_0) + MS(\boldsymbol{\rho}_0)$.

Proof: When the plant is represented as a coprime factorization $G = NM^{-1}$, then the zeros of $\psi(\boldsymbol{\rho}_0)$ represent the poles of all of the sensitivity functions of the closed-loop system. Therefore, the stability of $\psi^{-1}(\boldsymbol{\rho}_0)$ implies the stability of all sensitivity functions.

$\Re\{\psi(\boldsymbol{\rho}_0)\} > 0$ signifies that the Nyquist plot of $\psi(\boldsymbol{\rho}_0)$ will not encircle the origin $\forall\omega$. However, note that

$$\Re\{\psi(\boldsymbol{\rho}_0)\} > 0 \iff \Re\left\{\frac{1}{\psi(\boldsymbol{\rho}_0)}\right\} > 0.$$

Then by the SPR conditions in Lemma 4.1, the positive real constraint implies that

$$\psi^{-1}(\boldsymbol{\rho}_0) = [MS(\boldsymbol{\rho}_0)]^{-1}[1 + L(\boldsymbol{\rho}_0)]^{-1}$$

is stable (where $L(\boldsymbol{\rho}_0) = NR(\boldsymbol{\rho}_0)[MS(\boldsymbol{\rho}_0)]^{-1}$ is the open-loop FRF), and thus the closed-loop system is stable. ■

The feasible solution to this problem will generate a controller which will stabilize the closed-loop system and can be used in ψ_0 for the initialization.

7.4 Simulation Examples

Two simulation examples will now be presented in order to demonstrate the effectiveness of the proposed methods. The first example considers a controller design for an uncertain heat conducting system. The second example will investigate the performance for a family of unstable, non-minimum phase systems. The following criterion is used for measuring and

comparing the attained performance for each case study:

$$\mathscr{J}_{p,i}^{\star} = \left\| \mathscr{S}_2^i(\boldsymbol{\rho}^{\star}) - \mathscr{S}_2^d \right\|_p$$

for $p \in \{1,2,\infty\}$, where the p-norm is calculated as stated in Section 7.2.1. When a single model is considered, the subscript i is removed. For all of the case studies, the `MATLAB` software was used in conjunction with the `YALMIP` interface [130] to solve all of the problems in this work. A computer having the following hardware specifications was used: Intel-Core i7, 3.4 GHz CPU, 8GB RAM. The optimization algorithms were run using `MATLAB` version (R2017a) on a Windows 7 platform (64-bit).

Remark. *As with the preceding chapters, all of the optimization problems considered in this chapter are SIP problems since there are a finite number of optimization variables $\boldsymbol{\rho}$ and an infinite number of constraints with respect to ω. To solve any of these problems, the optimization algorithm can be converted to a SDP problem. In this manner, a predefined frequency grid can be implemented in order to solve a finite number of constraints. In other words, a set of frequency points $\Omega_\eta = \{\omega_1, \ldots, \omega_\eta\}$ is defined, where η constraints must be satisfied for each feasibility condition added to the optimization problem.*

7.4.1 Case 1: Heat Conductor

The proposed design method has the advantage of designing controllers for fractional order systems. Consider the heat conduction process which has the following transfer function:

$$G_i(s) = e^{-\sqrt{s/\tilde{a}_i}}, \tag{7.27}$$

where the output is the temperature of the system at a given position, the input is a constant temperature set at a boundary, and $\tilde{a}_i$ is the conduction constant and is an uncertain parameter which lies in the set $\tilde{a}_i \in \{2, 2.5, 3\}\,\mathrm{rad\,s^{-1}}$ for $i = 1,2,3$. The objective of this case study is to design an RST controller (with $\mathscr{H}_2$ and $\mathscr{H}_\infty$ performance) with integral action to ensure performance and stability for all of the uncertain values in $\tilde{a}_i$. In other words, it will be desired to minimize $\|\mathscr{S}_2^i - \mathscr{S}_2^d\|_p$ for all i and for $p \in \{2,\infty\}$.

Controller Synthesis

As shown in Theorem 7.1, a stabilizing initial controller is needed in order to ensure the closed-loop stability and desired performance. Since it was desired to have a controller with integral action, a simple initial stabilizing controller was selected as $R(z^{-1}, \boldsymbol{\rho}_0) = 10^{-2}$ and $S(z^{-1}, \boldsymbol{\rho}_0) = 1 - z^{-1}$ (which was confirmed to stabilize all G_i by investigating the Nyquist plot of the open-loop FRF). With this initializing controller, a 2^{nd} order controller (with integral action) was designed for achieving $\mathscr{H}_2$ and $\mathscr{H}_\infty$ performance (by using the methods in Sections 7.2.2 and 7.2.3 with the added constraint in (7.25)). These problems were solved using the SDP algorithm with a logarithmically spaced grid from 10^{-3} to $\pi/T_s\,\mathrm{rad\,s^{-1}}$ (with $\eta = 200$ and

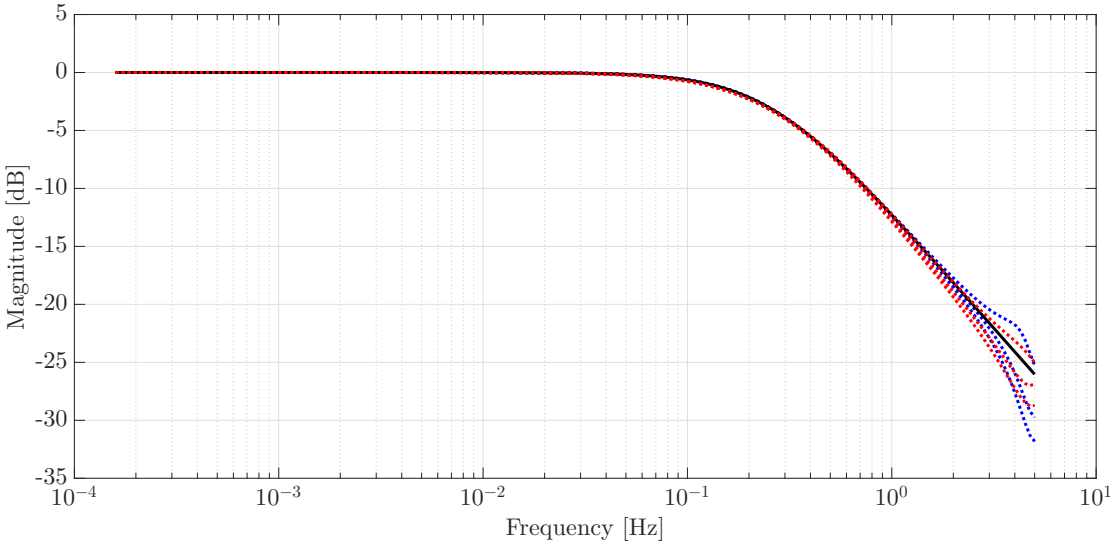

Figure 7.1 – Closed-loop FRFs for each G_i obtained by solving the $\mathscr{H}_2$ problem (dashed-blue) and solving the $\mathscr{H}_\infty$ problem (dashed-red). The desired closed-loop FRF is shown with the solid-black line.

Table 7.2 – Optimization results for $\mathscr{H}_2$ and $\mathscr{H}_\infty$ problems

	$\mathscr{H}_2$ Design			$\mathscr{H}_\infty$ Design		
	R	S	T	R	S	T
1	29.48	1	2.63	16.77	1	1.56
z^{-1}	-21.67	-1.54	1.99	-26.70	-2.16	-0.46
z^{-2}	-2.99	0.54	0.21	10.52	1.16	-0.51
Optimization Time [s]	65.1			41.2		
$\max_i \mathscr{J}^\star_{2,i}$	**0.016**			0.027		
$\max_i \mathscr{J}^\star_{\infty,i}$	0.038			**0.030**		

$T_s = 0.1$ s). For this case study, the desired reference model was selected as a simple first order transfer function, i.e., $\mathscr{S}_2^d = (\tau s + 1)^{-1}$, where τ is the desired time constant (which was selected as $(0.5\pi)^{-1}$ s). The tolerance for γ was selected as $\gamma_{tol} = 10^{-3}$.

Fig. 7.1 shows the magnitude of the closed-loop FRFs (for both the $\mathscr{H}_2$ and $\mathscr{H}_\infty$ designs) for all G_i. Table 7.2 shows the resulting optimization parameters for each design method with the associated optimization time. The parameters in the RST columns correspond to the polynomial variable in the left-most column. For example, the polynomial $S(z^{-1}) = 1 - 1.54z^{-1} + 0.54z^{-2}$ corresponds to the polynomial S in the $\mathscr{H}_2$ design method. From all of these results, it can be observed that even with an uncertain fractional-order transfer function, the proposed method can be used to obtain the desired model-reference objective with a low-order fixed-structure controller.

7.4.2 Case 2: Unstable robot prototype

Consider the following unstable, non-minimum phase system for the climbing robot prototype reported in [110] (which represents the dynamics for the axial movement of one of the robots' components):

$$G(z) = -0.006\frac{(z-6.502)(z+\nu)(z+0.6731)}{(z-1.021)(z-0.5054)(z-0.1672)}, \tag{7.28}$$

where $\nu = 3.890$ and the sampling time is given as $T_s = 0.025\,\text{s}$. Suppose that the unstable zero ν is an uncertain parameter that can vary to ±30% of its nominal value. Therefore, this parameter lies in the interval $\hat{\boldsymbol{\nu}} = \nu[0.7, 1.3]$. With the proposed approach, a multi-model design can be implemented where the uncertain parameter can be gridded with a finite set of values and a controller designed to ensure the performance for all of the gridded values. For this problem, the grid was chosen as $\hat{\nu}_i = \nu\{0.7, 0.8, \ldots, 1.3\}$ for $i = 1, \ldots, 7$. Thus the plant can be expressed as $G_i(z)$ (which represents the plant model with respect to the i^{th} parameter in $\hat{\nu}_i$).

Initial Stabilizing Controller Design

A stabilizing initial controller is needed in order to ensure the closed-loop stability and performance; therefore, the problem in (7.26) can be used to ensure the closed-loop stability for all of the models in G_i. The coprime factors $N_i(z)$ and $M_i(z)$ for $i = 1, \ldots, 7$ must first be established. Since each model is unstable, then each coprime factor must be selected such that $N_i(z)$ and $M_i(z)$ are stable and proper for all i. A simple choice is to divide both the numerator and denominator of each model by a factor $(z-\tilde{\xi})^3$, where $\tilde{\xi} \in]-1, 1[$. To simplify the design, the same $\tilde{\xi} = 0$ can be selected for each i^{th} coprime. For example, the coprime factors for the plant $G_1(z)$ can be formed as follows:

$$\begin{aligned} N_1(z) &= \frac{-0.006(z-6.501)(z+\hat{\nu}_1)(z+0.6731)}{z^3} \\ M_1(z) &= \frac{(z-1.021)(z-0.5054)(z-0.1672)}{z^3}. \end{aligned} \tag{7.29}$$

From these relations, it is evident that $G_1(z) = N_1(z)M_1^{-1}(z)$.

The problem in (7.26) was solved using a 5^{th} order controller and with a logarithmically spaced frequency grid of 100 points from 10^{-2} to π/T_s. Since there are $i = 7$ models to consider in the problem, then there will be a total of 700 linear constraints to satisfy. The optimization time for obtaining the polynomials $R(z^{-1}, \boldsymbol{\rho}_0)$ and $S(z^{-1}, \boldsymbol{\rho}_0)$ was calculated as 2.7 s; these controllers ensure the closed-loop stability for all of the models in G_i.

$$\begin{aligned} R(z^{-1}, \boldsymbol{\rho}_0) &= 15.09 - 2.349z^{-1} + 1.873z^{-2} - 6.644z^{-3} + 5.061z^{-4} + 0.4924z^{-5} \\ S(z^{-1}, \boldsymbol{\rho}_0) &= 1 + 2.142z^{-1} + 0.8225z^{-2} - 1.185z^{-3} - 1.896z^{-4} - 0.8832z^{-5}. \end{aligned} \tag{7.30}$$

Table 7.3 – Performance for different optimization criteria

Criteria	$\mathscr{H}_1$	$\mathscr{H}_2$	$\mathscr{H}_\infty$
$\max_i \mathscr{J}^\star_{1,i}$	**0.401**	0.425	0.426
$\max_i \mathscr{J}^\star_{2,i}$	0.455	**0.453**	0.456
$\max_i \mathscr{J}^\star_{\infty,i}$	1.615	1.250	**0.561**

Note that $S(z^{-1},\boldsymbol{\rho}_0)$ was prefixed with a term $(1-z^{-1})$ (since it was desired to have a final controller with integral action).

Controller Synthesis

A controller was designed to obtain $\mathscr{H}_p$ performance and stability for $p \in \{1,2,\infty\}$ for all of the models G_i. A 5^{th} order polynomial for both $R(\boldsymbol{\rho})$ and $S(\boldsymbol{\rho})$ are selected; however, to obtain adequate performance for the $\mathscr{H}_1$ model-reference objective, a 10^{th} order polynomial for $T(\boldsymbol{\rho})$ was selected. For comparative purposes, the same controller orders were used for all of the $\mathscr{H}_p$ model-reference objectives.

- For the $\mathscr{H}_2$ and $\mathscr{H}_\infty$ objectives, ψ_0 was selected such that it incorporated the stabilizing controllers obtained in (7.30). The tolerance used for γ was selected as $\gamma_{tol} = 10^{-3}$. The constraint in (7.25) was imposed on all problems in order to ensure that the conditions of Theorem 7.1 were satisfied.

- For the $\mathscr{H}_1$ objective, the final polynomials for $R(\boldsymbol{\rho}_1)$ and $S(\boldsymbol{\rho}_1)$ are given in (7.30) and $T(\boldsymbol{\rho}_2)$ is the only polynomial left to be optimized

For this case study, the desired reference model was selected as a simple first order transfer function, i.e., $\mathscr{S}_2^d = (\tau s+1)^{-1}$, where τ is the desired time constant (which was selected as $(5\pi)^{-1}$ s).

The frequency grid that was used for the stabilizing controller design was also used for all of the model-reference optimization problems. Figure 7.2 shows the closed-loop step responses with $\mathscr{H}_p$ performance for the nominal plant model (i.e., when $\hat{\nu}_i = \nu$). It can be observed that the responses are comparable. In order to conserve space, all of the closed-loop step responses for each model and each method are not shown. However, Table 7.3 shows the associated performance criteria for each $\mathscr{H}_p$ model-reference objective. As expected, the minimum value of $\max_i \mathscr{J}^\star_{p,i}$ is obtained when the respective $\mathscr{H}_p$ model-reference objective is minimized (which was also the case in the previous case study).

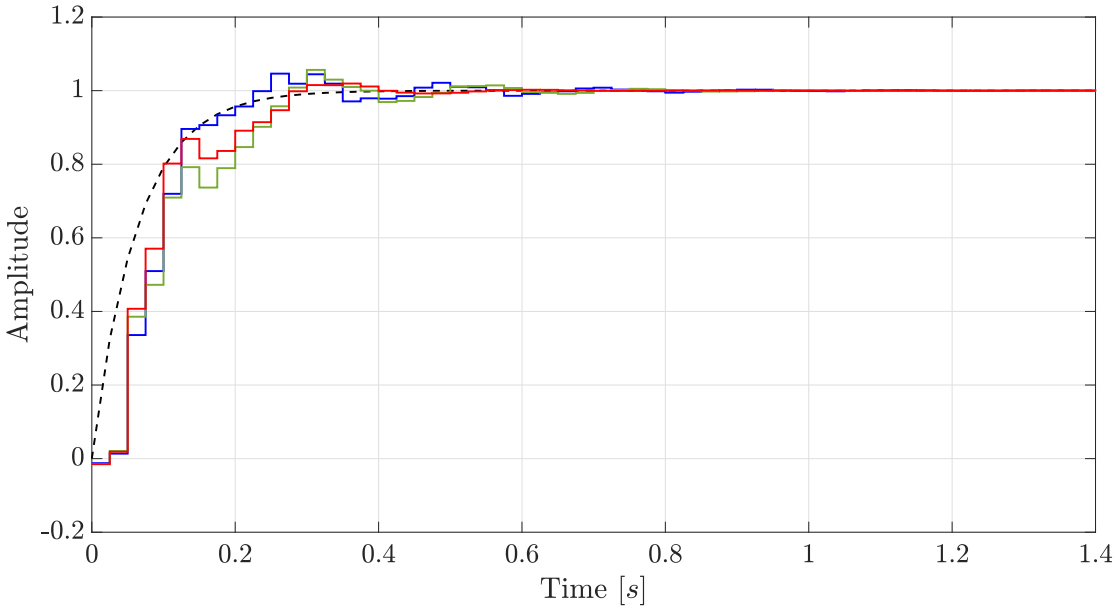

Figure 7.2 – Closed-loop step response for the nominal plant model with $\mathscr{H}_1$ performance (blue-line), $\mathscr{H}_2$ performance (green-line), and $\mathscr{H}_\infty$ performance (red-line). The dashed-black line is the desired response.

7.5 Case Study: Power Converter Control

The system considered in this case study is the power converter control system investigated in the case study of Chapter 4. Fig. 4.8 shows the structure of the control system. For this application, the same CANCUN converter is used to drive the load (which is shown in Fig. 4.10); however, for this application, the load and the reference profile are different (where a much larger closed-loop bandwidth is required to properly track the desired reference profile). The details with regards to the desired specifications are discussed in subsequent sections.

7.5.1 Controller Design

For this application, the following requirements must be satisfied:

- Achieve optimal tracking performance (i.e., minimize $\|\mathscr{S}_2(\boldsymbol{\rho}) - \mathscr{S}_2^d\|_p$) and obtain the desired error requirements (in parts-per-million (ppm)) for a specific reference profile (shown in Fig. 7.3).
- Obtain a modulus margin of at least 0.5.
- Ensure that the controller $[S'(\boldsymbol{\rho})]^{-1}$ is stable (which is a requirement set within the proprietary software of the CERN controller [141, 117]), where $S(\boldsymbol{\rho}) = (1-z^{-1})^{n_I} S'(\boldsymbol{\rho})$ and $S'(\boldsymbol{\rho})$ is the polynomial given in (2.28) (which signifies that $n_I \in [1,2,\ldots,\infty[$ pure integrators are allowed in the design).

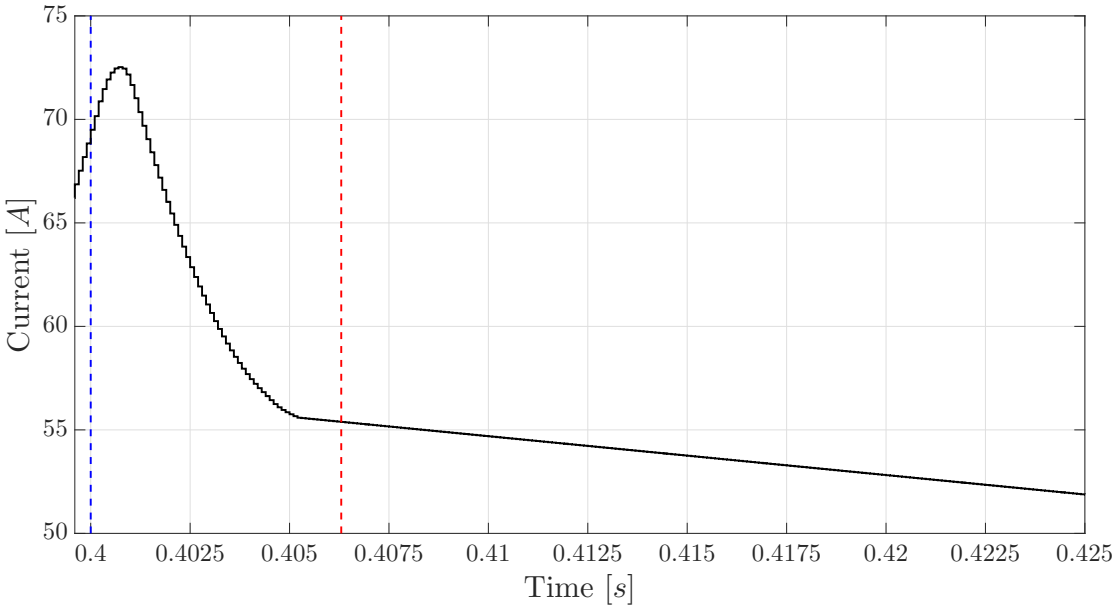

Figure 7.3 – The desired reference current i_R. The error between the blue-dashed line and the red-dashed line must remain within ±1000 ppm; the error after the red-dashed line must remain within ±100 ppm.

Given these constraints, the following optimization problem can be considered:

$$\begin{aligned} \underset{\boldsymbol{\rho}}{\text{minimize}} \quad & \|\mathscr{S}_2(\boldsymbol{\rho}) - \mathscr{S}_2^d\|_p \\ \text{subject to:} \quad & \|m_d \mathscr{S}_1(\boldsymbol{\rho})\|_\infty < 1 \\ & \Re\{S'(\boldsymbol{\rho})\} > 0 \\ & \forall \omega \in \Omega. \end{aligned} \tag{7.31}$$

The first constraint in this problem ensures the desired modulus margin for $m_d = 0.5$ while the second constraint ensures the stability of $[S'(\boldsymbol{\rho})]^{-1}$. Note that this second constraint implies that all of the zeros of $S'(\boldsymbol{\rho})$ are in $|z| < 1$; therefore, the constraint in (7.25) is not needed to guarantee the closed-loop stability.

Desired Reference Model

The tracking signal and error requirements for this application are shown in Fig. 7.3. At CERN, the error is calculated with respect to a delayed reference input (i.e., $e(t) = r(t - \tau_s) - y(t)$); τ_s can be determined by shifting the reference signal such that the minimum peak error is achieved. The calculation for obtaining the error in ppm is performed by taking the raw data for the error $e(t)$ and scaling it by a factor of $10^6/100$. The factor of 100 represents the nominal current (100 A) of the power converter for this application.

It is known that the open-loop process contains a fractional delay that lies in the interval

[200,400] μs; this delay comes from the filtering elements within the FGC along with the communication delay inherent in the system. This application requires a very large closed-loop bandwidth and this delay can inhibit the desired performance (since it is known that a delay limits the achievable closed-loop bandwidth [142]). Therefore, $\mathscr{S}_2^d$ should be selected such that the effect of the open-loop delay is compensated for and the desired bandwidth can be obtained. One such transfer function which can accomplish this requirement is as follows:

$$\mathscr{S}_2^d(s) = \frac{\omega_d^2}{s^2 + 2\zeta\omega_d s + \omega_d^2} e^{-sT_d}, \tag{7.32}$$

where ζ is the damping factor, T_d [s] is the desired shift of the reference profile, and

$$\omega_d = 2\pi f_d \left[1 - 2\zeta^2 + \sqrt{2 - 4\zeta^2 + 4\zeta^4}\right]^{-0.5},$$

where f_d [Hz] is the desired closed-loop bandwidth. As a worst case consideration, the delay shift can be selected as $T_d = 400\,\mu s$. Thus with respect to tracking, the delay shift T_d allows the effect of the open-loop delay to be nullified so that the bandwidth and damping requirements can be satisfied.

A simulation was performed to determine the bandwidth that was required in order to satisfy the desired error specifications. By assuming that the closed-loop response behaves as $\mathscr{S}_2^d$, the bandwidth and damping factor can be selected such that the error between the delayed reference input and output remains within the requirements set by the application (which are shown in Fig. 7.3); it was determined that $f_d = 2000\,\text{Hz}$ with $\zeta = 0.8$ satisfies these requirements.

Synthesis and Experimental Results

A PRBS signal was used as the input voltage reference of the open-loop system in order to capture the dynamics of the process. A total of 10 experiments were performed with the PRBS clock period $T_{cl} = 100\,\mu s$ (which is equal to the sampling time of the control loop); the acquired periods (with transients removed in post-processing) could then be merged together. A custom FGC signal is limited to 1023 data points; therefore, a 9-bit PRBS signal was used for identification purposes (which corresponds to a period with a length of 511 samples). For a signal of length 511, the frequency resolution is limited to 255 points. Fig. 7.4 shows the input and output signals acquired from the identification experiment. The FRF of the process was then obtained as $G(e^{-j\omega}) = \mathscr{F}\{i(t)\}/\mathscr{F}\{v(t)\}$.

For comparative purposes, it was desired to compare the controller obtained from a model-based design methodology (such as the `SYSTUNE` toolbox from the `MATLAB` environment) with the proposed methods. This method uses a non-smooth optimization algorithm to tune fixed-structure control systems in order to achieve a desired model-reference objective (in the $\mathscr{H}_2$ sense). This method requires a model to synthesize a controller; therefore, a 4^{th} order model was identified with `MATLAB` by using the PRBS input and output data. The following

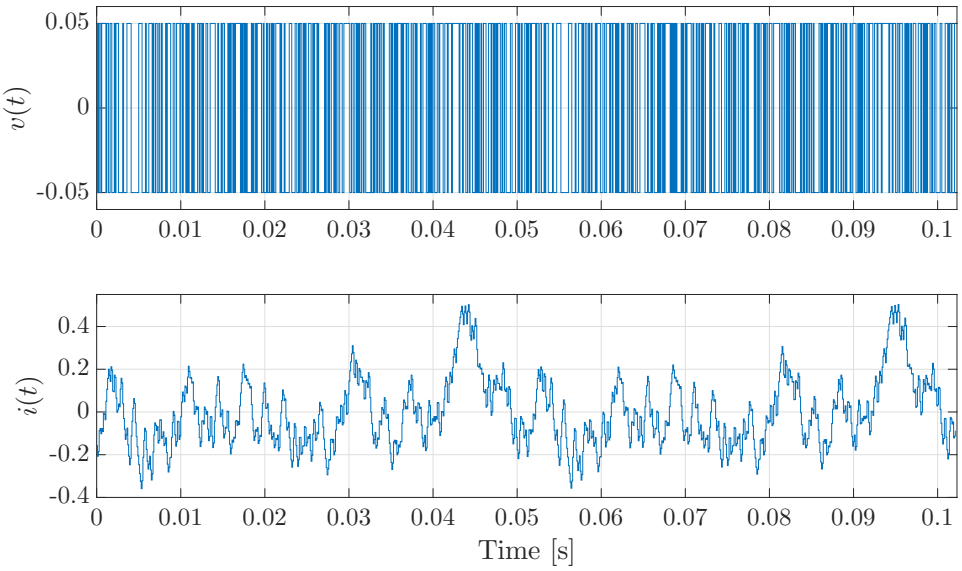

Figure 7.4 – PRBS signal used for the input voltage $v(t)$ of the open-loop system along with the resulting output current $i(t)$.

non-minimum phase model with delay was obtained through the identification experiment (using the ARX method):

$$G_m(z^{-1}) = \frac{0.7319(1+1.196z^{-1})z^{-4}}{(1-0.948z^{-1})(1+0.295z^{-1})(1-0.073z^{-1}+0.273z^{-2})}$$

The calculated model fit percentage was given as 93.5% (which was the value provided by `MATLAB`). Note that when the superposed noise is not white, the coupling between the deterministic and stochastic dynamics can bias the estimation of the ARX model [143]. Thus it is of interest to compare the proposed data-driven method with a biased model in order to determine how the modeling errors impact the stability and performance of the closed-loop system.

Remark. *Note that `SYSTUNE` cannot impose constraints to ensure controller stability and modulus margin (of the closed loop system). However, constraints for the gain and phase margins can be imposed. A modulus margin of* 0.5 *implies that the gain margin is at least* 6 dB *and that the phase margin is at least* 29 °*; these values were therefore used to ensure the stability margins. However, to obtain the controller stability, different optimization iterations were performed until this specification was obtained (since the method used by this toolbox produces different results for different iterations).*

For this case study, it was desired to have integral action for the final controller. Therefore, since the plant is stable, a simple selection for the initial stabilizing controller is $R(z^{-1},\boldsymbol{\rho}_0) = 10^{-3}$ and $S(z^{-1},\boldsymbol{\rho}_0) = 1-z^{-1}$ (which was confirmed to stabilize the closed-loop system in an experiment). Therefore, these values were used to initialize the proposed optimization

methods (i.e., $\psi_0 = 10^{-3}G + (1 - z^{-1})$). All of the proposed optimization methods were solved in SDP form (for all of the $\eta = 255$ frequency points obtained from the PRBS identification experiment). For comparison purposes, the same order controller was used for all design methods (i.e., a 5^{th} order polynomial for $R(\boldsymbol{\rho})$ and $S(\boldsymbol{\rho})$ and a 10^{th} order polynomial for $T(\boldsymbol{\rho})$).

- The following optimization problem was considered for minimizing the $\mathscr{H}_\infty$ model-reference objective:

$$
\begin{aligned}
\underset{\boldsymbol{\rho},\gamma}{\text{minimize}} \quad & \gamma \\
\text{subject to:} \quad & \begin{bmatrix} \psi^*(\boldsymbol{\rho})\psi_0 + \psi_0^*\psi(\boldsymbol{\rho}) - \psi_0^*\psi_0 & \left(\Delta_2(\boldsymbol{\rho}) - \psi(\boldsymbol{\rho})\mathscr{S}_2^d\right)^* \\ \Delta_2(\boldsymbol{\rho}) - \psi(\boldsymbol{\rho})\mathscr{S}_2^d & \gamma \end{bmatrix} \succ 0 \\
& \begin{bmatrix} \psi^*(\boldsymbol{\rho})\psi_0 + \psi_0^*\psi(\boldsymbol{\rho}) - \psi_0^*\psi_0 & \left(m_d S(\boldsymbol{\rho})\right)^* \\ m_d S(\boldsymbol{\rho}) & 1 \end{bmatrix} \succ 0 \\
& \Re\left\{S'(\boldsymbol{\rho})\right\} > 0 \\
& \forall \omega \in \Omega_\eta.
\end{aligned}
\tag{7.33}
$$

  A similar problem can be formulated for the $\mathscr{H}_2$ problem (as discussed in Section 7.2.3). The $\mathscr{H}_2$ and $\mathscr{H}_\infty$ model-reference problems were solved with $\gamma_{tol} = 10^{-4}$.

- In solving the $\mathscr{H}_1$ model-reference problem, the modulus margin constraint (along with the controller stability constraint) was first satisfied by obtaining a feasible solution to the condition in (7.15). The optimization problem in (7.16) was then solved to obtain $T(\boldsymbol{\rho}_2)$.

Fig. 7.5 shows the error obtained by comparing the proposed design approaches with the approach implemented by `SYSTUNE`. The dashed-black horizontal lines in the plot indicates the bounds set by the application. It can be observed that the controller from `SYSTUNE` violates all of the error requirements. With the proposed approaches, the $\mathscr{H}_1$ and $\mathscr{H}_\infty$ designs satisfy all of the requirements, while with $\mathscr{H}_2$ design violates the 100ppm error specification. Fig. 7.6 shows the magnitude of the closed-loop responses for all design approaches; it can be observed that the `SYSTUNE` controller is not adhering to the desired bandwidth requirements. Thus the modeling process and the type of model used for a real system can significantly impact the desired specifications (due to the inherent modeling errors).

Table 7.4 shows the values of the performance criteria for each design method. The values of $\mathscr{J}_p^\star$ for `SYSTUNE` were obtained by formulating $\mathscr{S}_2$ with the `SYSTUNE` controller and $G(e^{-j\omega})$ obtained from the PRBS experiment (which represents the FRF of the true process). From this table, it can be observed that the proposed controller design methods produce the best performance.

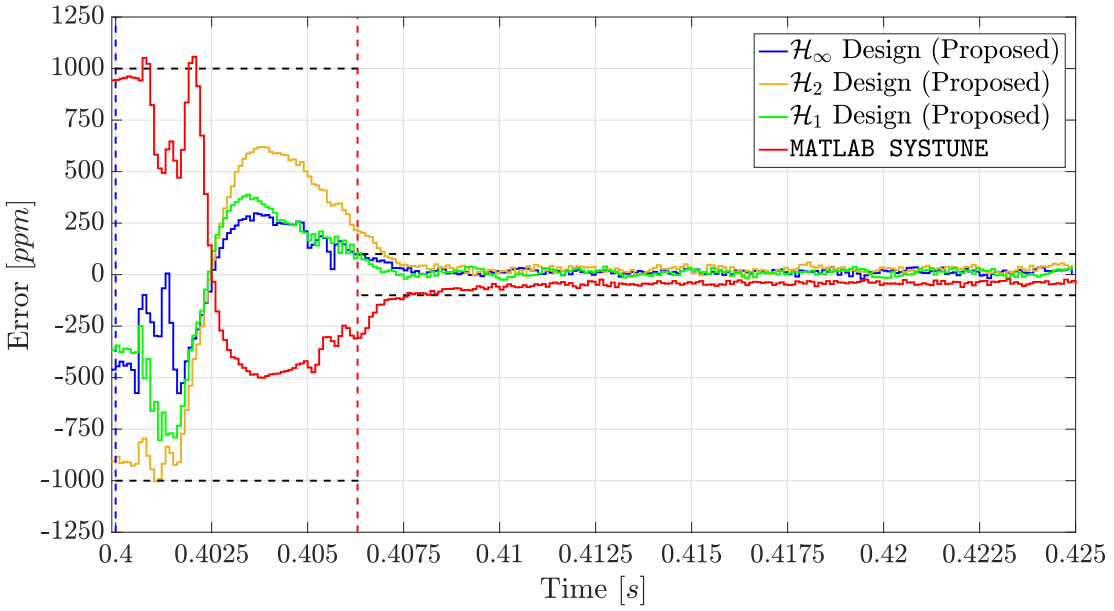

Figure 7.5 – Errors obtained using the proposed designs (blue, green and orange lines); error obtained using the SYSTUNE controller (red line).

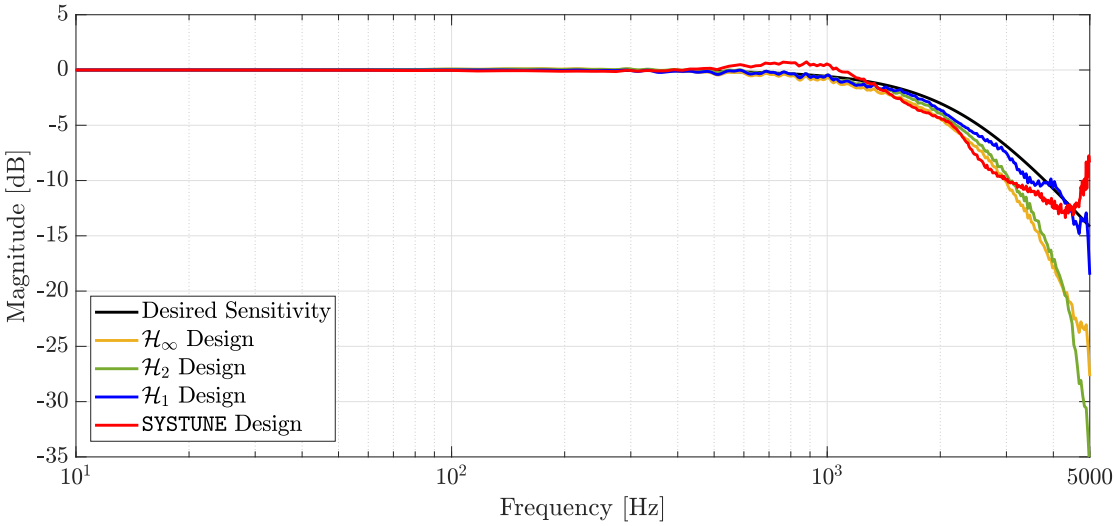

Figure 7.6 – $|\mathcal{S}_2|$ for all of the design methods discussed in this work.

Table 7.4 – Performance values for all methods

Criteria	$\mathscr{H}_1$	$\mathscr{H}_2$	$\mathscr{H}_\infty$	SYSTUNE
$\mathscr{J}_1^\star$	**0.1180**	0.1183	0.1392	0.1398
$\mathscr{J}_2^\star$	0.1413	**0.1383**	0.1467	0.1682
$\mathscr{J}_\infty^\star$	0.2905	0.2446	**0.1774**	0.5804

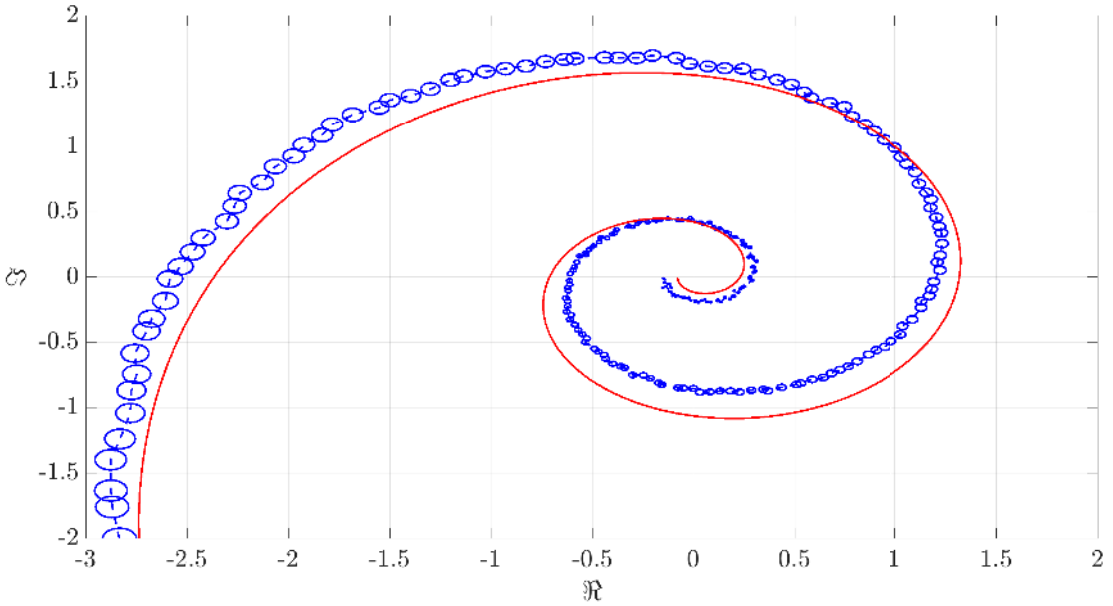

Figure 7.7 – $G(e^{-j\omega})$ (dashed-blue line) with the frequency-dependent uncertainty disks (blue circles) and $G_m(e^{-j\omega})$ (solid-red line).

Fig. 7.7 shows the comparison between the Nyquist plot of the process obtained via the PRBS and the Nyquist plot obtained from the model. The disks in this plot represent the uncertainty of the measurement process (which is assumed to be additive uncertainty, and can be obtained from the covariance of the estimates, as described Chapter 3). The uncertainty was determined for a 95% confidence interval; from Fig. 7.7, it can be observed that the FRF of the model is not coherent with the dynamics of the true process (since $G_m(e^{-j\omega})$ does not lie in the uncertain set of $G(e^{-j\omega})$). Thus with the model-based controller design, it is clear that the performance degradation comes from the modeling error. In other words, the performance degradation does not necessarily come from the controller design methodology of `SYSTUNE`, but rather from the unmodeled dynamics of the identified model. The proposed data-driven scheme, however, allows a controller design for the true process, and avoids the problem of unmodeled dynamics (where the acquired performance was confirmed through the experiments shown in Fig. 7.5).

7.6 Conclusion

A new data-driven method for computing a 2DOF fixed-structure controller that attains $\mathscr{H}_p$ performance (for $p \in \{1, 2, \infty\}$) has been presented. A frequency-domain approach has been used in order to avoid the problem of unmodeled dynamics associated with parametric models. In minimizing the $\mathscr{H}_2$ and $\mathscr{H}_\infty$ model-reference objectives, a non-convex model-reference constraint was convexified by linearizing the non-convex function around a stabilizing controller. This linearization process allowed the use of the Shur Complement Lemma to con-

struct an LMI and solve a convex optimization problem to obtain a local solution for the true fixed-structure $\mathscr{H}_p$ problem. In minimizing the $\mathscr{H}_1$ model-reference objective, the controller was optimized in two separate steps; in the first step, a design was implemented to ensure closed-loop stability and sufficient robustness margins. In the second step, an unconstrained model-reference objective was considered to achieve the desired performance. These methods have been applied in several case studies; with respect to the power converter control system at CERN, it has been shown that a data-driven approach was necessary for attaining the required performance of the application. In other words, the experiments have confirmed that the data-driven approach significantly reduces the conservativeness associated with the modeling process.

8 Conclusion and Future Outlook

8.1 Conclusion

This dissertation has presented a data-driven approach for computing robust controllers by only considering the frequency-domain data of a process. By parameterizing a controller as a ratio of two LP transfer functions, a convex optimization problem was formulated where the optimal solution of the problem converged to the global solution of the true $\mathscr{H}_\infty$ problem as the controller order increased. The necessary and sufficient conditions for the existence of robust controllers that guarantee bounded infinity norm on the sensitivity functions were developed. However, in typical engineering problems, it is of interest to shape multiple sensitivity functions simultaneously in order to achieve multiple desired specifications. Thus necessary and sufficient conditions for obtaining $\mathscr{H}_\infty$ performance and closed-loop stability have also been devised in the case when multiple sensitivity functions are considered in a design. This proposed method was used to design robust controllers for processes that contain frequency dependent uncertainties. This includes uncertainties that originate from a noise source or from a nonlinearity; in the case where a nonlinearity was present in the plant model, the methods in [99] were used to obtain a BLA with an associated frequency dependent uncertainty. A convex problem was then formulated to ensure the stability and performance for the underlying linear system of the nonlinear model. The main advantages of the proposed method(s) are as follows:

- No linearization around a given desired open-loop transfer function is performed and the convex constraints are necessary and sufficient for obtaining $\mathscr{H}_\infty$ performance.
- Since the controller is not LP (in contrast to most works where LP controllers are used to convexify an optimization problem), the denominator of a controller is optimized.
- The convergence of the method to the global optimal solution is proved.
- No initialization of a controller is needed for a design.

- Since the proposed design schemes depend only on the frequency-domain data, discrete-time controllers can be designed for continuous-time systems (and vice versa).

By using the necessary and sufficient conditions proposed for linear systems, a similar condition was derived for stabilizing linear systems that were subject to sector-bounded time-varying nonlinearities. Thanks to the Circle criterion, convex feasibility conditions were derived in a data-driven setting. The results for stabilizing this class of nonlinear systems were developed in a deterministic sense where no approximations or linearization techniques were implemented to achieve the desired specifications. Moreover, a sufficient condition was developed to achieve both stability and $\mathscr{H}_\infty$ performance for sector-bounded (time-invariant) nonlinear systems represented by describing functions (where performance was guaranteed for the fundamental component of the nonlinearity, since describing functions characterize nonlinear systems based on the fundamental frequency component of a sinusoidal signal).

The controllers for these design schemes were parameterized by a ratio of two LP transfer functions. These transfer functions used a set of orthogonal basis functions (i.e., Laguerre basis functions) which required the selection of a free parameter *a-priori*. Thus for low-order controllers, this method led to optimal solutions far from the true optimal solution of the $\mathscr{H}_\infty$ problem. Moreover, by convexifying the $\mathscr{H}_\infty$ problem, the global optimal solution to an approximate problem is obtained. Therefore, a non-convex problem was formulated to obtain the local solution of the $\mathscr{H}_\infty$ problem for fixed-structure low-order controllers. Several non-convex problems were proposed in which the local solution was obtained; in the BP problem, the solution was obtained by solving a set of convex optimization problems (with increasing orders of the function F) until convergence to a solution was obtained. For the general non-convex problems, a PSO algorithm was proposed to find the local solution. A major advantage of PSO is that the algorithm can be applied to problems of large dimensions, and often produces quality solutions more rapidly than alternative methods. It was shown that for low-order controllers (i.e., PID controllers), the PSO algorithm produces the best optimal solution (in a data-driven sense) in a short amount of time; however, for larger order controllers, the PSO algorithm requires more time to obtain a good solution. With the convex optimization algorithm, a reasonable solution (with respect to the optimal values of the non-convex problems) was obtained in a relatively short time. Thus there exists a trade off between the quality of the optimal solution and the optimization time for larger order controllers.

In addition to the large optimization time of the PSO algorithm, the choice of the free parameters within this algorithm were not trivial for large order controllers. Therefore, since convex problems are computationally tractable, it was desired to develop a convex optimization problem which can obtain the local solution to the $\mathscr{H}_\infty$ problem for fixed-structure controllers. A model-reference convex problem for obtaining this local solution was devised using a 2DOF controller where an initializing (stabilizing) controller was required to ensure the performance and stability of the closed-loop system. However, in addition to ensuring $\mathscr{H}_\infty$ performance, other problems were devised for ensuring $\mathscr{H}_1$ and $\mathscr{H}_2$ performance. Developing optimization problems with these other minimization criteria is important because minimizing different

norms in the frequency-domain is interpreted differently in the time-domain. The $\mathscr{H}_2$ and $\mathscr{H}_\infty$ criteria were convexified by linearizing a non-convex constraint around an initial operating point. Through an iterative process, the local optimal solution (for fixed-structure controllers) could then be obtained. The $\mathscr{H}_1$ problem was solved in a 2-step manner where, in the first step, a design was implemented to ensure closed-loop stability and sufficient robustness margins. In the second step, an unconstrained model-reference objective was considered to achieve the desired performance.

With all of the methods presented in this dissertation, it is evident what the advantages and disadvantages of each method are. With the method in which the plant is represented as a fraction of coprime factors, no initializing controller is needed for a design. Additionally, the global solution of the true $\mathscr{H}_\infty$ problem is achieved as the controller order increases. However, for low-order controllers, the optimal solution using this method may be far from the true optimal solution of the $\mathscr{H}_\infty$ problem (since the global optimal solution to an approximate (convex) problem is obtained). Thus for low-order controllers, another convex problem with fixed-structure controllers can be considered (which linearizes the $\mathscr{H}_\infty$ constraints); however, this method requires an initial stabilizing controller. Moreover, additional constraints on the controller are needed to guarantee the stability of the closed-loop system. Therefore, one must consider the constraints of the application before selecting a method for designing an appropriate controller.

8.1.1 Future Outlook

Extension to MIMO Systems

The results obtained from the proposed methods in chapters 3 to 5 are quite significant. The fact that convergence to the global optimal solution of the true $\mathscr{H}_\infty$ problem is achieved by increasing the controller order (using a convex formulation) is a remarkable result. Thus an important extension of this method would be to MIMO systems.

Frequency Gridding

All of the methods in this dissertation use frequency-domain data for controller synthesis and analysis. From a theoretical standpoint, the derived Theorems and Lemmas in this work hold for all real frequencies. However, from a practical standpoint, the optimization problems are solved in SDP form (i.e., for a finite number of frequencies). Thus the performance and stability for a given real system is guaranteed in a stochastic sense. This dissertation has considered some methods in which the performance and stability can be attained within a given probability level. However, this method may not be adequate for processes with many resonant modes. It is known that within a very small frequency range, the magnitude and phase at these resonant modes vary drastically. Since the proposed data-driven method uses frequency response data for controller synthesis, these modes should be properly captured

for an appropriate design. Thus a natural extension of the proposed method(s) is to adopt a frequency-domain method which guarantees the performance and stability of a closed-loop system given a finite amount of frequency-domain data.

Optimal Basis Functions

It has been observed that the proposed design schemes implement controllers with basis functions that contain a free design parameter (i.e., the Laguerre parameters ξ, ξ_z). In Chapter 3, it was shown that the effect of this parameter is reduced when the controller order increases (and that the effect can be significant for low-order controllers). Thus by developing a method which optimizes this parameter, the performance for low-order controller designs can be improved. In Chapter 6, this parameter was optimized by solving a non-convex problem, and it was shown that the results can be improved when this parameter is optimized. However, for larger order controllers, optimization of this parameter becomes more problematic (as the quality of the local solution is dependent on the free parameters of the nonlinear solver). Thus is it desired to develop a technique which optimizes this parameter using convex optimization algorithms.

Data-Driven Scheme with Nonsmooth Approach

The nonsmooth optimization technique implemented by `hinfstruct` in MATLAB's Robust Control Toolbox has been shown to be a very fast and effective approach for computing fixed-structure controllers with $\mathscr{H}_\infty$ performance. However, this method cannot synthesize controllers for systems with delay (where a Padé approximation is needed to implement the tool). Moreover, the tool cannot design controllers with a set of time-domain or frequency-domain data. Due to the efficient nonsmooth optimization technique implemented by this tool, it would be reasonable to consider this method in a data-driven setting and synthesize controllers with a set of data without the need to specify a model.

A H_∞ Smith Predictor Design for Time-Delayed MIMO Systems via Convex Optimization

A.1 Introduction

Many dynamical systems in the industry possess unavoidable time delays. These delays can be caused by accumulation of time lags for dynamic systems interconnected in series, transportation delay or measurement delay [144]. Time delays in control loops can cause significant complications in modern industrial applications. The rapid development in data and communication network technologies has caused a need for real-time data processing [145]. The first time-delay compensation method was proposed in the late 1950s by [146]. This method is known as the Smith Predictor (SP), and it has become one of the most widely implemented control schemes used to regulate industrial systems with time delays.

The SP, however, is somewhat limited in its performance, since an accurate model of the system is generally required for satisfactory operation. In certain circumstances, small modeling errors may lead to undesirable performance, where the system can become unstable. For this reason, research efforts have been focused on robustness issues of the SP.

Many researchers are interested in the optimal control of dead-time systems, especially H_∞ control, i.e., to find a controller to internally stabilize the system and to minimize the H_∞-norm of an associated transfer function. Many relevant results have been presented in this framework using modified versions of the SP. See, for instance, [147], [148] and [149]. Recently, the single-input-single-output (SISO) SP has been extended and generalized for multiple-input-multiple-output (MIMO) systems. In [150], a structured uncertainty approach was implemented for SP's with diagonal delay matrices. This method, however, does not consider general and distinct time delays for each element of the plant transfer matrix. A diagonal H_2 optimal controller for non-square plants is designed by factorization methods in [151]. In [152], a generalized predictive control (GPC) method is implemented on MIMO SP systems with multiple delays. These control techniques, although efficient, are quite complex from both the design and implementation perspective.

There are a wide variety of industrial applications that involve MIMO processes with time

delays, and it is of practical interest to develop robust control techniques for such systems. The proposed control scheme is based on the ideas presented in [153] for SP design of SISO systems and in [59] for designing decoupling MIMO controllers. However, in this paper, the SP design method for computing H_∞ controllers for SISO models is extended to MIMO SP's with process plants that possess uncertain time delays. A convex optimization approach is implemented to design a linearly parameterized primary controller in a SP structure for a MIMO system with uncertain time delays.

This paper is organized as follows: In Section (A.2), the class of models, controllers and control objectives are defined. Section (A.3) will discuss the control design methodology and stability conditions of the proposed method for the MIMO Smith predictor. This methodology is based on the convex constraints in the Nyquist diagram. Section (A.4) will demonstrate the effectiveness of the proposed method by considering several case studies from industrial processes. Finally the concluding remarks are given in Section (A.5).

A.2 Problem Formulation

In this section, the SP for MIMO systems with generalized time delays is investigated. For notation purposes, bold face characters will represent transfer function matrices.

A.2.1 Class of models

Let n_o and n_i represent the number of outputs and the number of inputs of a system, respectively. The set of LTI-MIMO stable strictly proper models with multiplicative uncertainty and uncertain time delays can be defined as follows:

$$\mathscr{P} = \{\mathbf{P}_c(s)[\mathbf{I} + \Delta_c(s)\mathbf{W}_{2_c}(s)]; \quad c = 1,\ldots,m\}, \tag{A.1}$$

where each element in $\mathbf{P}_c(s)$ possesses a time delay that can vary over a range of specified values, and $\mathbf{W}_{2_c}$ is a transfer function matrix that represents the multiplicative input uncertainty of the system. $\Delta_c(s)$ represents the unknown stable transfer function matrix satisfying $\|\Delta_c\|_\infty < 1$. For simplicity, one model from the set $\mathscr{P}$ will be investigated, and the subscript c will be omitted. The uncertain $n_o \times n_i$ time delayed plant has the following form:

$$\mathbf{P}(s) = \begin{bmatrix} G_{11}(s)e^{-\tau_{11}s} & \cdots & G_{1n_i}(s)e^{-\tau_{1n_i}s} \\ \vdots & \ddots & \vdots \\ G_{n_o1}(s)e^{-\tau_{n_o1}s} & \cdots & G_{n_on_i}(s)e^{-\tau_{n_on_i}s} \end{bmatrix}, \tag{A.2}$$

where $G_{qp}(s)$ is a strictly proper delay-free transfer function, and τ_{qp} is the uncertain time-delay of the process for $p = 1,\ldots,n_i$ and $q = 1,\ldots,n_o$. Note that τ_{qp} is a set that is composed of elements τ_{qp_i} for $i = 1,\ldots,l$ and belongs in the domain $\{\tau_{qp} \in \mathbb{R} : \tau_{qp_i} > 0 \ \forall \ \{p,q,i\}\}$.

A.2.2 Class of controllers

As stated in [59], an $n_i \times n_o$ matrix can be formed to represent the controller $\mathbf{C}(s,\boldsymbol{\rho})$. The elements of $\mathbf{C}(s,\boldsymbol{\rho})$ will possess linearly parameterized elements

$$C_{pq}(s,\boldsymbol{\rho}) = \boldsymbol{\rho}_{pq}^T \phi_{pq}(s), \tag{A.3}$$

where $\boldsymbol{\rho}_{pq}^T$ is a vector of parameters, and $\phi_{pq}(s)$ is a vector of stable transfer functions chosen from a set of orthogonal basis functions. The non-diagonal elements of $\mathbf{C}(s,\boldsymbol{\rho})$ strive to decouple the system, while the diagonal elements aim to control the single-loop subsystems. The main purpose of parameterizing the controller in this manner is due to the fact that the components of the open loop transfer function can be written as a linear function of the control parameters $\boldsymbol{\rho}$,

$$\boldsymbol{\rho} = [\rho_{11},\ldots,\rho_{1_{n_i}},\ldots,\rho_{n_o 1},\ldots,\rho_{n_o n_i}]. \tag{A.4}$$

A.2.3 Design specifications

Fig. A.1 displays the SP for the MIMO case, where $\mathbf{G}_n(s)$ is an $n_o \times n_i$ nominal delay-free transfer function matrix with elements $G_{qp}(s)$, and $\mathbf{P}_n(s)$ is an $n_o \times n_i$ nominal transfer function matrix that includes the nominal values of the time delays, which is comprised of elements $G_{qp}(s)e^{-\zeta_{qp}s}$ (where ζ_{qp} represents the qp-th nominal time delay). Both $\mathbf{Y}(s)$ and $\mathbf{R}(s)$ are $n_o \times 1$ column vectors that possess elements $y_q(s)$ and $r_q(s)$, respectively. The transfer function from the inputs of $\mathbf{C}(s)$ to $\mathbf{Y}_p(s)$ will represent the open-loop transfer function,

$$\mathbf{L}(s) = [\mathbf{P}(s) + \mathbf{H}(s)]\mathbf{C}(s), \tag{A.5}$$

where $\mathbf{H}(s) = \mathbf{G}_n(s) - \mathbf{P}_n(s)$. Notice that if $\mathbf{P}(s) = \mathbf{P}_n(s)$, then $\mathbf{L}(s) = \mathbf{G}_n(s)\mathbf{C}(s)$. Since the class of controllers to be designed for this system are linearly parameterized, the elements of the controller $\mathbf{C}(s)$ will actually be a linear function of the controller parameters $\boldsymbol{\rho}$. Therefore, $\mathbf{C}(s)$ will be represented as $\mathbf{C}(s,\boldsymbol{\rho})$ with elements $C_{pq}(s,\boldsymbol{\rho})$, as asserted in (A.3).

The transfer function from the output disturbance $\mathbf{D}(s)$ to $\mathbf{Y}(s)$ is the output sensitivity function $\mathbf{S}(s,\boldsymbol{\rho})$, while the transfer function from $\mathbf{R}(s)$ to $\mathbf{Y}(s)$ is the complementary sensitivity function $\mathbf{T}(s,\boldsymbol{\rho})$:

$$\begin{aligned} \mathbf{S}(s,\boldsymbol{\rho}) &= [\mathbf{I} + \mathbf{H}(s)\mathbf{C}(s,\boldsymbol{\rho})]\mathbf{Z}^{-1}(s,\boldsymbol{\rho}) \\ \mathbf{T}(s,\boldsymbol{\rho}) &= \mathbf{P}(s)\mathbf{C}(s,\boldsymbol{\rho})\mathbf{Z}^{-1}(s,\boldsymbol{\rho}), \end{aligned} \tag{A.6}$$

where $\mathbf{Z}(s,\boldsymbol{\rho}) = [\mathbf{I} + \mathbf{L}(s,\boldsymbol{\rho})]$. The objective is to determine the controller $\mathbf{C}(s,\boldsymbol{\rho})$ that will guarantee the robust performance and robust stability of the closed-loop SP system.

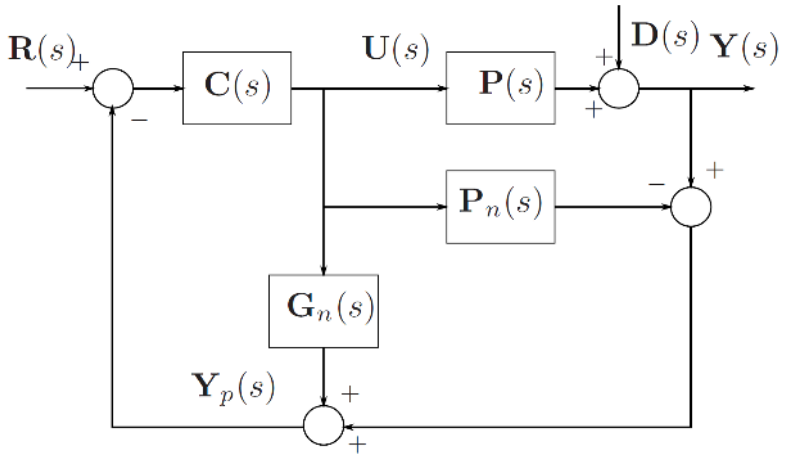

Figure A.1 – MIMO representation of the Smith Predictor

A.3 Proposed method

It is well known that if a SISO model is described by unstructured multiplicative uncertainty, and possesses both robustness and performance weighing functions W_1 and W_2, then the necessary and sufficient condition for robust performance is given by [96]:

$$\left\| |W_1 S(\boldsymbol{\rho})| + |W_2 T(\boldsymbol{\rho})| \right\|_\infty < 1, \tag{A.7}$$

where S and T are the sensitivity and complementary sensitivity functions of a SISO system, respectively.

For the moment, assume the case when a closed-loop MIMO system is fully decoupled. Then the MIMO sensitivity and complementary sensitivity functions can essentially be treated as functions containing independent SISO subsystems. Thus it is judicious to define $\mathbf{W}_1(s)$ as a diagonal filter with diagonal elements W_{1_q} and a diagonal filter $\mathbf{W}_2(s)$ with diagonal elements W_{2_q} representing, respectively, the nominal performance and multiplicative uncertainty for the SISO subsystems. This rationalization leads to the following theorem:

Theorem A.1. *Let $M_{qq}(j\omega,\boldsymbol{\rho})$ represent the diagonal elements of $\mathbf{H}(j\omega)\mathbf{C}(j\omega,\boldsymbol{\rho})$ and $N_{qq}(j\omega,\boldsymbol{\rho})$ represent the diagonal elements of $\mathbf{P}(j\omega)\mathbf{C}(j\omega,\boldsymbol{\rho})$. Suppose that $\mathbf{S}(s,\boldsymbol{\rho})$ and $\mathbf{T}(s,\boldsymbol{\rho})$ in (A.6) are diagonal transfer function matrices (the closed-loop system is fully decoupled). Then the linearly parameterized controller in (A.3) will guarantee the closed-loop stability of the system and satisfy the following robust performance criterion:*

$$\left\| |W_{1_q}(j\omega) S_{qq}(j\omega,\boldsymbol{\rho})| + |W_{2_q}(j\omega) T_{qq}(j\omega,\boldsymbol{\rho})| \right\|_\infty < 1 \quad \text{for } q = 1,\ldots,n_o \tag{A.8}$$

if

$$\left\{|W_{1_q}(j\omega)[1+M_{qq}(j\omega,\boldsymbol{\rho})]|+|W_{2_q}(j\omega)N_{qq}(j\omega,\boldsymbol{\rho})|\right\}\left|1+L_{D_q}(j\omega)\right|-\Psi_q(j\omega,\boldsymbol{\rho})<0 \quad \forall\omega \text{ for } q=1,\ldots,n_o, \tag{A.9}$$

where

$$\Psi_q(j\omega,\boldsymbol{\rho})=\Re\left\{\left[1+L^*_{D_q}(j\omega)\right]\left[1+L_{qq}(j\omega,\boldsymbol{\rho})\right]\right\}$$

and S_{qq} and T_{qq} are the q-th diagonal elements of $\mathbf{S}(s,\boldsymbol{\rho})$ and $\mathbf{T}(s,\boldsymbol{\rho})$, respectively. $L_{D_q}(s)$ is the q-th diagonal element of a diagonal transfer function matrix $\mathbf{L}_D(s)$ that contains strictly proper transfer functions which do not encircle the critical point, and $L^*_{D_q}$ is its complex conjugate.

Proof : If the closed-loop MIMO system is fully decoupled, then the MIMO sensitivity and complementary sensitivity functions can be considered as systems containing independent SISO systems. Since the real part of a complex number is less than or equal to its magnitude, we have

$$\Re\left\{\left[1+L^*_{D_q}(j\omega)\right]\left[1+L_{qq}(j\omega,\boldsymbol{\rho})\right]\right\}\leq\left|\left[1+L^*_D(j\omega)\right]\left[1+L_{qq}(j\omega,\boldsymbol{\rho})\right]\right|. \tag{A.10}$$

Then, by combining (A.10) and (A.9) (and noting that $|1+L_{D_q}|=|1+L^*_{D_q}|$), one obtains

$$\left|W_{1_q}\left[1+M_{qq}(j\omega,\boldsymbol{\rho})\right]\right|+\left|W_{2_q}N_{qq}(j\omega,\boldsymbol{\rho})\right|-\left|1+L_{qq}(j\omega,\boldsymbol{\rho})\right|<0 \quad \forall\omega, \quad \text{for } q=1,\ldots,n_o. \tag{A.11}$$

The above equation can be rearranged and expressed as follows:

$$\frac{\left|W_{1_q}\left[1+M_{qq}(j\omega,\boldsymbol{\rho})\right]\right|+\left|W_{2_q}N_{qq}(j\omega,\boldsymbol{\rho})\right|}{\left|1+L_{qq}(j\omega,\boldsymbol{\rho})\right|}<1 \quad \forall\omega \text{ for } q=1,\ldots,n_o. \tag{A.12}$$

Since M_{qq} and N_{qq} are the $q-th$ diagonal elements of $\mathbf{H}(s)\mathbf{C}(s,\boldsymbol{\rho})$ and $\mathbf{P}(s)\mathbf{C}(s,\boldsymbol{\rho})$ in (A.6), respectively, it can be seen that (A.12) leads directly to (A.8). ■

In order to fully decouple the MIMO system, a controller must be designed such that the off-diagonal elements of the open-loop transfer function matrix are equal to zero. The proposed method will be to define a diagonal open-loop transfer function matrix $\mathbf{L}_D(s)$, where the diagonal elements satisfy the desired performance for single loop systems. Therefore, by minimizing the objective function $\|\mathbf{L}(s,\boldsymbol{\rho})-\mathbf{L}_D(s)\|_2^2$, a controller can be designed to simultaneously minimize the magnitudes of the off-diagonal elements of $\mathbf{L}(s,\boldsymbol{\rho})$ and drive the diagonal elements to be approximately equal to $L_{D_q}(s)$.

However, the resulting controller will stabilize the closed-loop system only if it is fully de-

coupled. In practice, with a finite order controller, it is not always possible to make the off-diagonal elements of $\mathbf{L}(j\omega,\boldsymbol{\rho})$ equal to zero. In this case, the generalized Nyquist stability criterion should be used to guarantee the stability of the MIMO system. According to this theorem, the eigenvalues of the open-loop transfer function (A.5) should not encircle the critical point. However, these eigenvalues are non-convex functions of the linear control parameters, which complicates the design process. A possible solution to this problem is to implement the Gershgorin band theorem in order to approximate the eigenvalues of $\mathbf{L}(j\omega,\boldsymbol{\rho})$. The Gershgorin bands represent disks centered at the diagonal elements of a matrix that include the eigenvalues. For the open-loop transfer matrix $\mathbf{L}(j\omega,\boldsymbol{\rho})$, the radius of these disks are computed by:

$$r_q(\omega,\boldsymbol{\rho}) = \sum_{p=1,p\neq q}^{n_o} \left|L_{qp}(j\omega,\boldsymbol{\rho})\right|, \tag{A.13}$$

where $L_{qp}(j\omega,\boldsymbol{\rho})$ represents the qp-th element of $\mathbf{L}(j\omega,\boldsymbol{\rho})$. Note that $r_q(\omega,\boldsymbol{\rho})$ is convex with respect to the control parameter $\boldsymbol{\rho}$. The closed-loop stability of the MIMO system is guaranteed if these disks do not encircle the critical point. This precondition leads to the following theorem:

Theorem A.2. *Given the open loop transfer function matrix* $\mathbf{L}(j\omega,\boldsymbol{\rho})$*, the linearly parameterized controller (A.3) stabilizes the closed-loop system if*

$$\begin{aligned}\left|r_q(j\omega,\boldsymbol{\rho})[1+L_{D_q}(j\omega)]\right| - \Psi_q(\boldsymbol{\rho},\omega) < 0\\ \forall\omega, \quad \textit{for } q = 1,\ldots,n_o.\end{aligned} \tag{A.14}$$

Proof: By combining the constraint in (A.14) and (A.10) (and noting that $|1+L_{D_q}| = |1+L^*_{D_q}|$), one obtains

$$\begin{aligned}\left|r_q(j\omega,\boldsymbol{\rho})\right| < \left|1+L_{qq}(j\omega,\boldsymbol{\rho})\right|\\ \forall\omega \text{ for } q = 1,\ldots,n_o.\end{aligned} \tag{A.15}$$

The constraint in (A.15) guarantees that the disk with radius $r_q(j\omega,\boldsymbol{\rho})$ centered at $L_{qq}(j\omega,\boldsymbol{\rho})$ does not encircle the critical point $(-1+j0)$, and thus the system remains stable for all ω. ■

A.3.1 Primary controller design

In designing the controller $\mathbf{C}(s,\boldsymbol{\rho})$ for the MIMO SP, one must consider all of the possible combinations of the uncertain delay parameters τ_{qp}. Suppose that the cardinality of τ_{qp} is β_{qp}. Then the total number of possible combinations that must be considered in the design of the controller is given by the rule of product,

$$\begin{aligned}m &= \prod \beta_{qp}\\ \forall\ q &= 1,\ldots,n_o;\ p = 1,\ldots,n_i.\end{aligned} \tag{A.16}$$

If the number of uncertainties are equal for each τ_{qp} (i.e., $\beta_{qp} = \beta_{pq} = \beta \; \forall \; \{p,q\}$), then the total number of combinations will be $m = \beta^{n_o n_i}$. By combining the constraints presented in Theorems A.1 and A.2, one can define the following optimization problem for the multimodel system:

$$\begin{aligned}
\underset{\boldsymbol{\rho}}{\text{minimize}} \quad & \sum_{c=1}^{m}\sum_{k=1}^{N} \left\| \mathbf{L}_c(j\omega_k,\boldsymbol{\rho}) - \mathbf{L}_{D_c}(j\omega_k) \right\|_F \\
\text{subject to:} \quad & |r_{q_c}(j\omega_k,\boldsymbol{\rho})[1+L_{D_{qc}}(j\omega_k)]| - \Psi_{q_c}(j\omega_k,\boldsymbol{\rho}) < 0 \\
& \left\{ \left| W_{1_{q_c}}(j\omega_k)\left[1+M_{qq_c}(j\omega_k,\boldsymbol{\rho})\right] \right| + \left| W_{2_{q_c}}(j\omega_k) N_{qq_c}(j\omega_k,\boldsymbol{\rho}) \right| \right\} \left| 1+L_{D_{q_c}}(j\omega_k) \right| \\
& \qquad - \Psi_{q_c}(j\omega_k,\boldsymbol{\rho}) < 0 \\
& \text{for } k = 1,\ldots,N; \quad ; q = 1,\ldots,n_o; \quad ; c = 1,\ldots,m,
\end{aligned} \tag{A.17}$$

where

$$\begin{aligned}
\Psi_{q_c}(j\omega_k,\boldsymbol{\rho}) &= \Re\{[1+L^*_{D_{qc}}(j\omega_k)][1+L_{qq_c}(j\omega_k,\boldsymbol{\rho})]\} \\
M_{qq_c}(j\omega_k,\boldsymbol{\rho}) &= \sum_{z=1}^{n_o} G_{qz_c}(j\omega_k)(1-e^{-j\omega_k\zeta_{qzc}})C_{zq_c}(j\omega_k,\boldsymbol{\rho}) \\
N_{qq_c}(j\omega_k,\boldsymbol{\rho}) &= \sum_{z=1}^{n_o} P_{qz_c}(j\omega_k)C_{zq_c}(j\omega_k,\boldsymbol{\rho})
\end{aligned}$$

and $\|\cdot\|_F$ is the Frobenius norm. The objective function in (A.17), which is an approximation of the 2-norm, is convex with respect to the controller parameters $\boldsymbol{\rho}$. Note that the first inequality shows that the Gershgorin bands do not encircle the critical point and so the MIMO system remains stable even if it is not fully decoupled. The second inequality guarantees the robust performance for the SISO subsystems of the decoupled MIMO system.

A.4 Industrial Case Studies

The following examples will demonstrate the effectiveness of the proposed method for several industrial processes proposed in literature.

A.4.1 Case 1 - SP with fixed time delays

In [59], the proposed method was applied to a unity feedback MIMO system with fixed time delays. The plant model is represented by a 2×2 interactive chemical process which is used in industrial applications, and was defined as:

$$\mathbf{P}(s) = \begin{bmatrix} G_{11}(s)e^{-6s} & G_{12}(s)e^{-10s} \\ G_{21}(s)e^{-12s} & G_{22}(s)e^{-8s} \end{bmatrix} = \begin{bmatrix} \dfrac{10e^{-6s}}{8s+1} & \dfrac{5e^{-10s}}{30s+1} \\ \dfrac{-8e^{-12s}}{40s+1} & \dfrac{2e^{-8s}}{10s+1} \end{bmatrix}, \tag{A.18}$$

where the time scale is defined in minutes. The elements $G_{qp}(s)$ for $q = 1,2$ and $p = 1,2$ represent the strictly proper delay-free transfer functions in $\mathbf{G}_n(s)$. A relative-gain-array (RGA) analysis confirms that the system is not diagonally dominant.

Since the time delay parameters are fixed for this process, the nominal time-delayed plant model $\mathbf{P}_n(s)$ will be chosen to be equal to $\mathbf{P}(s)$. In this manner, the open loop transfer function will be $\mathbf{L}(s,\boldsymbol{\rho}) = \mathbf{G}_n(s)\mathbf{C}(s,\boldsymbol{\rho})$. The performance and uncertainty filters chosen for this case will be identical to those in [59],

$$W_{1_q} = 0.5 \quad , \quad W_{2_q} = 0.5\left(\frac{2s+1}{s+1}\right) \qquad q = 1,2. \tag{A.19}$$

For comparative purposes, a PI MIMO controller will be designed for this process. Thus the linearly parameterized controller will posses the following matrix form:

$$\mathbf{C}(s,\boldsymbol{\rho}) = \begin{bmatrix} [\rho_{11_1} \;\; \rho_{11_2}]\phi^T(s) & [\rho_{12_1} \;\; \rho_{12_2}]\phi^T(s) \\ [\rho_{21_1} \;\; \rho_{21_2}]\phi^T(s) & [\rho_{22_1} \;\; \rho_{22_2}]\phi^T(s), \end{bmatrix}, \tag{A.20}$$

where $\phi(s) = [1 \quad 1/s]$. Additionally, the desired diagonal open-loop transfer function $\mathbf{L}_D(s)$ will be chosen as simple integrators with time constants equal to 30 minutes (i.e., $\mathbf{L}_D(s) = (1/30s)\mathbf{I}$). The optimization problem in (A.17) can now be solved by repeating the stability constraints for each ω_k. The frequency grid will be chosen to be between 10^{-2} and 10 rad/min with $N = 150$ equally spaced points. The PI MIMO controller obtained from optimization is:

$$\mathbf{C}(s) = \begin{bmatrix} \dfrac{0.03289s + 0.001272}{s} & \dfrac{-0.03511s - 0.00311}{s} \\ \dfrac{0.05056s + 0.004511}{s} & \dfrac{0.2128s + 0.006133}{s} \end{bmatrix}.$$

Fig. A.2 displays the closed loop response of the system with the controller obtained in [59] and with the controller obtained with the SP. It can be seen that the controller for the SP produces no overshoot and asymptotically decouples the system much faster. Note that if the time constant of the desired open-loop transfer function matrix is decreased to 5 minutes, the rise and settling time of the system response is significantly improved.

A.4.2 Case 2 - SP with uncertain time delays

The proposed optimization problem will now be applied to an uncertain time-delayed MIMO SP. Consider the 2×2 plant process $\mathbf{P}(s)$ (i.e., $c = 1$) that was analyzed in Case (1). The time delays for this plant will now possess uncertain values that will belong to a set. This plant will

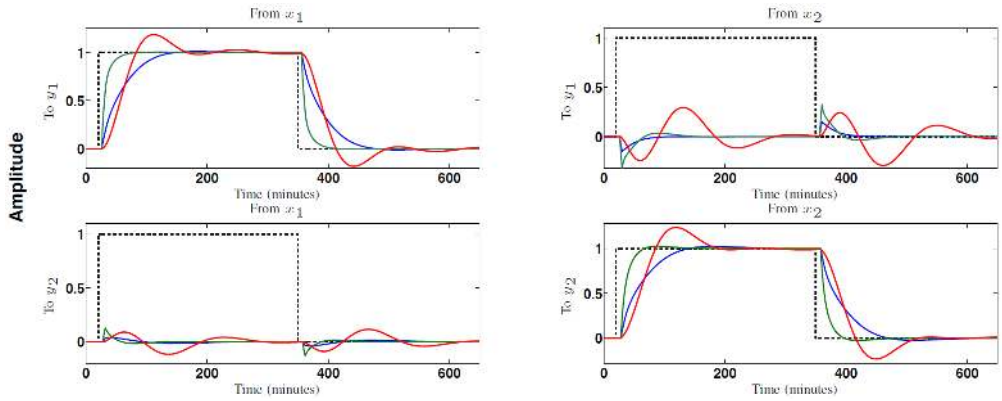

Figure A.2 – Closed loop comparison between time delayed MIMO system with unity feedback and time delayed MIMO SP: unit step reference signal (black, dash), response from system with no SP structure (red, solid), response with SP and with diag$(\mathbf{L}_D(s)) = \frac{1}{30s}$ (blue, solid), response with SP and with diag$(\mathbf{L}_D(s)) = \frac{1}{5s}$ (green, solid).

now be represented as follows:

$$\mathbf{P}(s) = \begin{bmatrix} \dfrac{10e^{-\tau_{11}s}}{8s+1} & \dfrac{5e^{-\tau_{12}s}}{30s+1} \\ \dfrac{-8e^{-\tau_{21}s}}{40s+1} & \dfrac{2e^{-\tau_{22}s}}{10s+1} \end{bmatrix}, \tag{A.21}$$

where the time delays τ_{qp} possess values in the sets:

$$\tau_{11} = \{3,9\} \quad \tau_{12} = \{7,13\} \quad \tau_{21} = \{9,15\} \quad \tau_{22} = \{5,11\}. \tag{A.22}$$

The nominal model is the same as defined in (A.18). Again, the elements $G_{qp}(s)$ for $q = 1,2$ and $p = 1,2$ represent the strictly proper delay-free transfer functions in $\mathbf{G}_n(s)$. The performance and uncertainty filters chosen for this example will be identical to those in section (A.4.1). The desired diagonal open-loop transfer function $\mathbf{L}_D(s)$ will be chosen as simple integrators with time constants equal to 7 minutes (i.e., $\mathbf{L}_D(s) = (1/7s)\mathbf{I}$).

For simplicity, a PI controller will be designed for this process. Note that in designing this controller, all possible combinations of the uncertainties in (A.22) must be considered. Therefore, since $\beta_{qp} = 2 \; \forall \; \{p,q\}$, there will be a total of $m = 2^4$ possible cases to consider. The optimization problem in (A.17) can now be solved by repeating the stability constraints for each combination of the uncertainties in (A.22). The frequency grid will be chosen to be between 10^{-2} and 10 rad/min with $N = 150$ equally spaced points. The PI MIMO controller

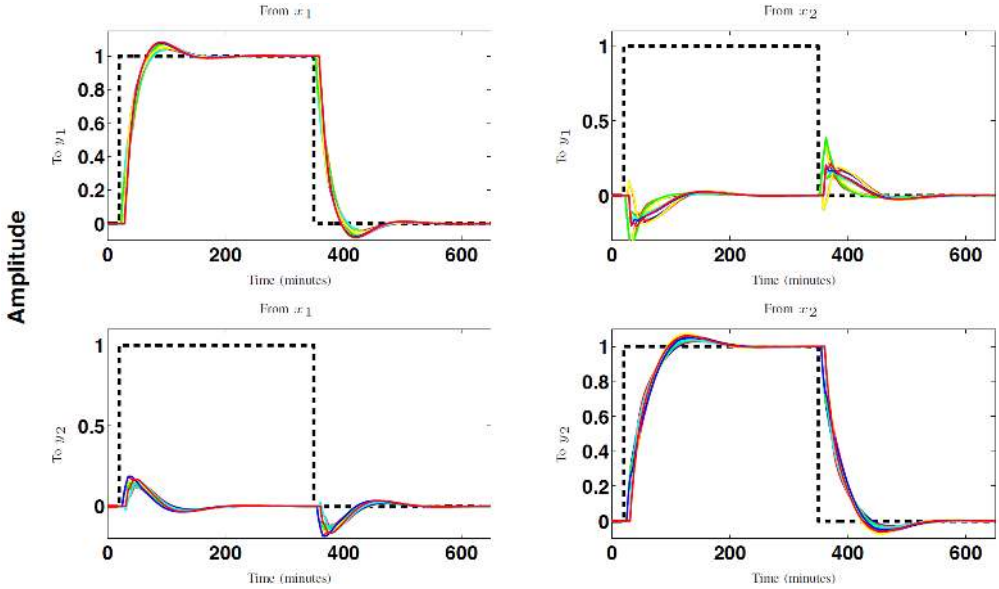

Figure A.3 – MIMO response to a unit step input: reference signal (black,dash), the remaining $\Omega = 16$ closed-loop responses are for all possible combinations of the time delay parameters in (A.22).

obtained from the optimization problem is:

$$\mathbf{C}(s) = \begin{bmatrix} \dfrac{0.06234s + 0.001464}{s} & \dfrac{-0.04803s - 0.005408}{s} \\ \dfrac{0.1585s + 0.0168}{s} & \dfrac{0.3113s + 0.005995}{s} \end{bmatrix}.$$

Fig. A.3 displays the closed-loop MIMO response to a step input. Notice that with this controller, the MIMO process achieves robust performance while simultaneously decoupling the system. The Gershgorin bands are depicted in Fig. A.4 for the system possessing the largest delay time uncertainty ($\tau_{11} = 9$, $\tau_{12} = 13$, $\tau_{21} = 15$, $\tau_{22} = 11$). The red and blue bands possess a radius of $|r_q(j\omega_k)|$ for $q = 1,2$ and $k = 1,\ldots,N$.

Notice how the Gershgorin bands never intersect with the performance filter centered at $(-1 + j0)$. This proves that the MIMO system is stable, robust, and satisfies the optimization criterion in (A.17).

A.4.3 Case 3 - The Shell control problem

The multivariable heavy oil fractionator (known as the Shell process) is a highly coupled system which is predominantly used in petrochemical processes. Efficient control methods are essential for attaining viable production rates, minimizing energy consumption, and reducing the overall operating costs. These types of systems are difficult to control for two reasons: the system interactions are strong, and the large time delays that are inherent to the

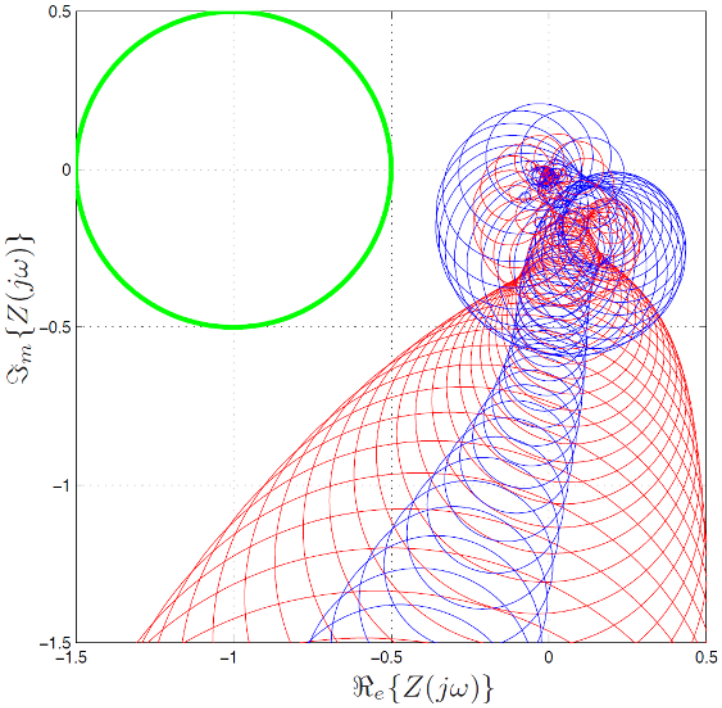

Figure A.4 – Gershgorin bands centered at L_{qq} with the largest time delay combination in (A.22): performance filter with $|W_{1_q}| = 0.5$ (green circle), Gershgorin bands corresponding to $q = 1$ (blue circles), Gershgorin bands corresponding to $q = 2$ (red circles). Note that $Z(j\omega)$ is simply the complex number representation of each circle in the plot.

system dynamics.

Consider the 2×3 industrial Shell problem in [154],

$$\mathbf{P}_n(s) = \begin{bmatrix} G_{11}(s)e^{-81s} & G_{12}(s)e^{-84s} & G_{13}(s)e^{-81s} \\ G_{21}(s)e^{-54s} & G_{22}(s)e^{-42s} & G_{32}(s)e^{-45s} \end{bmatrix} = \begin{bmatrix} \frac{4.05e^{-81s}}{50s+1} & \frac{1.77e^{-84s}}{60s+1} & \frac{5.88e^{-81s}}{50s+1} \\ \frac{5.39e^{-54s}}{50s+1} & \frac{5.72e^{-42s}}{60s+1} & \frac{6.9e^{-45s}}{40s+1} \end{bmatrix} \tag{A.23}$$

where the time scale is defined in minutes. Note that (A.23) is represented as the nominal model of the process. It should be noted that the controller outputs $[u_1(t)\ u_2(t)\ u_3(t)]^T$ should be within the saturation bounds of the physical system : $[-0.5, 0.5]$ (see [155]). The elements $G_{qp}(s)$ for $q = 1,2$ and $p = 1,2,3$ represent the strictly proper delay-free transfer functions in $\mathbf{G}_n(s)$. Now consider the case when the time delays are varied to +20% of their nominal values shown in (A.23). As with the previous example, the plant $\mathbf{P}(s)$ can be represented as a system with uncertain time delays. Since $\beta_{qp} = 2\ \forall\ \{p,q\}$, there will be a total of $m = 2^6 = 64$ possible cases to consider.

For comparative purposes, a PI controller will be designed for this process. Thus the controller $\mathbf{C}(s,\boldsymbol{\rho})$ will be a 3×2 transfer function matrix with $n = 12$ optimization parameters $\boldsymbol{\rho}$. The frequency grid will be chosen to be between 10^{-4} and 10 rad/min with $N = 200$ equally spaced points (since the frequencies of interest of the open-loop system lie within this range). The desired diagonal open-loop transfer function matrix will be chosen as simple integrators with bandwidths that are approximately 20% greater than the open-loop system bandwidths (i.e., $\mathbf{L}_D(s) = (1/35s)\mathbf{I}$). By solving the optimization problem in (A.17) for each combination of the uncertainties (i.e., $\{\tau_{11},\ldots,\tau_{qp}\}\ \forall\ \{p,q\}$, where $\tau_{qp} \in \{\zeta_{qp}, 1.2\zeta_{qp}\}$), one obtains the following PI controller

$$\mathbf{C}(s) = \begin{bmatrix} \frac{0.2053s+0.004997}{s} & \frac{-0.01315s-0.00146}{s} \\ \frac{-0.6735s-0.01008}{s} & \frac{0.4977s+0.008098}{s} \\ \frac{0.2839s+0.004451}{s} & \frac{-0.1041s-0.001432}{s} \end{bmatrix}.$$

Fig. A.5 displays the closed-loop step response of the SP for the nominal delay case, while Fig. A.6 displays the response with the worst case delay (the case where $\tau_{qp} = 1.2\zeta_{qp}\ \forall\ \{p,q\}$). The figures also show a comparison with the controller design method in [154] , which is based on a “squared down" approach.

From Fig. A.5 and Fig. A.6, it can be observed that the purposed method in this paper produces improved SISO subsystem performance with minimal overshoot. In addition, the decoupling transients are significantly reduced for both the nominal and worst case output responses. Fig. A.7 displays the controller outputs of the system.

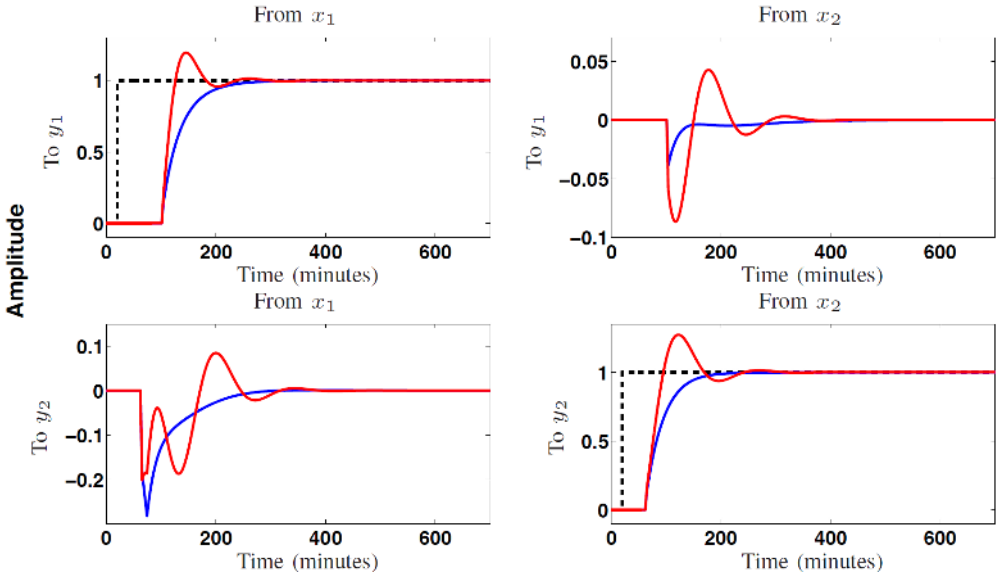

Figure A.5 – MIMO SP closed-loop response to a unit step input with $\tau_{qp} = \zeta_{qp}\ \forall\ \{p,q\}$: reference signal (black,dash), output response with the proposed optimization method (blue, solid), output response with the “squared down" method.

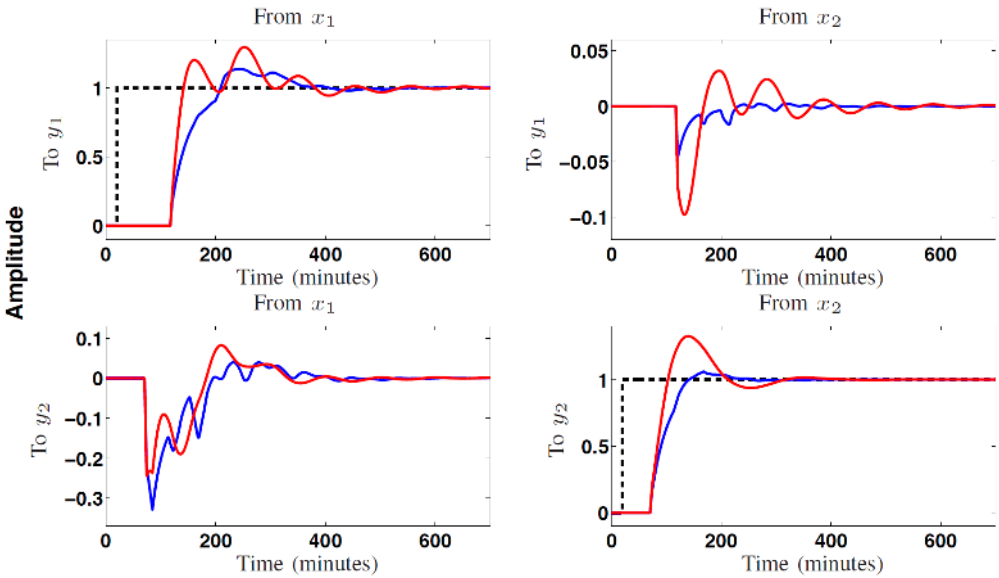

Figure A.6 – MIMO SP closed-loop response to a unit step input with $\tau_{qp} = 1.2\zeta_{qp}\ \forall\ \{p,q\}$: reference signal (black,dash), output response with the proposed optimization method (blue, solid), output response with the “squared down" method.

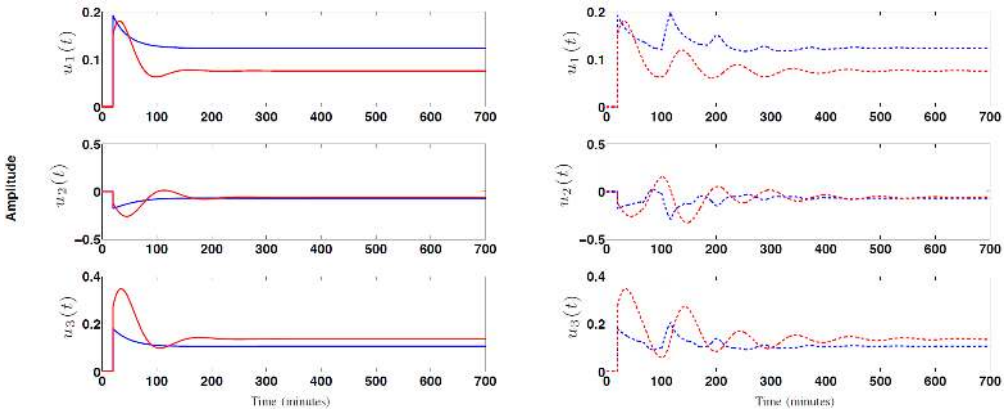

Figure A.7 – MIMO SP controller output response to a unit step reference: Controller output response of proposed method with $\tau_{qp} = \zeta_{qp}$ (blue, solid), controller output response of "squared down" method with $\tau_{qp} = \zeta_{qp}$ (red, solid), controller output response of proposed method with $\tau_{qp} = 1.2\zeta_{qp}$ (blue, dash), controller output response of "squared down" method with $\tau_{qp} = 1.2\zeta_{qp}$ (red, dash)

A.5 Conclusion

This paper has proposed a new method for computing multivariable SP controllers with H_∞ performance. The method is based on a convex approximation of the H_∞ robust performance criterion in the Nyquist diagram. This approximation relies on the choice of a desired open-loop transfer function $\mathbf{L}_D$ for the dead-time free model of the plant. With a linearly parameterized controller, one possesses the flexibility to design PI, PID, or higher order controllers for a system. For the industrial processes considered in this paper, the proposed method has been proven to be robust; H_∞ performance was achieved for MIMO systems with both multiplicative and time delay uncertainties. The solution to the optimization problem generates a controller such that a system becomes decoupled and simultaneously optimizes the single-loop performances of the SISO subsystems.

Bibliography

[1] O. Mayr, "The origins of feedback control", *Scientific American*, vol. 223, no. 4, pp. 110–119, 1970, ISSN: 00368733, 19467087.

[2] J. C. Maxwell, "On governors", *Proceedings of the Royal Society of London*, vol. 16, pp. 270–283, 1867.

[3] H. W. Bode, *Network Analysis and Feedback Amplifier Design*. New York, Van Nostrand, 1945.

[4] H. Nyquist, "Regeneration theory", *Bell System Technical Journal*, no. 11, pp. 126–147, 1932.

[5] G. Salvendy, *Handbook of industrial engineering: technology and operations management*. John Wiley & Sons, 2001.

[6] J. C. Willems, "In control, almost from the beginning until the day after tomorrow", *European Journal of Control*, vol. 13, no. 1, pp. 71 –81, 2007, SI: On the Dawn and Development of Control Science in the XX Century, ISSN: 0947-3580. DOI: https://doi.org/10.3166/ejc.13.71-81.

[7] Z.-S. Hou and Z. Wang, "From model-based control to data-driven control: survey, classification and perspective", *Information Sciences*, vol. 235, pp. 3–35, 2013.

[8] A. S. Bazanella, L. Campestrini, and D. Eckhard, *Data-driven Controller Design: The H_2 Approach*. Springer, 2012.

[9] X. Jing and Z. Lang, *Frequency Domain Analysis and Design of Nonlinear Systems based on Volterra Series Expansion: A Parametric Characteristic Approach*, ser. Understanding Complex Systems. Springer International Publishing, 2015, ISBN: 9783319123912.

[10] K. Zhou and J. C. Doyle, *Essentials of robust control*. N.Y.: Prentice-Hall, 1998.

[11] K. Åström and T. Hagglund, "The future of PID control", *Control Engineering Practice*, vol. 9, no. 11, pp. 1163 –1175, 2001, PID Control, ISSN: 0967-0661. DOI: https://doi.org/10.1016/S0967-0661(01)00062-4.

[12] Y. Meyer and G. Cumunel, "Active vibration isolation with a MEMS device. effects of nonlinearities on control efficiency", *Smart Materials and Structures*, vol. 24, no. 8, p. 085 004, 2015.

[13] E. d. A. Barboza, M. J. da Silva, L. D. Coelho, J. F. Martins-Filho, C. J. A. Bastos-Filho, U. C. de Moura, and J. R. F. de Oliveira, "Impact of nonlinear effects on the performance of 120 gb/s 64 QAM optical system using adaptive control of cascade of amplifiers", in *2015 SBMO/IEEE MTT-S International Microwave and Optoelectronics Conference (IMOC)*, 2015, pp. 1–5. DOI: 10.1109/IMOC.2015.7369212.

[14] D. Rijlaarsdam, P. Nuij, J. Schoukens, and M. Steinbuch, "A comparative overview of frequency domain methods for nonlinear systems", *Mechatronics*, vol. 42, no. Supplement C, pp. 11 –24, 2017, ISSN: 0957-4158. DOI: https://doi.org/10.1016/j.mechatronics.2016.12.008.

[15] S. Yin, X. Li, H. Gao, and O. Kaynak, "Data-based techniques focused on modern industry: an overview", *Industrial Electronics, IEEE Transactions on*, vol. 62, no. 1, pp. 657–667, 2015.

[16] S. Formentin, K. van Heusden, and A. Karimi, "A comparison of model-based and data-driven controller tuning", *International Journal of Adaptive Control and Signal Processing*, vol. 28, no. 10, pp. 882–897, 2014.

[17] I. D. Landau, R. Lozano, M. M'Saad, and A. Karimi, *Adaptive Control: Algorithms, Analysis and Applications*. London: Springer-Verlag, 2011.

[18] Z. Hou and S. Jin, *Model free adaptive control: theory and applications*. CRC press, 2013.

[19] ——, "A novel data-driven control approach for a class of discrete-time nonlinear systems", *IEEE Transactions on Control Systems Technology*, vol. 19, no. 6, pp. 1549–1558, 2011.

[20] ——, "Data-driven model-free adaptive control for a class of MIMO nonlinear discrete-time systems", *IEEE Transactions on Neural Networks*, vol. 22, no. 12, pp. 2173–2188, 2011.

[21] B. Gao, R. Cao, Z. Hou, and H. Zhou, "Model-free adaptive MIMO control algorithm application in polishing robot", in *2017 6th Data Driven Control and Learning Systems (DDCLS)*, 2017, pp. 135–140. DOI: 10.1109/DDCLS.2017.8068058.

[22] Z. Hou, S. Liu, and C. Yin, "Local learning-based model-free adaptive predictive control for adjustment of oxygen concentration in syngas manufacturing industry", *IET Control Theory Applications*, vol. 10, no. 12, pp. 1384–1394, 2016, ISSN: 1751-8644. DOI: 10.1049/iet-cta.2015.0835.

[23] Y. Zhu and Z. Hou, "Controller dynamic linearisation-based model-free adaptive control framework for a class of non-linear system", *IET Control Theory Applications*, vol. 9, no. 7, pp. 1162–1172, 2015, ISSN: 1751-8644. DOI: 10.1049/iet-cta.2014.0743.

[24] D. Liu and G. H. Yang, "Event-based model-free adaptive control for discrete-time non-linear processes", *IET Control Theory Applications*, vol. 11, no. 15, pp. 2531–2538, 2017, ISSN: 1751-8644. DOI: 10.1049/iet-cta.2016.1672.

[25] M. G. Safonov and T. C. Tsao, "The unfalsified control concept and learning", *IEEE Trans. on Automatic Control*, vol. 42, no. 6, 1997.

[26] G. Battistelli, D. Mari, D. Selvi, and P. Tesi, "Unfalsified approach to data-driven control design", in *53rd IEEE Conference on Decision and Control*, 2014, pp. 6003–6008. DOI: 10.1109/CDC.2014.7040329.

[27] R. Sánchez-Peña, P Colmegna, and F Bianchi, "Unfalsified control based on the H_∞ controller parameterisation", *International Journal of Systems Science*, vol. 46, no. 15, pp. 2820–2831, 2015.

[28] G. Battistelli, D. Mari, D. Selvi, and P. Tesi, "Direct control design via controller unfalsification", *International Journal of Robust and Nonlinear Control*, n/a–n/a, 2017, rnc.3778, ISSN: 1099-1239. DOI: 10.1002/rnc.3778.

[29] J. G. Ziegler and N. B. Nichols, "Optimum settings for automatic controllers", *trans. ASME*, vol. 64, no. 11, 1942.

[30] H. Hjalmarsson, "Iterative feedback tuning - an overview", *Int. Journal of Adaptive Control and Signal Processing*, vol. 16, pp. 373–395, 2002.

[31] H. Hjalmarsson, M. Gevers, S. Gunnarsson, and O. Lequin, "Iterative feedback tuning: theory and application", *IEEE Control Systems Magazine*, pp. 26–41, 1998.

[32] S. Veres and H. Hjalmarsson, "Tuning for robustness and performance using iterative feedback tuning", in *Proceedings of the 41st IEEE Conference on Decision and Control, 2002.*, vol. 4, 2002, 4682–4687 vol.4. DOI: 10.1109/CDC.2002.1185117.

[33] H. Prochazka, M. Gevers, B. D. O. Anderson, and C. Ferrera, "Iterative feedback tuning for robust controller design and optimization", in *Proceedings of the 44th IEEE Conference on Decision and Control*, 2005, pp. 3602–3607. DOI: 10.1109/CDC.2005.1582721.

[34] M. F. Heertjes, B. V. der Velden, and T. Oomen, "Constrained iterative feedback tuning for robust control of a wafer stage system", *IEEE Transactions on Control Systems Technology*, vol. 24, no. 1, pp. 56–66, 2016, ISSN: 1063-6536. DOI: 10.1109/TCST.2015.2418311.

[35] M. Heertjes, "Data-based motion control of wafer scanners", *IFAC-PapersOnLine*, vol. 49, no. 13, pp. 1 –12, 2016, 12th IFAC Workshop on Adaptation and Learning in Control and Signal Processing ALCOSP 2016, ISSN: 2405-8963. DOI: https://doi.org/10.1016/j.ifacol.2016.07.918.

[36] M. C. Campi, A. Lecchini, and S. M. Savaresi, "Virtual reference feedback tuning: a direct method for the design of feedback controllers", *Automatica*, vol. 38, pp. 1337–1346, 2002.

[37] S. M. Savaresi and G. O. Guardabassi, "Approximate I/O feedback linearization of discrete-time non-linear systems via virtual input direct design", *Automatica*, vol. 34, no. 6, pp. 715 –722, 1998, ISSN: 0005-1098. DOI: https://doi.org/10.1016/S0005-1098(97)00222-7.

[38] A. S. Bazanella, L. Campestrini, and D. Eckhard, *Data-driven controller design: the H_2 approach*. Springer Science & Business Media, 2011.

[39] P. Panizza, D. Invernizzi, F. Riccardi, S. Formentin, and M. Lovera, "Data-driven attitude control law design for a variable-pitch quadrotor", in *American Control Conference (ACC)*, 2016, pp. 4434–4439. DOI: 10.1109/ACC.2016.7525620.

[40] M. B. Radac and R. E. Precup, "Improving model reference control performance using model-free VRFT and Q-learning", in *2016 20th International Conference on System Theory, Control and Computing (ICSTCC)*, 2016, pp. 7–13. DOI: 10.1109/ICSTCC.2016.7790632.

[41] L. Campestrini, D. Eckhard, L. A. Chía, and E. Boeira, "Unbiased MIMO VRFT with application to process control", *Journal of Process Control*, vol. 39, pp. 35 –49, 2016, ISSN: 0959-1524. DOI: http://dx.doi.org/10.1016/j.jprocont.2015.12.010.

[42] E. L. Hedrea, M. B. Radac, and R. E. Precup, "Virtual reference feedback tuning for position control of a twin rotor aerodynamic system", in *2016 IEEE 11th International Symposium on Applied Computational Intelligence and Informatics (SACI)*, 2016, pp. 57–62. DOI: 10.1109/SACI.2016.7507431.

[43] S. Formentin, A. Bisoffi, and T. Oomen, "Asymptotically exact direct data-driven multivariable controller tuning", *IFAC-PapersOnLine*, vol. 48, no. 28, pp. 1349 –1354, 2015, 17th IFAC Symposium on System Identification SYSID 2015, ISSN: 2405-8963. DOI: https://doi.org/10.1016/j.ifacol.2015.12.319.

[44] A. Karimi, L. Mišković, and D. Bonvin, "Iterative correlation-based controller tuning", *Int. Journal of Adaptive Control and Signal Processing*, vol. 18, no. 8, pp. 645–664, 2004.

[45] L. Mišković, A. Karimi, D. Bonvin, and M. Gevers, "Correlation-based tuning of decoupling multivariable controllers", *Automatica*, vol. 43, no. 9, pp. 1481–1494, 2007.

[46] K. van Heusden, A. Karimi, and D. Bonvin, "Data-driven model reference control with asymptotically guaranteed stability", *Int. Journal of Adaptive Control and Signal Processing*, vol. 25, no. 4, pp. 331–351, 2011.

[47] G. Rallo, S. Formentin, and S. M. Savaresi, "On data-driven control design for non-minimum-phase plants: a comparative view", in *Decision and Control (CDC), 2016 IEEE 55th Conference on*, IEEE, 2016, pp. 7159–7164.

[48] P. Gahinet and P. Apkarian, "A linear matrix inequality approach to H_∞ control", *Int. Journal of Robust and Nonlinear Control*, vol. 4, no. 4, pp. 421–448, 1994.

[49] J. C. Doyle, K. Glover, P. P. Khargonekar, and B. A. Francis, "State-space solutions to standard H_2 and H_∞ control problems", *IEEE Transactions on Automatic Control*, vol. 34, no. 8, pp. 831–847, 1989, ISSN: 0018-9286. DOI: 10.1109/9.29425.

[50] A. Nemirovskii, "Several NP-hard problems arising in robust stability analysis", *Mathematics of Control, Signals and Systems*, vol. 6, no. 2, pp. 99–105, 1993, ISSN: 1435-568X. DOI: 10.1007/BF01211741.

[51] P. Apkarian and D. Noll, "Nonsmooth H_∞ synthesis", *IEEE Transactions on Automatic Control*, vol. 51, no. 1, pp. 71–86, 2006.

[52] P. Gahinet and P. Apkarian, "Decentralized and fixed-structure H_∞ control in MATLAB", in *50th IEEE Conference on Decision and Control (CDC)*, Orlando, FL, USA, 2011.

[53] P. Gahinet and P. Apkarian, "Structured H_∞ synthesis in MATLAB", *IFAC Proceedings Volumes*, vol. 44, no. 1, pp. 1435–1440, 2011.

[54] S. Khadraoui, H. Nounou, M. Nounou, A. Datta, and S. P. Bhattacharyya, "Robust control design method for uncertain system using a set of measurements", in *2013 American Control Conference*, 2013, pp. 4325–4330. DOI: 10.1109/ACC.2013.6580505.

[55] ——, "A control design method for unknown systems using frequency domain data", in *2013 9th Asian Control Conference (ASCC)*, 2013, pp. 1–6. DOI: 10.1109/ASCC.2013.6606148.

[56] E. van Solingen, J. van Wingerden, and T. Oomen, "Frequency-domain optimization of fixed-structure controllers", *International Journal of Robust and Nonlinear Control*, n/a–n/a, 2016, rnc.3699, ISSN: 1099-1239. DOI: 10.1002/rnc.3699.

[57] A. Karimi and G. Galdos, "Fixed-order H_∞ controller design for nonparametric models by convex optimization", *Automatica*, vol. 46, no. 8, pp. 1388–1394, 2010.

[58] A. Karimi and Z. Emedi, "H_∞ gain-scheduled controller design for rejection of time-varying narrow-band disturbances applied to a benchmark problem", *European Journal of Control*, vol. 19, no. 4, pp. 279–288, 2013, ISSN: 0947-3580. DOI: 10.1016/j.ejcon.2013.05.010.

[59] G. Galdos, A. Karimi, and R. Longchamp, "H_∞ controller design for spectral MIMO models by convex optimization", *Journal of Process Control*, vol. 20, no. 10, pp. 1175 –1182, 2010.

[60] A. Karimi, "Frequency-domain robust control toolbox", in *52nd IEEE Conference on Decision and Control*, 2013, pp. 3744–3749. DOI: 10.1109/CDC.2013.6760460.

[61] A. J. Den Hamer, S. Weiland, and M. Steinbuch, "Model-free norm-based fixed structure controller synthesis", in *48th IEEE Conference on Decision and Control*, Shanghai, China, 2009, pp. 4030–4035.

[62] A. den Hamer, "Data-driven optimal controller synthesis, a frequency domain approach", PhD thesis, Eindhoven University of Technology, Eindhoven , The Netherlands, 2010.

[63] M. Saeki, M. Ogawa, and N. Wada, "Low-order H_∞ controller design on the frequency domain by partial optimization", *International Journal of Robust and Nonlinear Control*, vol. 20, no. 3, pp. 323–333, 2010.

[64] M. Hast, K. J. Aström, B. Bernhardsson, and S. Boyd, "PID design by convex-concave optimization", in *European Control Conference*, Zurich, Switzerland, 2013, pp. 4460–4465.

[65] S. Boyd, M. Hast, and K. J. Åström, "MIMO PID tuning via iterated LMI restriction", *International Journal of Robust and Nonlinear Control*, vol. 26, no. 8, pp. 1718–1731, 2016.

[66] A. Karimi and C. Kammer, "A data-driven approach to robust control of multivariable systems by convex optimization", *Automatica*, vol. 85, no. Supplement C, pp. 227 –233, 2017, ISSN: 0005-1098. DOI: https://doi.org/10.1016/j.automatica.2017.07.063.

[67] A. Isidori and A. Astolfi, "Disturbance attenuation and H_∞ control via measurement feedback in nonlinear systems", *IEEE transactions on automatic control*, vol. 37, no. 9, pp. 1283–1293, 1992.

[68] J. A. Ball, J. W. Helton, and M. L. Walker, "H_∞ control for nonlinear systems with output feedback", *IEEE Transactions on Automatic Control*, vol. 38, no. 4, pp. 546–559, 1993.

[69] M. Aliyu, *Nonlinear H_∞ control, Hamiltonian systems and Hamilton-Jacobi equations*. CRC Press, 2011.

[70] H. C. Ferreira, P. H. Rocha, and R. M. Sales, "Nonlinear H_∞ control and the Hamilton-Jacobi-Isaacs equation", *IFAC Proceedings Volumes*, vol. 41, no. 2, pp. 188 –193, 2008, 17th IFAC World Congress, ISSN: 1474-6670. DOI: https://doi.org/10.3182/20080706-5-KR-1001.00032.

[71] X. Wang, E. E. Yaz, S. C. Schneider, and Y. I. Yaz, "$H_2 - H_\infty$ control of discrete-time nonlinear systems using the state-dependent Riccati equation approach", *Systems Science & Control Engineering*, vol. 5, no. 1, pp. 215–223, 2017. DOI: 10.1080/21642583.2017.1310635. eprint: http://dx.doi.org/10.1080/21642583.2017.1310635.

[72] H. Jiang, H. Zhang, Y. Luo, and X. Cui, "H_∞ control with constrained input for completely unknown nonlinear systems using data-driven reinforcement learning method", *Neurocomputing*, vol. 237, no. Supplement C, pp. 226 –234, 2017, ISSN: 0925-2312. DOI: https://doi.org/10.1016/j.neucom.2016.11.041.

[73] N. Krylov, N. Bogolyubov, and S. Lefschetz, *Introduction to Non-linear Mechanics*, ser. Annals of mathematics studies. Princeton University Press, 1943.

[74] D. Rijlaarsdam, P. Nuij, J. Schoukens, and M. Steinbuch, "Spectral analysis of block structured nonlinear systems and higher order sinusoidal input describing functions", *Automatica*, vol. 47, no. 12, pp. 2684 –2688, 2011, ISSN: 0005-1098. DOI: https://doi.org/10.1016/j.automatica.2011.08.049.

[75] H. Li, S. Wang, J. Lu, X. You, and X. Yu, "Stability analysis of the shunt regulator with nonlinear controller in PCU based on describing function method", *IEEE Transactions on Industrial Electronics*, vol. 64, no. 3, pp. 2044–2053, 2017, ISSN: 0278-0046. DOI: 10.1109/TIE.2016.2623579.

[76] C. K. Wei, H. A. F. Almurib, S. Yahya, and M. Moghavvemi, "Sinusoidal input describing function analysis for coupled tanks system", in *2016 IEEE Industrial Electronics and Applications Conference (IEACon)*, 2016, pp. 261–268. DOI: 10.1109/IEACON.2016.8067389.

[77] I. Tsypkin, *Relay Control Systems*. Cambridge University Press, 1984, ISBN: 9780521243902.

[78] M. C. Campi and S. M. Savaresi, "Direct nonlinear control design: the virtual reference feedback tuning (VRFT) approach", *IEEE Trans. on Automatic Control*, vol. 51, no. 1, pp. 14–27, 2006.

[79] M. B. Radac, R. E. Precup, E. M. Petriu, and S. Preitl, "Iterative data-driven tuning of controllers for nonlinear systems with constraints", *IEEE Transactions on Industrial Electronics*, vol. 61, no. 11, pp. 6360–6368, 2014, ISSN: 0278-0046. DOI: 10.1109/TIE.2014.2300068.

[80] D. Piga, S. Formentin, and A. Bemporad, "Direct data-driven control of constrained systems", *IEEE Transactions on Control Systems Technology*, vol. PP, no. 99, pp. 1–8, 2017, ISSN: 1063-6536. DOI: 10.1109/TCST.2017.2702118.

[81] C. Novara and S. Formentin, "Data-driven controller design for nonlinear systems: a two degrees of freedom architecture", *CoRR*, vol. abs/1407.2068, 2014.

[82] S. Formentin, C. Novara, S. M. Savaresi, and M. Milanese, "Data-driven inversion-based control of nonlinear systems", *IFAC-PapersOnLine*, vol. 48, no. 28, pp. 1343 –1348, 2015, 17th IFAC Symposium on System Identification SYSID 2015, ISSN: 2405-8963. DOI: https://doi.org/10.1016/j.ifacol.2015.12.318.

[83] S. Formentin, D. Piga, R. Tóth, and S. M. Savaresi, "Direct learning of LPV controllers from data", *Automatica*, vol. 65, pp. 98–110, 2016.

[84] V. A. Yakubovich, "The solution of certain matrix inequalities in automatic control theory", in *Soviet Math. Dokl*, vol. 3, 1962, pp. 620–623.

[85] H. K. Khalil, *Nonlinear Systems*. New Jersey: Prentice Hall, 1996.

[86] S. Ibrir, "Circle-criterion approach to discrete-time nonlinear observer design", *Automatica*, vol. 43, no. 8, pp. 1432–1441, 2007.

[87] C. Pittet, S. Tarbouriech, and C. Burgat, "Stability regions for linear systems with saturating controls via circle and Popov criteria", in *Proceedings of the 36th IEEE Conference on Decision and Control*, vol. 5, 1997, 4518–4523 vol.5. DOI: 10.1109/CDC.1997.649683.

[88] T. Kiyama, S. Hara, and T. Iwasaki, "Effectiveness and limitation of circle criterion for LTI robust control systems with control input nonlinearities of sector type", *International Journal of Robust and Nonlinear Control*, vol. 15, no. 17, pp. 873–901, 2005.

[89] M. Arcak and P. Kokotović, "Nonlinear observers: a circle criterion design and robustness analysis", *Automatica*, vol. 37, no. 12, pp. 1923–1930, 2001.

[90] M. Arcak, M. Larsen, and P. Kokotović, "Circle and Popov criteria as tools for nonlinear feedback design", *Automatica*, vol. 39, no. 4, pp. 643–650, 2003.

[91] P. Grabowski and F. M. Callier, "On the circle criterion for boundary control systems in factor form: Lyapunov stability and Lur'e equations", *ESAIM: Control, Optimisation and Calculus of Variations*, vol. 12, no. 1, pp. 169–197, 2006.

[92] G. Schmitt, "Frequency domain evaluation of circle criterion, popov criterion and off-axis circle criterion in the MIMO case", *International Journal of Control*, vol. 72, no. 14, pp. 1299–1309, 1999.

[93] S. Boyd and L. Vandenberghe, *Convex Optimization*. Cambridge,UK: Cambridge University Press, 2004.

[94] A. Nicoletti and A. Karimi, "H_∞ Smith predictor design for time-delayed MIMO systems via convex optimization", in *2014 IEEE Conference on Control Applications (CCA)*, IEEE, 2014, pp. 1418–1424.

[95] L. Ljung, *System Identification - Theory for the User*, second. NJ, USA: Prentice Hall, 1999.

[96] C. J. Doyle, B. A. Francis, and A. R. Tannenbaum, *Feedback Control Theory*. New York: Mc Millan, 1992.

[97] K. Zhou, *Essentials of Robust Control*. New Jersey: Prentice Hall, 1998.

[98] M. Schetzen, *The Volterra and Wiener theories of nonlinear systems*. Wiley, Apr. 1980, ISBN: 0471044555.

[99] R. Pintelon and J. Schoukens, *System identification: a frequency domain approach*. John Wiley & Sons, 2012.

[100] I. D. Landau and G. Zito, *Digital control systems: design, identification and implementation*. Springer, 2006.

[101] A. Karimi, "Frequency-domain robust control toolbox", in *52nd IEEE Conference in Decision and Control*, Florance, Italy, 2013, pp. 3744 –3749.

[102] J.-J. E. Slotine, W. Li, *et al.*, *Applied nonlinear control*, 1. Prentice hall Englewood Cliffs, NJ, 1991, vol. 199.

[103] A. Rantzer and A. Megretski, "Convex parameterization of robustly stabilizing controllers", *IEEE Trans. on Automatic Control*, vol. 39, no. 9, pp. 1802–1808, 1994.

[104] K. Glover and D. McFarlane, "Robust stabilization of normalized coprime factor plant descriptions with H-bounded uncertainty", *Automatic Control, IEEE Transactions on*, vol. 34, no. 8, pp. 821–830, 1989.

[105] P. Heuberger, P. Van den Hof, and B. Wahlberg, *Modelling and identification with rational basis functions*. London, UK: Springer-Verlag, 2005.

[106] H. Akcay and B. Ninness, "Orthonormal basis functions for continuous-time systems and L_p convergence", *Mathematics of Control, Signals, and Systems*, vol. 12, pp. 295–305, 1999.

[107] G. Calafiore and M. C. Campi, "The scenario approach to robust control design", *IEEE Trans. on Automatic Control*, vol. 51, no. 5, pp. 742–753, 2006.

[108] T. Alamo, R. Tempo, and A. Luque, "On the sample complexity of probabilistic analysis and design methods", in *Perspectives in Mathematical System Theory, Control, and Signal Processing*, Springer, 2010, pp. 39–55.

[109] G. Tao and P. A. Ioannou, "Necessary and sufficient conditions for strictly positive real matrices", *IEEE Proceedings G - Circuits, Devices and Systems*, vol. 137, no. 5, pp. 360–366, 1990, ISSN: 0956-3768. DOI: 10.1049/ip-g-2.1990.0057.

[110] J. Salt, A. Sala, and P. Albertos, "A transfer-function approach to dual-rate controller design for unstable and non-minimum-phase plants", *IEEE Transactions on Control Systems Technology*, vol. 19, no. 5, pp. 1186–1194, 2011, ISSN: 1063-6536. DOI: 10.1109/TCST.2010.2076386.

[111] G. Galdos, A. Karimi, and R. Longchamp, "RST controller design by convex optimization using frequency-domain data", in *Proceedings of the 18th IFAC World Congress*, Milan, Italy, 2011.

[112] W. Zhang, M. Tomizuka, P. Wu, Y. H. Wei, Q. Leng, S. Han, and A. K. Mok, "A double disturbance observer design for compensation of unknown time delay in a wireless motion control system", *IEEE Transactions on Control Systems Technology*, vol. PP, no. 99, pp. 1–9, 2017, ISSN: 1063-6536. DOI: 10.1109/TCST.2017.2665967.

[113] W. Shi, H. Zhao, J. Ma, and Y. Yao, "Dead zone compensation of ultrasonic motor using adaptive dither", *IEEE Transactions on Industrial Electronics*, vol. PP, no. 99, pp. 1–1, 2017, ISSN: 0278-0046. DOI: 10.1109/TIE.2017.2760854.

[114] C. Hu, B. Yao, and Q. Wang, "Adaptive robust precision motion control of systems with unknown input dead-zones: a case study with comparative experiments", *IEEE Transactions on Industrial Electronics*, vol. 58, no. 6, pp. 2454–2464, 2011, ISSN: 0278-0046. DOI: 10.1109/TIE.2010.2066535.

[115] W Bartmann, K Hanke, J. Abelleira, and M Kowalska, "Upgrades of the CERN PS booster ejection lines", No. CERN-ACC-2014-0202, Tech. Rep., 2014.

[116] L. Rossi and O. Brüning, *The High Luminosity Large Hadron Collider: The New Machine for Illumination the Mysteries of the Universe*. World Scientific Publishing Co, 2015. DOI: 10.1142/9581.

[117] Q. King, "The all-digital approach to LHC power converter current control", in *Accelerator and Large Experimental Physics Control Systems*, vol. 1, 2001, pp. 453–455.

[118] H Thiesen, S Page, V Montabonnet, Q King, G Hudson, D Nisbet, and M Cerqueira Bastos, "High precision current control for the LHC main power converters", in *International Particle Accelerator Conference (IPAC)*, 2010.

[119] M Bastos, G Fernqvist, A Cantone, and Q King, "Developments in high-precision aspects of power converter control for LHC", No. CERN-LHC-PROJECT-Report-1044, Tech. Rep., 2007.

[120] D Calcoen, Q King, and P. Semanaz, "Evolution of the CERN power converter function generator/controller for operation in fast cycling accelerators", in *International Conference on Accelerator and Large Experimental Control Systems (ICALEPCS)*, Grenoble, France, 2011.

[121] E. E. Kriezis, T. D. Tsiboukis, S. M. Panas, and J. A. Tegopoulos, "Eddy currents: theory and applications", *Proceedings of the IEEE*, vol. 80, no. 10, pp. 1559–1589, 1992, ISSN: 0018-9219. DOI: 10.1109/5.168666.

[122] R Shafer, "Eddy currents, dispersion relations, and transient effects in superconducting magnets", *IEEE Transactions on Magnetics*, vol. 17, no. 1, pp. 722–725, 1981.

[123] I. Schafer and K. Kruger, "Modelling of lossy coils using fractional derivatives", *Journal of Physics D: Applied Physics*, vol. 41, no. 4, p. 045 001, 2008.

[124] L. Zhou and L. Li, "Modeling and identification of a solid-core active magnetic bearing including eddy currents", *IEEE/ASME Transactions on Mechatronics*, vol. 21, no. 6, pp. 2784–2792, 2016, ISSN: 1083-4435. DOI: 10.1109/TMECH.2016.2582644.

[125] I. Petras, L. Dorcak, P. O'Leary, B. M. Vinagre, and I. Podlubny, "The modelling and analysis of fractional-order control systems in frequency domain", *ArXiv Mathematics e-prints*, Aug. 2000. eprint: math/0008186.

[126] K. C. Toh, M. J. Todd, and R. H. Tutuncu, "SDPT3: a MATLAB software package for semidefinite programming", *Optimization Methods and Software*, vol. 11, pp. 545–581, 1999.

[127] M. Vidyasagar, *Nonlinear systems analysis*. SIAM, 2002.

[128] D. Liberzon, *Switching in systems and control*. Springer Science & Business Media, 2012.

[129] J. Daafouz, P. Riedinger, and C. Iung, "Stability analysis and control synthesis for switched systems: a switched lyapunov function approach", *IEEE transactions on automatic control*, vol. 47, no. 11, pp. 1883–1887, 2002.

[130] J. Löfberg, "YALMIP: a toolbox for modeling and optimization in MATLAB", in *CACSD Conference*, http://control.ee.ethz.ch/joloef/yalmip.php, 2004.

[131] K Vinida and M. Chacko, "A novel strategy using H_∞ theory with optimum weight selection for the robust control of sensorless brushless DC motor", in *IEEE Symposium on Sensorless Control for Electrical Drives (SLED)*, IEEE, 2016, pp. 1–5.

[132] K. Suzuki, J. Kobayashi, T. Otani, and S. Iwamoto, "A multi-input lead-lag power system stabilizer with H_∞ control performance", in *IEEE Conference on Innovative Smart Grid Technologies-Asia (ISGT ASIA)*, IEEE, 2015, pp. 1–6.

[133] S. Qaraawy, H. Ali, and A. Mahmood, "Particle swarm optimization based robust controller for congestion avoidance in computer networks", in *International Conference on Future Communication Networks (ICFCN)*, IEEE, 2012, pp. 18–22.

[134] H. Konno, "A cutting plane algorithm for solving bilinear programs", *Mathematical Programming*, vol. 11, no. 1, pp. 14–27, 1976.

[135] D. Simon, *Evolutionary optimization algorithms*. John Wiley & Sons, 2013.

[136] Ö. Yeniay, "Penalty function methods for constrained optimization with genetic algorithms", *Mathematical and Computational Applications*, vol. 10, no. 1, pp. 45–56, 2005.

[137] Z. Zhen-ping, "Determination of the admissible parameter set in designing PID controllers with guaranteed robust performance", in *Electrical and Control Engineering (ICECE), 2010 International Conference on*, IEEE, 2010, pp. 3625–3628.

[138] M.-T. Ho, "Synthesis of H_∞ PID controllers: a parametric approach", *Automatica*, vol. 39, no. 6, pp. 1069–1075, 2003.

[139] A. Nicoletti, M. Martino, and A. Karimi, "A data-driven approach to power converter control via convex optimization", in *Proceedings of the 1st IEEE Conference on Control Technology and Applications*, IEEE, 2017.

[140] A. Ben-Tal, L. El Ghaoui, and A. Nemirovski, *Robust optimization*. Princeton University Press, 2009.

[141] Q. King, A. Nicoletti, R. Murillo Garcia, M. Magrans De Abril, K. T. Lebioda, and M. Martino, "CCLIBS: the CERN power converter control libraries", in *International Conference on Accelerator and Large Experimental Physics Control Systems*, Melbourne, Australia, 2015.

[142] K. J. Åström, "Control system design", *Department of Mechanical and Environmental Engineering University of California Santa Barbara*, p. 333, 2002.

[143] O. Nelles, *Nonlinear System Identification: From Classical Approaches to Neural Networks and Fuzzy Models*. Springer Berlin Heidelberg, 2013, ISBN: 9783662043233.

[144] J. E. Normey-Rico and E. F. Camacho, *Control of dead-time processes*. Springer Verlag, 2007.

[145] C. Lai, P. Hsu, and B. Wang, "Design of the adaptive Smith predictor for the time-varying network control system", in *SICE Annual Conference, 2008*, IEEE, 2008, pp. 2933–2938.

[146] O. J. M. Smith, "Closer control of loops with dead time", *Chemical Engineering Progress*, vol. 53, no. 5, pp. 217–219, 1957.

[147] L. Mirkin, "On the extraction of dead-time controllers and estimators from delay-free parametrizations", *IEEE Trans. on Automatic Control*, vol. 48, no. 4, pp. 543–553, 2003.

[148] G. Meinsma and H. Zwart, "On H_∞ control for dead-time systems", *IEEE Trans. on Automatic Control*, vol. 45, no. 2, pp. 272–285, 2000.

[149] Q. C. Zhong, "On standard H_∞ control of processes with a single delay", *IEEE Trans. on Automatic Control*, vol. 48, no. 6, pp. 1097–1103, 2003.

[150] R. Sánchez-Peña, Y. Bolea, and V. Puig, "MIMO Smith predictor: global and structured robust performance analysis", *Journal of Process Control*, vol. 19, no. 1, pp. 163–177, 2009.

[151] W. Zhang and C. Lin, "Multivariable Smith predictors design for nonsquare plants", *Control Systems Technology, IEEE Transactions on*, vol. 14, no. 6, pp. 1145–1149, 2006.

[152] J.E. Normey-Rico and E.F. Camacho, "Multivariable generalised predictive controller based on the Smith predictor", *IEE Proceedings-Control Theory and Applications*, vol. 147, no. 5, pp. 538–546, 2000.

[153] V. De Oliveira and A. Karimi, "Robust Smith predictor design for time-delay systems with H_∞ performance", in *IFAC Joint Conference*, Grenoble, France, 2013, pp. 2933–2938.

[154] S. Rao and M. Chidambaram, "Smith delay compensator for multivariable non-square systems with multiple time delays", *Computers & chemical engineering*, vol. 30, no. 8, pp. 1243–1255, 2006.

[155] C. Vlachos, D. Williams, and J.B. Gomm, "Solution to the shell standard control problem using genetically tuned PID controllers", *Control Engineering Practice*, vol. 10, no. 2, pp. 151–163, 2002.

Achille Nicoletti

Scientist / Control Systems Specialist

My passion and general research interests lie in designing robust controllers for challenging uncertain applications by using various optimization tools.

Education

2013–2017 **Ph.D**, *Swiss Federal Institute of Technology (EPFL)*, Lausanne, Switzerland.
Major: Electrical Engineering - Advisor: Alireza Karimi
Thesis: *A Data-Driven Frequency-Domain Approach for Robust Controller Design via Convex Optimization*

2011–2012 **M.S**, *Cleveland State University*, Cleveland, USA, *GPA: 4.0/4.0*.
Major: Electrical Engineering - Advisor: Zhiqiang Gao

2007–2011 **B.S**, *Cleveland State University*, Cleveland, USA, *GPA: 3.99/4.0*.
Major: Physics

2007–2011 **B.E.E**, *Cleveland State University*, Cleveland, USA, *GPA: 4.0/4.0*.
Major: Electrical Engineering (University Honors)

Certifications

2013 **Six Sigma Green Belt Certificate**, *Philips*, Highland Heights, USA.
License: GB-018-2013-05
Mentor: Manoj Mohta (Master Black Belt)

2013 **Lean Certificate**, *Philips*, Highland Heights.
Mentor: Surindra Mathur (Master Black Belt)

Patents

2013 **Automatic Folding via Image Processing**.
United States - US61/927,866

Research Experience

2014–present **Doctoral Fellow**, *CERN*, Geneva, Switzerland.

- Research and develop data-driven robust control methods via convex optimization
- Design and implement RST controllers for power converters in particle accelerators
- Develop $\mathcal{H}_\infty$ control methods for nonlinear systems
- Formulate stability and robustness margins to ensure quality operation
- Create GUI for semi-automated controller design processes

171 Rue du Puits Mathieu – Thoiry – France
+33 (672) 990 063 • anicoletti10@yahoo.com

2013-2014 **Research Assistant**, *Swiss Federal Institute of Technology*, Lausanne, Switzerland.

- Designed controllers with $\mathcal{H}_\infty$ performance for systems with delay
- Created new data-driven algorithms using 2-degree-of-freedom controllers
- Assist master-level courses and aid students in the laboratory sessions of the course

2010–2011 **Research Collaborator**, *Michigan State University*, USA.

- Collaborated with NSCL scientists and engineers for developing a new disturbance rejection control strategy for LINAC systems
- Implemented adaptive control techniques to eliminate disturbances caused by microphonics
- Analyzed the relationship between closed loop performance and cavity deformations
- Employed MATLAB to mathematically model and simulate a LINACs response to disturbances

Professional Experience

2011–2013 **Electrical Design Engineer II**, *Philips*, Highland Heights, USA.

- Design motion control system for next generation computed tomography products
- Implement simulation tools (MATLAB, Mathcad, Simulink) in order to model and analyze multidomain dynamic systems
- Develop control algorithms using CoDeSys (IEC 61131-3 development software) through PLC based drives
- Implement Six Sigma tools for engineering related process improvements
- Provide resolution of voltage anomalies associated with the motion control system including spikes and radiated EMC
- Construct state machines (via the Structured Text language) for preliminary design considerations
- Ensure motion control system reliability through systematic FMEA techniques

2008–2009 **Power Systems Engineer (Internship)**, *Philips*, Highland Heights, USA.

- Performed circuit analysis for various analog and digital interfaces on the CT system
- Failure analysis of single phase and three phase transformers
- Utilized MATLAB to program and analyze Focal Spot Deflection
- Implemented harmonic filtering methods for power systems
- Developed mathematical models to determine G-forces for stochastic vibration systems

Awards & Honors

2010–present Eta Kappa Nu Electrical Engineering Honor Society

2009–present Tau Beta Pi Honor Society

2009–present Golden Key Honor Society

2007–present Alpha Lambda Delta Honor Society

2011 Valedictorian of CSU Engineering department

2011 Outstanding Electrical Engineering Senior Award - CSU EE

2011 Outstanding Physics Senior Award - CSU Physics

2011 Certificate of Recognition - CSU College of Science and Health Professionals

2010 Engineering Student Enrichment Program (ESEP) Junior Award

2009 Engineering Student Enrichment Program (ESEP) Sophomore Award

2008 Cleveland State University Honors Program scholarship

Publications

Book Chapters

1. Vinicius de Oliveira, Achille Nicoletti, Alireza Karimi. *Robust Smith Predictor design for time-delayed systems with $\mathcal{H}_\infty$ performance*. Advances in Delays and Dynamics, Springer, 2014.

Journals

1. Achille Nicoletti, Michele Martino, Alireza Karimi. *Model-reference control via convex optimization: a data-driven approach*, submitted to Control Engineering Practice, 2017.
2. Achille Nicoletti, Alireza Karimi. *Robust control of systems with sector nonlinearities via convex optimization: a data-driven approach*, submitted to International Journal of Robust and Nonlinear Control, 2017.
3. Achille Nicoletti, Michele Martino, Alireza Karimi. *A robust data-driven controller design methodology for particle accelerator power converters*, accepted to IEEE Transactions on Control Systems Technology, 2017.
4. Alireza Karimi, Achille Nicoletti, Yuanming Zhu. *Robust $\mathcal{H}_\infty$ controller design using frequency-domain data via convex optimization*, International Journal of Robust and Nonlinear Control (ISSN: 1049-8923), Wiley-Blackwell, 2016.
5. John Vincent, Dan Morris, Nathan Usher, Zhiqiang Gao, Shen Zhao, Achille Nicoletti, Qinling Zheng. *On active disturbance rejection based control design for superconducting RF cavities*, Nuclear Instruments and Methods in Physics Research, Elsevier, Volume 643, Issue 1. Cleveland, OH, 2011.

Conferences

1. Achille Nicoletti, Alireza Karimi. *Robust controller design for linear systems with nonlinear distortions: a data-driven approach*, submitted to European Control Conference, Limassol, Cyprus, 2017.
2. Achille Nicoletti, Alireza Karimi. *A data-driven method for computing fixed-structure low-order controllers with $\mathcal{H}_\infty$ performance*, submitted to European Control Conference, Limassol, Cyprus, 2017.
3. Massimo Giovannozzi, Alexander Huschauer, Olivier Michels, Achille Nicoletti, Guido Sterbini. *Analysis of performance fluctuations for the CERN proton synchrotron multi-turn extraction*, International Particle Accelerator Conference (IPAC), Copenhagen, Denmark, 2017.
4. Achille Nicoletti, Michele Martino. *Data-driven controller design for high precision pulsed power converters for bumper magnets of the PS Booster*, International Particle Accelerator Conference (IPAC), Copenhagen, Denmark, 2017.
5. Achille Nicoletti, Michele Martino, Alireza Karimi. *A data-driven approach to power converter control via convex optimization*, IEEE Conference on Control Technology and Applications, Hawaii, USA, 2017.
6. Quentin King, Raul Murillo-Garcia, Marc Magrans de Abril, Krzysztof Lebioda, Michele Martino, Achille Nicoletti. *CCLIBS: The CERN Power Converter Control Libraries*, 15th International Conference on Accelerator and Large Experimental Physics Control Systems, Melbourne, Australia 2015.
7. Achille Nicoletti, Zlatko Emedi, Alireza Karimi. *A data-driven approach in designing RST controllers with $\mathcal{H}_\infty$ performance via convex optimization*, IEEE Conference on Decision and Control, Osaka, Japan 2015.
8. Achille Nicoletti, Alireza Karimi. *$\mathcal{H}_\infty$ Smith Predictor Design for time-delayed MIMO systems via convex optimization*, IEEE Multi-Conference on Systems and Control, Antibes/Nice, France, 2014.

Skills

Software

- MATLAB/Simulink
- C/C#
- VHDL
- LaTeX
- Mathcad
- Mathematica
- PSPICE
- MS Office

Hardware

- PIC microcontrollers
- FPGA's
- Analog and digital filters
- ADC's & DAC's
- Digital Signal Processors
- Spectrum analyzers
- VFD's & servo drives
- Asynchronous motors

Languages

English	Native language
French	Reading: C1 | Listening: C1 | Writing: B2
Italian	Reading: C1 | Listening: C1 | Writing: B2
Russian	Reading: A1 | Listening: A1 | Writing: A1

References

- Alireza Karimi, Ph.D.
  Professor of Mechanical Engineering, Swiss Federal Institute of Technology (EPFL)
  Phone Number: +41 21 693 5925
  Email: alireza.karimi@epfl.ch

- Michele Martino, Ph.D.
  Research Engineer, CERN
  Phone Number: +41 75 411 9422
  Email: michele.martino@cern.ch

- Kiril Streletzky, Ph.D.
  Associate Professor of Physics, Cleveland State University
  Phone Number: +1 216 687 2433
  Email: k.streletzky@csuohio.edu

- Zhiqiang Gao, Ph.D.
  Associate Professor of Electrical Engineering, Cleveland State University
  Phone Number: +1 216 687 3528
  Email: z.gao@csuohio.edu